STUDIES ON CAISSON TYPE BREAKWATER – A PHYSICAL AND NUMERICAL APPROACH

Thesis
submitted in partial fulfillment of the requirements for the degree of

DOCTOR OF PHILOSOPHY

by

KUMARAN V.
(177134AM500)

DEPARTMENT OF WATER RESOURCES AND OCEAN ENGINEERING
NATIONAL INSTITUTE OF TECHNOLOGY KARNATAKA
SURATHKAL, MANGALORE - 575 025, INDIA

DECEMBER, 2022.

STUDIES ON CAISSON TYPE BREAKWATER – A PHYSICAL AND NUMERICAL APPROACH

Thesis
submitted in partial fulfillment of the requirements for the degree of

DOCTOR OF PHILOSOPHY

by

KUMARAN V.
(177134 AM500)

Under the guidance of

Dr. MANU and Prof. SUBBA RAO

**DEPARTMENT OF WATER RESOURCES AND OCEAN ENGINEERING
NATIONAL INSTITUTE OF TECHNOLOGY KARNATAKA
SURATHKAL, MANGALORE - 575 025, INDIA**

DECEMBER, 2022

DECLARATION

I hereby declare that the Ph.D. Thesis entitled **"STUDIES ON CAISSON TYPE BREAKWATER – A PHYSICAL AND NUMERICAL APPROACH"** which is being submitted to **National Institute of Technology Karnataka, Surathkal,** for the partial fulfillment of the requirement for the award of degree of **Doctor of Philosophy** in the **Department of Water Resources and Ocean Engineering** is a bonafide report of the work carried out by me. The material contained in this Ph.D. Thesis has not been submitted to any university or Institution for the award of any degree.

....
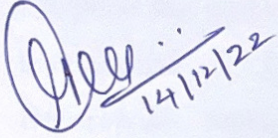
KUMARAN V. (177134AM500)

Department of Water Resources and Ocean Engineering

National Institute of Technology Karnataka, Surathkal

Place: NITK, SURATHKAL.

Date:

CERTIFICATE

This is to certify that the Ph.D. Thesis entitled **"STUDIES ON CAISSON TYPE BREAKWATER – A PHYSICAL AND NUMERICAL APPROACH"** submitted by **KUMARAN V. (177134 AM500),** as the record of the work carried out by him, is accepted as the Ph.D. Thesis submission in partial fulfillment of the requirements for the award of the degree of **Doctor of Philosophy** in the **Department of Water Resources and Ocean Engineering, National Institute of Technology Karnataka, Surathkal**, is a bonafide work carried out by him under our supervision and guidance.
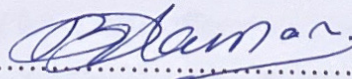
14/12/22

Dr. MANU

(Research Guide)

14/12/22

Prof. SUBBA RAO

(Research Guide)

Dr. Subba Rao Ph.D. (Coastal Engg.)
Professor
Department of Water Resources and Ocean Engineering
National Institute of Technology Karnataka, Surathkal
Srinivasnagar- 575 025, Mangaluru - INDIA
Email: surakrec@gmail.com

NITK Surathkal — Dept. of Water Resources & Ocean Engineering

Chairman - DRPC

Department of Water Resources and Ocean Engineering

National Institute of Technology Karnataka, Surathkal

Chairman (DRPC)
Dept. of Water Resources & Ocean Engineering

ACKNOWLEDGEMENT

ABSTRACT

The design and construction of coastal structures such as breakwaters, at greater water depths is rapidly increasing as a result of the increasing draught of large vessels and off-shore land reclamations. Vertical caisson-type breakwaters may be the best alternative compared to ordinary rubble mound breakwaters in larger water depths, in terms of performance, total costs, environmental aspects, construction time and maintenance. To fulfil the functional utility and impact of the structure on the sea environment, it is necessary to study the hydraulic performance of such breakwaters. In the present project, the hydrodynamic performance of caisson breakwater with various geometric configurations are studied in detail. In the first phase, a physical model approach is carried out extensively to study the stability of toe protection for vertical caisson breakwater. The determination of the size of the toe armour units and their cross-section for the stable design are investigated. The applicability of the Brebner and Donnelly (Coast Eng Proc 1: 24, 1962) design curve for depth-limited conditions is validated for a certain fixed relative foundation depth (d_1/d). In the second phase, an investigation of the non-perforated caisson type breakwater is performed considering different wave conditions. The variation of dynamic wave pressure, wave force, wave run-up, and wave reflection are determined for this structure. The maximum wave force on the caisson breakwater is calculated from measured pressure values and is compared with the wave forces calculated by Goda's and Sainflou wave theories. The comparison of results illustrate that the Goda's formula provides a good estimation of wave force distribution compared with the experimental findings. In the third phase, a numerical model of caisson breakwater is developed to study its performance using the computational fluid dynamics (CFD) approach using Ansys-Fluent and validated the same using experimental data. In the fourth phase, the experimental investigations are carried out on non-perforated vertical wall breakwater with the presence of a vertical and horizontal slotted barrier. In the fifth phase, the perforations (i.e 8 %, 10%, 13%, 15%, 20%) are introduced in the front face of the caisson breakwater to analyse the hydraulic performance to arrive at better perforations in reducing the wave forces, wave reflection and wave runup.

Keywords: Caisson Breakwater, Slotted Barrier, Perforated Caisson, CFD

TABLE OF CONTENTS

CHAPTER 4

HYDRODYNAMIC PERFORMANCE CHARACTERISTICS OF VERTICAL CAISSON TYPE BREAKWATER   **75**

LIST OF FIGURES

LIST OF PLATES

LIST OF TABLES

NOMENCLATURE

H_o	Deepwater Wave Height
z	Depth below SWL
D	Depth of Toe
d_l	Depth from MSL to top of Toe
d_s	Height of the structure
H_i	Incident Wave Height
H_r	Reflected Wave Height
Re	Reynolds Number
ξ_0	Surf Similarity Parameter
d	Water Depth
t	Instant of Time
T	Wave Period
L	Wave Length
F	Wave Force
B	Width of Toe
H_i / L	Wave Steepness
H_i / d	Relative Wave Height
d / L	Relative Water Depth
z / d	Relative depth parameter on the wall

LIST OF ABBREVIATIONS

CB   Caisson Breakwater

CFD   Computation Fluid Dynamics

FDM   Finite Difference Method

HSB   Horizontal Slotted Breakwater

MSL   Mean Sea Level

OWC   Oscillating Water Column

PCB   Perforated Caisson Breakwater

RANS   Reynolds Averaged Navier – Stokes Equation

SWL   Still Water Level

UDF   User Defined Function

VCB   Vertical Caisson Breakwater

VSB   Vertical Slotted Breakwater

VOF   Volume of Fluid

WCSPH   Weakly Compressible Smoothed Particle Hydrodynamics

CHAPTER 1

INTRODUCTION

1.1 GENERAL

In maritime structures, breakwaters are designed to protect a valuable part of the coast. In general, the main purpose of such a structure is to reduce the energy of waves in inshore waters for providing safe harbourage or reducing coastal erosion. Breakwater can be built using natural stones, a combination of natural stone and artificial armor units (if the waves are more powerful), or concrete caissons. The rubble mound breakwater gains stability because of its trapezoidal cross-section shape and hence, consumes a high volume of materials. To ensure the breakwater integrity and infrastructure serviceability, a comprehensive structural design of this structure is required. The recent years has witnessed rapid upsurge in population growth and infrastructure developments along the coast belt. In addition, there is a significant rise in the natural threats and impacts of natural hazards such as rising sea levels, cyclones, and tsunamis. Due to the increase in global trade, many new ports, marinas, and harbours are constructed in developing countries. During the last fifty years, there has been a lot of pressure on the coastal area for the development of safe navigation and safety of the coastal infrastructures. The design and construction of breakwaters have played a vital role in several measures for the protection of coastal infrastructure. In extreme storm weather conditions, the rise in wave loads on these structures leads to failure. To reduce such impact, different types of coastal structures are introduced either near or at a finite distance to dissipate the wave energy and hence the effect of waves on the structures.

1.2 BREAKWATER

The purpose of this type of coastal structure is to protect areas of human residence, conservation, and protecting beaches from the action of waves and tides (Kamphuis 2010). The energy of ocean waves is one of the most challenging tasks for ocean engineers to combat for various reasons. On the one hand, coastal infrastructures, amenities, and communities are protected from destructive waves. To ensure safe navigation and berthing within harbour basin, reasoble clam sea condition is expected

in ports, harbours and marinas. On the other hand, importance is given to safeguard the eroded beaches by modifying the profile and shape of the beach. Coastal protection by breakwaters is particularly relevant for beaches of high commercial and recreational values as the defense structures may save lives, more valuable resources, properties, and commercial activities in coastal areas. These structures provide necessary tranquillity on the lee-side of it. The selection of appropriate breakwater is influenced by several factors such as water depth, geomorphologic conditions of the seabed, availability of materials, and its functional utility.

1.3 TYPES OF BREAKWATERS

Breakwaters are generally categorized as fixed, floating, and special types, as shown in Figure 1.1. The most feasible one is chosen for construction based on the prevailing environment and depending on the required degree of shelter (Rajendra et al., 2017). The following are some of the types of breakwaters basically in use :

> - Rubble mound breakwaters
> - Vertical wall breakwaters
> - Composite breakwaters
> - Special type of breakwaters
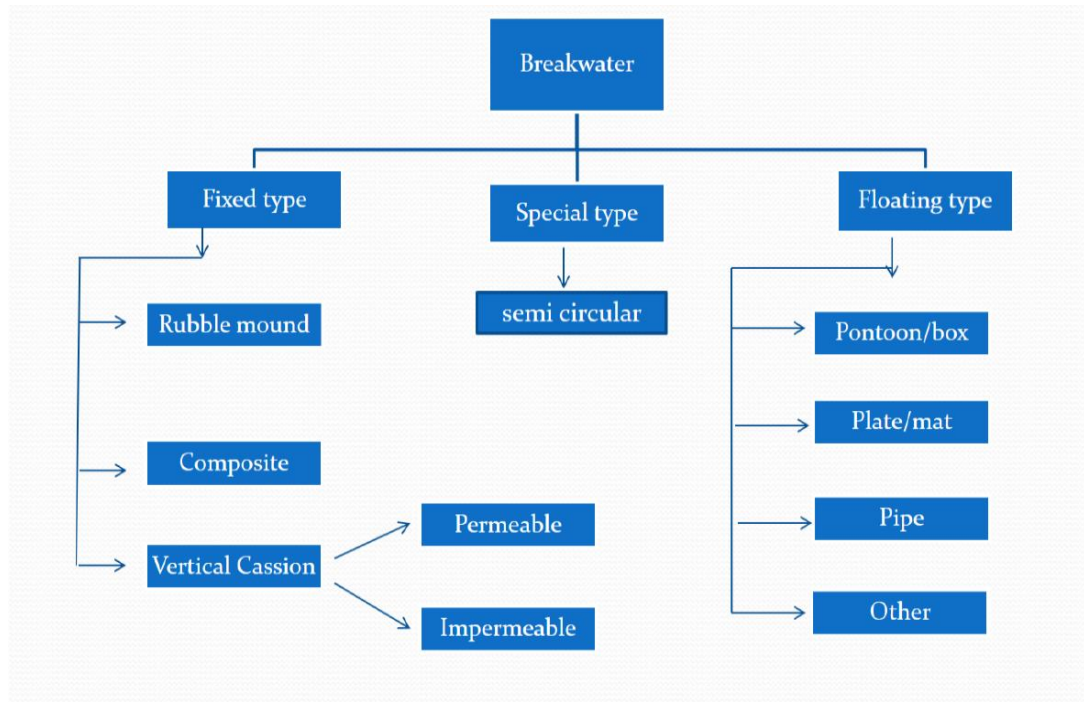
Figure 1.1: Classification of Breakwater (Rajendra et al. 2017).

1.3.1 Rubble Mound Breakwaters (RMB)

The most widely used in places where natural stones are abundantly available. The (RMB) is typically constructed with a core, secondary layer, and a primary layer to protect from wave action. The RMB is constructed mainly to break the wave and vertical wall breakwaters to reflect the waves. The RMB is limited to shallow water environments from a technical and economical point of view. Modern-day constructions with concrete blocks could be used in deep waters as well. Functionally, (RMB) mainly dissipate the wave energy of the incoming waves by forcing them to break on a slope. The slope of the structure is usually between 1:1 and 1:2, depending upon the materials used. In shallow water, rubble mound breakwaters are generally relatively inexpensive. As water depth increases, the material requirements increase significantly, and hence it reflects in high construction costs.

Rubble mound breakwaters have been used at ports of New Mangalore, Madras, Paradeep, and Tuticorin. They are economical up to depths of approximately 15 to 20

meters [Ramamurthy (1974)]. But there are cases where they have been used up to 50 meters, like Sines breakwater in Portugal.

Rubble mound breakwaters are further classified into and shown in Figure 1.2:

- Conventional breakwater

- Berm breakwater

- Reef breakwater

- Tandem breakwater
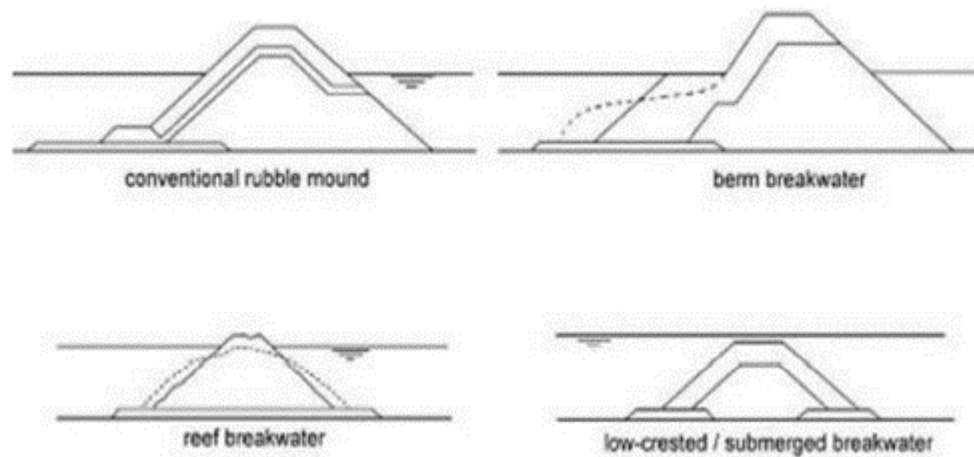
Figure 1. 2: Types of rubble mound breakwaters (CIRIA, CUR, CETMEF 2007)

1.3.2 Vertical Caisson Breakwaters

Vertical caisson or wall-type breakwater is predominantly used to protect the inner harbour region from the high-water levels and waves to maintain tranquility for safe marine operations, especially in deeper waters. The vertical-caisson structure breakwaters function as an effective barrier against the waves and maintain calm sea conditions on their leeward side for safe operations. These breakwaters are effective for water depths larger than 15–20 m; the most common type of vertical / caisson breakwaters are cellular reinforced concrete caissons, which are sunk with seawater ballast and then filled with sand. They are also called upright or vertical-caisson breakwater (Franco 1994).

Arrays of concrete caissons or vertical caisson are widely used as a breakwater in various countries (ex: Japan, Italy) when it is viable and cost-effective. The functional aspect of vertical breakwater is to reflect the incident wave energy, whereas the rubble mound breakwater acts as a dissipative mechanism. Typical photography of Vertical breakwater is illustrated in Figure 1.3.
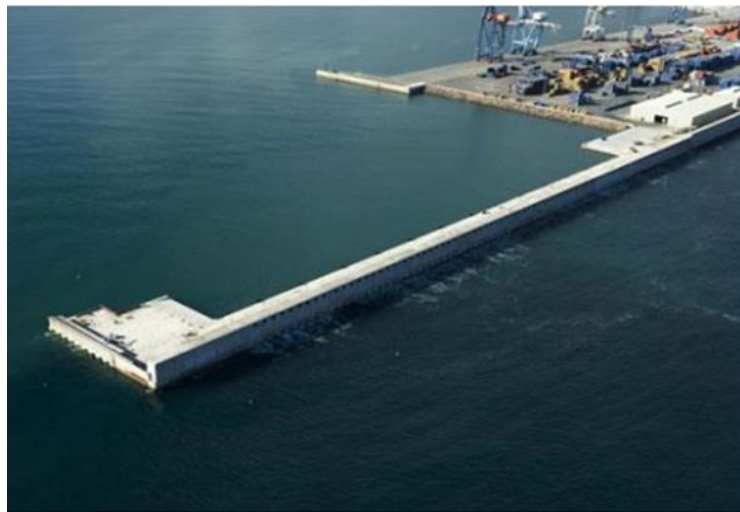
Figure 1.3: Vertical breakwaters

(Source:https://www.gravityeng.com/exp_tinnel_pid=122&type=Harbor)

The installation of caisson-type breakwaters is done by towing the caisson to the required location and ballasting it using rubble, concrete, or sand fill to lower it to the sea bed. Caisson-type breakwaters are the most suitable for rough sea conditions due to relatively fast and easier installation. The main factors influencing the design and selection of vertical caisson breakwater are foundation stability and incident wave forces. Such kinds of breakwater are regularly designed as structures subjected to forces causing failure in the following ways:

- Sliding from one block to the another

- By overturning as a solid mass and continuous wave action leads to the uplifting of horizontal layers.

- Collapsing or fracture of massive blocks.

The installation of vertical wall breakwaters requires skilled labour, advanced construction equipment, and high knowledge of confidence. Many such breakwaters are failed in the past (e.g.) japan, Italy, Algeria, etc. (Goda 1992)

A few of the merits and demerits of the caisson-type breakwater are listed below:

Merits

- Provide a larger harbour area and a narrower entrance.

- Reduce the amount of material

- Avoid dangers of unequal settlement

- Where rock is unavailable, it saves time and money

Demerits

- Difficult to repair if damaged

- Construction requires more extensive and heavier equipment

- Required formwork, quality concrete, and skilled labour, batching plants, floating crafts

- It can be constructed only where foundation conditions are favorable.

1.3.3 Composite Breakwaters

The combination of the RMB and the wall breakwaters is shown in Figure 1.4. The concrete caissons of different configurations are used to substitute the wall section to reduce the effect of wave reflection. Such kinds of breakwaters are significant in deeper waters or at sites where the variation of tidal is high. High mound composite breakwaters are unstable as the breaking waves induce impulsive pressure and scouring, due to which low mound breakwaters have commonly been used. These composite configurations function as mound breakwaters at low tide and vertical breakwaters at high tide. (Goda, 2000).
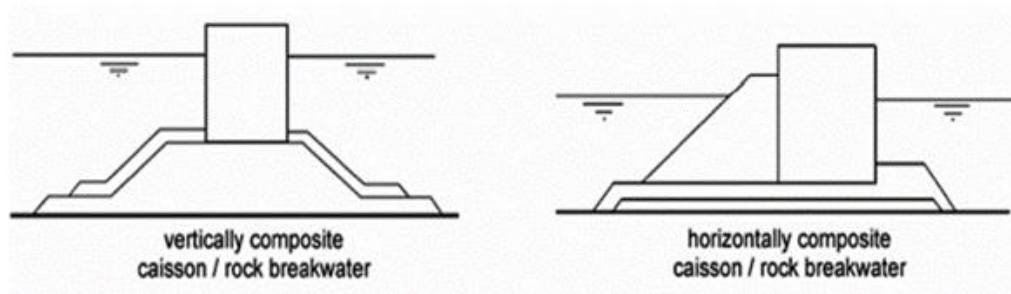
Figure 1.4: Types of the composite breakwater (CEM 2012)

The final choice of the type is governed by the equipment available and technical-know how in handling the job. During the low tide, the rubble mound will function as a rubble mound breakwater. During the high tide, the composite breakwater will perform the role of a caisson breakwater, and the rubble mound offers scour protection. It provides a platform for handling cargo. It makes it possible for ships to come close to the breakwater wall on the inner or harbourside for loading and unloading cargo.

1.3.4 Special Types of Breakwaters

The special kind of breakwater is still in use though limited to special conditions. The curtain wall breakwater is used as secondary breakwaters to protect small craft harbours. Sheet pile or continuous pile vertical wall breakwaters are used to break small waves. A Horizontal plate breakwater can reflect and break waves. A floating breakwater is very useful as a breakwater in deep waters, but its effect is limited to relatively short waves. Some of the special types of breakwaters are explained in the subsequent sections.

Floating breakwaters, In low wave energy environments, floating breakwater is employed as an alternative to conventional gravity breakwaters. It does not have any kind of bottom-founded structure. Further, for practical applications, it floats over the water surface assisted by pontoons and supported by mooring lines as shown in Figures 1.5-1.6.

7
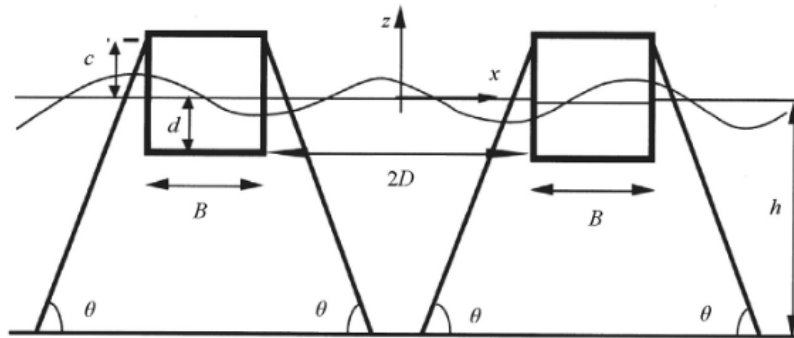
Figure 1.5: Floating double-box breakwater (Williams et al., 2000)

Figure 1.6: (a) Holy Loch breakwater (Maritimejournal.com, 2017), (b) breakwater at

Fezzano, SP-Italy (Ingemar, 2017)

Mobile breakwaters are considerably used for their speedy installation at the site. The wave height is appreciably reduced on the leeward side of the structure which supports ready transportation.

Horizontal plate breakwater is preferable in a less energy-wave environment with weak and soft subsoil conditions. The structural configuration breaks and reflects the wave energy significantly. Mostly steel jacket frames are used to support these structures.
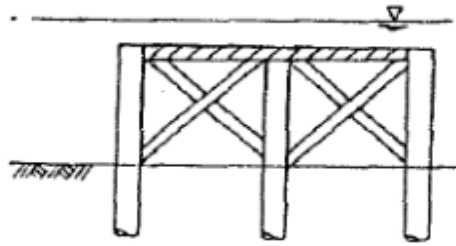
Figure 1.7: Horizontal plate breakwater (D'Angremond et.al., 2008)

Pile breakwater

Figure 1.8 illustrates the configuration of pile breakwater formed by a series of piles arranged in rows. It has more advantages than the conventional rubble mound breakwaters in allowing the free passage of sediments and thus reducing coastline erosion on its down-drift side.
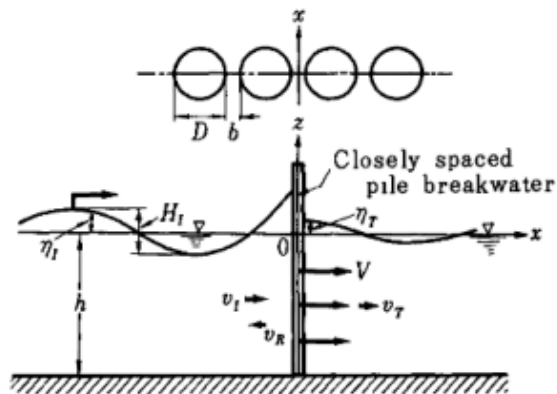
Figure 1.8: Pile breakwater (D'Angremond et.al., 2008)

Curtain wall breakwater It is frequently utilized as a supplemental breakwater to safeguard small vessel harbors.
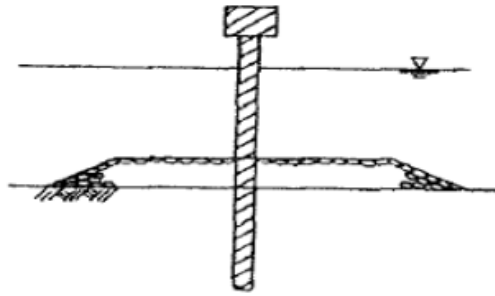
Figure 1.9: Curtain wall breakwater (D'Angremond et.al., 2008)

1.4 COMPUTATIONAL APPROACH FOR BREAKWATER

In the structural design of breakwaters in the last few decades, the advancement in computation tools has increased enormously for solving wave structure problems (Ning et al., 2007).With the rapid development of advanced computers and computational fluid dynamics (CFD) techniques, several software applications have been developed based on linear wave theory or diffraction models, such as ANSYS-Aqwa, Fluent, Oracflex, WAMIT, etc., Computational Fluid Dynamics (CFD) has led to a decisive step in the simulation of wave actions on breakwaters, both submerged and emerged. The successive advances in the computational tool and signs of progress in graphics capabilities of numerical models and analyzing outcomes are considerably more accessible compared to physical model study.

Two-Dimensional or Three-Dimensional flow simulation is quickly becoming standard practice. It involves a typical procedure for the numerical integration of Reynolds Averaged Navier–Stokes equations and volume of fluid with one of the traditional turbulence models (K-eps, K-ω, RNG) and a free surface tracking procedure generally based on the Volume of Fluid Method. However, computational fluid dynamic (CFD) methods based on the Navier-Stokes equation model are promising for non-linear hydrodynamic characteristics between waves and floating bodies, viscous flow separations, and even possible wave overtopping and breaking.

1.5 NEED AND SCOPE OF THE PRESENT STUDY

In general, coastal structures and in particular, the breakwaters are built since ancient times, but the major research still is extensively focused on the hydraulic performance, structural characteristics, and the design process. The social, environmental, and aesthetic factors are increasingly influencing the design of breakwater. There is a need to develop a safe and economical breakwater as capital investment contributes more to designing breakwaters in port design, developing a safe and economical breakwater is vitally important.

Figure 1.10: (a) Breakwater Structure   (b) Caisson Towing to site

(c) Caisson installation on site   (d) Installation flooded with water to sink

(e) Foot protection installation work (f) Final caisson on site
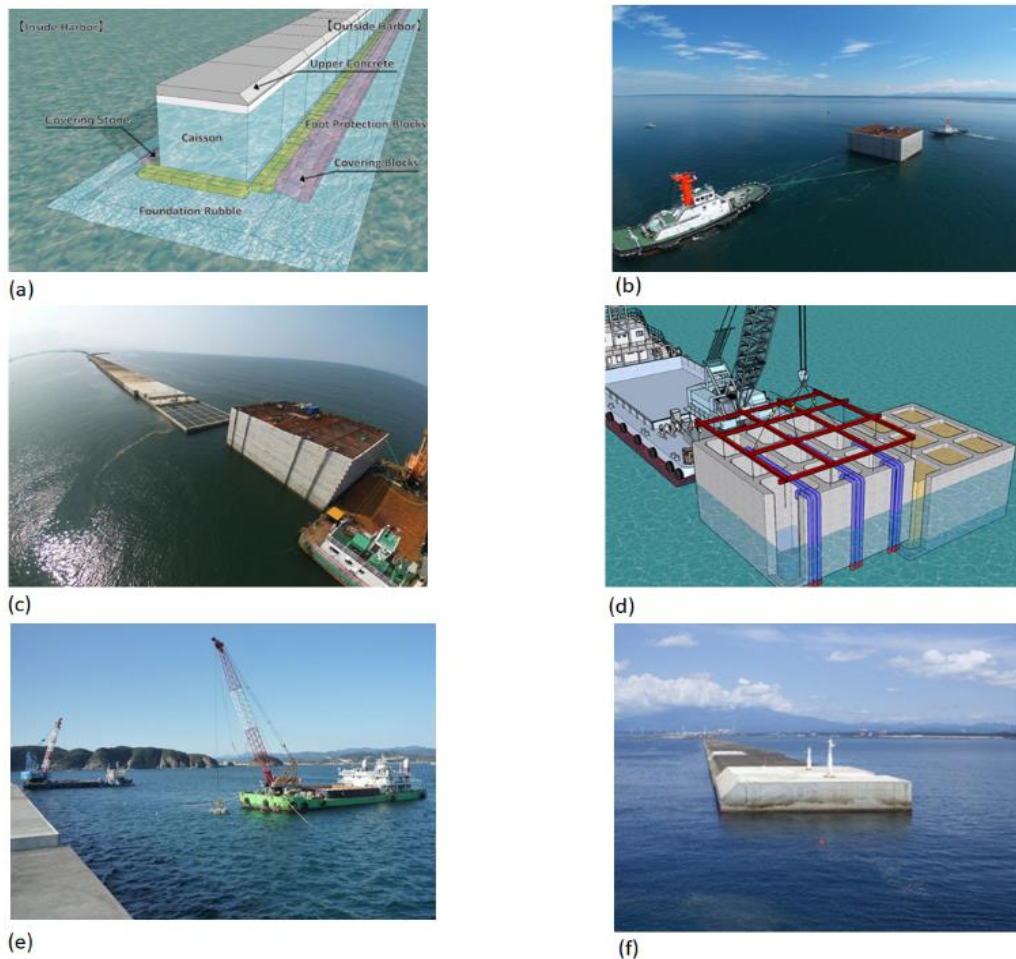
(Port of Akita, Japan / Source: https://www.aomi.co.jp/en/tech/cason.html)

Figure 1.10 illustrates the pictorial representation of the step-by-step installation of caisson breakwater from shore to site. (Port of Akita, Japan). The first vertical breakwater in the modern age of Japan is those at Yokohama Port, which is designed by H. S. Palmer (a retired British Major General) and built from 1890 to 1896 at the same time as new thoughts and developments are in process by various investigator around the globe. The present research focus on the hydrodynamic performance of a vertical caisson breakwater. The experimental studies are carried out in the wave mechanics laboratory to investigate the performance of vertical caisson breakwater with various combinations such as slotted barrier, protection of toe, and perforated caissons by using suitable test models wave characteristics under non-breaking wave conditions.

In an experimental study, understanding the scale effects for the desired wave parameters is a critical task for all conditions. Hence, it is also necessary to develop an appropriate numerical model to understand the hydrodynamics of the various test model considered in the present study. An attempt is made to develop an appropriate numerical model using the CFD approach, a 2D numerical wave flume is established using ANSYS- Fluent platform. The numerical results of the wave forces, free surface elevations, wave reflection, and wave runup are validated with the physical model test results, and good agreement is found.

1.6 BRIEF OVERVIEW OF THE THESIS

This thesis comprises of eight chapters, and the content of each chapter is as outlined below :

In Chapter 1, a basic introduction and motivation behind the current work are presented. And introduces the history of breakwaters and types of breakwaters with special emphasis on vertical caisson breakwater. Further, it also includes the need and scope of the present research work.

In Chapter 2, the relevant literature survey to the present work is performed thoroughly, followed by a brief introduction of several concepts related to physical modelling and the equivalent numerical modelling, which in turn leads to the motivation and objectives of the present research work.

Details of the present experimental investigation, including the details of laboratory conditions, physical modelling, wave conditions, methodology, and experimental setup for the present work, are explained in **Chapter 3.**

Chapter 4 deals with the stability of the toe for caisson breakwater and the determination of the size of the toe armour units and its cross-section. The applicability of the Brebner and Donnelly (Coast Eng Proc 1: 24, 1962) design curve for depth-limited conditions is validated to know the stability and % damage level for toe armour units. Finally, the hydrodynamic parameters on the vertical caisson breakwater are also discussed.

Chapter 5 presents the numerical modelling of vertical caisson breakwater using the computation fluid dynamics (CFD) tool using Ansys- Fluent. A 2D numerical wave flume is developed using ANSYS- Fluent platform by considering the VOF method and incompressible open channel fluid flow. The wave boundary conditions are adopted by solving the Reynolds-Averaged Navier Stokes equations (RANS equation) with the k—ε model to examine the effects of turbulence on the numerical results.

Chapter 6 elaborates on the work on the slotted barrier in the front of the caisson breakwater as one of the areas of extended interest in the field of ocean engineering. The emphasis of the study is on dynamic pressures, wave forces, wave reflection, and wave run-up on the vertical caisson-type breakwater. A CFD approach is also performed to ensure the level of confidence for a wide range of input conditions.

Chapter 7 discusses the performance characteristics of vertical caisson breakwater with perforations by varying porosity percentages and relative spacing between them. Finally, arriving with an optimum porosity on vertical caisson breakwater.

Chapter 8 presents the summary and conclusion of the work done in the thesis, followed by the future scope of research. In this chapter, the major contributions from the present study are highlighted. The limitations of the present study and indications of future directions from this study are also presented here.

The relevant literature used for the present study are presented in the references section

In Appendix 1, the measurement of wave reflection, wave force calculation are presented, and Uncertainty analysis is presented in Appendix 2.

13

A list of publications based on the present research work and a brief resume are given at the end of the report.

CHAPTER 2

LITERATURE REVIEW

This chapter is split into four phases. The first and second phase of the chapter highlights the background and the evolution of caisson-type breakwater. It also provides an in-depth understanding of such breakwater's performances and failure modes in different wave conditions. The main objective of this section is to figure out the cost-effective design of coastal structures for multi-purpose: protecting the coast from erosion or providing the safe, tranquil condition for safe marine operations.

In the third phase of the chapter (Section 2.3), the comprehensive literature review of the perforated breakwater is reported. Through a comprehensive review of past literature in terms of hydrodynamic performance and design wave loads on the wall-type breakwater, with the combinations of the horizontal and vertical slotted barrier, the research gaps are identified and have been taken further for a thorough investigation.

In the fourth phase of the chapter (Section 2.4), a review of numerical approaches is taken place for a better understanding of the wave structure problem.

2.1 GENERAL

The literature study provides a general overview of the use of vertical breakwater in coastal engineering practice, while the emphasis of the study is on vertical walls placed on top of a rubble foundation. The literature study aims to gain a fundamental understanding and insight into the design and response characteristics of vertical caisson breakwater.

2.1.1 Vertical Breakwater

The vertical breakwater design philosophy is reasonably well developed by Tanimoto (1976), Goda (1985), Takahashi (2001), and many more in the past. They have modelled the intricacies of its hydraulic, structural behaviour, and performance. The

literature available in the area of design of vertical breakwaters and sliding stability of caisson breakwaters is presented in this section. The definition sketch of a vertical breakwater is shown in Figure 2.1. A vertical structure consists of a caisson, made up of reinforced concrete, which may or may not be filled with sand. A literature survey is carried out to understand the results of the works done by various authors in the field of Hydrodynamic characteristics of the vertical breakwater, and stability against sliding of the concrete caisson breakwater.
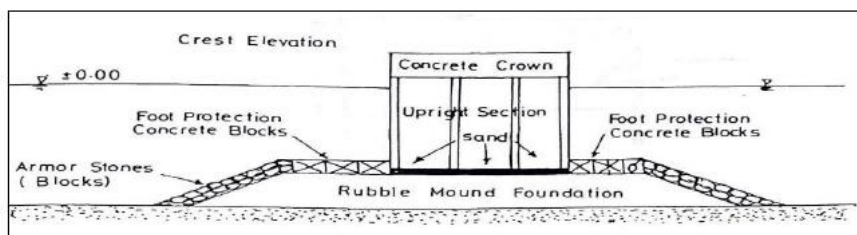
Figure 2.1: Idealized typical section of a Caisson breakwater

A vertical seawall is a retaining structure in which wave attack is primarily resisted by the "wall" of the structure, either extended directly from the seabed or built atop a rubble foundation, as illustrated in Figure 2.2. Vertical seawalls are considered for their efficient use of space and economical construction material utilization and are further classified by Allsop (2009) as:

- Full depth, where the vertical structure extends over the full depth of water

- Vertically composite, where the vertical wall is constructed atop a rubble foundation

- Armoured or horizontally composite, where a mound of armour units is placed against the seaward face of the wall.
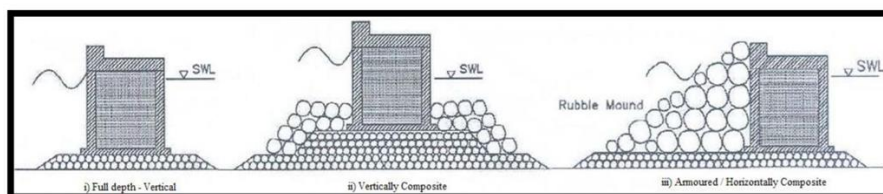
Figure 2.2: Vertical seawall/ Breakwater (Allsop, 2009)

16

Vertical structures comprising reinforced concrete (i.e. caissons) are common forms used in practice. These structures are primarily floated from a dry/floating dock and placed atop the correct foundation location. (Ching, 2004).

In the design of vertical caisson breakwater, both functional and structural considerations play a significant role. Functional considerations are mainly wave overtopping, and reflection by a breakwater. A few structural elements are mentioned below majorly to be considered for functional and structural consideration.

- Self-weight of the structure
- Crest elevation
- Toe protection

The stability of vertical caisson breakwater is assessed in terms of factors of safety against sliding, overturning modes of failure, shear failure in foundations, and influence of shock pressures, including earthquakes that could cause liquefaction of its foundation.

2.1.2 Wave Pressure Formulae for Vertical Breakwater

Depending upon the positions or orientation, the vertical wall breakwater is subjected to various kinds of wave forces. The wave force is the dominant factor in the stability analysis of any breakwater. So the forces and moments resulting in the structure should be analysed based on the type of wave. The waves may be classified as:

- Non-Breaking Waves
- Breaking Waves
- Broken Waves

2.1.3 Non-Breaking Waves

When the depth of water at the structure is greater than about 1.5 times the maximum expected wave height, non-breaking waves occur. The forces due to the non-breaking waves are primarily hydrostatic. Sainflou (1928) presented a formula for the pressure of a standing wave on a vertical wall as shown in Fig 2.3. This method has been in

general use for many years. Sainflou used a regular sine wave and assumed that there will be a perfect reflection from the wall. The wave pressure is calculated according to first-order theory.
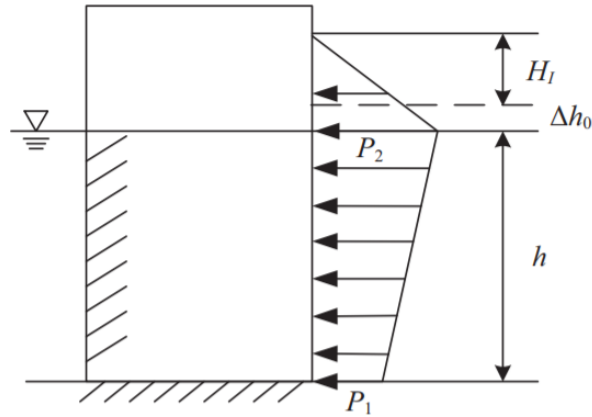
Figure 2.3: Sainflou wave pressure distribution diagram

The formulae involved are as follows:

$$p_1 = \frac{\gamma H}{Coshkd} \tag{2.1}$$

$$p_2 = \frac{(p_1 + \gamma d)(h + h_0)}{Coshkd} \tag{2.2}$$

$$h_o = \frac{\pi H^2}{L} coshkd \tag{2.3}$$

Where,

k - Wavenumber; d - Depth of structure from still water level; H - Wave height; L - Wavelength; γ - The unit weight of seawater; Δh_0 - lifted distance for the mean water level.

The total resultant pressure F and overturning moment are calculated from the pressure distribution diagram. Sainflou's formula is applicable for relative depth, h/L_0, between 0.1 and 0.15 where L_0 is the wavelength (Yu-Shu Kuo et al., 2015).

2.1.4 Breaking Wave Forces

Waves breaking directly against the vertical face of the structures exerts high, short-duration pressures that act near the region where the wave crest hits the structure. Breaking waves create short impulsive loads on the vertical structures which introduce localized damages. When the water depth is less than about 1.5 times the maximum expected wave height, breaking waves may occur. Minikin (1955, 1963) introduced a design procedure based on observations of full-scale breakwaters and the results of Bagnold's study. The dynamic pressure Pm is maximum at the SWL and decreases to zero at $0.5H_b$ (breaking wave height) below and above the SWL as shown in Figure 2.4.

Minikin (1955) developed a procedure to determine the maximum dynamic pressure that the vertical wall would experience and the expression for maximum dynamic pressure is given as:

$$p_m = 101\rho g \frac{dH_b}{L_D D}(D + d) \qquad (2.4)$$

Where

P_m – Maximum wave pressure; H_b – Breaking wave height; L_D - Wavelength at depth D ; D – Depth at a distance of one wavelength seaward of the structure; D=hs (m+1) where m is the slope of the seabed; ρ - Density of seawater ; d – water depth at the toe of the structure

The total horizontal force is represented by the area under the dynamic and hydrostatic pressure distribution (SPM, 1984).
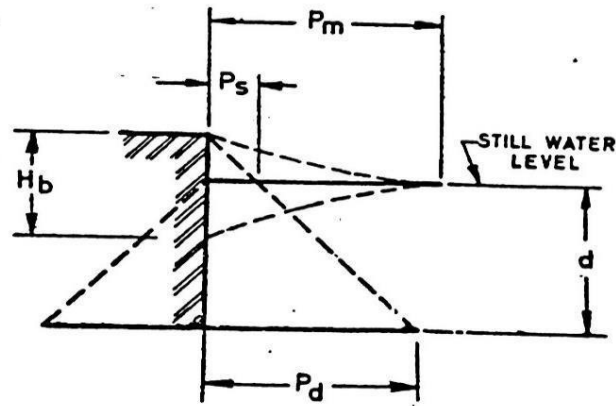
Figure 2.4: Minikin Wave pressure distribution diagram (Mani, 2012)

Goda (1974) proposed a new wave pressure formula, which can be applied for the whole range of wave action from nonbreaking to post-breaking waves with a smooth transition between them. The design wave height is specified as the maximum wave height possible at the site of the breakwater. The new formulae, as well as the existing formulae of Hiroi, Sainflou, and Minikin, with the cases of 21 sliding and 13 not sliding of the upright sections of prototype breakwaters. The results establish that the new formulae are the most accurate ones. With the new formulae, engineers will be able to design composite breakwaters under any wave condition with consistent principles. Figure 2.5 illustrates the Goda wave pressure distribution.
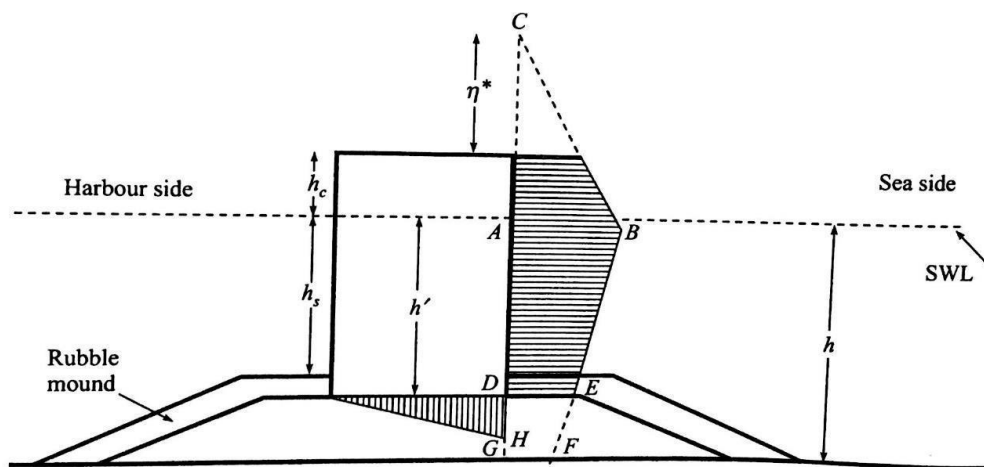
Figure 2.5: Goda Wave pressure distribution diagram (Mani J. S. 2012)

20

$$\eta^* = 0.75(1 + cos\beta)H_m \qquad (2.5)$$

Where,

η^* is the height up to which the wave pressure is exerted, β is the angle between the direction of wave approach and a line normal to the breakwater, H_m is maximum wave height. The recommended value for β is 15^0.

$$\alpha_1 = 0.6 + 0.5 \left[\frac{2kh}{Sinh2kh}\right]^2 \qquad (2.6)$$

$$\alpha_2 = min \left\{ \frac{h_b - h_s}{3h_b} \left(\frac{H_m}{H_s}\right)^2, \quad \frac{2h_s}{H_m} \right\} \qquad (2.7)$$

$$\alpha_3 = 1 - \frac{h^1}{h}(1 - \frac{h}{Coshkh}cos\beta)H_m \qquad (2.8)$$

$$P_1 = 0.5(1 + cos\beta)(\alpha_1 + \alpha_2 cos^2\beta)\gamma w_m H_m \qquad (2.9)$$

$$P_2 = \frac{P_1}{Coshkh} \qquad (2.10)$$

$$P_3 = \alpha_3 P_1 \qquad (2.11)$$

$$\gamma_w - \text{Specific weight of seawater}$$

$$P_4 = \begin{cases} P_1\left(1 - \frac{h_c}{n}\right) for \ \eta^* > h_c \\ 0 \qquad\qquad for \ \eta^* > h_c \end{cases} \qquad (2.12)$$

$$h_c = min \ (\eta^*, h_c) \qquad (2.13)$$

H_s is significant wave height, h_s is the height from toe crest to SWL, h_c height of the structure above the SWL.

Total horizontal force P is given by the following formula

$$P = \frac{(P_1 + P_3)h^1}{2} + \frac{(P_1 + P_4)h^*}{2}$$ (2.14)

2.1.5 Stability and Failures of Vertical Breakwater

Breakwater stability and performance depend upon the following hydraulic parameters.

- Wave height
- Wave period
- Wave direction relative to the breakwater
- Duration of wave attack
- Design water level
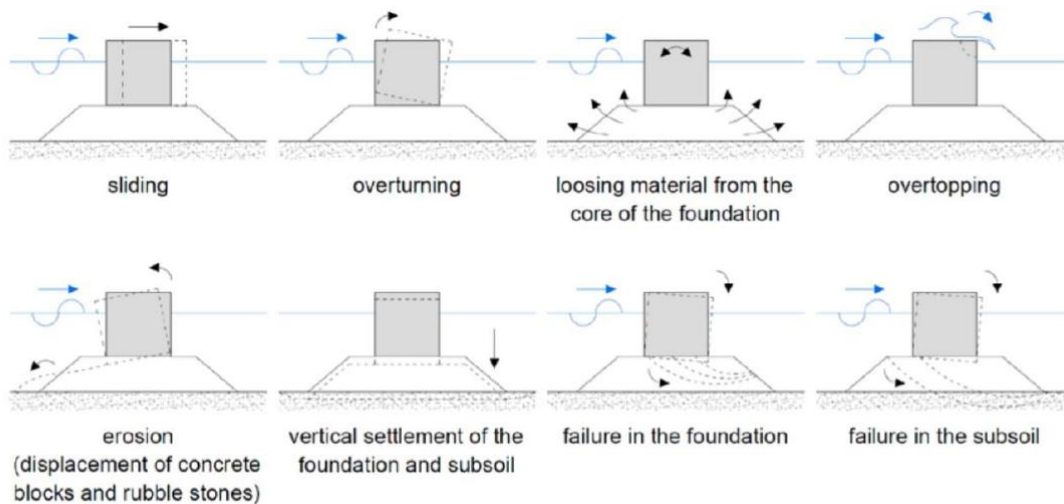
Figure 2.6: Failure modes of vertical wall breakwaters (Ruol et al., 2000)

In Figure 2.6, illustrates the different failure modes of vertical caisson breakwater. The failures experienced by vertical and composite breakwaters (Oumeraci, 1994) can be briefly classified into:

- Reasons inherent to structure itself
- Reasons inherent to hydrostatic and load conditions
- Reasons inherent to foundation and seabed morphology.

Reasons inherent to structure itself, among the various reasons for failures which are inherent to the concrete structure and its rubble mound foundations, one may distinguish the inadequacy of the concept of reflective structures (vertical structures have to reflect all the incoming wave energy), the crest level of the rubble mound foundation which is generally too high, and the crest level of the concrete structure which is too low. In addition, there are further reasons related to the non-monolithic structure and the weakness of the concrete material.

Reasons inherent to hydrostatic and load conditions, the reasons due to hydraulic influencing factors and loads, there is the exceedance of design wave conditions, the focusing of wave action at certain zones along the breakwater, wave breaking, subsequent impact loads and wave overtopping.

Reasons inherent to foundation and seabed morphology, are among the factors which have contributed to the failures reported

- Unfavourable configuration of the contour lines of the seabed in front and offshore of the Breakwater.

- Seabed scour and erosion of the rubble mound foundation,

- Settlement of the structure and shear failure of the foundation (failure of geotechnical nature).
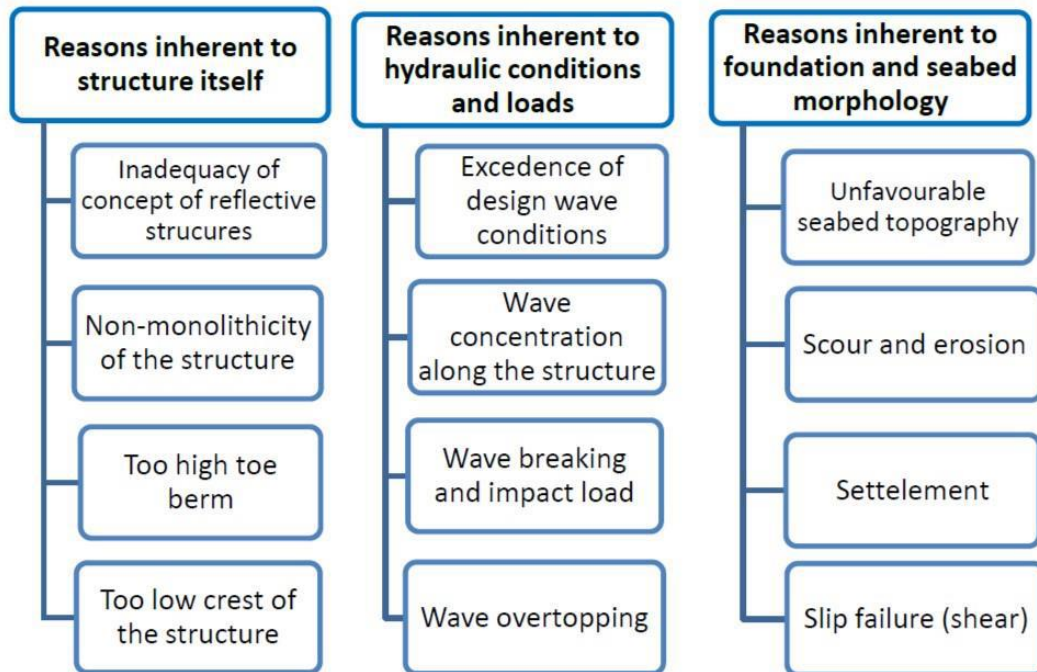
Figure 2.7: Failures of vertical wall breakwater (Oumeraci 1994)

Figure. 2.7 shows the failure modes of caisson breakwater and the stability of the upright section of vertical wall breakwaters has to be performed against

- Sliding
- Overturning
- Maximum soil stresses
- Slip circle failure

Apart from the above aspects, the vertical wall breakwaters are checked for shear and liquefaction. Stability calculation of breakwaters, the external forces such as the wave forces, hydrostatic pressure, buoyancy, and deadweight shall be considered.

The various external forces are:

1. **Wave forces:** For the stability determination for a breakwater, the loads on all four sides and shock pressures have to be taken into consideration.

2. **Hydrostatic pressure:** When there is a water level difference between harbour and seaward sides of a breakwater, hydrostatic pressures corresponding to the water level difference shall be considered.

3. **Buoyancy:** In the structural section of the breakwater below the still water level, buoyancy shall be considered.

4. **Deadweight:** The deadweight of breakwater may be calculated by using unit weights of respective materials in the assumed section.
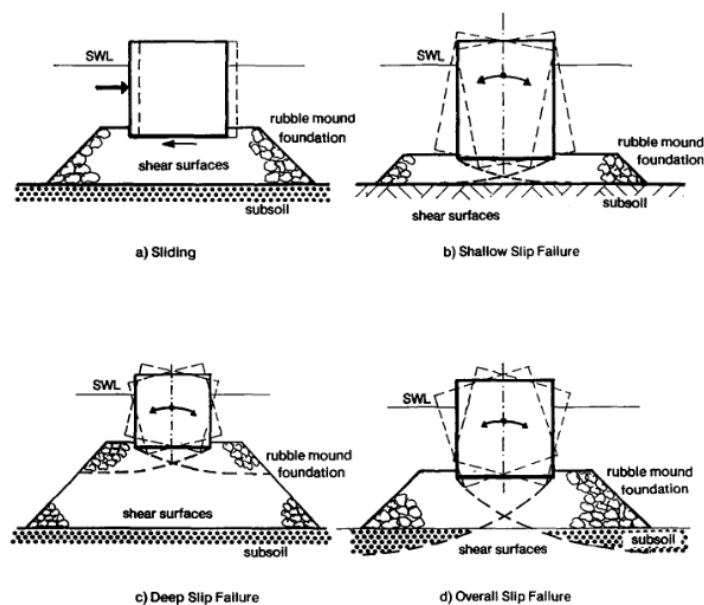
Figure 2.8: Sliding and Slip Failure Modes (Oumeraci, 1994)

Because of the complexity of the phenomena leading to failures of geotechnical nature as shown in Figure 2.8, it is obvious that conventional bearing capacity calculations are of limited use to explain the failure mechanisms observed. Indeed, more reliable models are needed to simulate the dynamic behaviour of the structure-foundation-water system for complex loads, boundary conditions and soil characteristics.

2.1.6 Stability Against Sliding

Horizontal forces caused by wave action act upon the vertical wall, which tends to slide the caisson on the rubble base. Thus, the reaction develops at the contact surface of rubble and the base of the wall due to friction. This force, due to friction, must be sufficient to keep down the vertical wall in its position. The frictional force at the

contact surface is the total vertical load multiplied by the coefficient of friction at the contact plane as shown in Figure 2.9.
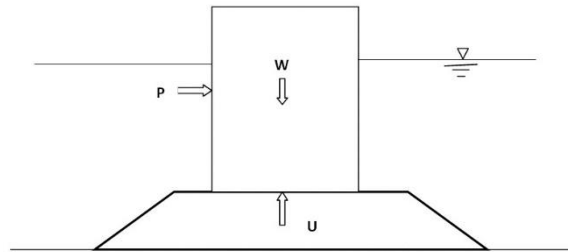
Figure 2.9: Sliding of Caisson breakwater

So, the stability against sliding is checked using the expression

$$\mu(W - U) \geq P_{max} \tag{2.15}$$

Where

μ = coefficient of static friction,

W = Total vertical force of the submerged structure,

U = Uplift force,

P_{max} = the maximum resultant horizontal force exerted on the wall of the structure.

The factor of safety against sliding =

$$Factor\ of\ safety\ against\ sliding = \frac{\mu(W - U)}{P_{max}} \tag{2.16}$$

Here μ, the coefficient of friction between the upright section and the rubble mound is usually taken as 0.6 [Japanese standards for ports and harbour facilities, (1980)]. The factor of safety obtained should not be less than 1.2 in the case of Goda's (1985) approach, and should not be less than 1.5, as per IS 9527(Part I)-1981.

26

2.1.7 Stability Against Overturning

The moment due to horizontal force about the heel of the vertical wall gives an overturning moment. This moment is resisted by a moment of the weight about the same point. If the overturning moment exceeds the resisting moment, it results in the overturning of the breakwater shown in Figure 2.10.
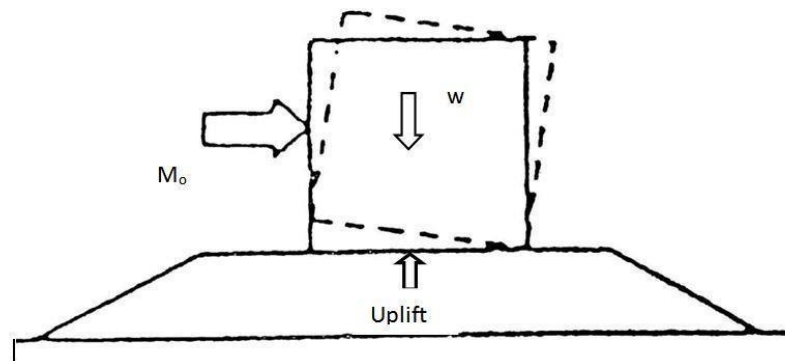
Figure 2.10: Overturning of Caisson breakwater

For checking the stability against overturning, the resisting moments ($\sum M_R$) and the overturning moments ($\sum M_0$) are calculated. The resisting moment should be higher than the overturning moment for the structure to be safe against overturning.

The factor of safety against overturning is calculated as

$$Factor\ of\ safety\ against\ \text{overturning} = \frac{\sum M_R}{\sum M_o} \qquad \qquad (2.17)$$

The factor of safety against overturning should not be less than 1.2 in the case of the Goda (1985) approach, Takahashi (1996) and should not be less than 2 as per IS 9527 (Part I)-1981.

2.2 TOE PROTECTION

Vertical breakwater mainly relies on the bottom foundation material for vertical support. The horizontal wave action resulting in loss of bottom materials, can lead to scoring ultimately leading to structural failure as in Figure 2.11. In breakwater

27

construction in Japan, it is customary to provide the toe protection stones at the front and rear of the upright sections
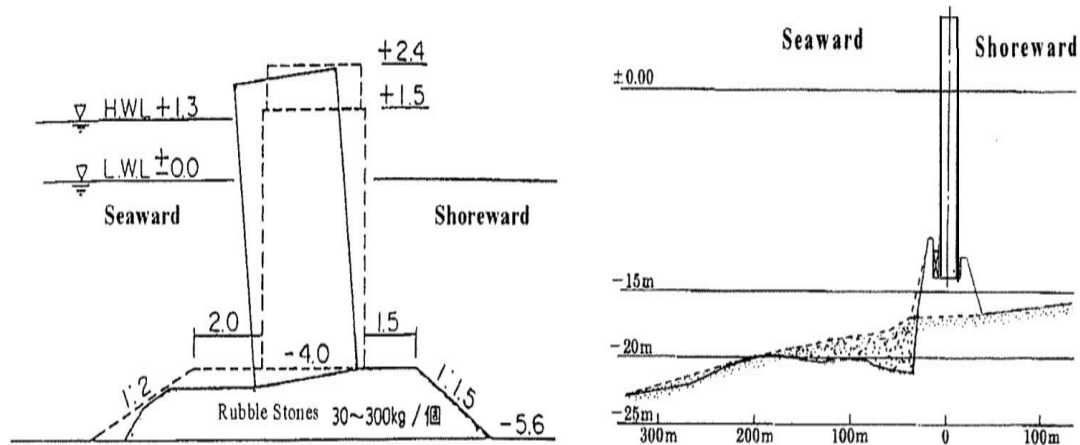
Figure 2.11: Failure due to scouring of bottom material (Takahashi et al., 2002)

When reviewing the history of various vertical wall breakwaters that failed earlier, it is concluded that the toe protection at the base of the structure plays a vital role in their failure mechanism. The present knowledge about toe protection and the material to be used for the protection is limited. The design of the toe protection and the determination of armour unit weight has to rely on the available empirical formula.

Toe stability is often addressed using modified forms of Hudson's equation.

$$W = \frac{\gamma_r\, H^3}{K_D \Delta^3 cot\theta} \tag{2.18}$$

Where,

W – is the weight of the armour (N)

γ_r – is the specific weight of the armour units (N/m^3)

H –is the design wave height at the toe of the structure(m)

K_D – is the dimensionless stability coefficient

Δ - is the dimensionless relative buoyant density of rock, i.e. ($\rho_r = \rho_w - 1$)

28

ρ_r *and* ρ_w are the densities of rock and seawater

θ – is the angle of revetment with the horizontal

Brebner and Donnelly (1962) performed a series of experiments to determine the stability characteristics of pell-mell placed rubble of uniform shape and size used as a foundation or as toe protection for the vertical superstructure of composite breakwaters. The toe cross-section and the armour units are affected by various parameters such as the shape of rubble units, inertia and drag coefficients, wave steepness, specific gravity and relative depth (d/L). An experimental investigation was carried out for the stability of toe protection and rubble, based on varying relative depth d_1/d (i.e. $d_1/d = 0\%$, 25%, 50% and 75%) as shown in Figure 2.12.

Where d_1 is the depth from SWL to the top of the toe and d is the depth of water.
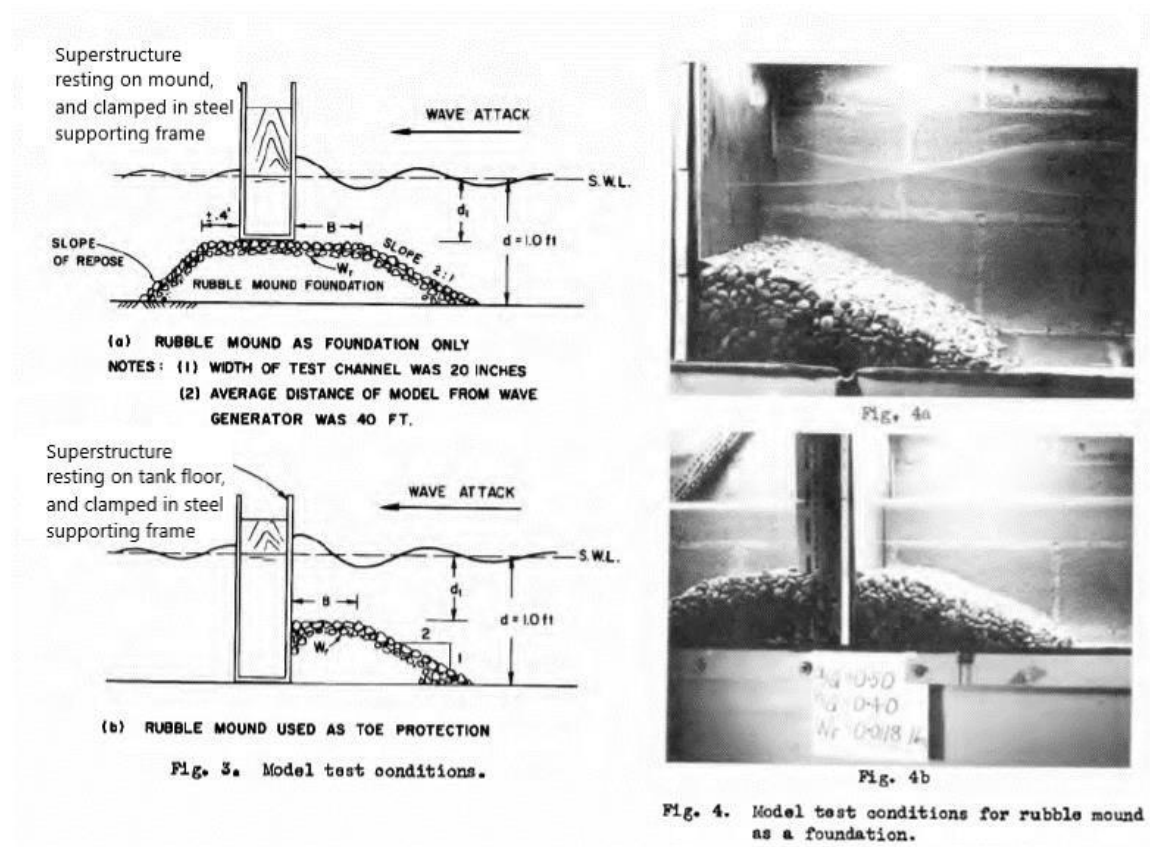
Figure 2.12: Model Test conditions adopted by Brebner and Donnelly (1962)

They obtained a relationship between the relative depth of toe d_1/d and the stability number (H/ΔD_{n50}), where, Δ is the relative mass density of armour units and D_{n50} is the

29

nominal diameter of the armour unit. They observed larger values of $H/\Delta D_{n50}$ for large values of d_1/d_s, where d_1 is the depth of toe protection below the still water level, and d_s is the water depth at the structure site.

Tanimoto et al. (1982) investigated the effects of wave action on a composite breakwater, atop a rubble foundation, by using irregular waves. The tests proved that irregular waves are more destructive than regular waves. The investigation was conducted to determine the stability of armour units under wave attack. The equation (2.18) is written in the form of the stability equation which was derived by Hudson (1959) for the armour units of rubble mound breakwaters and N_s is called the stability number.

The equation guiding their experimental work was given as:

$$W = \frac{\rho_r \ H_{\frac{1}{3}}^{3}}{N_s^{\ 3} \ (S_r - 1)^3} \qquad (2.19)$$

Where,

W = weight of the armour (N)

S_r = specific weight of the armour units (N/m^3)

$H_{1/3}$ = design wave height at the toe of the structure (m)

$\rho_r \ and \ \rho_w$ are the densities of rock and seawater.

Baart (2008) investigated toe bunds for rubble mound breakwaters and more specifically the stability of rocks in toe bunds under wave attack and the maximum velocities of the incoming waves to relate the wave load to damage. Baart used data from Gerding (1993) for toes in the deep water for his analysis. As this study is about toe stability in shallow water, surging waves do not describe the wave behaviour at the breakwater. The insight into the behaviour of the design equation for determining the required toe rock size by Gerding (1993) and Van der Meer (1998). The stability equation is damage level, expressed in N_{od}.

$$\mathbf{N_{od}} = \boldsymbol{B} \ (\boldsymbol{H_s}/\Delta \boldsymbol{D_{n50}})^4 \tag{2.20}$$

$$\mathrm{N_{od}} = B \ \alpha^2{}_{shore} \tag{2.21}$$

$$\mathbf{N_{od}} = \boldsymbol{B}(\frac{\boldsymbol{tan_{\alpha shore}}}{\sqrt{\boldsymbol{S_{op}}}}) \tag{2.22}$$

Where,

N_{od} = damage number

B = width of wave flume

s_{op} = fictitious wave steepness (0.008 to 0.04)

tan (α_{shore}) = Fore shore angle (1:50 to 1:10)

A damage level can be chosen to calculate the stone size for the tolerated damage level. Baart (2008) concluded that, if a design value N_{od} = 0.5 is used in Van Der Meer equation, it is considered that a flume test will result in higher damage than expected N_{od} = 0.5. The Van der Meer model predicts lower damage than occurred for 65% of Gerding's tests.

Gert Victor Muller (2016) investigated the stability of the armour layer toe rock in transitional water depths and analyzed past literature to formulate a new possible equation and predict the minimum stability numbers needed for certain site-specific parameters. It was noted that the present formulas available in practice lack information regarding small relative foundation depths (d_1/d) ranging from [0.35 – 0.55] (Brebner & Donnelly (1962). The results determined from the literature were considered for the estimation of a new formula for the relative foundation depth (d_1/d) ranging from [0.35 – 0.55]. Apart from the stability analysis, the overtopping for the different wave conditions of the structure is measured during the physical model tests and evaluated by the present empirical design formulas.

2.3 PERFORATED AND SLOTTED BREAKWATER

The research on the slotted vertical barrier and perforated structures is one of the areas of importance in the ocean engineering field. The study mainly involves wave transmission, reflection, dissipation, wave forces, dynamic pressures on the slotted wall, and runup of waves on the perforated walls. Knowledge of these topics is needed for the optimal design of this type of breakwater. As the water depth increases, a breakwater that extends through the full water depth may be uneconomic, and partial protection breakwaters may be required. There are many types of the partial protection breakwaters such as pneumatic and hydraulic breakwaters, submerged breakwaters, floating breakwaters, flexible floating breakwaters, detached breakwaters, perforated breakwaters, piles breakwaters, pipe breakwaters and slotted breakwaters.

Jarlan (1961) was the first to introduce the perforated-wall caisson concept consisting of a perforated wall, a solid rear wall and a wave energy absorbing chamber in between known as Jarlan-type breakwater. The parameters such as wave reflection, the wave forces and the wave run-up are reduced on the rearward side of breakwater due to the introduction of perforated wall (Suh et al., 2006; Li, 2007). The relative wave chamber width, B/L affects the hydrodynamic performance of breakwater. It is named a Jarlan-type breakwater, shown in Figure 2.13.
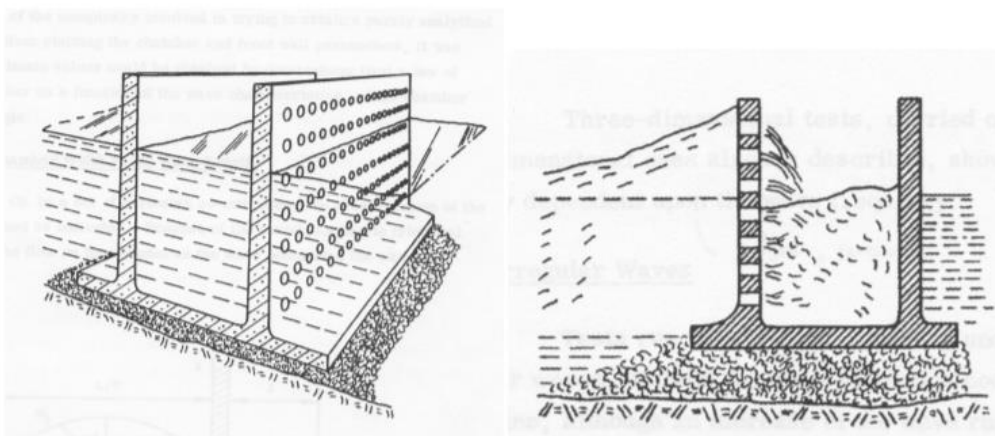
Figure 2.13: Typical Jarlan-type breakwater

Slotted barriers help in reducing the wave force, dynamic pressure, wave runup, reflection coefficient, and other hydrodynamic parameters on the caisson breakwater. To minimize the disturbances in the coastal environment such kinds of barriers are highly beneficial in reducing the cost, especially for increased water depths.

Many researchers tried out several modifications for the Jarlan-type breakwater. One such model proposed is a combination of a permeable barrier and an impermeable back wall and filling rock in the core. Weigel (1960) first gave a scientific account of the slotted breakwaters, also known as slotted wave screens. Also, slotted walls coupled with an impermeable vertical sea wall can be used as coastal protection structures against erosion due to wave action.

Neelamani et al. (2017) studied the wave reflection characteristics of slotted vertical barriers with a solid impermeable back wall. In the irregular wave fields, 37 various wave barrier configurations (1 vertical wall, 6 distinct sloping breakwaters, and 30 slotted vertical barriers with porosity ranging from 10 to 50% and 1-6 slotted barriers) are invetigated. The findings of this study reveal that by increasing the number of porous walls from one to six, the reflection coefficient may be reduced from 0.9 to 0.3, especially for d/Lp values larger than 0.2. Furthermore, the results suggest that increasing the number of porous walls did not significantly reduce wave reflection for d/Lp less than 0.2.

Fugazza and Natale (1992) studied the wave attenuation produced by a permeable structure and proposed a formula to optimize the hydraulic design of breakwaters of the Jarlan-type. For a perforated-wall caisson lying on a flat sea bottom, they showed that the reflection of waves normally incident to the caisson is at its minimum when the wave chamber width is about one-quarter of the wavelength. In contrast to the conclusion made by Kondo (1979), Fugazza and Natale showed that the perforated-wall breakwater with a single wave chamber could give the most significant reduction of wave reflection in the range of practical applications.

Losada et al. (1993) investigated an analytical model to study the energy dissipation on multilayered porous media under obliquely impinging waves. The variation of the reflection coefficient with kA (where k is the wavenumber and A is the width of a unit

cell consisting of two layers) was discussed. By increasing the number of absorber units the reflection could be reduced and an increase in the angle of wave incidence decreases the dependence of the reflection coefficient on kA, and for large angles of incidence, the reflection is almost constant and negligible.

Zhu and Chwang (2001) established an analytical model to study the interaction between ocean waves and a slotted seawall. The model has been verified with experimental data and they concluded that reflection characteristics mainly depend on the porosity of the test model and incident wave height. They found that the reflection coefficient reaches its minimum value when the chamber width is about a quarter of the incident wavelength.

Isaacson et al. (1998) investigated the mechanism of wave interactions numerically with a thin vertical partially submerged slotted barrier extending from the water surface the typical artist view is illustrated in Figure 2.14. The numerical model is compared with experimental measurements of the reflection, transmission, and energy dissipation coefficients for a partially submerged slotted barrier. The numerical results compared well with the theoretical predictions for the limiting cases of an impermeable barrier and a permeable barrier extending down to the seabed, and close agreement was found in all cases. Also, the effects of porosity of the slotted barrier, relative wavelength, and wave steepness are discussed in this paper. It is found that the method used here slightly overpredicts the wave transmission at high wave steepness.
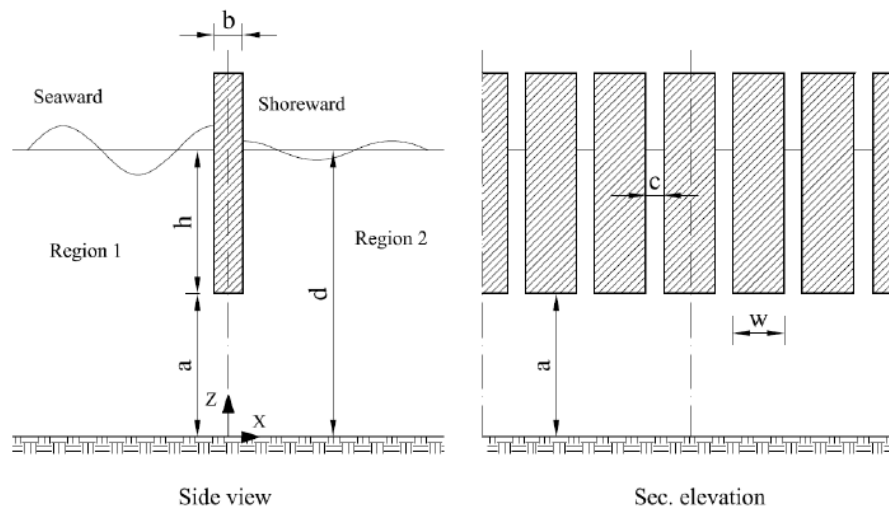
Figure 2.14: Vertical slotted barrier (Isaacson (1998))

The numerical solution explained that the reflection, transmission and head loss coefficients depend on the permeability parameter G is generally complex and depend on the friction coefficient f and inertia coefficient s where the inertia coefficient depends on the added mass coefficient cm.

Suh et al. (2006) investigated the performance of a pile-supported vertical wall breakwater, the upper part of which consisted of an impermeable vertical wall and the lower part consisted of an array of vertical piles as shown in Figure 2.15. An Eigenfunction expansion method is used for the analysis and estimated reflection, transmission, run-up and wave forces acting on the breakwater. The method adopted is similar to Isaacson et al. (1998) except for the formulation of permeability parameter G, for which the method of Mei et al. (1974) was adopted.
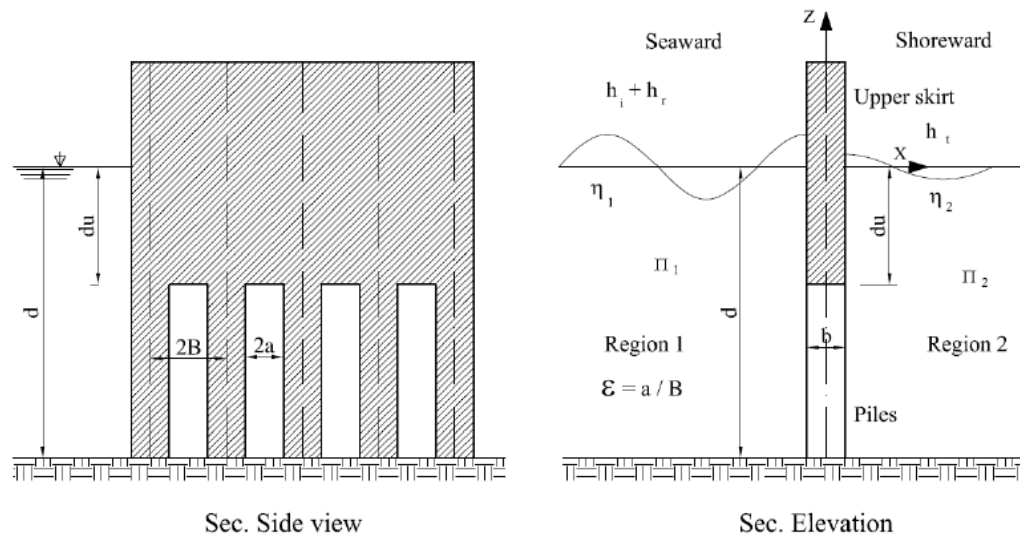
Figure 2.15: Pile supported vertical breakwater (Suh, 2006))

The pile-supported vertical wall breakwater always gave smaller transmission and larger reflection than a curtain wall breakwater with the same draft as that of the upper wall, or a pile breakwater with the same porosity as that of the lower part, of the pile-supported vertical wall breakwater.

Bergmann and Oumeraci (1999) investigated a single and multiple chamber system with porosity varying between 11 % and 40.5 % and proposed analytical expressions for transmission CT and reflection CR coefficients. The multi-chamber system with progressively decreasing porosity of the screens was reported to be efficient in wave damping. Multi-chamber systems were found to be effective over a wider range of B/L beyond 0.3.

Reddy et al. (2013) conducted a series of physical model tests to examine the wave pressure reduction at the different heights of the breakwater corresponding to the local water depth. From the physical model test, the author arrived at the modification factor associated with Goda's formula to estimate the shoreward pressure on the seawall in the presence of the offshore breakwater. An increase in height of protecting offshore structure reduces the wave pressure on seawall/caisson and the sliding stability increases as illustrated in Figure 2.16.
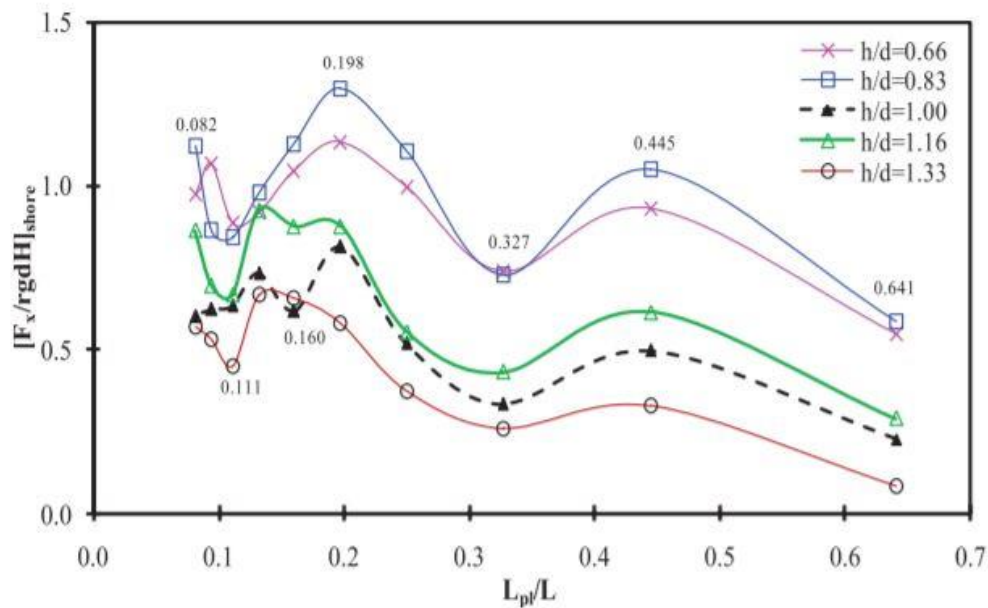
Figure 2.16: Dimensionless shoreward force for different h/d ratio

(Sreenivasa Reddy et.al., 2013)

Li et al. (2003) investigated a completely perforated wall breakwater with two perforated front walls. The inclusion of the middle-slotted barrier had minimal effect, particularly on large waves. For a perforated single chamber breakwater with a small geometrical porosity of a perforated plate (i.e 15 %, 25 % and 35 %), the addition of a middle-perforated plate does not significantly change the reflection coefficient for B/L < 0.1, but it can significantly reduce the reflection of short waves (B/L>0.4) and increase the reflection of intermediate waves (0.1<B/L<0.4). The effect of porosity, relative width, and relative water depth is discussed and compared to experimental data. When both the geometrical porosity of the first wall and the B/L ratio are high, however, a middle-slotted barrier can greatly lower the reflection coefficients; similar expected effects have been observed in previous experimental testing for breakwaters with two completely slotted barriers. (Sawaragi and Iwata,1978; Kondo, 1979).

Chiu et al. (2007) conducted a series of hydraulic model tests with regular/irregular waves to investigate the wave forces acting on a vertical breakwater, and wave pressures on the vertical wall and at the bottom of the caisson. They compared the maximum horizontal force and uplift force with Goda's wave force theories. They obtained that Goda's theory gives a higher safety factor. However, the measured uplift

force was smaller than Goda's and non-zero at the land-side end of the bottom which might be caused by the path of water flow in the porous media beneath the caisson. Their results show that the different irregular wave trains with the same spectrum are different and thus the effectiveness of conventional irregular wave tests with several repeats of the same wave train should have to be reconfirmed.

Alkhalidi et al. (2015) investigated the variation of wave pressures and forces on slotted vertical wave barriers. The porosity of a slotted wall is the ratio between the opening areas of the slotted wall to the total vertical area of the wall from still water level to the flume bed as shown in Figure 2.17. They inferred that increasing porosity reduces the dynamic pressures. This is because when porosity increases, wave energy propagates more freely through the porous wall, generating smaller wave runup on the wall and thus smaller dynamic pressures. Also, increasing porosity from (0% to 30%) affects dynamic pressures on porous wall panels significantly near the still water surface, but not so near the seabed.
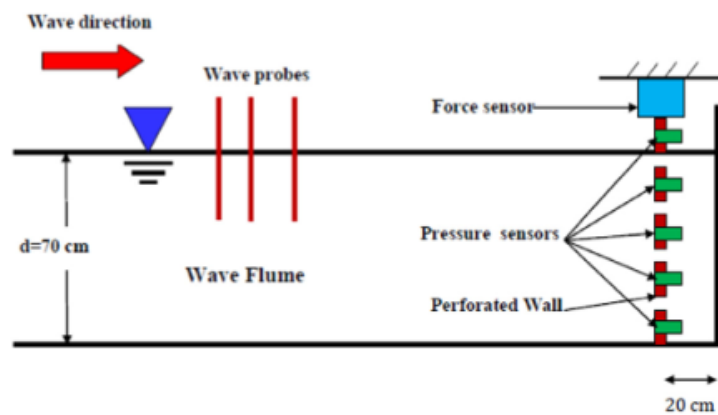
Figure 2.17: Typical experimental arrangement for measuring dynamic pressure and wave forces (Alkhalidi et.al., 2015)

The study concludes that horizontal shoreward forces decrease significantly as porosity increases, especially for smaller values of d/L since the total area exposed to wave action decreases due to the increased porosity. Seaward forces decrease marginally with increases in porosity, especially as d/L decreases.

Ibrahim et al. (2019) studied two different types of breakwaters. The first type consists of two vertical perforated walls. The first wall is 50% permeable in the lower, and the upper part is impermeable.
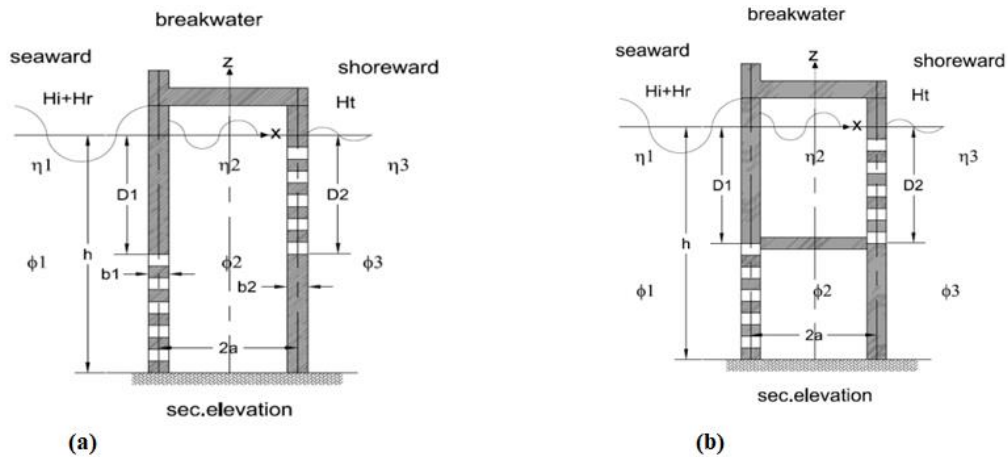
Figure 2.18: Definition sketch for a vertical perforated wall breakwater with
(a) horizontal slot   (b) without horizontal slot

And the second wall is 50% permeable in the upper and lower parts is impervious, and has a horizontal slotted wall between them. The second type is the same construction as the first type but without the horizontal slotted wall as illustrated in Figure 2.18. The study shows that the hydrodynamic performance of the first type is better than that of the second type by 10-15% in performance because of the presence of the horizontal slotted wall.

2.4 NUMERICAL APPROACH

The structural interaction of ocean waves is a common phenomenon of free-surface fluid flow hydrodynamics in coastal engineering. Understanding the basic physical properties and analytical computations of the same are imperative to assess the various loads on coastal structures and their responses. Experimental studies on ocean wave structure interaction require well-sophisticated laboratory facilities and wave response measuring systems. The experimental studies on ocean wave structure interaction are time-consuming and expensive. The rapid development in modern computational methods resulted in CFD-based simulation of ocean wave structure interaction which

is becoming more popular. Many researchers are working on CFD-based simulations to study ocean wave hydrodynamics, sediment transport, ocean wave energy, etc. due to less time consumption, economic, and reliability of results when compared to the experimental methods.

In the recent past, many researchers (Xie et al., 1981; Xueping Gao and Kunimitsu Inouchi., 1997; Kasem and Sasaki., 2010) have developed CFD models to simulate ocean waves which are nonlinear and unsteady in their behaviour. Xueping Gao and Kunimitsu Inouchi (1997) studied the clapotis interaction for broken waves along with vertical breakwater and classified their wave motions as a standing wave, breaking clapotis, and broken clapotis. The authors concluded that broken clapotis is a more serious wave motion than the other two wave motions. Xie et al. (1981) worked on experimental studies on the interaction of the clapotis wave with a vertical breakwater and simultaneously measured the maximum horizontal orbital velocity distributions for non-breaking wave conditions.

Kamath (2012) investigated mesh grid size analysis with several grid cell densities starting from 10 grid cells per wavelength. A large reduction in wave amplitude as the wave propagates through the wave tank is observed for small grid cell densities. This happens due to numerical diffusion which occurs due to the low grid density and results in the damping of the amplitude. It is seen that the numerical solutions start to match the theoretical values at a grid density of 100 grid cells per wavelength and that the numerical diffusion of the wave amplitude ceases considerably at a grid density of 200 cells per wavelength. Thus, a minimum grid density of 200 cells per wavelength can be adopted.

Similarly, **Afshar (2010)** conducted a study in which, space discretization was carried out by a finite volume approach and the free surface was determined by the VoF method. The study concluded that a minimum of 200 to 400 grids per wavelength were required to obtain acceptable results. **Fabio et al. (2018)**, used ANSYS CFX, to study the generation and propagation of regular waves. Waves were generated in two different ways and it was concluded that a piston wavemaker provided more precise results. Additionally, different ways of preventing reflection in the NWF were analysed. The

optimized solution when compared to Stokes's second-order theory, showed good agreement.

Tae et al. (2012) analyzed the wave reflection of vertical and slit caissons with porous structures using the numerical model based on the Navier-Stokes equations. In the case of regular waves, the reflection coefficient was significantly reduced, whereas the reflection coefficient for irregular waves was reduced by a relatively small amount by using porous structures. As the wave height was increased, the reflection coefficient was found to be decreasing for both vertical and slit caissons. The waves were observed to be more dissipated at the slit caisson than at the vertical caisson. The reflection coefficient was rarely affected by the variation of the significant wave period.

(a) Combination of the vertical caisson and the porous structure

(b) Combination of the slit caisson and the porous structure
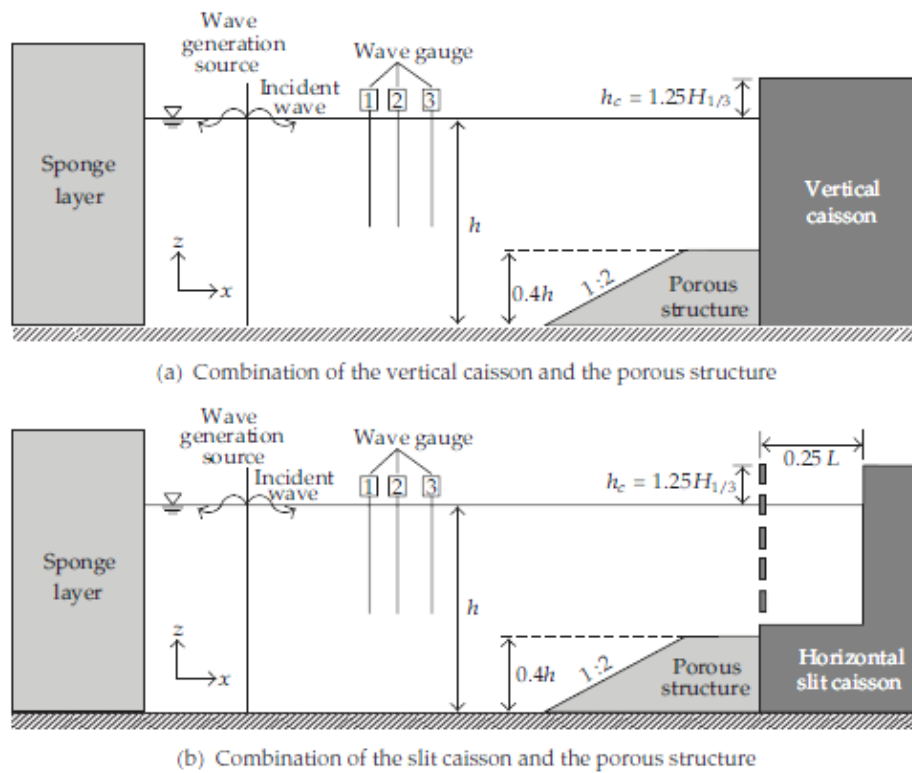
Figure 2.19: Schematic diagram of Numerical wave flume (Tae et al., 2012)

The rectangular and trapezoidal porous structures showed obvious energy dissipation, whereas the triangular porous structure showed a little reduction effect on the slit caisson and almost no reduction on the vertical caisson. Because a porous structure with a low height is not able to dissipate wave energy effectively, a proper height is required for efficiency. Although rectangular and trapezoidal porous structures showed almost

the same energy dissipation, the trapezoidal structure is preferred because it has superiority in workability and stability. Ref. Figure 2.19.

Poguluri et al. (2020) investigated the wave interaction on the vertical slotted barrier based on an analytical and numerical approach in regular waves. The 3-Dimensional the implicit unsteady turbulent model illustrated in Figure 2.20 is based on incompressible Reynolds-averaged Navier–Stokes (RANS) equations that were adopted to assess the analytical MEEM solutions. The horizontal harmonic forces on the vertical slotted barrier are estimated by harmonic decomposition analysis of the time-series forces on the slotted barrier, and the comparison was good with the analytical solution for the first harmonic. The magnitudes of the second and third harmonics are 2%–10% of the first harmonic force.
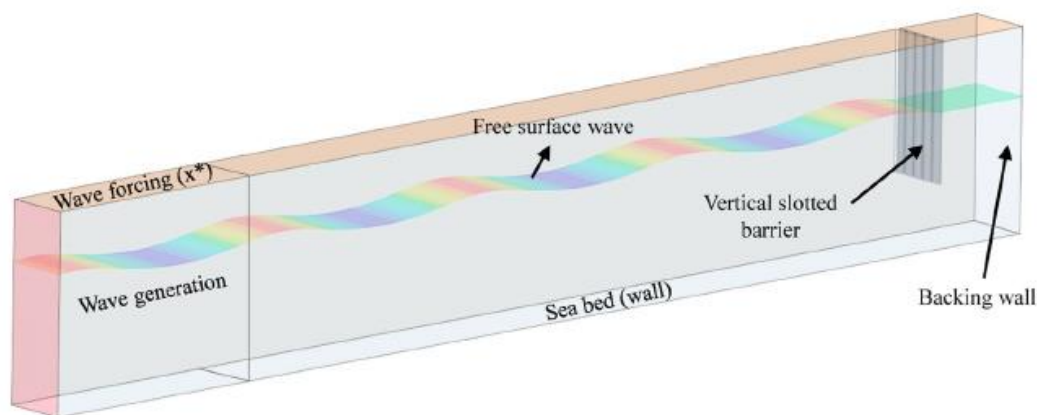
Figure 2.20: Schematic diagram of numerical wave flume
(Poguluri et al., 2020)

Finnegan and Goggins (2012) studied the linear deep-water waves using the ANSYS CFX tool. Several tests are performed to see the influence of various parameters on the waves generated which include the computational grid size, the domain length and height, time step interval, and beach slopes. The results showed good agreement in comparison with the linear wave theory. The subject of implementing a beach slope at the end of the numerical wave tank has different studies conducted by several authors in the past decade. Maguire (2011) studied various beach slopes and recommends a slope value greater than 1:10. Fabio et al. (2018) and Finnegan and Goggins (2012)

investigated slopes 1:3 to 1:6, and both works concluded that 1:5 is the ideal slope condition, contradicting the conclusions attained by Lal and Elangovan (2008) and Elangovan (2011), where in both cases, a beach slope of 1:3 gives a better reduction in wave reflection.

2.5 SUMMARY

The need for developing an innovative coastal structure for protecting the coastal areas has led to the development of various types of breakwater. With the advancement in technology different types of breakwaters are developed in different parts of the world. Breakwaters are usually designed and constructed to satisfy several criteria such as functional performance, environmental impact, cost of construction and maintenance which adds challenge to the designer's task. Hence, to economize the utilization of construction materials and to provide an eco-friendly solution to coastal engineering problems alternative types of breakwaters are evolved. The high construction cost of most coastal structures requires that risk analysis and life-cycle costing be an integral part of each design effort (SPM, Volume II, 1984). The performance of any type of breakwater depends on the primary objective to be satisfied which in turn depends on the environmental conditions and the purpose of it is construction. The analysis of breakwater after conducting a series of experiments is very significant to prevent the consequence of occasional damage, particularly in the case of extreme events.

The hydraulic performance evaluation together with the structural stability is very important while designing the structure. The extreme wave condition nearby the breakwater structure and the resulting phenomena are to be studied in detail before designing a breakwater structure. Therefore to evaluate the performance of breakwater, the hydrodynamic characteristics such as wave forces, wave reflection and wave runup are to be studied. Perforated breakwaters are preferred over solid-type breakwaters due to their advantage of dissipating wave energy in front of the breakwater.

Dissipation of energy reduces both wave forces on the caisson and wave reflection (CEM, Part VI, 2006). In this chapter, a comprehensive review of the literature on the hydraulic performance of caisson breakwater is discussed in detail. The research gap from the past studies is identified to improve and evaluate the performances of a

caisson-type breakwater by both physical model approaches. These breakwaters are subjected to several drawbacks, e.g. insufficient wave protection, and high reflection, due to the onslaught of extreme waves, which may have disastrous consequences or in some cases impossible to rebuild the structure.

The present study involves the analysis of the hydraulic performances of vertical caisson breakwater with the protection of the toe, perforated caisson breakwater, and slotted barriers in front of the caisson breakwater. However, in addition to that, the study focuses on the development of a numerical model using the computational fluid dynamics approach and validates the same using model test results. The outcome of the present work forms a good reference for the effective development of caisson breakwater.

2.6 NECESSITY AND RELEVANCE OF PRESENT STUDY

The literature review showcases, that the wave forces acting on a vertical caisson breakwater cause severe turbulence at the toe of the structure. The continuous action of breaking and non-breaking waves makes the toe of the structure vulnerable to the erosion of the seabed material and toe scour which finally leads to the collapse of the entire structure. So, provisions must be made to stabilize the toe of the structure against these forces and also to protect the main structure. Several Analytical, experimental, Numerical, and field studies are carried out by several investigators such as Van der meer (1988), Goda (1985), Mani (1993), Tanimoto and Takahashi (1994) Neelamani (2002), Deo (2015), Munni Reddy (2007), Zhu (2010), Binumol (2017), Sundar (2017), Vijay (2019) and Sunny Kumar (2020).

Even though several theoretical, experimental, and field studies were carried out, the literature study showed that no comprehensive work was undertaken on the effects of toe protected caisson breakwater with the combination of slotted barriers and perforations on its performance. As the design of such a structure is complex with many parameters in control of its performance, it is decided to take up the physical model study on the hydrodynamic performce of toe protected caisson type breakwater with perforations and slotted barriers in front of it.

2.7 OBJECTIVES OF PRESENT STUDY

The objectives of the proposed investigation are the followings:

1. To study the stability of toe protection for vertical caisson breakwater.

2. To investigate the hydraulic performance characteristics such as wave reflection, wave runup, and wave forces on vertical caisson breakwater and to develop a numerical model using the computational fluid dynamics approach and validate the same using experimental data.

3. To study the effects of slotted barriers in front of caisson breakwater and its performance characteristics experimentally and validate the numerical results with physical model tests.

4. To investigate the performance characteristics of caisson breakwater with perforations by varying the percentage of perforations.

DETAILS OF EXPERIMENTAL AND NUMERICAL INVESTIGATION

3.1 BACKGROUND

Breakwaters are necessary for building ports, and harbours, their structural stability and economy in construction are the need of the hour. The fast-growing advances in technology lead to different types of breakwaters and it is almost impossible to predict the actual performance of a structure at the site since the complications encountered on site cannot be modelled theoretically. Constructing these large structures, transportation, and placement of such structures in shallow or deep water is always a difficult task for engineers. Hence, to optimize design aspects, it becomes necessary to test the performance of a model of the prototype under laboratory simulated conditions. To arrive at a safe and stable design of breakwaters, model studies are extensively used which proves to be one of the best tools for the designer.

This chapter deals with the details of laboratory conditions, experimental setup, dimensional analysis, hydraulic modelling, methodology and test procedures adopted for the experimental and numerical investigations.

3.2 PHYSICAL MODELLING

Physical models have an important role in the development of complex hydrodynamic phenomena on coastal structures. Physical models are representing the physical system in the laboratory so that the major parameter acting in nature are represented in the model in the correct proportion. They can give a good simulation of reality as they include all the processes that take place in reality (Hughes, 1993). Physical models have scaled representations of reality in which a prototype system is duplicated as closely as possible on a smaller scale. Model studies have their own technical and practical limitations, but prove to be one of the best tools for the designer in arriving at a safe and stable design for breakwaters. The purpose of the model is to approximate

and anticipate the prototype behaviour through certain prescribed modelling laws. Many modelling approaches are followed in the study of natural systems. The physical model provides insight into a physical phenomenon that is not fully understood (Chakrabarthi, 1996).

Froude's model law is applied because the essential forces involved are inertia, pressure and gravity whereas viscous and surface tension forces are neglected. The scale effects and uncertainty are the two major issues that decide the reliability of the model studies. To reduce scale effects the model should be as large as possible (Hughes, 1993) so that the Reynolds number of the flow is high and the flow is turbulent (Ouellet, 1970). And to minimize uncertainty the experiment has to be properly planned, experimental procedures and extrapolation methods should be standardized and sources of errors have to be minimized (Mishra, 2001).

3.3 FROUDE SCALING LAW

The Froude criterion is a ratio of inertial forces to the gravitational forces, as follows.

$$\sqrt{\frac{Interia\ force}{Gravity\ Force}} = \sqrt{\frac{\rho L^2 V^2}{\rho L^3 g}} = \frac{V}{\sqrt{gL}} \qquad (3.1)$$

where 'V' and 'g' are the velocity of the flow and gravitational acceleration, respectively, and 'L' is the wavelength of the gravitational waves.

The Froude scaling law is applicable only when the predominant reaction force on the system is due to gravity, which controls the fluid flow in addition to the force of inertia. The application of the Froude scaling law in the physical model study requires that the Froude number in the prototype must be equal to the Froude number in the model.

$$\left(\frac{V}{\sqrt{gL}}\right)_p = \left(\frac{V}{\sqrt{gL}}\right)_m \qquad (3.2)$$

where the subscripts 'p' and 'm' denote the corresponding Froude number at prototype and model scale.

$$\lambda = \frac{L_p}{L_m} \qquad (3.3)$$

From the above equation, the parameter 'λ' is defined as the ratio of the prototype characteristic wavelength to the model wavelength. In this way, all the similitude parameters of the Froude scaling law can be defined. Based on Froude's scaling law, the main parameters used in the present research work.

3.3.1 Predominant Variables

The present model study involves a complex structure comprising of a toe protected caisson breakwater and slotted barrier. The waves break over the barrier, loosing a major portion of energy and then loose some more energy while propagating in the zone between the structures. This phenomenon is difficult to express mathematically and one has to depend upon experimental investigations. The results of such investigations are more useful when expressed in the form of dimensionless relations. To arrive at such dimensionless relationships between different variables, dimensional analysis is carried out. The predominant variables considered for dimensional analysis in the present investigation are listed in Table 3.1.

Table 3.1 Predominant parameters influencing the performances of
Vertical caisson Breakwater

Predominant Variable		Dimension
Wave Parameters	Incident Wave Height (H_i)	L
	Water Depth (d)	L
	Wave Period (T)	L
	Wavelength (L)	L
	Run-up (R_u)	L
	Particle Velocity (v)	LT^{-1}
Structural Parameter	Armour Unit Weight (W)	M
	Nominal Diameter (Dn_{50})	L
	Structural Height	L

	Relative mass density of Armour unit Weight (Δ)	$M^oL^oT^o$
Fluid Parameters	Mass Density (ρ)	ML^{-3}
	Dynamic Viscosity (υ)	$M L^{-1}T^{-1}$
External Effects	Acceleration due to Gravity (g)	LT^{-2}

3.3.2 Details of Dimensional Analysis

For deep water wave conditions L and T are related by

$$L = \frac{gT^2}{2\pi} \qquad (3.4)$$

The term gT^2 is used in the above equation to represent the wave length L, instead of taking L directly. This is because if L is used it would be depth specific while, gT^2 is independent of depth and represents the deep water wave characteristics which can easily be transformed to shallow waters depending upon local bathymetry.

Considering the damage level S of the toe of caisson breakwater which is dependent on several independent parameters, their relationship can be expressed as follows:

$$S = f \{H_i, T, d, L, D, d_1, \xi_{o,} \Delta, A_e, g, \rho, N_s, D_{n50}\} \qquad (3.5)$$

By the application of Buckingham's π theorem, an equation of the form shown below is obtained.

$$S = A_e/D^2_{n50} = f [H_i/gT^2, H/\Delta Ns, d/L,] \qquad (3.6)$$

Similarly, wave force (F) on caisson breakwater which is dependent on several independent parameters, their relationship can be expressed as follows:

$$F = f \{P, H_i, L, d, z, g, \rho,\} \qquad (3.7)$$

By the application of Buckingham's π theorem, an equation of the form shown below is obtained.

$$F = f\{P/\rho g d, \ z/d, \ H_i/d, \ H_i/L, \ d/L\} \qquad (3.8)$$

By the application of Buckingham's π theorem, an equation of the form shown below is obtained.

$$K_r = H_r/H_i = f \ \{H_i/d, \ H_i/L, \ d/L\} \qquad (3.9)$$

Where,

A_e/D^2_{n50}	:	Dimensionless damage (S)
H_r/H_i	:	Transmission coefficient (K_r)
H_i/gT^2	:	Deepwater wave steepness
$H/\Delta D_{n50}$	:	Hudson's stability number (N_S)
d/L	:	Relative water depth
H_i/d	:	Relative water depth
H_i/L	:	Relative Wave Steepness
z/d	:	Relative depth parameter
$P/\rho g d$	:	Relative wave pressure

3.4 WAVE CONDITIONS

The wave climates off the Mangalore coast as given by the Dattatri et al. (1994) are considered while planning the present investigations. During the monsoon, the maximum recorded wave height off the Mangalore coast is about 4.5 m to 5.4 m. During fair weather season wave height hardly exceeds 1 m. The predominant wave period

during monsoon is 8 sec to 11 sec. Occasionally, during the fair-weather season, wave periods up to 15 sec are observed. The tides at Mangalore are mixed type and predominance of semi-diurnal components. The tidal variation for mean sea level is approximately ± 1.68 m. Hence, for the present study wave height range of 1 m to 5.4 m and wave period range of 8 sec to 12 sec are considered.

3.5 MODEL SCALE SELECTION

In the present study, the selection of similitude is achieved by the method of dimensional analysis. The non-dimensional parameters of the complex wave interaction phenomenon decide the similitude achieved between the model and the prototype. By taking into account the wave climate off the Mangaluru coast, the similitude criteria in the present study are achieved by considering the non-dimensional parameter, wave steepness H_i/L as given in Table 3.2. Using the existing facilities of the two-dimensional wave flume in the Department of Water Resources and Ocean Engineering, National Institute of Technology Karnataka, regular waves of heights ranging from 0.03 m to 0.24 m and periods ranging from 1 sec to 3 sec can be produced.

Table 3.2 Wave parameters of Prototype and Model

Wave Parameter	H_i (m)	T (sec)	H_i/L
Protype	1 – 5.4	8 to 12	0.00070 to 0.0086
Model	0.030 to 0.24	1.0 to 3.0	0.00030 to 0.0244

To simulate the field conditions of wave height, period and diameter of perforation by application of Froude's law (Hughes, 1993) a geometrically similar model scale of 1:30 is selected for the present experimental investigations. The viscous effects are predominant if the Reynolds number in the model is too small. In the present investigation, the Reynolds number is always maintained above 3.5×10^4 and therefore, viscous effects are not significant (Owen and Briggs, 1986). The details for the selection of the model scale were presented in Table 3.3.

Table 3.3 Selection of model scale

Scale	H_i (m)		T (sec)		D (m)			
	1	5.4	8	12	0.25	0.5	0.75	1
1:10	0.1	0.54	2.53	3.8	0.25	0.05	0.075	0.10
1:20	0.05	0.27	1.79	2.68	0.0125	0.025	0.0375	0.05
*1:30	**0.033**	**0.18**	**1.46**	**2.19**	**0.0083**	**0.0166**	**0.025**	**0.033**
1:40	0.025	0.135	1.26	1.9	0.0063	0.0125	0.0188	0.025

* Scale selected for the present study

3.6 EXPERIMENTAL SETUP

3.6.1 Wave Flume

The wave flume of the Department of Water Resources and Ocean Engg. of N.I.T.K, Surathkal is 50 m long, 0.71 m wide, and 1.1 m deep. It has a 42 m long smooth concrete bed. About 15m of the wave flume is provided with glass panels on one side to facilitate observations and photography. The flume is widened to 1.5 m and deepened to 1.4 m and the generating chamber is 6.35 m long. A gradual transition is ensured between the average flume bed level and the level of the generating chamber by a ramp of a series of vertical asbestos sheets spaced at 0.1 m distance from each other and kept parallel to the length of the flume. The purpose of the filter is to dampen the disturbance caused by successive reflections and to smoothen the generated waves.

The wave generating chamber has a bottom-hinged flap controlled by an induction motor (11 kW at 1450 rpm), which in turn is regulated by an inverter drive (0-50 Hz) rotating at a speed range of 0-155 rpm. A flywheel and a bar chain link the motor with the flap. Regular waves of heights 0.08 m to 0.24 m and periods of 0.8 sec to 4.0 sec in a maximum water depth of 0.5 m can be generated with this facility. Figure. 3.1 gives an artist's view of the experimental setup.
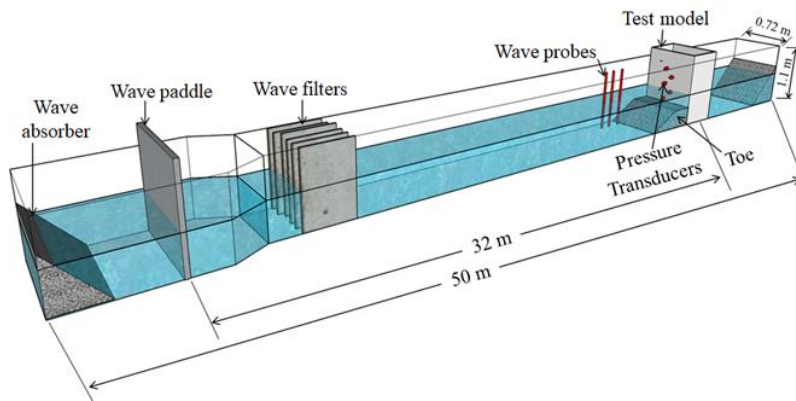
Figure 3.1: Schematic experimental setup

3.6.2 Data Acquisition System

Capacitance type wave probe along with amplification units is used for acquiring the data. The probe will be used for acquiring incident wave height, along with computer data acquisition system. The main parameter, wave surface elevation on seaward side of model is converted into electrical signal using relevant instruments. The digital voltage signals are converted into wave heights and wave periods using the laboratory wave recorder software provided by EMCON (Environmental Measurements and Controls), Kochi, India. The DAQ and the system is complete with its capacitance based high sensitive wave sensor, multichannel Data logger (LAOWR) and Windows based data acquisition software. The data acquisition speed is 30 Hz. The data protocol sensor input ranges from 0 to 5 volt, with power + 12 Volt DC.

3.6.3 Wave Probes

The Capacitance-type wave probes (Figure 3.2) are used to measure the free surface elevation and the incident reflected wave heights. The accuracy of measurements using wave probes is 0.001 m. Wave Probes are used to record the incident and transmitted wave characteristics. The recorded analogue data is converted into digital data and is stored in digital form by a software-controlled A/D converter. Per sec 20 samples of data are collected per second of time in our Data Acquisition System (DAS). The spacing of probes and decomposition of incident wave characteristics from superposed waves is accomplished using the three-probe method suggested by Isaacson (1991).

54

Figure 3.2: Capacitance-type wave meter

3.6.4 Runup Probe

Similar to the principle of the wave probe, the run-up probe is fabricated to measure the water-free surface oscillation on the front face of the caisson breakwater. The run-up probe consisted of stainless steel 1 mm in diameter and 0.7 m long. The wires dipped into the water and the current that flowed between them is proportional to the depth of immersion. The current is sensed by an electronic circuit, which provided an output voltage proportional to the instantaneous depth of immersion or the run-up of the water. A closer view of the run-up meter on the test model is shown in Figure 3.3
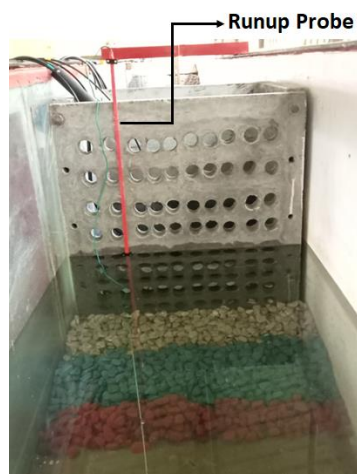
Figure. 3.3: A closer view of the run-up probe on the test model.

3.6.5 Pressure Transducers

The piezoresistive submersible 316 L type of pressure transducers (Make: KELLER W 26) are used for measuring water and air pressures. The change in strain due to the application of external pressure develops an output voltage and then it is converted into physical measurements through the multiplication of calibration constants. The pressure transducers with a sensing range of 0.5 bars are used for measuring water pressure on the front face of the caisson breakwater. A view of the pressure transducer is shown in Figure 3.4.

Figure. 3.4: A closer view of the Pressure Transducer.

3.7 CALIBRATION OF DATA ACQUISITION SENSORS / INSTRUMENTS

The sensors produce the output in voltage, which corresponds to the physical quantities that are under investigation. The calibration checks were performed for each test to reduce the calibration errors. The output of the sensor in terms of voltage for a known input physical quantity was recorded and the output was plotted against the known input. A slope of the best fit line for the plot was taken as the calibration constant.

3.7.1 Wave Probes

The calibration of the wave probe is done in the static condition to obtain the calibration constants. The wave probe is fitted to a channel and placed inside the wave flume with a certain depth of water. The wave probe is immersed into the flume, till half of the

wave probe length and this level is initially noted as zero reading by balancing the bridge circuit of the wave probe. Later, the probe is slowly immersed from 0.05 m to 0.2 m and the proportionate output voltages are registered. Likewise, the probe is moved above the still water level up to 0.2 m for the initial reading and the output voltage is noted. This depth of submergence of the wave probe for calibration was chosen such that the area covered is sufficient to capture the wave surface elevation profile. The voltage marked for known water level immersion is plotted and the slope of the best fit line gives the calibration constants. Typical calibration charts obtained for the different wave probes used in the present study are shown in Figure 3.5.
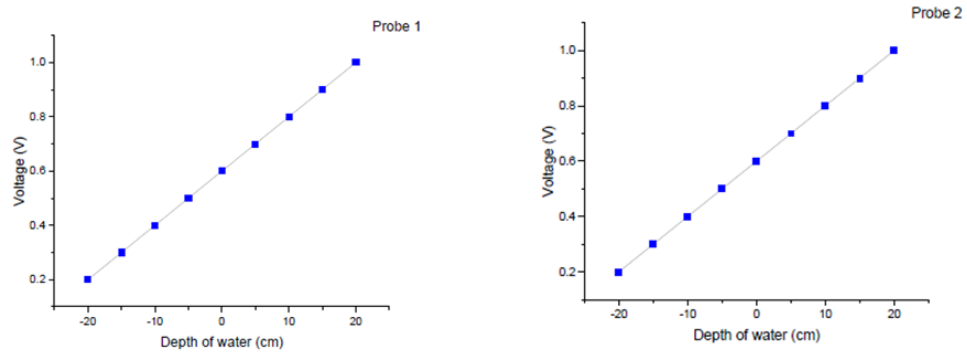
Figure. 3.5: Calibration plots for wave probes

3.7.2 Run-up Probes

A similar calibration procedure to that of wave probe is adopted for the static calibration of the run-up probe. The run-up probe is immersed inside the test facility and water is filled at certain depth to arrive the consistency of run-up probe as the initial stage. Then, the water level inside the test facility is raised in an internal of 10 cm. At each step, the corresponding variation in voltage is recorded. The voltage marked for known water level immersion is plotted and the best fit line gives the calibration chart. Typical calibration charts obtained for the run-up probe used in the present study are illustrated in Fig.3.6. Similarly, the calibration is repeated to check for the repeatability.
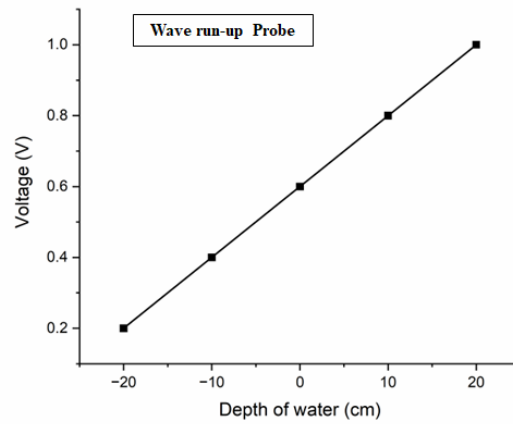
Figure. 3.6: Calibration plot for wave run-up probe

3.7.3 Wave Flume

The calibration of wave flume is to obtain a relationship between the frequency of the inverter and wave period and eccentricity and wave height for a particular water depth. Desired wave period can be generated by changing of frequency through the inverter drive. The wave period is inversely proportional to the frequency of the inverter with an increase in the frequency the value of the wave period will decrease. Similarly, the eccentricity motor is directly proportional to the wave height with an increase in the eccentricity the value of wave height will increases. The regular waves of height (H) ranging from 0.03 m to 0.18 m with varying periods (T) from 1.2 sec to 3.0 sec for different water depths are required for the experiment. Wave height for a particular wave period can be produced by changing the eccentricity of the bar chain on the flywheel. Combinations that produced secondary waves in the flume are not considered for the experiments. Figure 3.7 illustrates the calibration charts for wave heights at different wave periods and water depths of (a) 0.50 m, (b) 0.45 m and (c) 0.40 m.
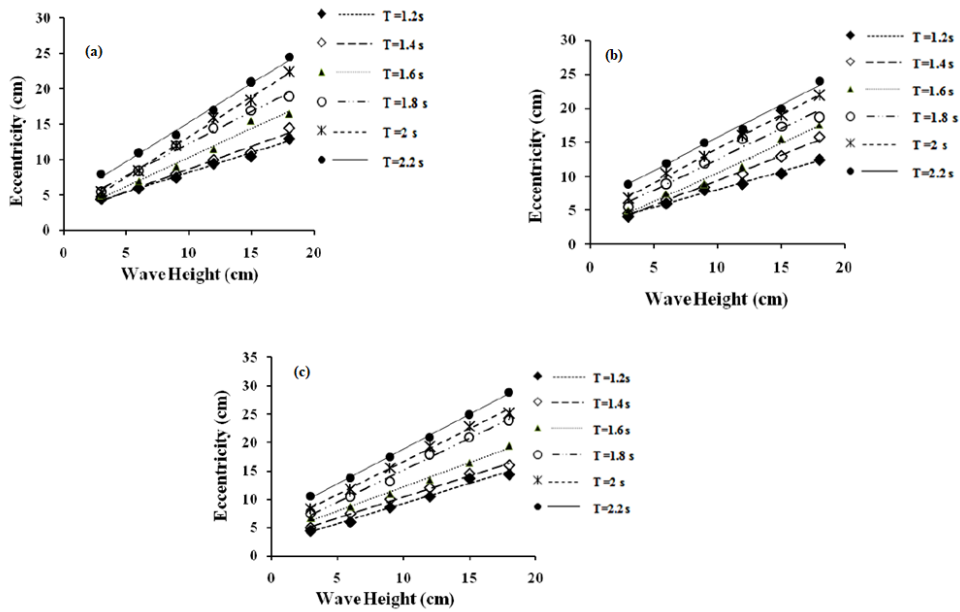
Figure. 3.7: Calibration plots for wave flume for (a) d = 0.50 m, (b) d = 0.45 m,
(c) d = 0.40 m.

3.7.4 Pressure Transducer

The usual methods of calibrating pressure sensors are based on exerting pressure on a VoF (volume of fluid). This pressure is measured precisely and is compared to the output signal from the test object. The voltage noted is plotted against the known water level, which is multiplied by a unit weight of water. And the pressure is measured in the unit of a Pa/volt, the slope of best fit. Typical calibration charts obtained for the pressure transducers are presented in Figure. 3.8.
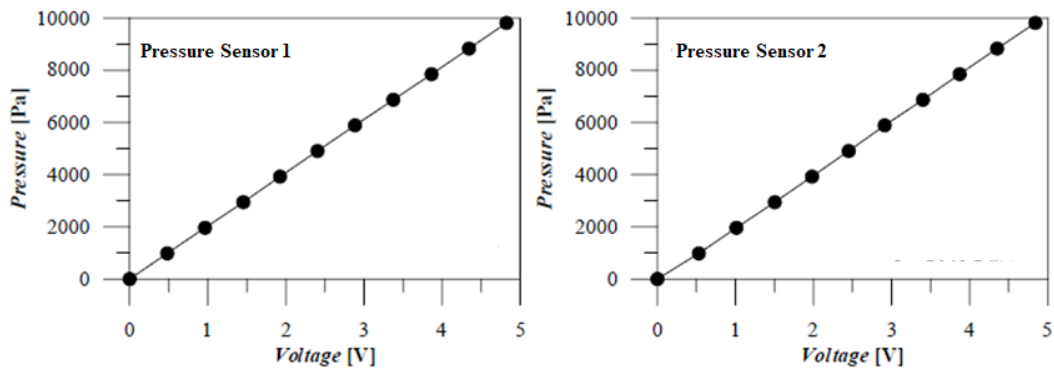
Figure 3.8: Calibration plots for pressure transducer

3.8 BREAKWATER TEST MODEL

Physical models are constructed to study the behaviour of the caisson breakwater. Due to the predominant gravity effect in the free surface wave motion, Froude's model law is used for physical modelling. A model scale of 1:30 is used for testing all physical models considering the Arabian Sea wave climate as detailed in section 3.2. The experimental studies are carried out in the wave mechanics laboratory to investigate the performance of vertical caisson breakwater with various combinations such as slotted barrier, protection of toe and perforated caissons by using suitable test models by varying wave characteristics under non-breaking wave conditions.

3.8.1 Casting and Placing of Test Models

For the present study, the test model is constructed using concrete and the dimensions of the model are 0.70 m in length, 0.5 m in breadth, and 0.90 m in height for the present study. The dimensions selected are based on the prototype of two caisson breakwaters integrated with OWC plants one in Vizhinjam port, Kerala and another from Sakata harbour, Japan. (Antonio F.O Falcao 2016). Also, the height of the Vertical caisson breakwater is selected in such a way that there is no wave overtopping occurs. On the seaside of the model, rubble mound toe protection is constructed. The toe protection is designed as quoted in the Shore protection manual (1984) Vol-II / CEM (2011). The design procedure is based on the experimental work conducted by Brebner and Donnelly (1962). Figure 3.9 illustrates the positions of pressure transducers and the cross-section of the test model with toe protection and the cross-section of the test model is presented in Figure 3.10.
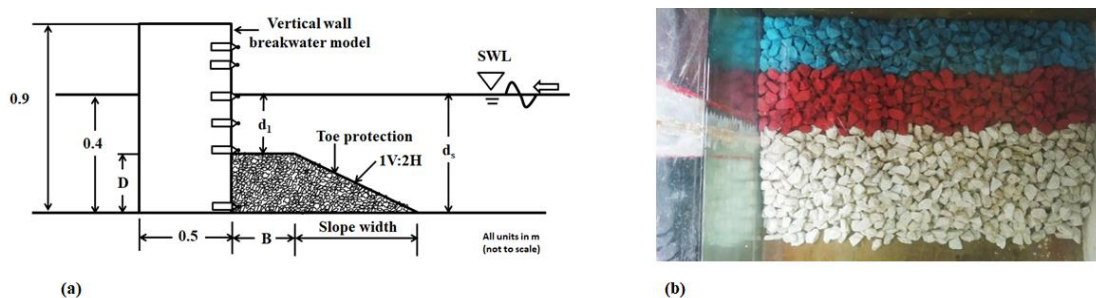
Figure 3.9: (a) Positions of Pressure Transducers (b)Toe protection for VCB
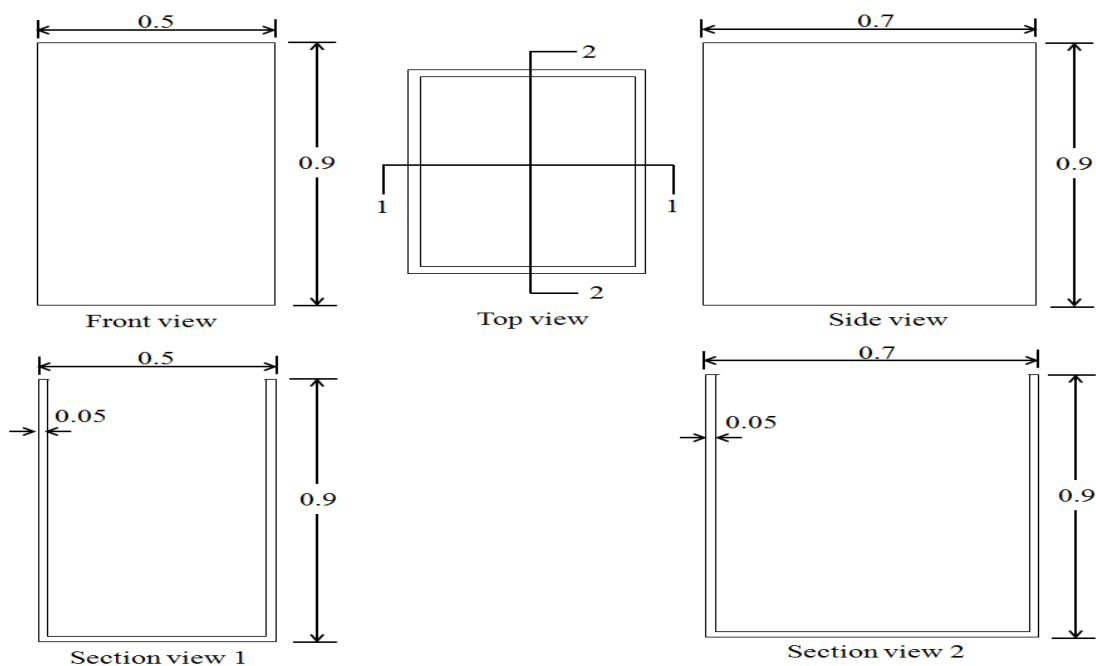
Figure 3.10: Cross-section of the test model (All units in m- not to scale)

The dimensions for the caisson breakwater model are chosen in such a way to avoid the overtopping of incident waves and to ensure there is no transmission of waves. Also, the dimensions of test models are selected in such a way that the structure should not slide for the least value of incident wave height (H_i) and wave period (T) used in the experiment.

Table 3.4. Toe cross-section for vertical / caisson breakwater as per Brebner and Donnelly (1962) / SPM (1984)

Water Depth (d) (m)	Depth of Toe D=0.25d (m)	Width of Toe B=0.4 d (m)	Depth from MSL to top of Toe d_1=0.75d (m)
0.35	0.088	0.14	0.263
0.40	0.10	0.16	0.30
0.45	0.113	0.18	0.338
0.50	0.125	0.20	0.375

The toe is constructed and the relative depth ratio is maintained constant for all four varying water depths, the dimensions of the cross-section are depicted in Table 3.4. The

trapezoidal cross-section of the toe consists of a homogenous pile of stones of 20g weight (i.e., nominal diameter, dn_{50} of 0.019 m) on the seaward side of the vertical caisson breakwater.

3.9 RANGE OF EXPERIMENTAL VARIABLES

Different wave-specific parameters, structure-specific parameters, and scaled parameters considered in the present study are listed in Tables 3.5 - 3.6.

Table 3.5 Wave and structure-specific parameters

Parameters	Experimental range of values
Wave specific Parameters	
Incident wave height, Hi (m)	0.12, 0.14, 0.16, 0.18
Wave period, T (sec)	1.2, 1.4, 1.6, 1.8, 2 [Toe Stability]
	2.2, 2.4, 2.6, 2.8 [Remaining All cases]
Depth of water, d (m)	0.35, 0.40, 0.50 [Toe Stability]
	0.5 [Remaining All cases]
Wavelength, L (m)	4.05 - 6.10
Structure specific parameters	
Vertical caisson Breakwater	
Height of structure (m)	0.90
Length of structure (m)	0.70
Breadth of structure (m)	0.50
Weight of caisson structure (N)	3120
Toe	
The weight of the armour units (g)	20
Nominal diameter, d_{n50} (m)	0.019

Table 3.6 Range of Scaled Parameters

Parameter	Definition	Range
H_i/L	Wave Steepness	0.029 – 0.089
d/L	Relative Water Depth	0.057 – 0.223
H_i/d	Relative Wave Height	0.24 – 0.51
ξ_{eq}	Relative surf similarity parameter	0.10 – 0.40

For the direct application of field conditions, the dimension analysis is carried out and the range of scaled parameters is shown in Table 3.6. The d/L ranged from 0.057-0.223,

which indicates the study covered a range of shallow to intermediate water-depth conditions.

3.10 METHODOLOGY

The test model is casted using concrete and the dimensions of the model are 0.70 m in length, 0.5 m in breadth, and 0.90 m in height for the present study. The dimensions selected are based on the prototype of two caisson breakwaters integrated with OWC plants one in Vizhinjam port, Kerela and another from Sakata harbour, Japan. (Antonio F.O Falcao 2016). Also, the height of the Vertical caisson breakwater is selected in such a way that there is no wave overtopping occurs. On the seaside of the test model, rubble mound toe protection is constructed. The toe protection is designed as quoted in the Shore Protection Manual (1984) Vol-II / CEM (2011). The design procedure and geometry are based on the experimental work conducted by Brebner and Donnelly (1962).

The wave flume is filled up with fresh water to the desired level and calibrated to produce the selected wave height and period without keeping the model. The measuring instruments are also calibrated. The test model is placed at a distance of 32 m away from the wave generator flap as shown in Figure 3.1.

The methodology adopted for the present research work is as follows:

1. The wave climates off the Mangalore coast as given by the KREC study team (1994) are considered as the input parameters while planning the experimental investigations.

2. Dimensional analysis is carried out using the Buckingham π theorem and non-dimensional parameters were identified.

3. The scale of the model is then selected based on the available site conditions and the predominant wave parameters of the Mangalore coast.

4. Before conducting the experiments every day, the calibration of the instruments is undertaken frequently to check and ensure accuracy.

5. In the first phase, the percentage damage of toe protection for vertical caisson breakwater experiments are conducted to arrive at a stable toe design.

6. In the second phase, the hydrodynamic performance of caisson breakwater such as pressure distribution, wave forces, wave runup, and wave reflection is analyzed and the experimental results are compared with the existing theoretical approaches (Sainflou, Goda).

7. In the third phase, a numerical model of caisson breakwater is developed to study its performance using the computational fluid dynamics (CFD) approach using Ansys-Fluent and validated the same using experimental data.

8. In the fourth phase, to examine the dissipation of the wave energy, wave runup, and wave reflection by the presence of a slotted barrier in the front of a vertical caisson type breakwater.

9. In the fifth phase, perforations are introduced on the front face of caisson breakwater to know the effects of perforation on the performance of it.

For better clarity, the complete workflow is described in Figure 3.11.
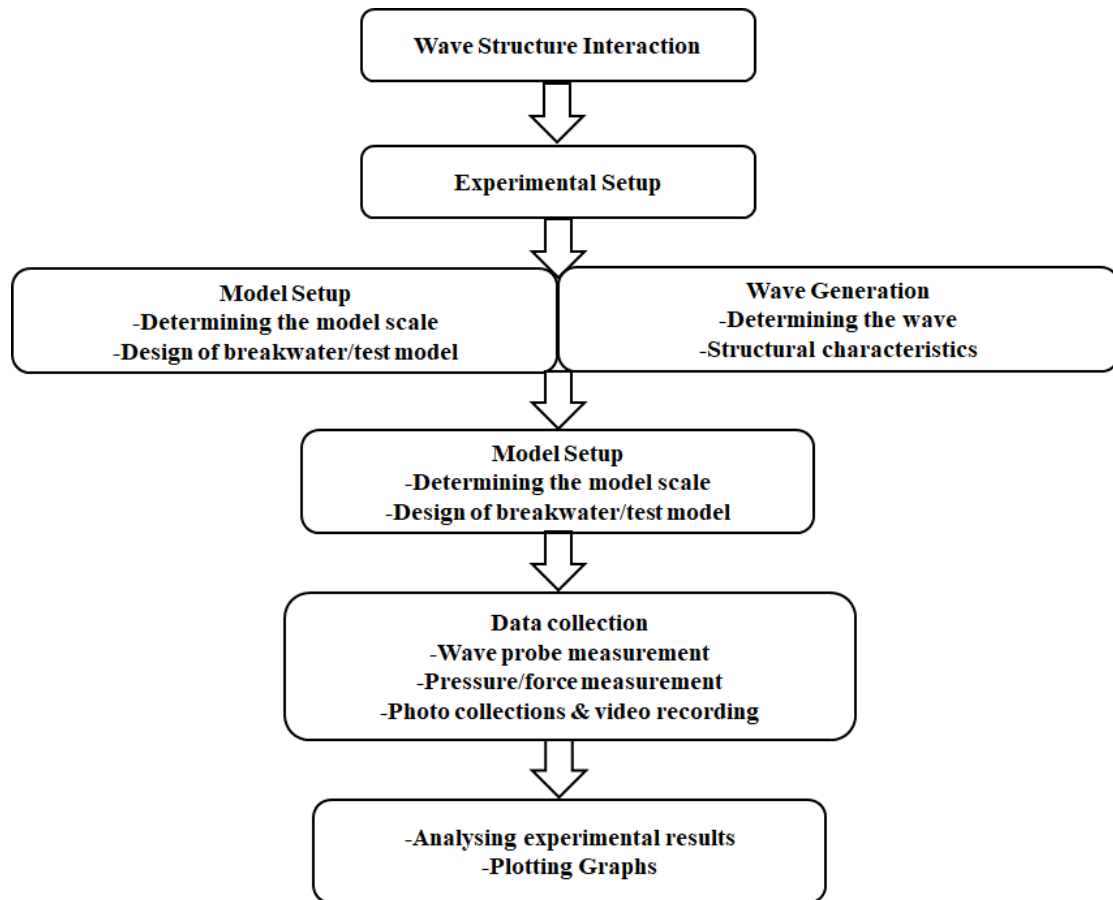
Figure 3.11: Methodology for present work

3.11 MODEL TEST CONDITIONS

The present experimental investigations are carried out with the following test conditions:

- The sea bed is rigid and horizontal and it is assumed that the sediment movement does not interfere with the wave motion and does not affect the model performance.

- The waves are periodic and monochromatic.

- Wave reflection from the structure does not interfere with freshly generated incident waves, since the waves are generated in bursts of five.

- Secondary waves generated during the test are not considered.

- Wave reflection from the flume bottom or flume side walls is not considered.

- The density difference between freshwater and seawater is not considered.
- Bottom frictional effects have not been accounted.

The experimental setup is prepared to produce ideal conditions as per the assumptions mentioned in section 3.11. However, there may be some factors that cannot be satisfied fully. The errors are small and do not have a significant influence on the results of the present study.

3.12 UNCERTAINTY ANALYSIS

The use of uncertainty analysis is indispensable in physical model studies. There is no single way to describe uncertainty in measurements and there are many different situations that demand somewhat differing descriptions. The distribution of uncertainty between precision and bias is arbitrary. Whatever may the method used for calculating uncertainty, the method used should be reported in some appropriate way and the report includes the method employed (Kline, 1985). Uncertainty is an estimate of experimental error and it describes the degree of goodness of measurement or experimentally determined result. (Misra, 2001).

Experimental error sources should be identified and the error (δ) should be determined from calibration and conducting simple experiments respectively. The distribution of uncertainty between precision and bias is arbitrary. The confidence interval gives an estimated range of values, which is likely to include an unknown population parameter. The estimated range is calculated from a given set of observations. The 95% confidence interval limits must always be estimated and this concept of confidence level is fundamental to uncertainty analysis (Misra, 2001). The details of the uncertainty analysis are explained in Appendix I.

3.13 PHOTOS OF EXPERIMENTAL SETUP AND TEST MODELS

Plate 3.1: Photographic view of (a) Inventer drive and (b) motor
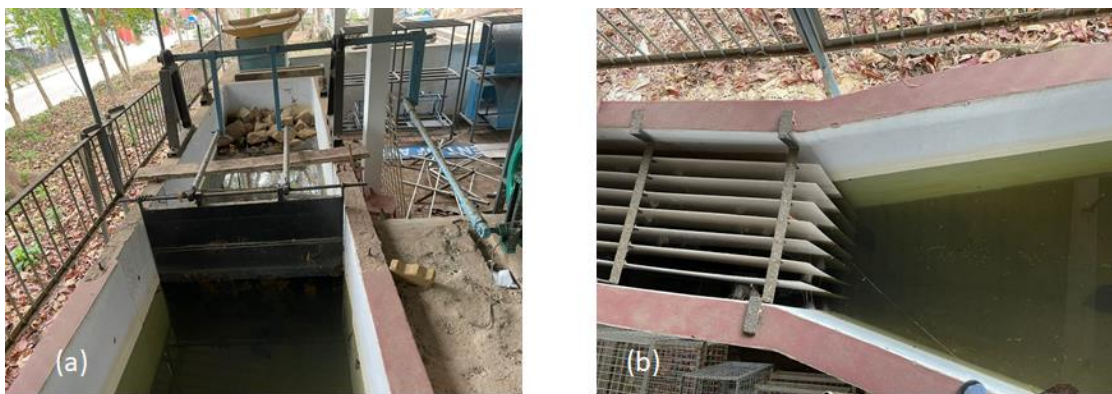
Plate 3.2: Photographic view of (a) Flap type Wave Generator and (b) Wave Filters
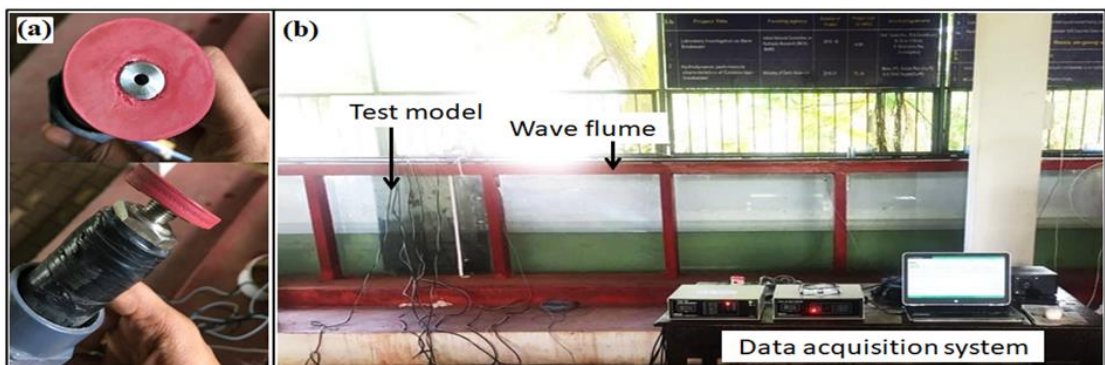
Plate 3.3: (a) Pressure sensor and (b) experimental setup along with data acquisition system

Plate 3.4: (a) - Aggregate mix, (b) &(c) – Preparation of mesh of vertical wall, (d), (e), (f) - Armour units for the protection of toe, (g) – Bedding Layer or base layer on flume bed, (h)- arrangement of a toe, (i)- Vertical wall with the protection of toe.
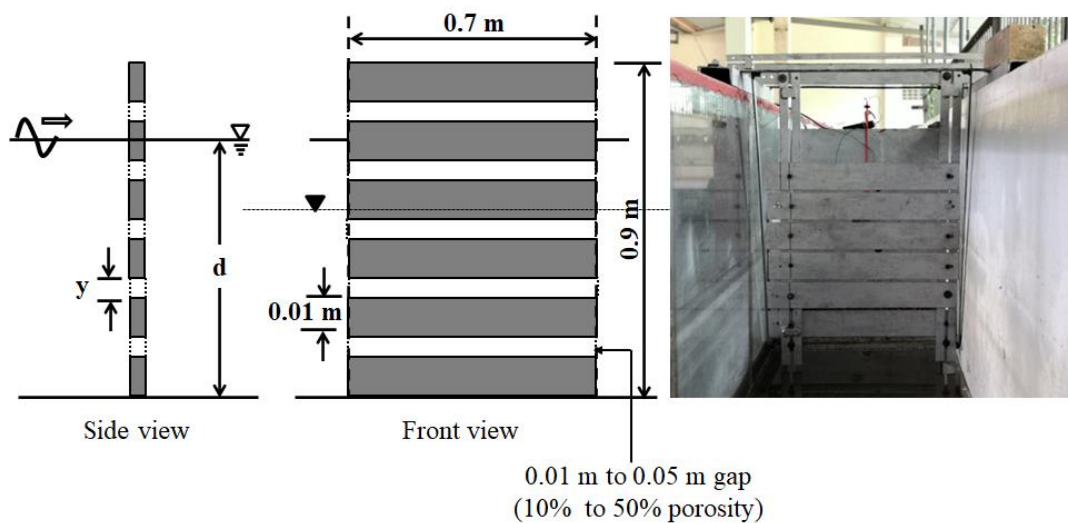
Plate 3.5: (a) Schematic sketch and photographic view of horizontal slotted barriers
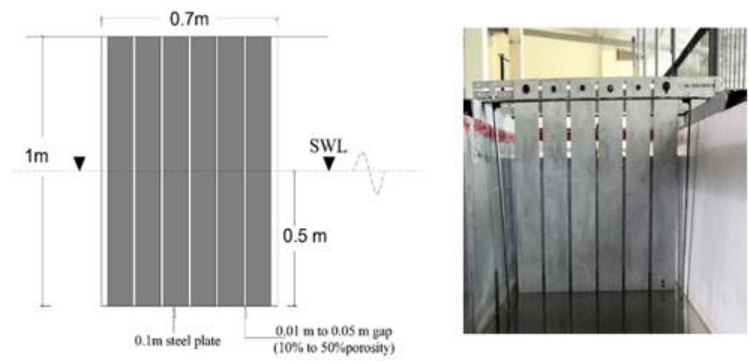
Plate 3.5. (b) Schematic sketch and photographic view of vertical slotted barriers

(b)

(c)

(d)

(d)

(e)

Plate 3.6: Perforated test model

3.14 NUMERICAL SETUP

Experimental and analytical approaches are often infeasible because of the cost, time involved, and real-life industrial problems. Therefore, the third approach is emerging in the engineering community, which is called Computational Fluid Dynamics (CFD). CFD is the technique, which can reduce the experimental cost and time without making much approximation to the governing equations. In CFD, the governing equations of given physics (maybe differential form or integral form) are solved using some numerical techniques such as Finite Difference Method (FDM), Finite Element Method (FEM), or Finite Volume Method (FVM). In the present study, an attempt is made to study the fluid-structure interaction using the commercial CFD tool ANSYS - FLUENT.

3.14.1 Details of Numerical Wave Flume

A two-dimensional numerical wave flume is modelled with dimensions of length 20 m, the height of 1.1 m. To nullify the effects of wave reflection in NWT, three different end slope conditions (1: 3, 1:5 slope and numerical beach condition) are performed as shown in Figure 3.12.
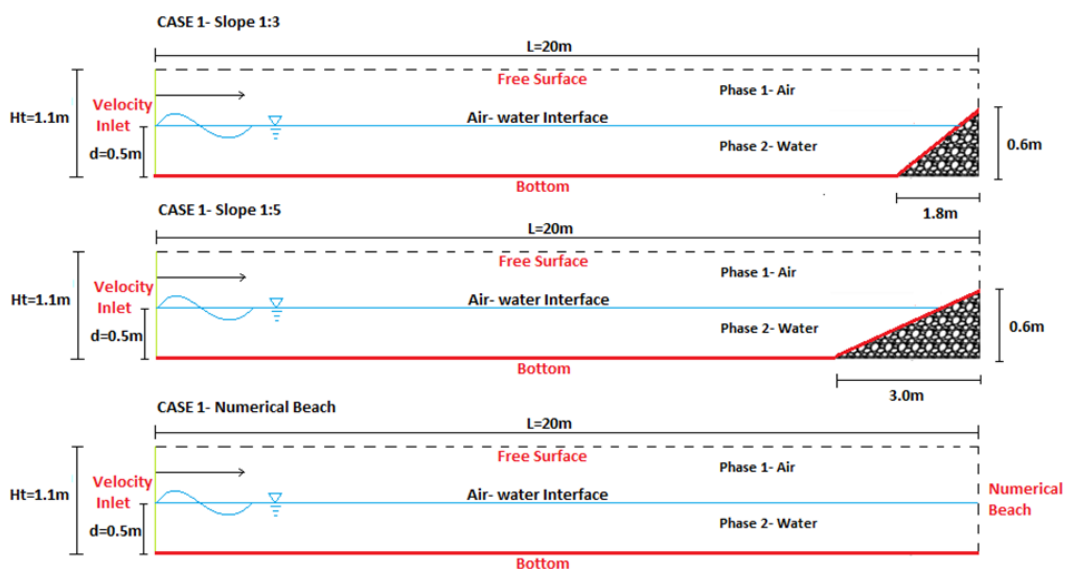
Figure 3.12: The geometry of numerical wave flume with varying end slopes.

Initially, under the hydrostatic conditions (water at rest) of the flume, the generation of the wave process has been initiated by assigning a regular wave motion in the wave flume using a user-defined function with the movement of the flap-type paddle. In general, the governing equations (conservation of mass and moment) are solved by making the computational space into a finite number of control values. As an initial condition, static pressure is given for the liquid face, and the volume of the fluid model is used to generate the free surface between the air and water medium. The general steps involved in numerical simulation of ANSYS FLUENT can be broadly classified into three steps.

1. Pre-processing
2. Solver
3. Post-processing.

Pre-processing can further be subdivided into Geometry building, Meshing, and defining the boundary conditions as illustrated in Figure 3.13.
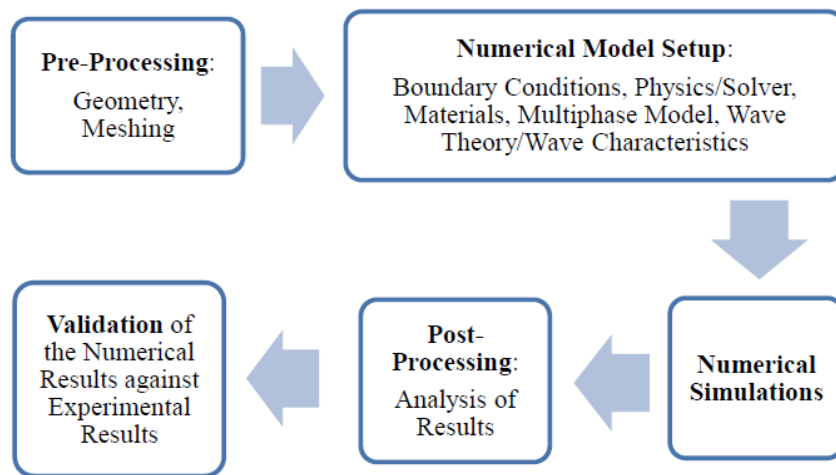
Figure. 3.13. Workflow in Numerical Simulations Ansys-Fluent.

3.15 Meshing Details

The computational mesh is created using ANSYS Fluent Meshing. The face meshing method is firstly used to create a structured mesh, in which the domain is divided into square elements of specified dimensions. Initially, to determine the effect of mesh size on the accuracy of results generated by ANSYS Fluent, a two – dimensional Numerical

Wave Tank with no caisson structure is modelled and the wave surface elevations are obtained. Numerical simulations are carried out for three mesh sizes viz. 0.01m x 0.0 m, 0.02 m x 0.02 m and 0.03 m x 0.03 m as shown in Figures 3.14 (a-c). And Table 3.7 shows the base grid dimensions for which the trials are carried out.
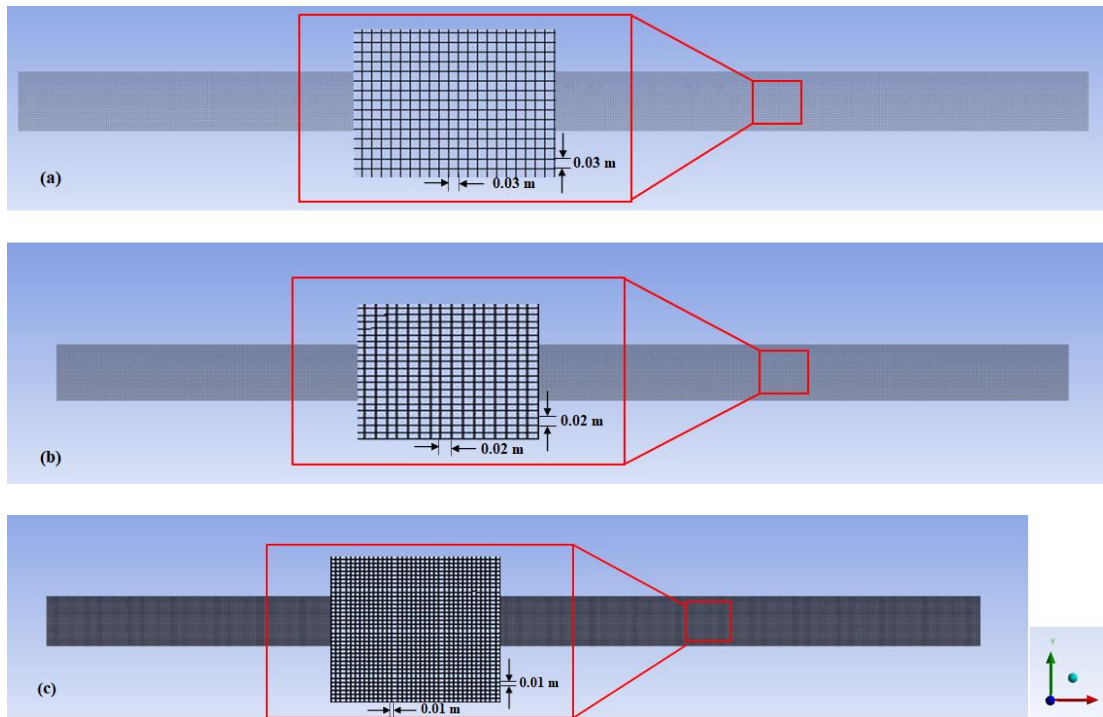
Figure. 3.14: (a-c) Fluent meshing closer to the test model.

Table 3.7 Mesh Size Parameters

Meshing Details	Δx (m)	Δz (m)	Grid Cell Density	No. of Elements	No. of Nodes
1.	0.03	0.03	200	24076	24775
2.	**0.02**	**0.02**	**300**	**55742**	**56796**
3.	0.01	0.01	600	220008	222119

The inappropriate selection of mesh can affect the accuracy of simulation results, computational efficiency, and solution stability. The proper wave formation can be obtained when the model is developed with a minimum of 200 grids per wavelength (Arun Kamath 2012) and the aspect ratio (ratio of higher dimension to lower dimension of element) of an element should be less than 10 (Marques Machado et al. 2018). In the

present study, to generate waves at a maximum wavelength of 6 m conditions maximum element length of 0.03 m is required. So, all the experiments are simulated with a mesh size of 0.02 m and at an element aspect ratio of one. The detailed grid cell density and elements details as shown in Table 3.7.

HYDRODYNAMIC PERFORMANCE CHARACTERISTICS OF VERTICAL CAISSON TYPE BREAKWATER

4.1 BACKGROUND

Vertical caisson breakwater/wall type breakwater are predominantly used to protect the inner harbour region from the high-water levels and waves to maintain the tranquillity condition for safe marine operations. The breakwaters are generally classified as rubble mound (mound breakwater), caisson-vertical breakwater, and a combination of both which is termed as a composite breakwater. The selection of appropriate breakwater is influenced by several factors such as water depth, geomorphologic conditions of the seabed, availability of materials, and its functional utility. In the cases of caisson breakwater and its toe design is the paramount important parameter. In many cases, improper design and instability of the toe will lead to damage to the main structure, the failure of the toe is not always easy to diagnose because a toe is not visible from the waterline. In most cases, the instability of the toe is unnoticed until the failure occurs on the main structure. Further, the replacement of the stone is also difficult, therefore the most stable and economical toe armour size design is required.

For effective design, it is necessary to know the hydrodynamics in and around the toe of the caisson-type breakwater. The stability relationship between $H_S/(\Delta D_{n50})$ and h_t /H_S (h_t – depth of the toe from the SWL), is assumed lower the value of h_t /H_S (higher toe) corresponds to more damage. Higher values of wave steepness (short period waves) give more damage to the toe than the lower wave steepness. However, this statement is valid only based on a few data points (Gravesen and soreson). The experimental study conducted by Brebner and Donnelly is quoted in SPM/CERC/CEM, for rubble toe protection in front of the vertical-faced breakwater in which a relationship may be assumed between the ratio h_t /h and the stability number H_S /(ΔD_{n50}) or N_S. (Where h is the water depth).

In the first phase of the chapter (Section 4.2), deals with the stability of the toe armour units for caisson-type breakwater and analyses the percentage damage level for varying

wave characteristics. The applicability of the Brebner and Donnelly (Cost Eng Proc 1:24, 1962) design curve for depth limited conditions is validated for a certain fixed relative foundation depth (d_1/d).

In the second phase of the chapter (Section 4.9), to assess the dynamic pressure, wave forces, wave runup, and wave reflection for caisson type breakwater. And, finally, the maximum wave forces on caisson breakwater are calculated from measured pressure values and are compared with the forces calculated by Goda's and Sainflou's wave theories.

4.2 SELECTION OF TEST MODEL DIMENSIONS AND CONFIGURATION

The selection of wall breakwater /caisson model dimensions are made by considering the two prototype models, one in Vizginjam port, Kerala and another from Sakata harbour, Japan.

On the seaside of the model, rubble mound toe protection is designed. The design procedures are adopted from CEM / SPM Vol-II (the experimental work conducted by Brebner and Donnelly (1962). Markle et al. (1995) evolved a relationship between N_S (toe stability number) and depth ratio, d_1/d.
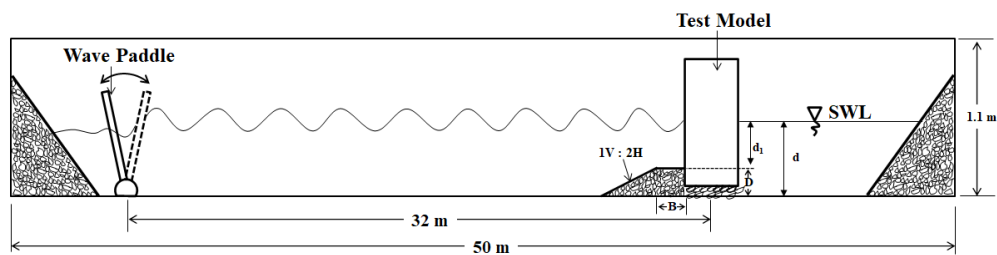
Figure. 4.1: Schematic experimental setup in a wave flume

The seaside slope of the toe is 1V:2H and the value of the d_1/d_S [Where d_1 - depth from MSL to top of the toe, D –Height of toe, B- Width of the toe, d – Depth of water]. Figure 4.2, illustrates the artist's view of the test model with the protection of the toe and bedding layer provided at the bottom of the test model. The dimensions of the toe

protection are dependent on water depths which are depicted in Table 4.1. The line sketch of the experimental setup model in wave flume is presented in Figure 4.1.
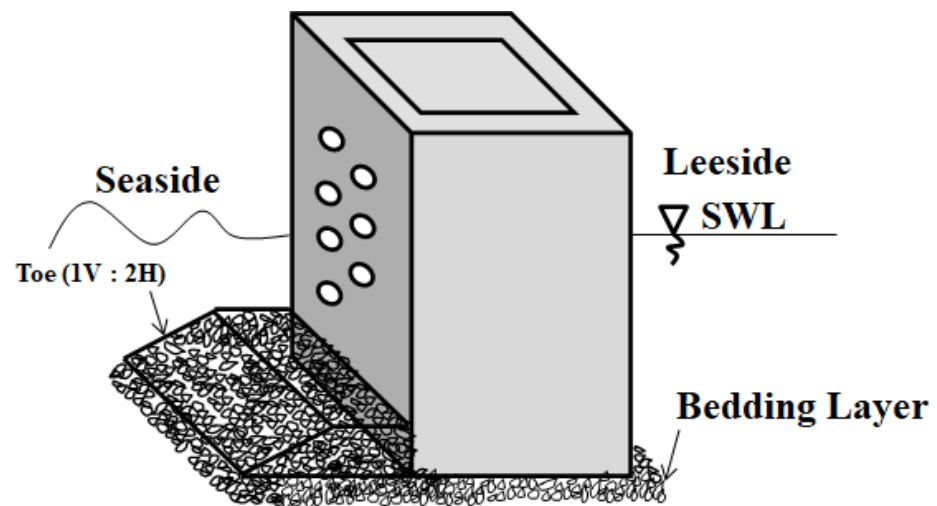
Figure 4.2: Test Model

Table 4.1 Dimensions of the toe for vertical wall breakwater as per

Brebner and Donnelly (1962) / SPM (1984)

Water Depth (d) (m)	Depth of Toe D=0.25d (m)	Width of Toe B=0.4d (m)	Depth from MSL to top of Toe d_1=0.75d (m)
0.35	0.0875	0.14	0.2625
0.40	0.10	0.16	0.30
0.50	0.125	0.20	0.375

4.3 CALCULATION OF TOE ARMOUR WEIGHT

The design inputs cover the wave characteristic existing along the Mangalore coast and then designed as follows:

Mass density of armour unit at site (γ) $= 2.8$ t/m^3

Design wave height (H_s) $= 3$ m (Prototype)

         ($H_{1/10}$) $= 1.27$ x H_s = 1.27 x 3 = 3.81 m

Stability coefficient (K_D) $= 3.2$

(from SPM for Rough angular quarry stone)

$$\text{Cot}\alpha = 2$$

Hudson (1959) formula provides the basis for primary armour weight (W_{50}) calculations

$$W = \frac{\gamma_\gamma\, H^3}{K_D\, (S_r - 1)^3\, \cot\alpha}$$

$$W = \frac{2.8 \times 3.81^3}{3.2\left(\frac{2.8}{1.025} - 1\right)^3 2}$$

The weight of the armour unit in prototype (W) = 4.659 tones = 4659 kg

The weight of the armour unit for toe, gradation W/10 is 465.9 kg

The values obtained from Hudson's formula are scaled down to 1:30

$$N_{wa} = N_{\gamma a}\, (N_L)^3$$

$$N_{wa} = (2.8/2.8) \times (30)^3 = 27000$$

$$(W_a)_m = \frac{(W_a)_p}{(N_w)_a} = \frac{465900}{27000}$$

$$(W_a)_m = 17.2 \text{ grams}$$

Approximate to 20 g

The trapezoidal cross-section of the toe consists of a homogenous pile of stones of 20g weight (i.e., nominal diameter, d_{n50} of 0.019 m) on the seaward side of the vertical caisson breakwater. In the free surface wave motion, the gravity effect is predominant and hence Froude's model law is used for physical modelling. A scale of 1:30 is used for the present study to suit the wave characteristics off the Mangaluru coast are detailed in chapter 3.

4.4 MEASUREMENT OF DAMAGE LEVEL

To determine the percentage of damage (S) and relative damage (D) the number of armour units placed are monitored using video device and photographs during the course of experiments. The number of armour units displaced after the experiments from their original position can then be compared to the total number of units within the reference area as quoted in Coastal Engineering Manual (CEM-2011), Eq.4.1.

$$S = \frac{Placement\ of\ armour\ units\ before\ experiments}{Displacement\ of\ armour\ units\ after\ the\ experiments}\ \text{X}\ 100 \qquad (4.1)$$

From the top to the bottom of armour units or in-between vertical levels is described as references area from the strip width a typical case shown in Figure 4.3. From the literature of Van der Meer (1988), the term, N_{od}, is for units displaced out of the armour layer. More in-depth studies are performed and the wave boundary conditions are established for damage criteria as tabulated in Table 4.2
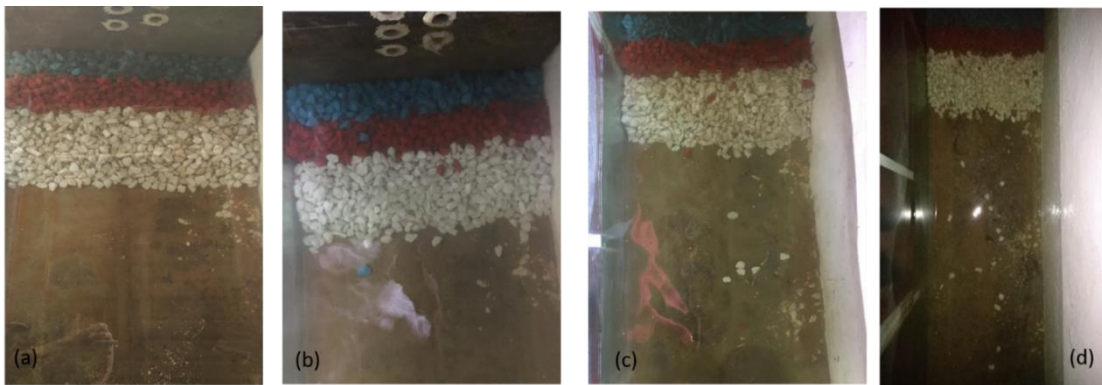
Figure 4.3: (a) Initial Condition (b) After 800 waves (c) After 2000 waves (d) After 3000 waves depth of water of 0.35 m & wave height (H) of 0.14 m and wave period (T) of 2 sec.

Table 4.2 Damage Classification

% CIRIA(1991)	Description	% Damage (Greding 1993)	Description
0 to 3 %	No movement of stones (or only a few) in the toe	< 0.5	Hardly any damage
3 to 5 %	Toe flattened out, but still functioning with acceptable damage	0.5 - 2.0	Acceptable Damage
> 20- 30 %	Failure (toe has lost its function)	> 4	Unacceptable Damage (toe has lost its function); Failure

4.5 ZERO DAMAGE WAVE HEIGHT

Figure 4.4, illustrates the variation of dimensionless damage (S) with incident wave height. It is observed from this figure that as the wave height increases, the damage level S also increases. Zero damage wave height is the wave height corresponding to a specified percentage damage level S (i.e., normally S=3%). When the size of armour unit is fixed, the wave height (H) is the only variable in the stability number ($H/\Delta D_{n50}$) that influences damage. In Figure 4.4. the wave height is varying from 0.08 m to 0.18 m for the water depth of 0.40 m and the wave period T is changing from 1.4 sec to 2 sec (corresponding relative water depth ranges from 0.09865 to 0.15564).
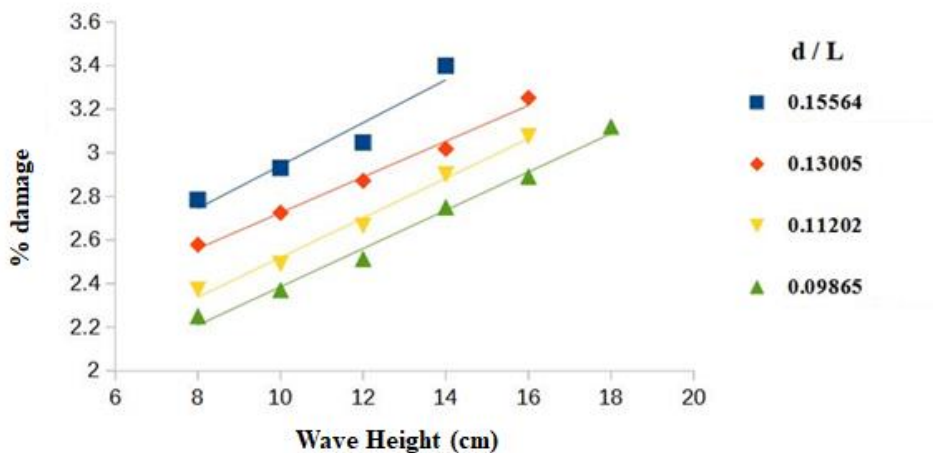
Figure 4.4: Variation of dimensionless damage (S) with incident wave height (H)

From the above graph, the equation of a line for a relative depth of 0.15564 is,

$$S = 0.08H + 1.9602 \qquad (4.2)$$

The zero-damage wave height (H_Z) from the above equation, If S = 3%, H = H_Z.

$$0.08H + 1.9602 = 3 \qquad (4.3)$$

$$0.0335Hz = 1.0398 \qquad (4.4)$$

Solving the equation (4.4),

$$H = H_Z = 0.13 \text{ m} \qquad (4.5)$$

From the experimental observations, it is observed that the values of H_Z are greater than the design wave height, and the structure will not be susceptible to damage under design conditions.

4.6 VARIATION OF PERCENTAGE DAMAGE (S) WITH INCIDENT WAVE STEEPNESS PARAMETER (H_i/gT^2)

Figure 4.5 (a) shows the effect of wave steepness (H_i/gT^2) on % damage (S) for different crest width of Toe (B) [0.20 m], depth of toe (D) [0.12 m] at water depth of 0.5 m. For the water depth of 0.5 m, the percentage of damage increased from 0.1 to 4.4 with an increase in wave steepness from 0.002 to 0.008. The steeper waves resulted in more damage at all the water depths. Similarly, in Figure 4.5 (b), at the depth of water of 0.4 m, the percentage of damage increased from 0.1 to 5 with an increase in wave steepness from 0.002 to 0.008. Lower the % damage occurs in the higher water depth since the wave interaction with the toe protection has a less significant effect. (i.e. the energy of the wave gets reduced with depth).

(a) for d = 0.50 m, B = 0.2 m, D= 0.12 m
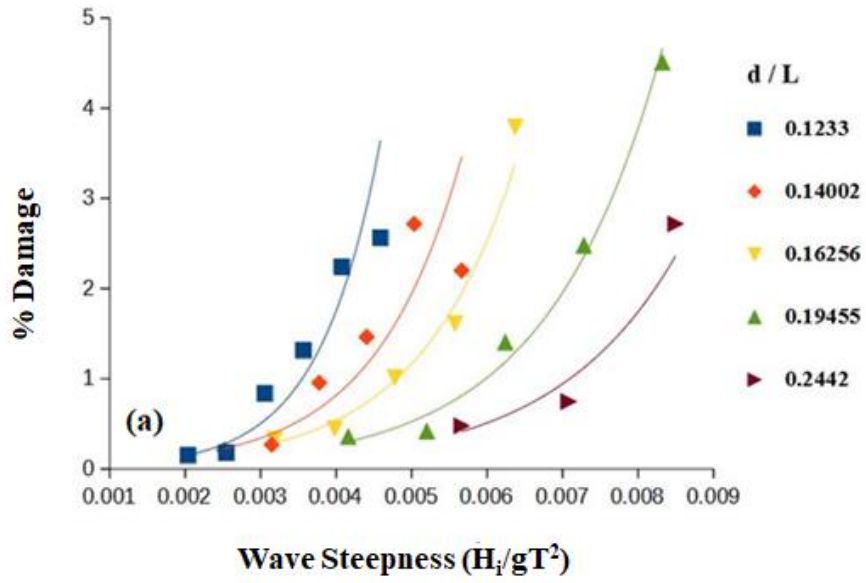
(b) for d = 0.4 m, B = 0.16 m, D = 0.10 m
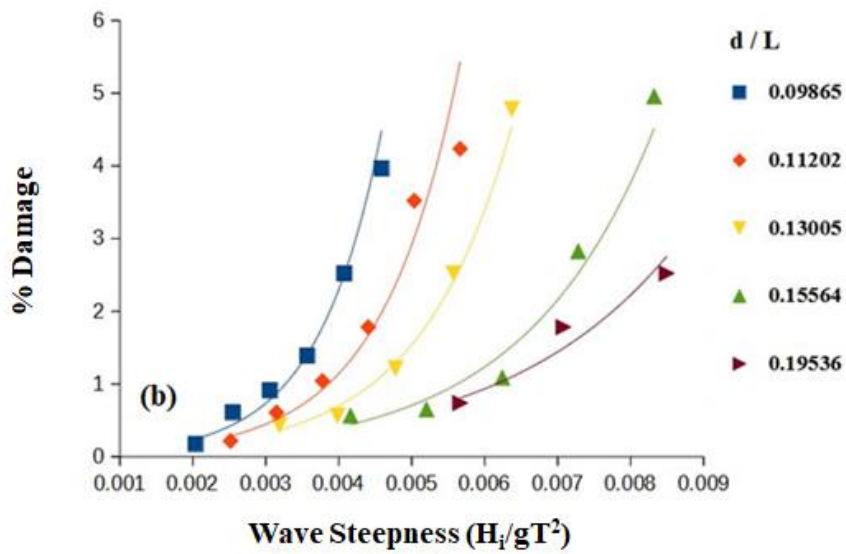
(c) for d = 0.35 m, B = 0.14 m, D = 0.0875 m
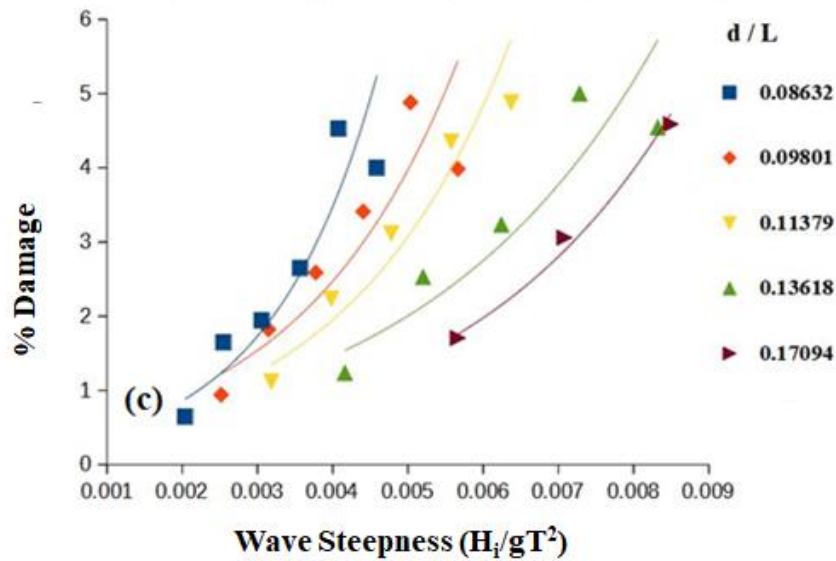
Figure 4.5: Variation of % damage (S) with wave steepness H_i/gT^2

At the depth of 0.35 m (Figure 4.5 (c)), the percentage of damage increased from 0.8 to 5.2 with an increase in wave steepness from 0.002 to 0.008. The percentage of damage is more even at the lower steepness of waves when the depths of water are low. At all the considered water depths in the present study, the percentage of damage increased with an increase in relative water depth. The fact might be the wave exceedance in deep water, where the Rayleigh distribution is valid. But since most of the experiments are in-depth limited conditions and also the frequency of occurring at higher wave heights is limited. On the other hand, wave steepness is an influencing parameter for the damage to the toe and the highest waves that are possible at the attack on the toe are frequent which further increases the damage. Such behaviour is observed in very shallow water. As the incident water wave steepness increases, the percentage of damage increases for the range of variables considered in the present study. The maximum percentage of damage observed for the depth of water of 0.35 m is 5.2 %. Similarly, for other depths of water 0.50 m and 0.40 m, the percentage of damage is within the acceptable limit as illustrated in Table 4.2.

4.7 VARIATION OF PERCENTAGE DAMAGE (S) WITH SURF SIMILARITY PARAMETER (ξ_o)

Figure 4.6 (a), shows the variation Percentage Damage (S) on Surf Similarity Parameter(ξ_o) for the water depth of 0.5 m. The surf similarity parameter is a ratio between the bottom slope (tanβ) and the value for the wave steepness (H$_i$/L). Surf Similarity Parameter used the local wave height (design condition) for wave height H and the wavelength L.

$$\xi_0 = \left\{ \tan\beta / \sqrt{H_i/L} \right\} \qquad (4.6)$$

Where,

tanβ = Bottom Slope

H_i = Incident Wave Height

 L = Wave Length

a) d = 0.50 m, B = 0.2 m, D= 0.12
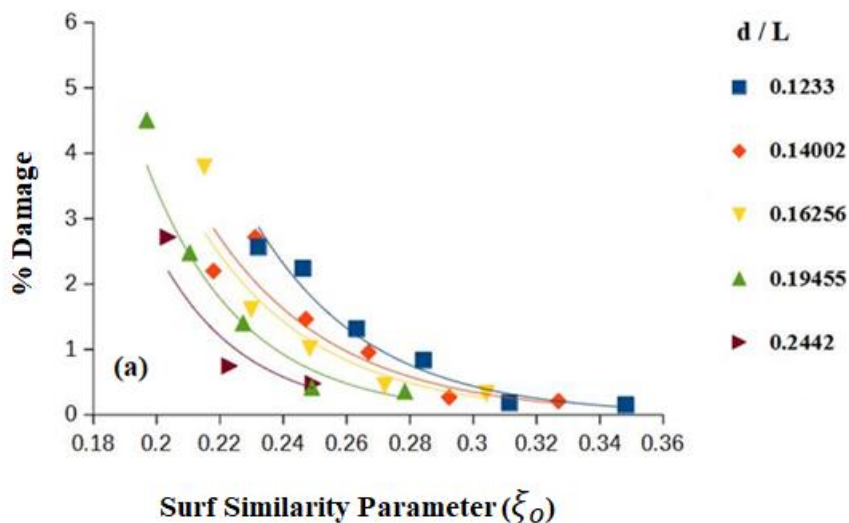
(b) d = 0.4 m, B = 0.16 m, D = 0.10 m
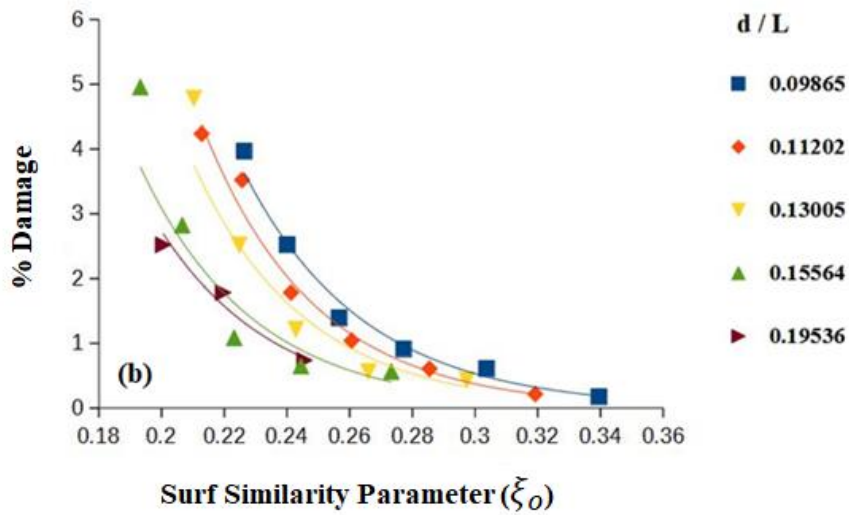
(c) d = 0.35 m, B = 0.14 m, D = 0.0875 m
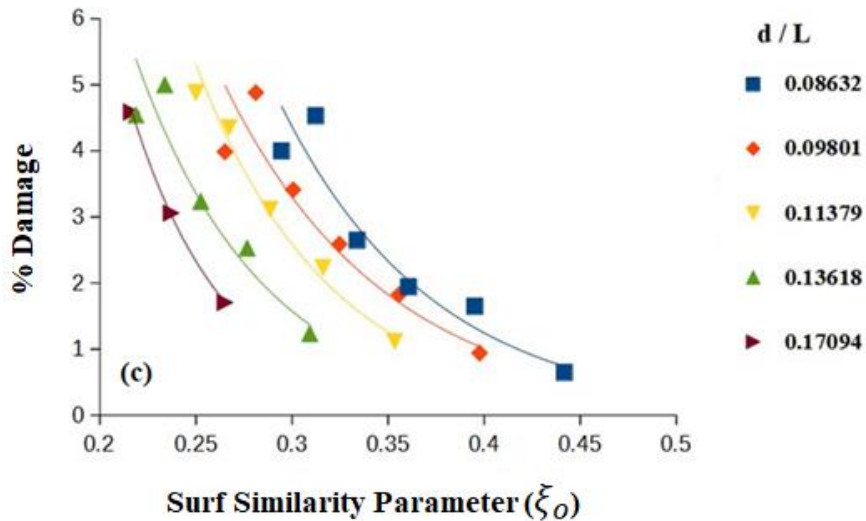
Figure 4.6: Variation of % damage (S) with Surf Similarity Parameter (ξ_o)

The breaking of the wave depends on the combined effect of wave height, wavelength, wave steepness and bottom slope, (tanβ). For relatively high-water level in comparison to the wave height, the waves can reach the test model without breaking. For lower

water levels in comparison to the wave height, the waves already broke on the foreshore slope. From the graph, it is observed that percentage damage (S) increases from 2.5 to 3.0 (which is an increase of 16 %) with a decrease in surf similarity parameter from 0.282 to 0.235 (which is a decrease of 20 %) for the relative water depth of 0.123. Similarly, Figure 4.6 (b) and Figure 4.6 (c) show the variation of % damage (S) on the surf similarity parameter (ξ_o) for the water depths of 0.40 m and 0.35 m. The surf similarity parameter varies from 0.2 to 0.50, a higher value is observed at a water depth of 0.35 m for the relative water depth of 0.0863.

It is observed that the surf similarity parameter increased with a decrease in relative water depth. The percentage damage decreased with an increase in the surf similarity parameter. Since the armour unit is pushed in an upward direction for long waves. The steeper waves lead mainly to the downward movement of armour units. The high wave impact on toe structures mainly depends on the higher wave heights and longer waves. In shallow water conditions, wave-breaking phenomena occur on the foreshore and the toe structure. Such waves dissipate their wave energy and more damage is observed.

4.8 STABILITY ANALYSIS

Figure 4.7, shows the variation of the stability number, N_S, with relative water depth d/L. The applicability of the Brebner and Donnelly (Cost Eng Proc 1:24, 1962) design curve for depth limited conditions is validated for a certain fixed relative foundation depth (d_1/d) is compared with the present study and it is significant in generating accurate response results for the toe armour layer stability. The accuracy of the results of the test is ensured by carrying out a series of repeatability of experimental tests for various test conditions. The present experimental results match well with the results of Brebner and Donnelly, as shown in Figure 4.7.
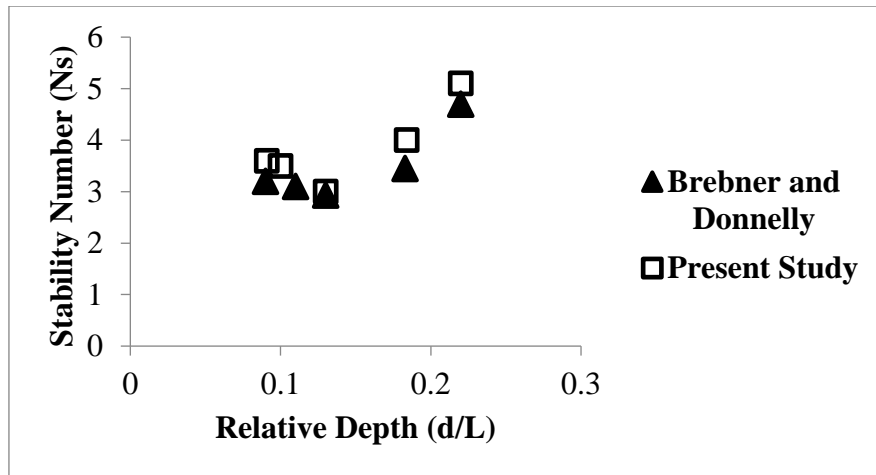
Figure 4.7: Variation of the stability number, N_s with relative depth parameter (d/L)

It is observed that the relative foundation depth (d_1/d) plays a vital role in the stability of the armour layer. Thus, the results of the tests are illustrated by analysing the data graphically by depicting the minimum stability numbers needed for the corresponding relative foundation depth.

4.9 CLOSURE

In this Section, the percentage damage of toe for wall type breakwater is analyzed and a comparison of stability parameter N_S with Brebner and Donnelly (1962) is also presented. The main findings are listed below point-wise.

- Wave steepness is an influencing parameter for the damage development of the toe. Such behavior is observed in very shallow water. As the incident water wave steepness increases the percentage of damage increases for the range of variables considered in the present study. The maximum percentage of damage observed for the depth of water of 0.35 m is 5.2 %. Similarly, for other depths of water 0.50m and 0.40m, the percentage of damage is within the acceptable limit.

- In shallow water conditions, it is observed significantly different hydrodynamic behavior. The toe structure is attacked by breaking or already broken waves. Although a reduced wave height reaches the toe, the damage is larger because the toe is exposed to turbulent wave attacks.

87

- The stability number is significantly affected by the depth of the rubble mound foundation and by the relative depth (d/L). Further increase in wave height causes steeper waves resulting in more damage. Similarly, it is observed that the surf similarity parameter decreases to a maximum of 20 % for the relative depth (d/L) of 0.1233.

4.10 EVOLUTION OF WALL PRESSURE FORMULAE ON VERTICAL CAISSON TYPE BREAKWATER

The wave pressure distribution and stability of vertical breakwater have been studied by several investigators since 1919. Based on the assumption of uniformly distributed loads with averaged wave pressure acting on the vertical wall, Hiroi proposed the first wave pressure formula in 1920. Sainflou (1928), proposed the simple form of the clapotis wave formation formula for the vertical wall without foundation. The modified sainflou formulae which apply the Miches high-order were proposed by Rundgren (1958). Minikin formula (1950), for wave pressure calculation, is based on the maximum wave height and impact test concepts. Figure 4.8 shows the evolution of wave pressure formulae.
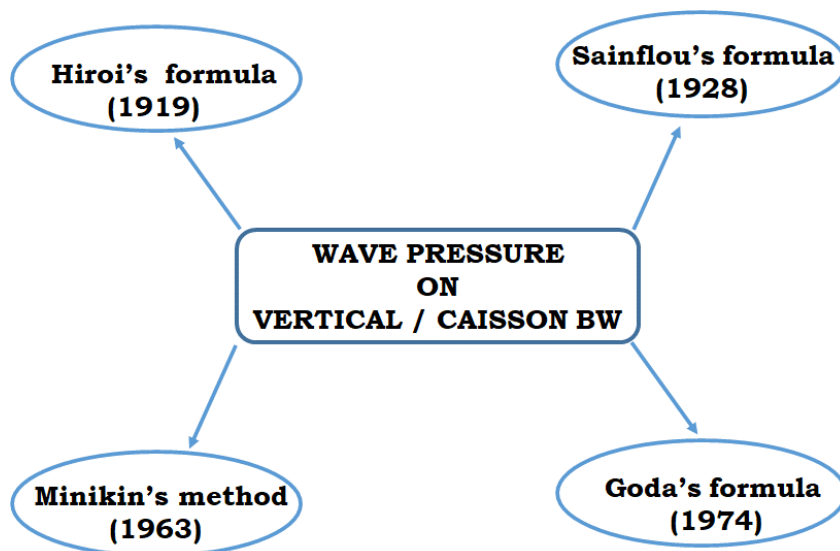
Figure. 4.8: Evolution of Wall Pressure Formulae

Goda (1973), obtained four equations for the design load on vertical walls and they are widely used for both breaking and non-breaking wave conditions. SPM (1984) suggests the Minikin (1963) formulae for the design of composite breakwaters. IS-4651 (Part-III) also suggests the use of the Minikin (1963) method and Sainflou (1928) method for the estimation of breaking wave forces and non-breaking wave forces, respectively. Ergin and Abdalla (1993), attempted computation of horizontal breaking wave forces on vertical structures using the empirical methods of Minikin (1963) and Goda (1974). Muni Reddy (2007) reveals that the most reliable methods available for both non-breaking and broken waves are Sainflou (1928), and Goda (2000). These two methods are mostly used to design, such as seawalls and vertical breakwaters, whereas Minikin's (1963) method is recommended for structures placed in breaking wave conditions. The results reveal that these methods give a significant difference in predicting the wave forces and Minikin's method usually predicts higher wave forces than Goda's method

In this section, the main objective is to analyse the hydraulic performance of wall/caisson breakwater such as dynamic wave pressure distribution, wave reflection, wave runup and wave force on the test model for varying wave characteristics and depth of water.

4.11 TYPICAL TIME HISTORIES OF WATER SURFACE ELEVATION AND PRESSURE ALONG WITH THE DEPTH OF THE WALL

Typical time histories plots sensed by the wave probes and pressure transducers at different locations on the test model along with its depth such that the depth of submergence of the pressure sensors, z/d (z is the depth below still water and d is water depth) ($z/d= -1$, $z/d= -0.2$, $z/d= -0.1$, $z/d= 0$) as shown in Figure 6.3.

From this experimental analysis data, water surface elevation(η) and the dynamic pressure exerted on the test model are obtained. At the beginning of the formation of the partial standing wave, some disturbance takes place. After that, the wave tends to be stable for some time ($t = 7$–17 sec), which is the suitable duration to estimate the wave forces, wave runup and wave reflection coefficients. After this time, the form of

the partial standing wave changes due to the new reflection of the wave from the wave generator, which generates a new incident wave with different characteristics.
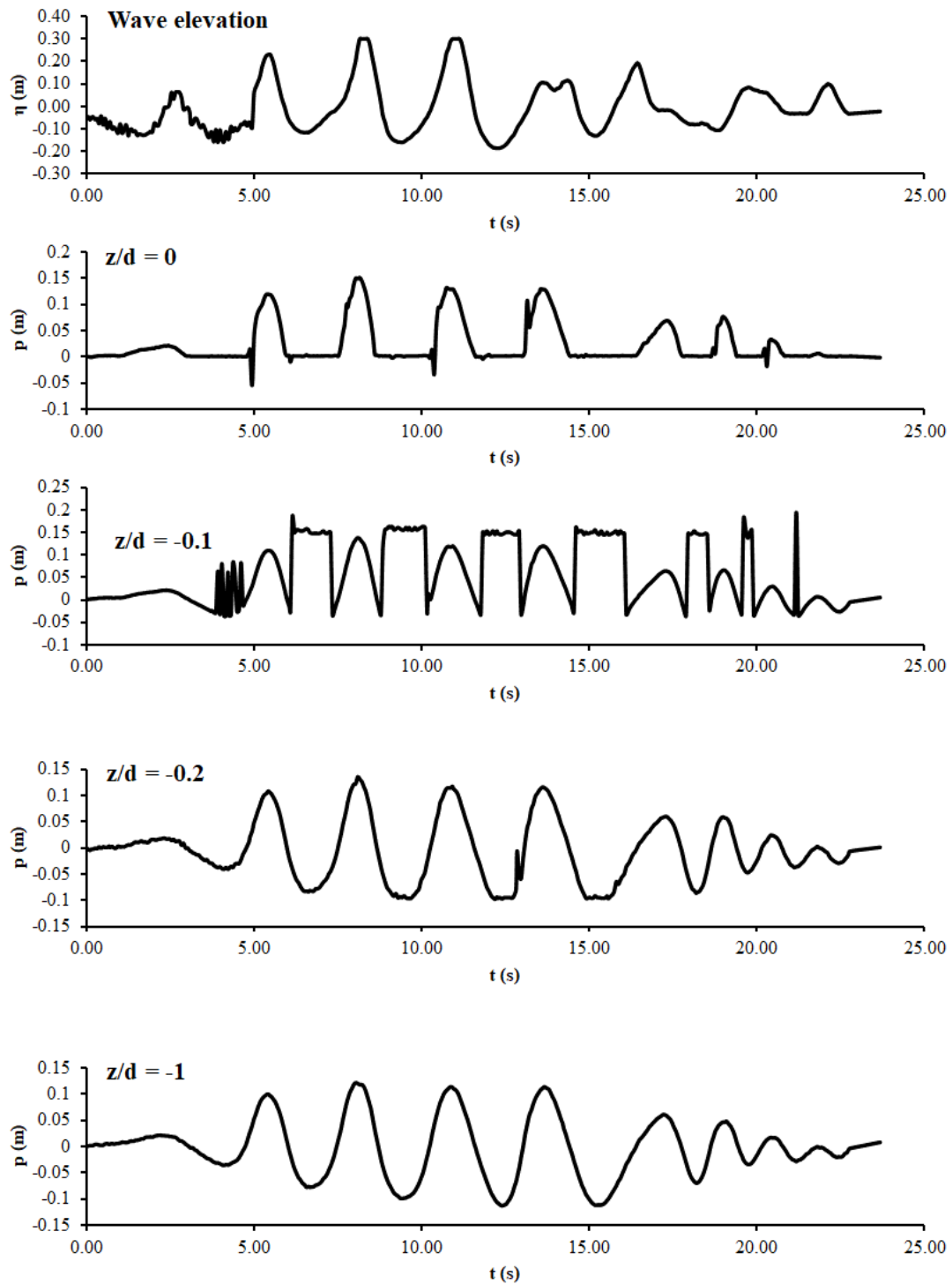
Figure. 4.9. Typical Time Histories of water surface Elevation and pressure along the depth of model (d/L = 0.08432, H_i/d= 0.36)

4.12 VARIATION OF RELATIVE WAVE PRESSURE (P/ρgd) WITH RELATIVE DEPTH PARAMETER (z/d) ON THE WALL FOR EXPERIMENTAL AND THEORETICAL APPROACHES

The artists and photographic view of the test model with toe protection are presented in Figure 4.9. Pressure transducers, P1 immersed at bottom of the test model, P2 sensor placed at a distance of 0.26 m from the position of P1 and P3, P4, P5, and P6 are positioned in a zigzag manner (Muni Reddy (2007)) at an equal height of 0.05 m depth from P2 as shown in Figure 4.11. The pressure transducers are completely immersed in wave action. Figures 4.12 to 4.15, illustrate the variation of relative wave pressure (P/ρgd) with relative depth parameter (z/d) on the front wall and it is compared with the corresponding values calculated by the theoretical formulae of Sainflou and Goda. The dynamic pressure distribution on the test model for varying wave characteristics along the depth of the wall (z/d= -1, z/d= -0.2, z/d= -0.1, z/d= 0) is studied. The variations of dimensionless pressure, P/ρgd, (where P, - Pressure, d, - the depth of water, g- acceleration due to gravity 9.81 m/s^2) with the relative depth parameter on the wall, z/d (z is negative below Still Water Level, SWL) is plotted in these graphs. Similarly, at still water level (z=0), the vertical particle accelerations are maximum and negative.
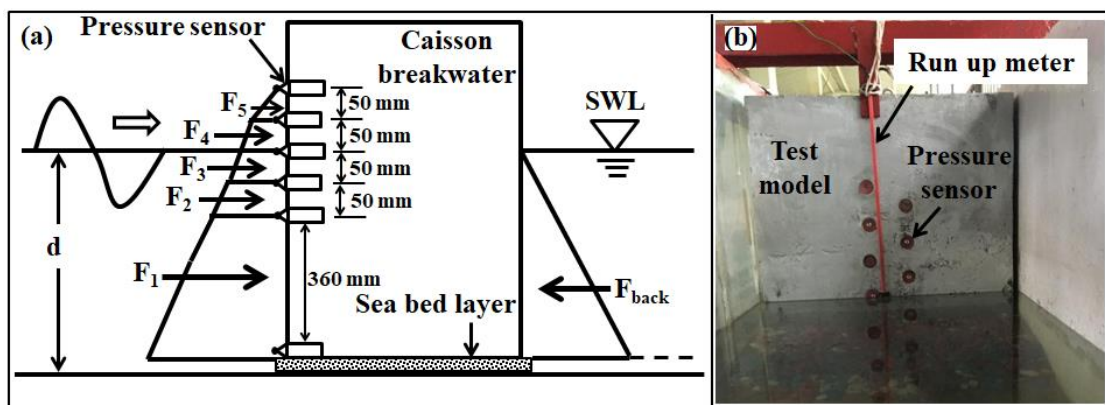
Figure 4.10: (a) Schematic diagram of pressure sensor locations and (b) photographic view of pressure sensors and run-up meter on the test model.

The dynamic pressure value reduces towards the bottom of the test model according to the cos hyperbolic reduction principle. From the unsteady Bernoulli equation, the pressure response factor kp becomes 1, at z=0 (at SWL). At any water depth (−z) under a wave crest, the wave pressure is at a peak and consists of the static pressure and dynamic pressure shown in (eq. 4.7).

$$P = -\rho gz \text{ (static Pressure)} + \rho gHKp/2 \text{ (dynamic pressure)} \qquad (4.7)$$
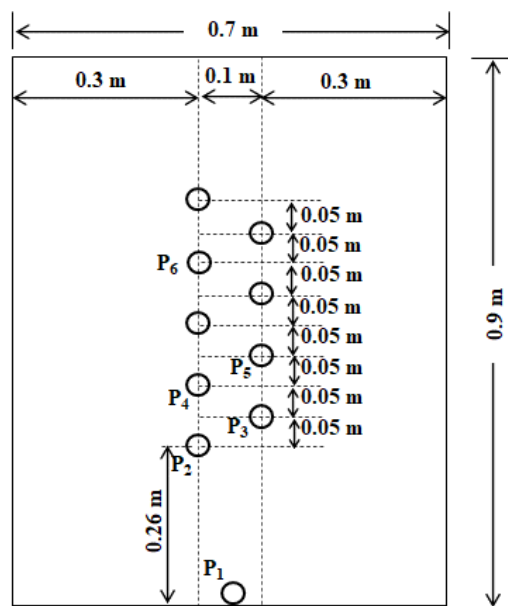
Figure. 4.11: Positions of Pressure Transducers
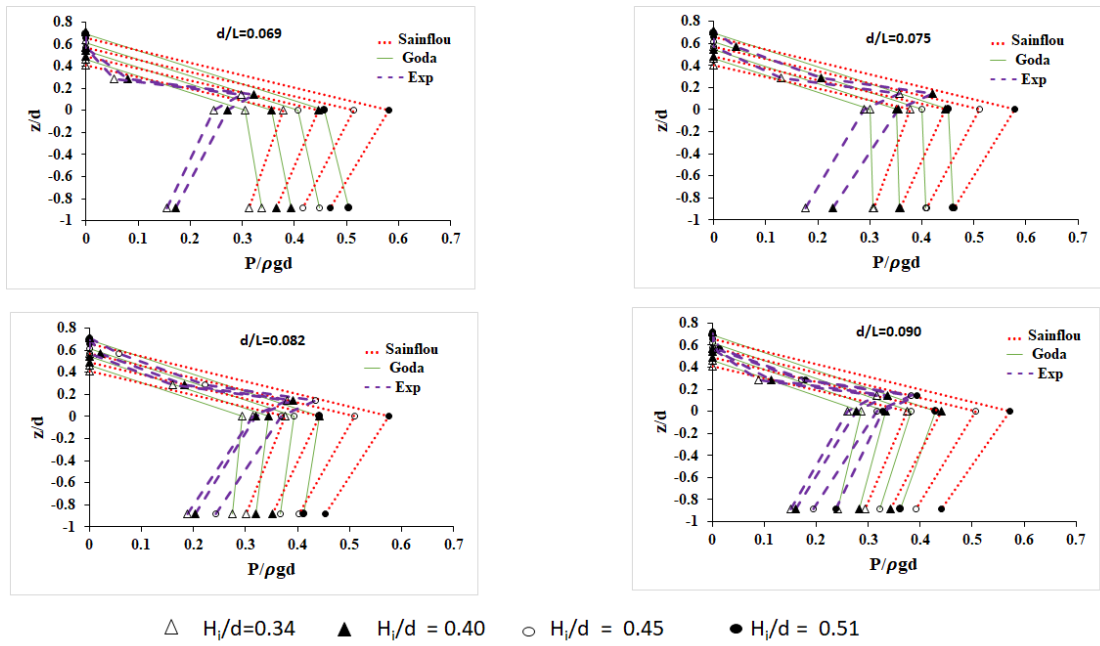
Figure 4.12: Variation of relative wave pressure (P/ρgd) with relative depth parameter on the wall (z/d), d = 0.35 m
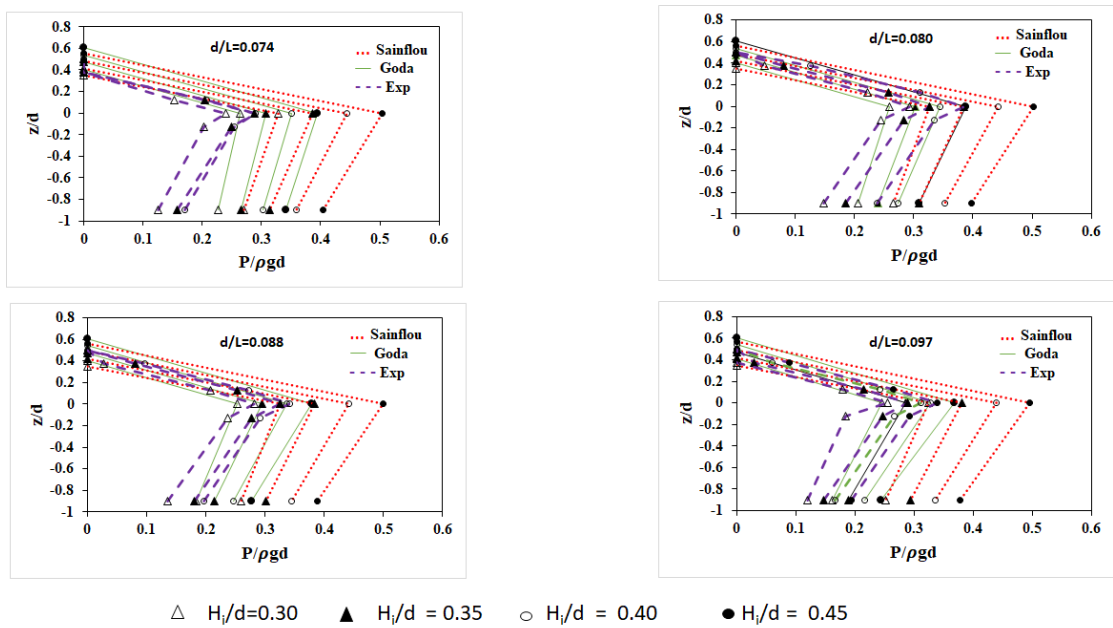
Figure 4.13: Variation of relative wave pressure (P/ρgd) with relative depth parameter on the wall (z/d), d = 0.40 m
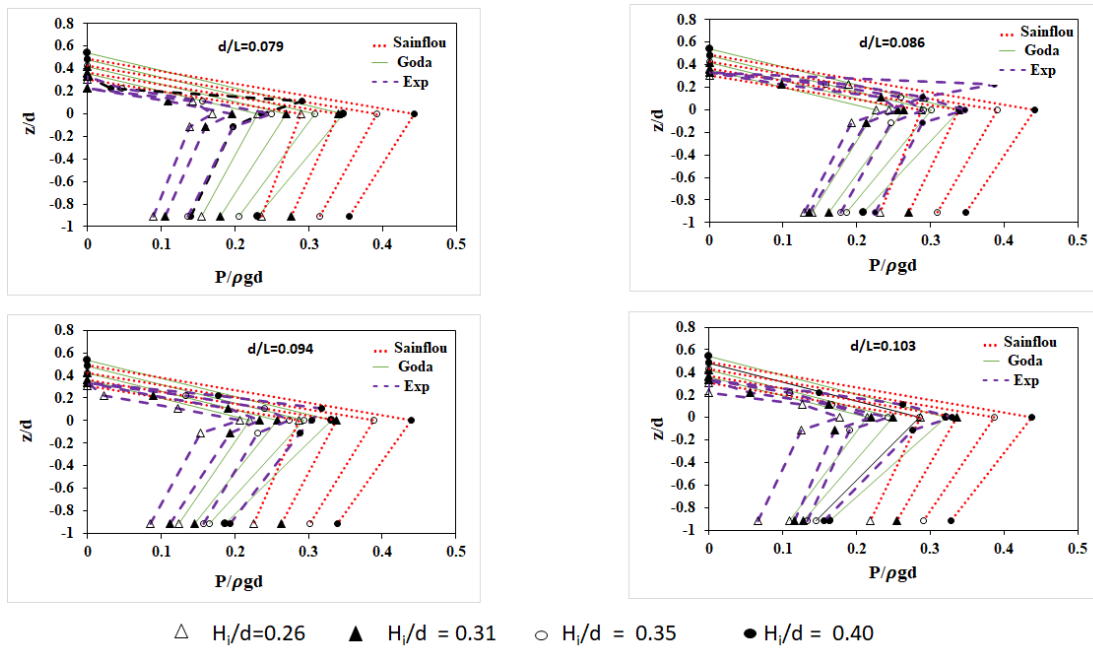
Figure 4.14: Variation of relative wave pressure (P/ρgd) with relative depth parameter on the wall (z/d), d = 0.45 m
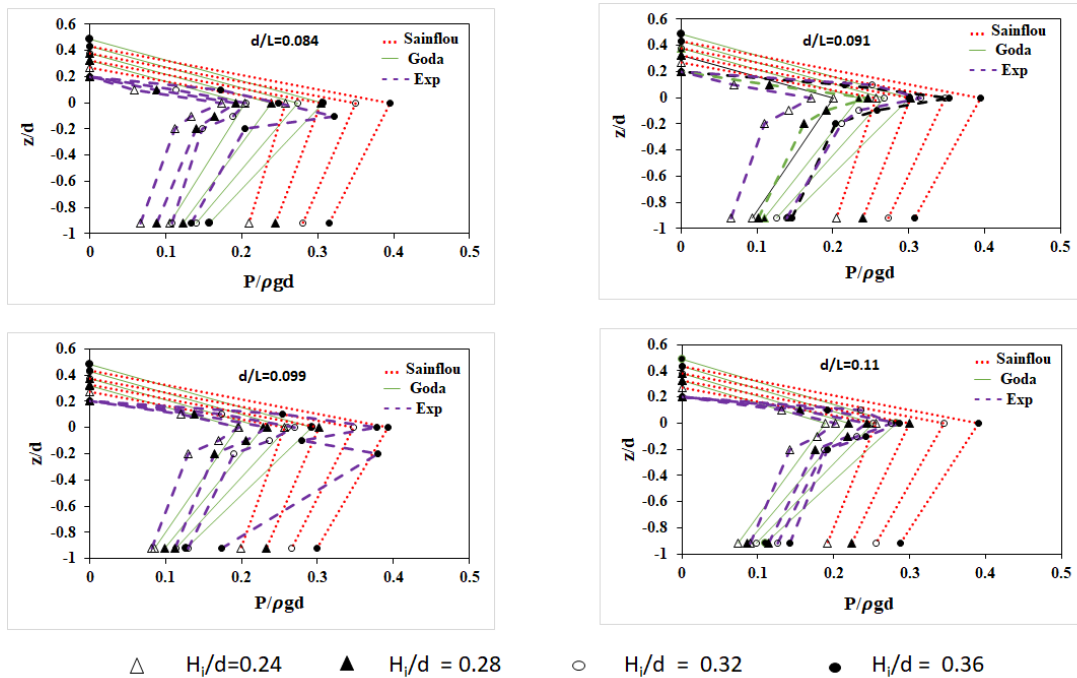
Figure 4.15: Variation of relative wave pressure (P/ρgd) with relative depth parameter on the wall (z/d), d = 0.50

The relative wave pressure is increasing with relative depth till the still water level, & it is maximum at still water level and then decreases with z/d & becomes minimum at the bottom of the wall. The wave pressure has a trapezoidal distribution both above and below the still water level, while the uplift pressure acting on the bottom of the upright section is assumed to have a triangular distribution which is similar to the Goda approach. The wave pressure is calculated using Sainflou's and Goda's theoretical approach. The relative wave pressure is found increasing with an increase in wave height and period, as long waves exert more pressure compared to short periods waves. The comparison of results reveals that the Sainflou method is overestimating the wave pressure by 15 % compared with the experimental results. Meanwhile, Goda's method provides a good estimation of dynamic pressure distribution which is comparable with the experimental results.

4.13 VARIATION OF RELATIVE FORCE PARAMETER ($F/\rho gd^2$) WITH INCIDENT WAVE STEEPNESS (H_i/L)

The horizontal wave force generated by the regular wave field is presented for a range of wave steepness (H_i/L) and relative depth parameter (d/L). The wave force F is made non-dimensional by dividing over the term (ρgd^2) and plotted on the y-axis. The x-axis indicates the wave steepness (H_i/L). The dashed-dot line dashed line, and solid line represents the theoretical results as shown in Figures 4.16 to 4.19. It is observed that the Sainflou method overestimates the wave force for an increasing wave steepness and increasing depth parameter.
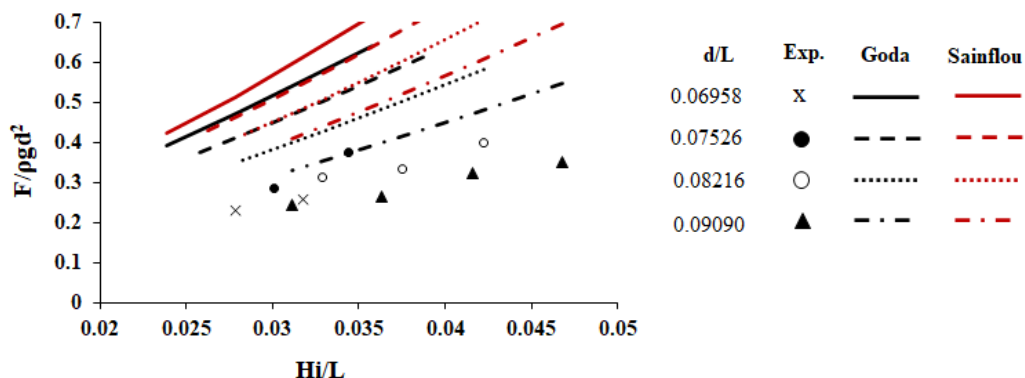
Figure 4.16: Variation of Wave force Parameter ($F/\rho gd^2$) with incident wave Steepness (H_i/L), for d=0.35 m

95
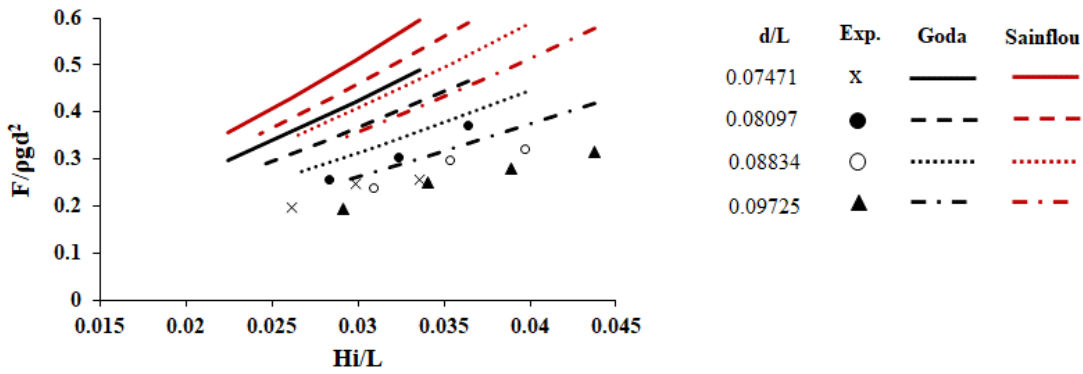
Figure 4.17: Variation of Wave force Parameter ($F/\rho gd^2$) with incident wave Steepness (H_i/L), for d=0.40 m
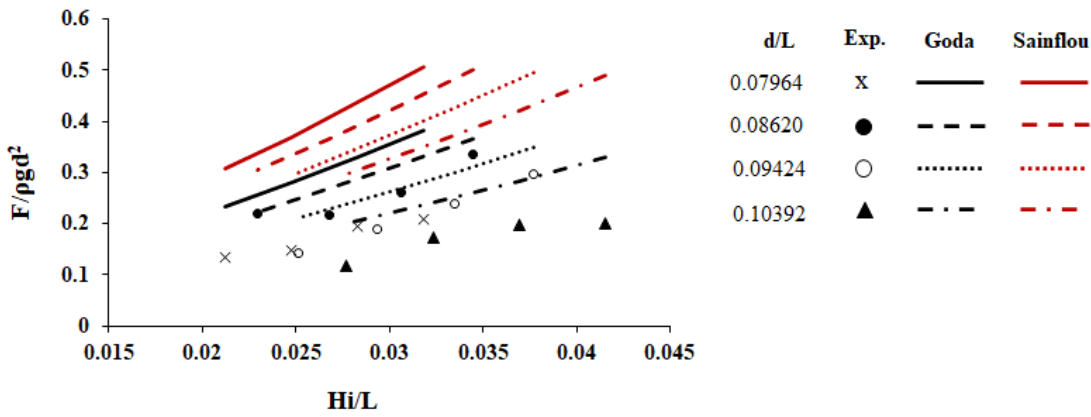
Figure 4.18: Variation of Wave force Parameter ($F/\rho gd^2$) with incident wave Steepness (H_i/L), for d=0.45 m
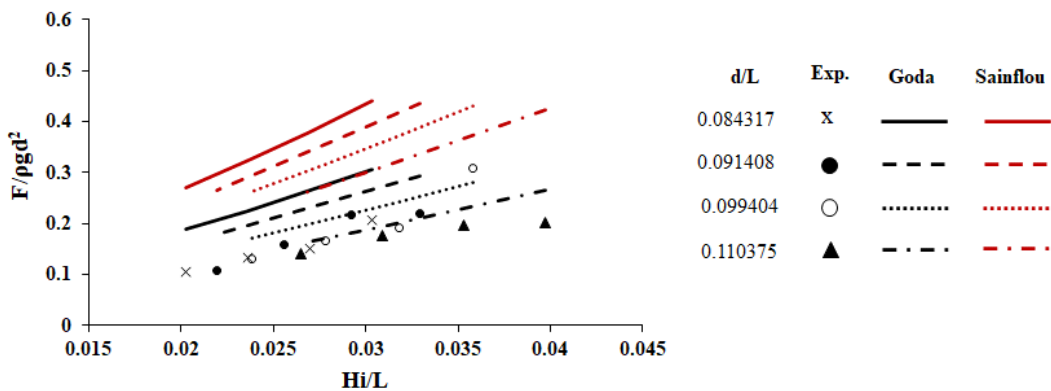
Figure 4.19: Variation of Wave force Parameter ($F/\rho gd^2$) with incident wave Steepness (H_i/L), for d=0.50 m

This increase may be due to the linear pressure distribution which is a simplification of the actual pressure distribution with z/d. Goda formula slightly underestimates the wave

96

forces in shallow water conditions and also provides a good estimation of wave force distribution compared with the experimental results for certain d/L (0.8 – 0.11) ratios.

4.14 EFFECT OF ON VARIATION OF RELATIVE WAVE RUNUP (R_u/H_i) WITH RELATIVE DEPTH PARAMETER (d/L)

The variation of relative wave run-up (R_u/H_i) as a function of relative water depth (d/L) is illustrated in Figure 4.20, for various relative wave heights (H_i/d). In general, the wave runup is defined as the vertical rise of water above the still-water level to which the water rushes up on the front face of the test model. This helps in determining the design wave crest level of the structure depending on the allowable overtopping level.
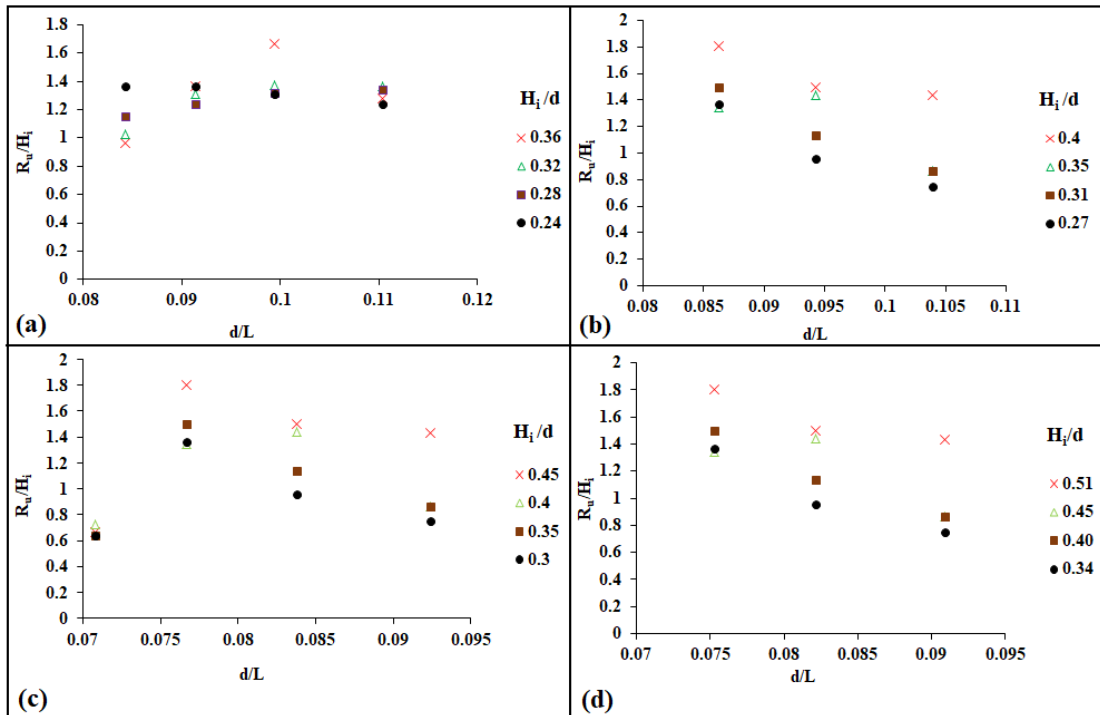
Figure 4.20: Variation of relative wave runup (R_u/H_i) with relative depth parameter (d/L) for (a) d = 0.5 m, (b) d = 0.45 m, (c) d = 0.4 m and (d) d = 0.35 m.

It is observed that the relative run-up (R_u/H_i) is decreasing with an increase in the relative depth (d/L) for the depths of water. The (R_u/H_i), increases with an increase in H_i/d because the higher wave heights rush up the waves above still water level. From the experimental results, the relative run-up (R_u/H_i) varies between 0.6 to 1.8.

4.15 INFLUENCE OF WAVE HEIGHT (H_i/d) ON WAVE REFLECTION COEFFICIENT (K_r)

Figure 4.21, shows the effect of wave height on the coefficient of reflection K_r, in terms of wave steepness, H_i/L for varying wave periods, and depth of water on a caisson-type breakwater. The wave surface elevation time histories from the wave probes are used to estimate the reflected wave heights (K_r). Three-wave probes are positioned at L (wavelength), L/3, and 2L/3 distance from the test model used to measure incident and reflected wave heights.
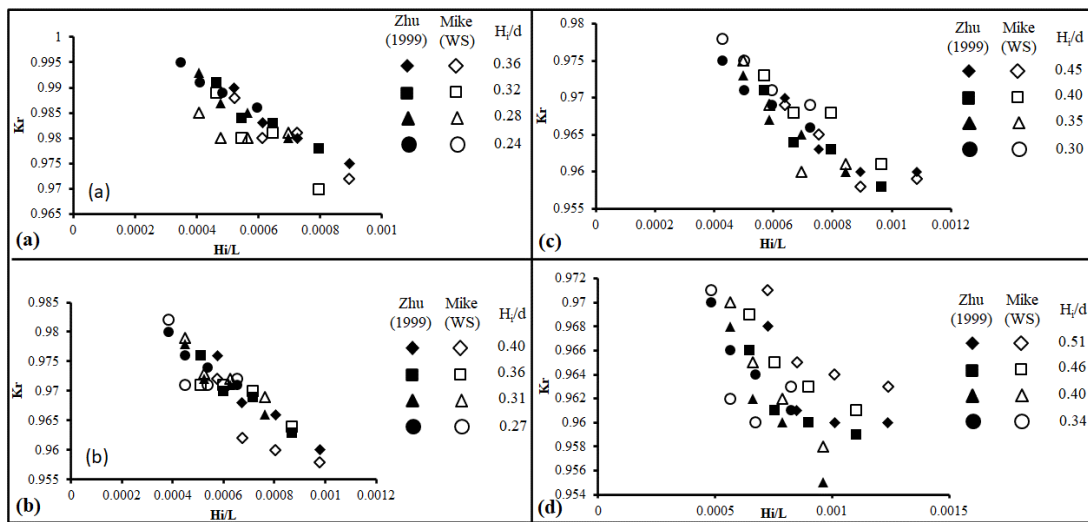
Figure 4.21: Variation of wave reflection coefficient (K_r) with wave steepness parameter (H_i/L), for (a) d = 0.5 m, (b) d = 0.45 m (c) d = 0.40 m and (d) d = 0.35 m.

The reflection coefficient K_r is obtained from the analysis of composite wave elevation using the transfer function method discussed by Zhu (1999) and also calculated using the MIKE Zero WS reflection analysis module, which is used for the calculation of wave reflection analysis. The analysis requires measurements of wave probe data at a minimum of two different locations are more to solve the governing equations by using the least-squares fit approach.

Based on the method proposed by Goda and Suzuki (1976), Mansard and Funke (1987) and extended by Zelt and Skjelbreia (1992). The wave reflection coefficient, K_r, is defined as the square root of the ratio of the area between the reflected wave to the incident wave. The reflection co-efficient K_r values decrease with an increase of H_i/L,

98

due to excessive dissipation of wave energy for the steeper waves. And it is observed that the reflection coefficient K_r is found to be more than 0.95 for both approaches.

4.16 STRUCTURAL STABILITY ANALYSIS

4.16.1 Stability Against Sliding

The horizontal forces caused by the wave action act upon the vertical wall, which tends to slide the structure, and the frictional force at the bottom contact surface is the resisting or stabilizing force. So, the stability against sliding is observed using the below expression (Goda Approach)

$$\mu \, (W-U) \geq P_{max} \tag{4.16}$$

$$\text{Factor of safety against sliding} = \mu \, (W-U) \, / \, P_{max} \tag{4.17}$$

Where

μ =   Coefficient of static friction,

W =   Total vertical force,

U =   Uplift force,

P_{max} = The maximum resultant horizontal force exerted on the vertical wall

4.16.2   Stability Against Overturning

The moment due to horizontal force about the toe of the vertical wall gives an overturning moment and the resisting or stabilizing moment is due to the self-weight of the structure about the same point. If the overturning moment exceeds the resisting moment, it results in the overturning of the structure. The stability against overturning is determined by comparing the resisting moments ($\Sigma \, M_R$) with the overturning moments ($\Sigma \, M_O$).

$$\text{The factor of safety against overturning} = \Sigma \, M_R \, / \, \Sigma \, M_O \tag{4.8}$$

The resisting moment should be higher than the overturning moments for the structure to be safe against overturning.

4.17 INFLUENCE OF DEPTH PARAMETER (d /gT²) ON FACTOR OF SAFETY (FOS)

The stability of vertical caisson breakwater is determined by the factor of safety against sliding and overturning. The lesser the factor of safety, the lower the stability of the structure. So, the factor of safety indicates the stability of the structure. In Figures 4.22 to 4.25, the factor of safety is plotted against the relative depth parameter (d/gT^2) for different wave characteristics.
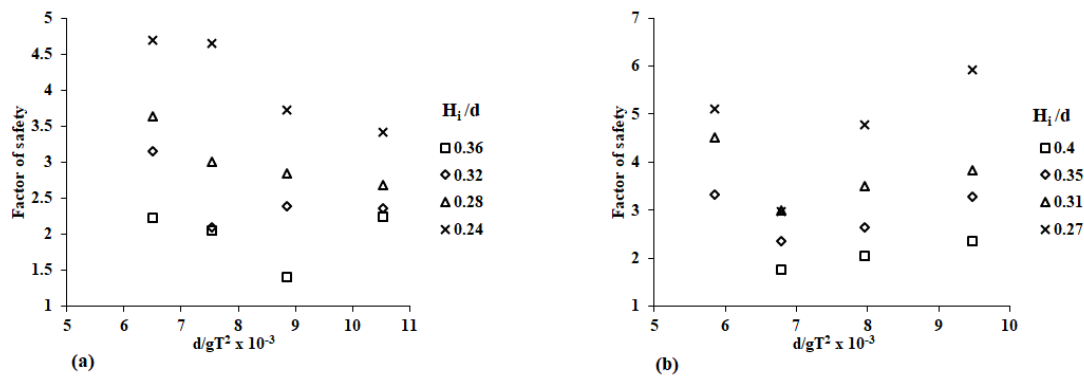
Figure 4.22: FOS against sliding for relative depth parameter (d/gT^2)

(a) for depth of water d=0.50 m (b) for depth of water d=0.45 m
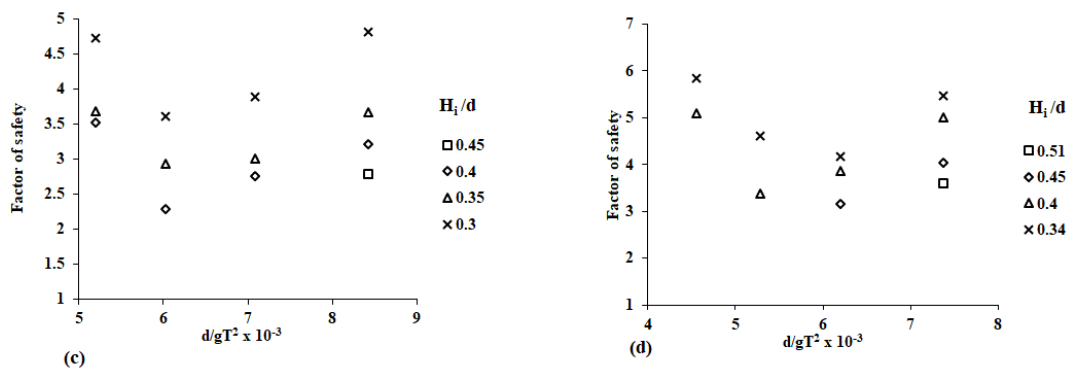
Figure 4.23: FOS against sliding for relative depth parameter (d/gT^2)

(b) depth of water 0.40 m (d) depth of water 0.35 m

100
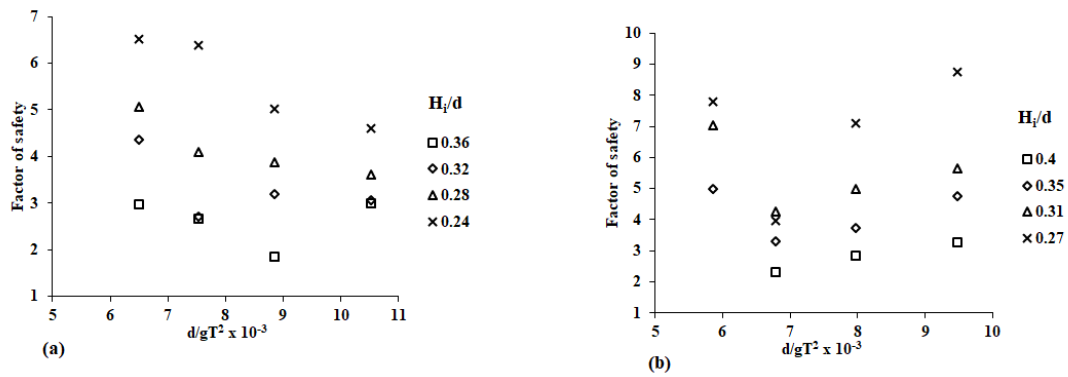
Figure 4.24: FOS against overturning for relative depth parameter (d/gT^2)

(a) depth of water 0.50 m (b) depth of water 0.45 m
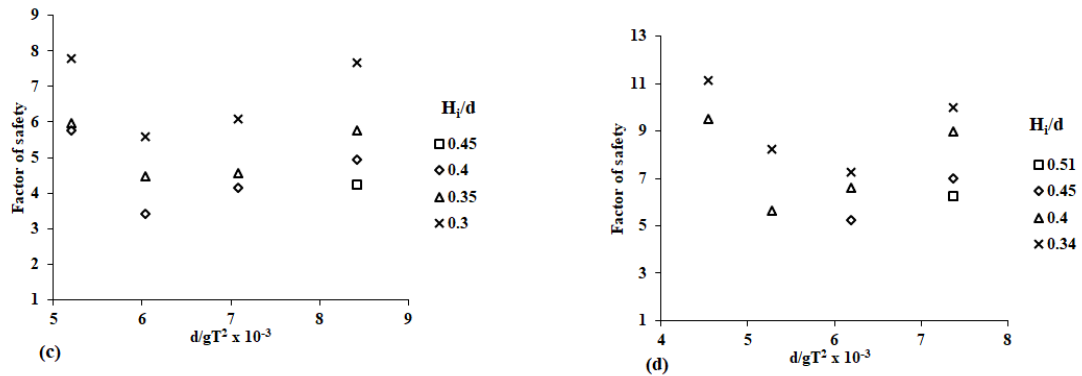
Figure 4.25: FOS against overturning for relative depth parameter (d/gT^2)

(a) depth of water 0.40 m (b) depth of water 0.35 m

It is observed that as wave height increases the factor of safety decreases. This is because, the increase in wave height increases the forces on a caisson, which intern reduces the factor of safety. In all test conditions, it is found that the factor of safety decreases with the increase of depth parameter for higher wave heights. Further from the observations, the factor of safety against sliding ranges from 5.9 to 2.1, and for overturning it ranges from 10.5 to 2.2 for the wave heights of 0.12 m to 0.18 m.

The factor of safety against sliding should not be lesser than 1.2 in the case of Goda (1985) approach, and should not be lesser than 1.5, as per IS 9527(Part I)-1981. Similarly, the factor of safety against overturning should not be less than 1.2 in the case of Goda's (1985) approach and should not be less than 2 as per IS 9527(Part I)-1981. It is found that the minimum FoS against sliding and overturning for the entire

range of experimental values are greater than the minimum FoS specified and hence the test model is safe against both sliding and overturning.

4.18 CLOSURE

In this section, the hydrodynamic performances of caisson/wall type breakwater are analyzed and a comparative study is also presented with an empirical approach. The main findings are outlined below point-wise.

- The dynamic pressure near the seabed is significantly less compared to the still water level because the vertical particle acceleration is maximum and it is negative. Goda's formula provides a good estimation of wave force distribution compared with the experimental results for certain d/L (0.8 – 0.11) ratios. Similarly, the Sainflou method is overestimating the wave forces by 15 % compared with the experimental results.

- The relative run-up (R_u/Hi) is decreasing with an increase in the relative depth (d/L) for the depths of water. The (R_u/Hi), increases with an increase in H_i/d because the higher wave heights rush up the waves above still water level.

- The reflection co-efficient K_r values decrease with an increase of H_i/L, due to more excessive dissipation of wave energy for the steeper waves. And it is observed that the reflection coefficient K_r is found to be more than 0.95 for both approaches.

- From the observations, the factor of safety against sliding ranges from 5.9 to 2.1, and for overturning it ranges from 10.5 to 2.2 for the wave heights of 0.12 m to 0.18 m. The factor of safety against sliding should not be lesser than 1.2 in the case of Goda (1985) approach, and should not be lesser than 1.5, as per IS 9527(Part I)-1981. Hence the test model is safe against both sliding and overturning.

NUMERICAL PERFORMANCE CHARACTERISTICS OF VERTICAL CAISSON TYPE BREAKWATER

5.1 BACKGROUND

The structural interaction of ocean waves is a common phenomenon for free-surface fluid flow hydrodynamics in coastal engineering. Understanding the fundamental physical properties and analytical computations is imperative to assess the various loads on coastal structures and their responses. Experimental studies on ocean wave structure interaction require well-sophisticated laboratory facilities and wave response measuring systems. The rapid development in modern computational methods resulted in CFD-based simulation of ocean wave structure interaction getting more popular. Many researchers are working on CFD-based simulations to study ocean wave hydrodynamics, sediment transport, ocean wave energy, etc., due to less time consumption, economical, and accuracy of results when compared to the experimental methods. In the recent past, many researchers (Xie et al., 1981; Xueping Gao et al., 1997; Kasem et al., 2011) have developed CFD models to simulate ocean waves, which are non-linear and unsteady in their behaviour. Xueping Gao et al. (1998) studied the clapotis interaction for broken waves along with vertical breakwater and classified their wave motions (standing wave, breaking clapotis, and broken clapotis). The authors concluded that broken clapotis is a more severe wave motion than the other two wave motions.

Xie et al. (1981) worked on experimental studies on the interaction of the clapotis wave with a vertical breakwater and simultaneously measured the maximum horizontal orbital velocity distributions for non-breaking wave conditions. George et al. (2019) studied the hydrodynamic performances of vertical slotted barriers with the combination of impermeable upper, and lower parts and a permeable middle part theoretically. And also, a comparative study is performed with experimental data and in StarCCM+. The combination of large eddy simulation and Volume of Fluid is performed to analyze the solitary waves propagating on single and double rows of vertical slotted piles (Yao et al., 2018). In a physical model study, the wave reflection

is analyzed by various methods available in the literature (Goda 1972, Mansard and Funke 1980, Zhu 1999, Isaacson 1991). Maguire et al. (2011) studied various beach slopes and recommended a slope value greater than 1:10. Similarly, Fabio et al. (2018) and Finnegan et al. (2012) investigated slopes 1:3 to 1:6, and both works concluded that 1:5 is the ideal slope condition. Elangovan (2011) investigated the effect of beach slope on wave reflection and concluded that a beach slope of 1:3 is better in reducing wave reflection.

Keeping this in view and to effectively dissipate wave energy for wide range of coastal engineering applications, a comprehensive study was attempted using the Reynolds Averaged Navier -Stokes (RANS) equation.

5.2 THEORETICAL METHOD

5.2.1 Stokes Wave Theory

Stokes wave theory, a nonlinear one, describes regular finite amplitude progressive waves. Real waves have shorter crests and deeper troughs, while sinusoidal waves have the same height and length of crests and troughs, respectively. The equation in the dimensional form of Laplace is given in Eq. 5.1. At the same time, the wave steepness H_i/L is small but not infinitely small as for regular waves. This assumption is reasonable since, in actual waves, the steepness never exceeds 0.10-0.15.

$$\nabla^2\emptyset = \frac{\partial^2\emptyset}{\partial x^2} + \frac{\partial^2\emptyset}{\partial x^2} = \emptyset_{xx} + \emptyset_{zz} = 0 \tag{5.1}$$

The boundary conditions to be satisfied are the free surface kinetic boundary condition

$$\emptyset_{z\,=}\,0\ ; \qquad\qquad z = -h \tag{5.2}$$

$$\eta_t\,0 +\ \emptyset_x\eta_x - \emptyset_z = 0\ ;\ z = -\eta \tag{5.3}$$

$$\eta + \frac{1}{2g}(\emptyset_x^2 + \emptyset_z^2) + \frac{1}{g}\emptyset_t = \frac{C(t)}{g}\ ;\ z = \eta \tag{5.4}$$

Where C(t) is the arbitrary function in the generalized Bernoulli equation.

In addition, we assume the waves are periodic in x, which we express as

$$\emptyset_x(0, z, t) = \emptyset_x(L, z, t) = 0 \tag{5.5}$$

The dimensional form of the equations and solutions are based on the assumption that if we define the parameter γ as

$$\gamma = \delta\epsilon = \frac{H}{h}\frac{h}{L} = \frac{H}{L} \tag{5.6}$$

Then we have nonlinear terms = $O(\gamma)$. Linear terms.

$$\eta = a\cos\theta + \frac{\pi}{L}a^2 f_2\left(\frac{d}{L}\right)\cos 2\theta + \left(\frac{\pi}{L}\right)^2 a^3 f_3\left(\frac{d}{L}\right)\cos 3\theta \tag{5.7}$$

Equation (1) gives the free surface elevation (η) of the wave according to Stokes third-order theory. Where a = amplitude of the wave for the first-order term in the expression of surface elevation, d= water depth (m), L= wavelength (m).

$$f_2\left(\frac{d}{L}\right) = \frac{\cosh\frac{2\pi d}{L}\left(\cosh\frac{4\pi d}{L} + 2\right)}{2\left(\sinh\frac{2\pi d}{L}\right)^3} \tag{5.8}$$

$$f_3\left(\frac{d}{L}\right) = \frac{3}{16} \cdot \frac{8\left(\cosh\frac{2\pi d}{L}\right)^6 + 1}{\left(\sinh\frac{2\pi d}{L}\right)^6} \tag{5.9}$$

In the third-order approximation, the eq. (5.7) can be written as

$$\eta = a_1\cos\theta + a_2\cos 2\theta + a_3\cos 3\theta \tag{5.10}$$

And finally, the stokes higher-order expressed in eq.8

$$c^2 = \frac{gL}{2\pi} \tanh\frac{2\pi d}{L}\left\{1 + \left(\frac{2\pi a}{L}\right)^2 \frac{\cosh\frac{8\pi d}{L} + 8}{8(\sinh\frac{2\pi d}{L})^4}\right\}$$ (5.11)

The eq 5.11 (stokes higher-order) waves have dispersive frequency and amplitude.

5.3 MATHEMATICAL FORMULATION AND NUMERICAL SIMULATION

The numerical model implemented in the present study using Fluent is a computational fluid dynamics toolbox within the framework of Ansys. It is based on the finite volume Reynolds-Averaged Navier-Stokes (RANS in Eq. 5.12 and 5.13) (where u_i is the velocity component averaged over time t, p is the fluid pressure, and ρ is the fluid density) multiphase solver and assumes that the fluids (air and water) are incompressible and viscid. The parameters in the computational domain for the two fluids are solved simultaneously in the governing equations, including mass conservation and momentum conservation. The additional terms represent the effects of turbulence
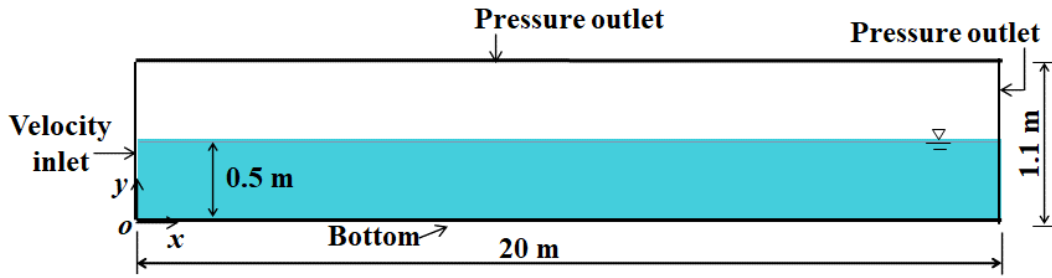
Figure. 5.1: Geometry of the flume model with boundary conditions.

Navier-Stokes's equation and continuity equation are used to formulate the nonlinear and free surface wave motion. The water is assumed to be incompressible, Newtonian fluid, and the density of water does not change with time. The computational domain of the numerical 2D-wave flume model and its dimensions are given in Figure 5.1. Reynolds stresses defined by $-\overline{u_i' u_j'}$; νT is the eddy viscosity and can be defined as $V_T = C_\mu k^2 / \varepsilon$, k is the turbulence kinetic energy, and its rate of dissipation is ε. C_μ is a constant and is defined as 0.0845. (Ansys Fluent User's Guide, 2019).

106

$$\frac{\partial u_i}{\partial x_i} = 0 \tag{5.12}$$

$$\frac{\partial u_i}{\partial t} + u_j \frac{\partial u_i}{\partial x_j} = -\frac{\partial p}{\partial x_i} + \frac{\partial}{\partial x_j}\left[(v + v_T)\left(\frac{\partial u_i}{\partial x_j} + \frac{\partial u_j}{\partial x_i}\right)\right] + \frac{\partial}{\partial x_j}\left(-\overline{u_i' u_j'}\right) \tag{5.13}$$

$$\nabla \cdot u = 0 \tag{5.14a}$$

$$\rho\left(\frac{\partial u}{\partial t}\right) = -\nabla p + \nabla^2 \mu + F_e \tag{5.14b}$$

Navier-Stokes equation in two-Dimensional Cartesian coordinate systems can be rewritten as

$$\rho\left(\frac{\partial u}{\partial t} + u\frac{\partial u}{\partial x} + v\frac{\partial u}{\partial y}\right) = -\frac{\partial p}{\partial x} + \mu_w\left(\frac{\partial^2 u}{\partial x^2} + \frac{\partial^2 u}{\partial y^2}\right) + \rho g_x \tag{5.15a}$$

$$\rho\left(\frac{\partial v}{\partial t} + u\frac{\partial v}{\partial x} + v\frac{\partial v}{\partial y}\right) = -\frac{\partial p}{\partial x} + \mu_w\left(\frac{\partial^2 v}{\partial x^2} + \frac{\partial^2 v}{\partial y^2}\right) + \rho g_y \tag{5.15b}$$

Where u and v are components of the velocity field in the x and y-direction, respectively. P is the fluid pressure and ρ is density. μ_w is the kinematic viscosity and g_x and g_y are the gravitational acceleration components. In Eq. (5.14b), the first term corresponds to the inertial forces; the second term corresponds to pressure/forces; the third term corresponds to viscous forces; the fourth term corresponds to external forces applied to the fluid. Eqs. 5.15 a and 5.15 b represent the Navier-Stokes equation in a 2D Cartesian coordinate system. Eq. 5.16 presents the continuity equation, Eq. 5.17 presents the continuity equation for incompressible flow and Eq. 5.18, based on the conception of the control volume, the motion of the free surface is tracked by solving the transport equation of the VOF function.

$$\frac{\partial}{\partial x}(\rho x) + \frac{\partial}{\partial y}(\rho y) + \frac{\partial \rho}{\partial t} = 0 \qquad (5.16)$$

$$\frac{\partial u}{\partial x} + \frac{\partial y}{\partial y} + \frac{\partial w}{\partial z} = 0 \qquad (5.17)$$

$$\frac{\partial F}{\partial t} + u_i \frac{\partial F}{\partial x_i} = 0 \qquad (5.18)$$

F is the volume fraction of fluid in the control volume, defined as 1 in the fluid, 0 in the void, and $0 < F < 1$ at the free surface. The primary focus of the study is on numerical wave generation and consequently free surface elevation capture. Hence, for surface tracking Volume of the Fluid method is taken into consideration. Hirt et al. (1981) developed the volume of fluid (VOF) method to solve the two-phase problems. The kinematic free surface boundary condition and dynamic free surface boundary conditions are presented and satisfied using Volume of Fluid in Ansys - Fluent. In the present work, the governing equations are solved considering the relevant boundary conditions for the computational domain. At the vicinity of the water surface elevation, the mesh densities are increased for better capture of wave surface elevation.

5.4 SOLVER CONTROLS

Fluent offers a wide variety of solvers which can affect the solution quality and convergence. The segregated solver is the solution algorithm used by ANSYS Fluent for this class of problems. Using this approach, the governing equations are solved sequentially (i.e., segregated from one another). Because the governing equations are non-linear, several iterations of the solution loop must be performed before a converged solution is obtained. The non-Iterative Time Advancement (NITA) technique is also available and has been shown to speed up the iteration process significantly (ANSYS Fluent User Guide, 2020). The idea underlying the NITA scheme is that, to preserve overall accuracy, it is not necessary to reduce the error from each sequential solution step to zero, but only to make it the same order as the time discretisation error. The computational flow of the NITA scheme, as seen in Figure 5.2 illustrates that only a

single global iteration per time step is performed. Sub-iterations are performed within each time step, but the outer, velocity-pressure iteration is performed just once (hence the term "non-iterative") within a given time step which significantly speeds up simulations. This approach effectively drives the error in each sub-iteration to the time discretisation error, not zero and has the net effect of allowing a computation in the order of 3 to 4 times faster than standard iterative techniques.

```
                    ┌─────────────────┐
          ┌────────→│   t = t+n Δ t   │
          │         └────────┬────────┘
          │                  ↓
          │         ┌─────────────────┐   No    ╱───────────────╲
          │         │ Solve u and v   │←────────┤  Converged ?  │
          │         │   equations     │         ╲───────────────╱
          │         └────────┬────────┘                  │ Yes
          │         ←────────┤←───────────────────────────
          │         ┌─────────────────────────────┐  No   ╱───────────────╲
          │         │ ┌─────────────────────────┐ │←──────┤  Converged ?  │
          │         │ │ Solve Pressure Correction│ │       ╲───────────────╱
          │         │ └─────────────────────────┘ │              │ Yes
          │         │ ┌─────────────────────────┐ │
          │         │ │Correct velocity Pressure Flux│
          │         │ └─────────────────────────┘ │
          │         └────────┬────────────────────┘
          │         ←────────┤←───────────────────────────
          │         ┌─────────────────┐   No    ╱───────────────╲
          │         │ Solve k and ξ   │←────────┤  Converged ?  │
          │         │     Flux        │         ╲───────────────╱
          │         └────────┬────────┘                  │ Yes
          │         ←────────┤←───────────────────────────
          │         ┌─────────────────┐
          │         │ Solve other     │
          │         │    scalars      │
          │         └────────┬────────┘
          │                  ↓
          │         ┌─────────────────┐
          └─────────│   Next time     │
                    │     n+=1        │
                    └─────────────────┘
```
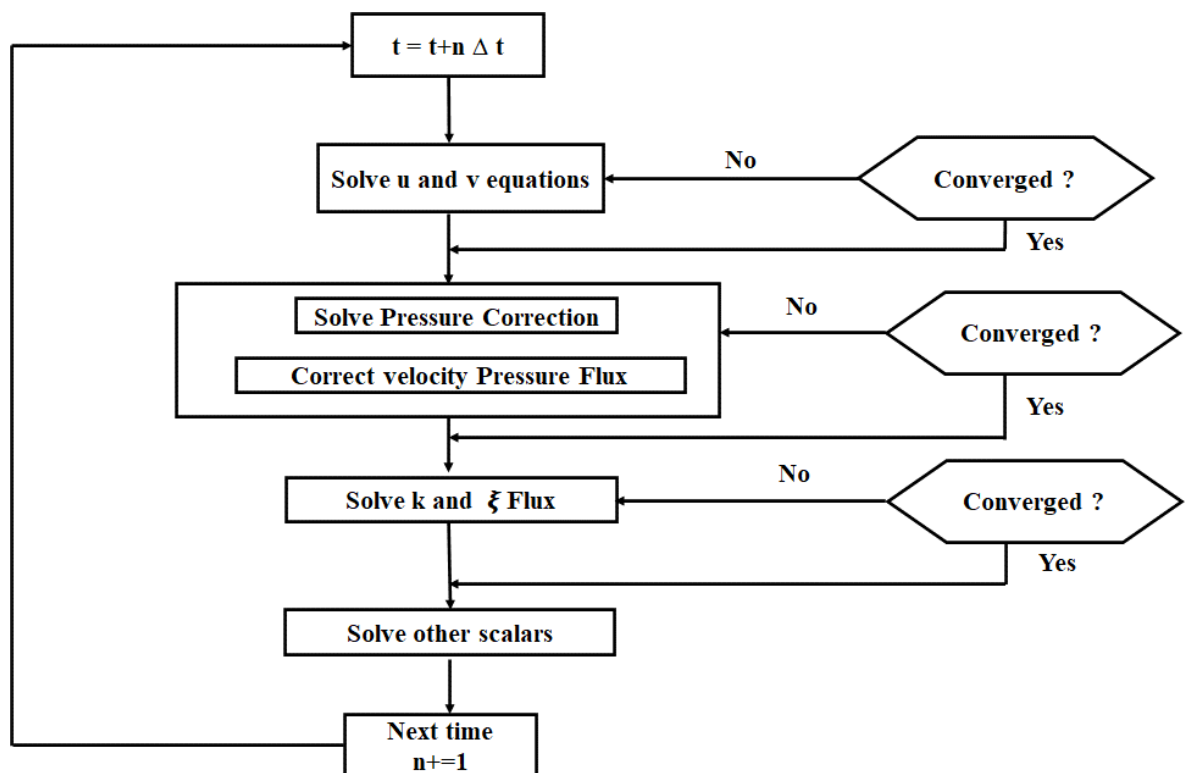
Figure 5.2: Non-Iterative Time Advancement flow chart
(ANSYS Fluent User Guide, 2020)

Because of the non-linearity of the equation set being solved, it is necessary to control the change of variables. This is achieved by a process called under-relaxation. This process effectively reduces the change of each variable, ϕ, during each iteration. In a simple form, the new value of the variable within a cell depends upon the old value plus the computed change in the variable multiplied by the under-relaxation factor, α.

5.5 PRELIMINARY INVESTIGATION

The preliminary investigation is carried out to arrive at suitable wave flume length, mesh or grid size and beach slope by using a numerical tool based on computational fluid dynamics. At first, a numerical wave flume (NWF) is created with different mesh sizes to select the optimum mesh size. In addition, different beach slope conditions are introduced such as 1:3, 1:5 and numerical beach at the far end of the NWT to optimize the wave reflection solutions. In the sub-sections, an elaborate discussion is carried out to arrive at an optimum numerical wave flume for the study.

5.5.1 Modelling of geometry

A 2-D NWF geometrical model has a length of 20 m, and a height of 1.1m with a 0.5 m water depth, and the NWF length is chosen to be twice the wavelength (L) of the maximum L considered in the study. It is enough to generate a fully matured wave to capture the proper wave-structure interaction. So that the wave-making area is not influenced by wave reflection from the downstream end. (Length of NWF as 20m (>12m)), and the height of NWF is kept the same as the experimental setup. The geometrical model is designed by the Ansys design modeller tool. The geometry for numerical simulations for varying beach slopes with boundary conditions is illustrated in Figure 5.3. Similarly, the slope characteristics are tabulated in Table 5.1.
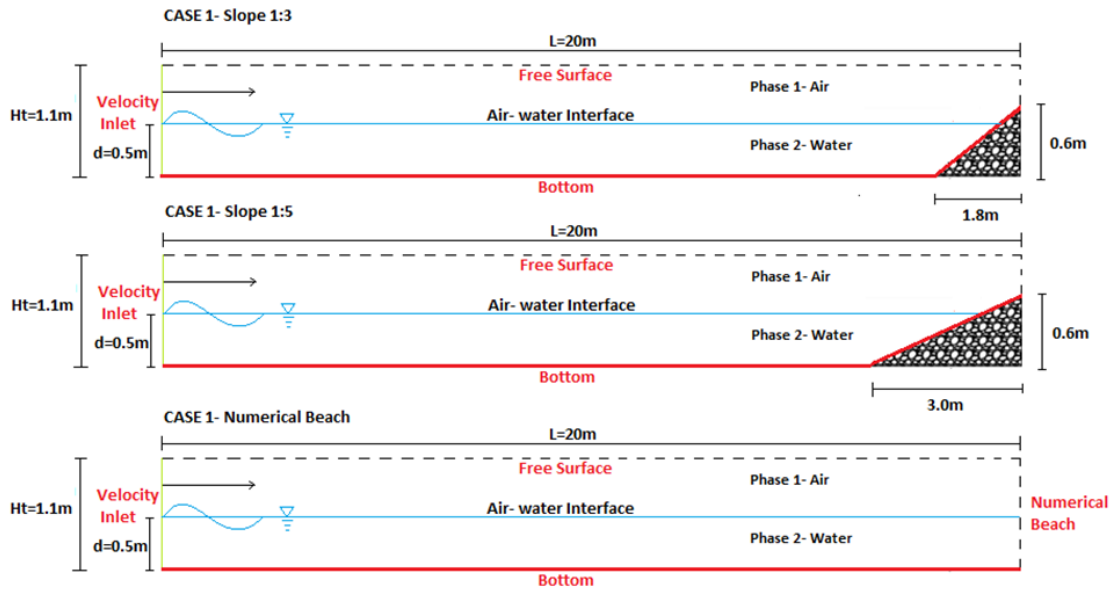
Figure 5.3: Schematic NWF with boundary conditions and varying beach slopes
(not to scale)

Table 5.1 Slope Characteristics

Slope Characteristics	Case 1- Slope 1:3	Case 2- Slope 1:5	Case 3- Numerical Beach
V	0.6m	0.6m	-
H	1.8m	3.0m	-

The general steps involved in numerical simulation of ANSYS - FLUENT can be broadly classified into three. Pre-processing, Solver, and Post-processing. Pre-processing can be subdivided into Geometry building, Meshing, and defining the boundary conditions, as illustrated in Figure 5.4.
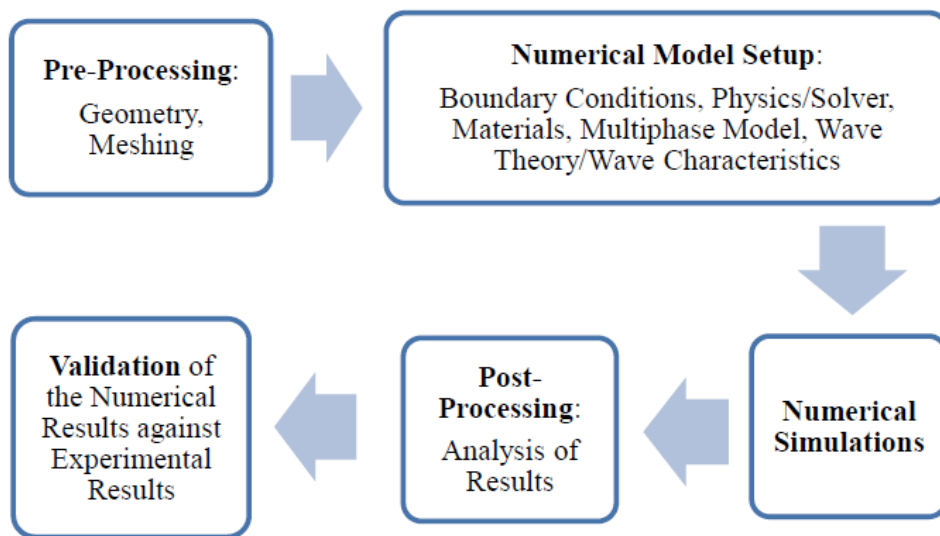
Figure 5.4: Workflow in Numerical Simulations Ansys-Fluent.

5.5.2 Meshing details

The suitable mesh selection determines the solution's accuracy, stability, and computational efficiency. Hence, in this segment, we devote a detailed discussion on the grid size or mesh details. The numerical grid pattern is created using the Ansys mesh tool. Using the face meshing method, the solution region is split into square elements of chosen dimensions, and then a structured mesh is created. Initially, to determine the effect of mesh size on the accuracy of ANSYS Fluent results, a two–dimensional numerical wave tank is modelled, and the wave surface elevations are obtained. The computational simulations are carried out for three mesh sizes, viz. 0.01m x 0.01m. 0.02m x 0.02m and 0.03m x 0.03m as shown in Figures. 5.5 (a-c). Table 6.2 shows the base grid dimensions for which the trials are carried out. Havn (2011) recommended the criteria for sizing the mesh and time step for better accuracy. The mesh size parameters are illustrated in Table 5.2.
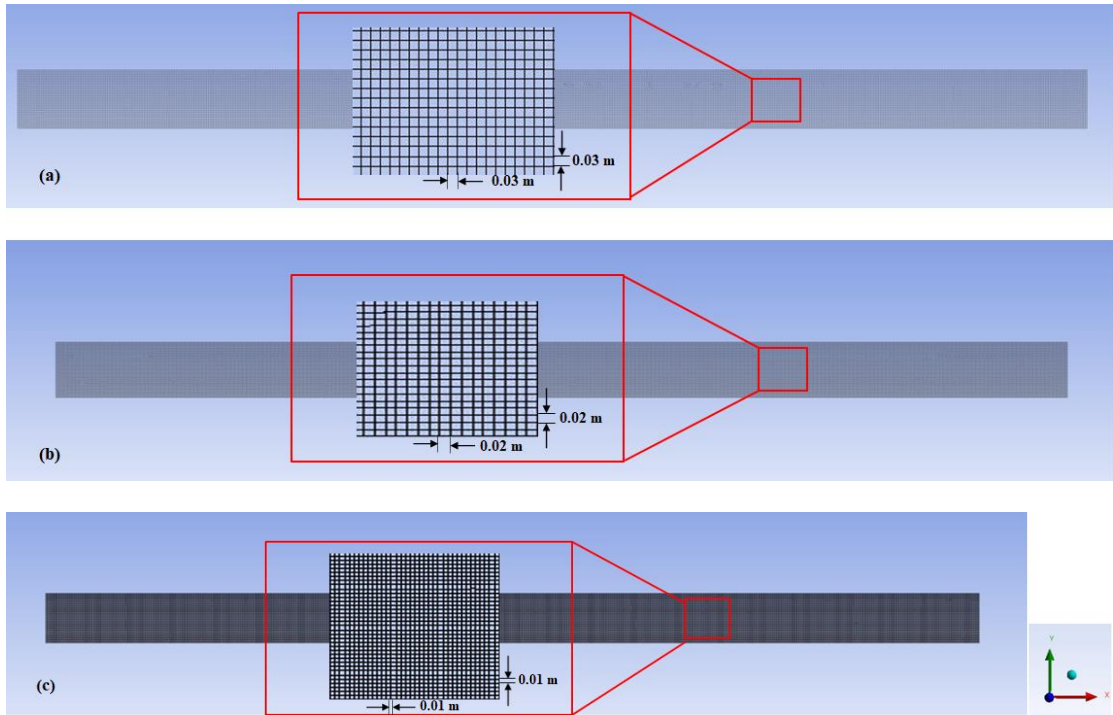
Figure 5.5: (a-c) Fluent meshing closer to the test model.

Table 5.2 Grids Parameters

Meshing Details	Δx (m)	Δz (m)	Grid Cell Density	No. of Elements	No. of Nodes
1.	0.03	0.03	200	24076	24775
2.	**0.02**	**0.02**	**300**	**55742**	**56796**
3.	0.01	0.01	600	220008	222119

From the mesh convergence results obtained for the cases mentioned above, inferences are drawn that higher grid cell density gives more accurate results. But the computational time is very high compared to the normal. Hence, it can be concluded that higher grid cell density is preferred for more accurate results while increasing the nodes and elements in the computation domain with finer mesh results more in time. But from the mesh convergence study shown in Table 5.3, the grid size of 0.02 m is observed with similar trends compared with the 0.01 m grid size. Hence, for the present study, the numerical wave flume meshes into structured square meshes of 0.02 m grid size, and the whole structure meshes uniformly into a square structured mesh of 0.02 m x 0.02 m. Due to that, the computational time reduces since fewer elements are used.

113

Meanwhile, varying the beach slope at the downstream end of NWF doesn't significantly affect mesh size.

Table 5.3 Mesh convergence study

Mesh size	0.01 m	0.02 m	0.03 m
	0.10	0.10	0.11
Incident Wave Height (m)	0.12	0.12	0.13
	0.14	0.14	0.16

5.5.3 Boundary Conditions

As we solve the 2nd order governing equation in 2-D, we need four boundary conditions to get the solution mathematically. Here in the physical domain, we have the following four boundary conditions.

(i)   Inlet = velocity inlet

(ii)   Outlet = pressure outlet

(iii)   Bottom = wall (no-slip condition)

(iv)   Top = free surface

The boundary conditions are illustrated schematically in Figure 5.6.
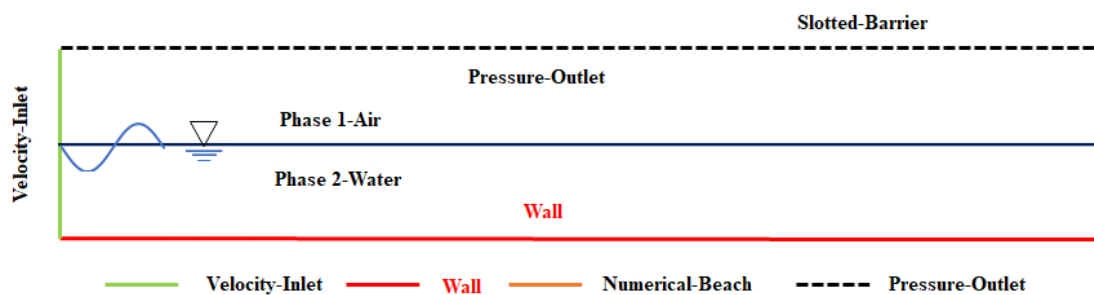
Figure 5.6: Boundary conditions

The numerical wave flume involves multiple phases, i.e., air and water. Flowing media (water) is always set as the secondary phase, and the medium over that is a primary phase (air). Fluent automatically assumes that the preliminary phase species is present in every cell unless otherwise mentioned. Creating the secondary phase (water) within the domain is assigned over the required portion to provide a constant fill level equal to

114

the chosen water depth (d=0.5m). For clarity, the actual boundary conditions are shown in Figure 5.6. The ocean wave is generated using a User Defined Function (UDF) to the inlet velocity boundary within the Fluent analysis module. A unique UDF is created in the setup part for each water depth (d), wavelength (L), wave height (H), and wave period (T) combination.

As an initial condition, static pressure is given for the liquid face, and the free surface between the air and water interface is generated by the volume of the fluid model (VOF). The implicit formulation is used for the volume fraction parameter.
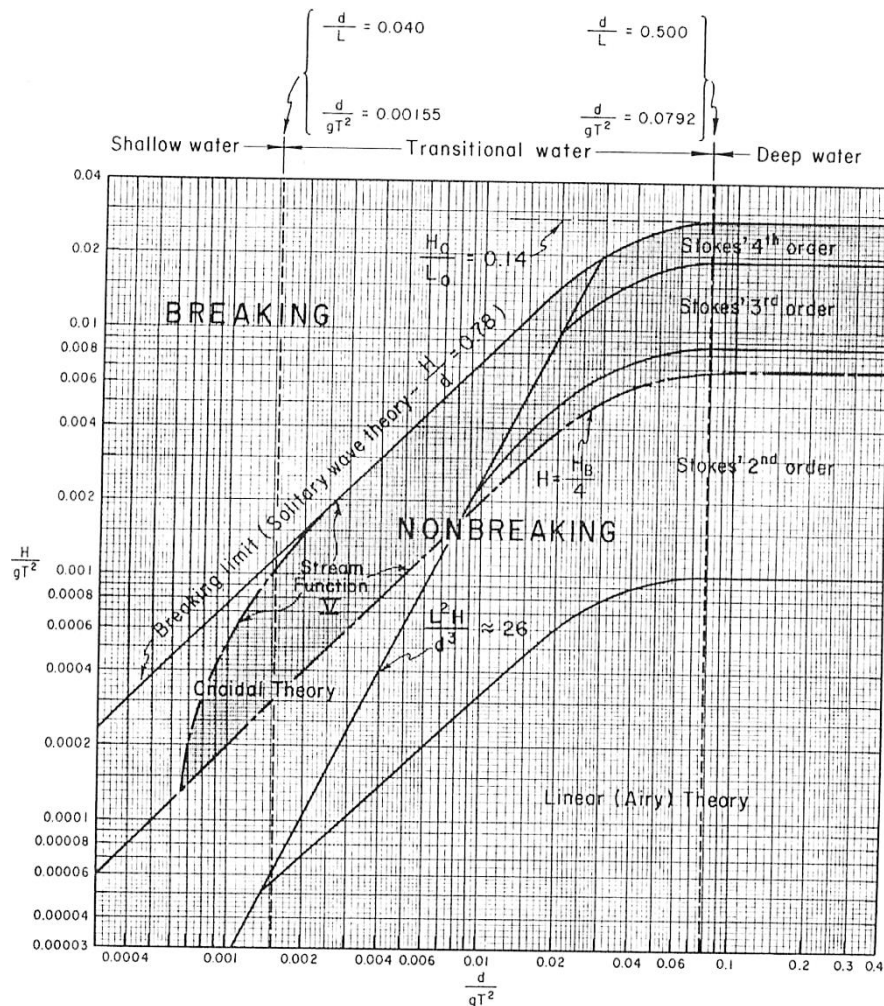
Figure 5.7 Ranges of validity for various wave theories (Le Mehaute, 1969)

The numerical simulations are frameworks with two-phase air and water, having a constant density of 998 kg/m^3 for water and 1.225 kg/m^3 for air. The turbulence model

chosen is a standard k-ε viscous model. To simulate the wave condition, the wave theory is selected based on the plot given by Le Mehaute (1969), wherein the analysis involves the wave conditions from (1/20 ≤ d/ L ≤1/2) shown in Figure 5.7.

5.5.4 Wavemaker Theory

The wave height in a physical model study is resolved by the amplitude and frequency of the wave plate (Dean and Dalrymple, 1984). The wavemaker driven by an electric motor on the other side of motor rotation is attached to a flap or piston-type wave marker. The wavemaker theory introduces a relation between the wall movement at the wave-making side of NWF and the free surface elevation originating from that same movement. For d/L ≤ 0.05 shallow-water waves, a simple theory is introduced by Galvin in the year 1964 for the propagation of a wave profile. The flap-type wavemaker with a hinged end possesses a maximum stroke S. The water depth in the towing tank is d. The displaced water volume by the flap deviation is 0.5 x S x d (where S is stroke and d (or h) – depth of water as illustrated in Figure 5.8.
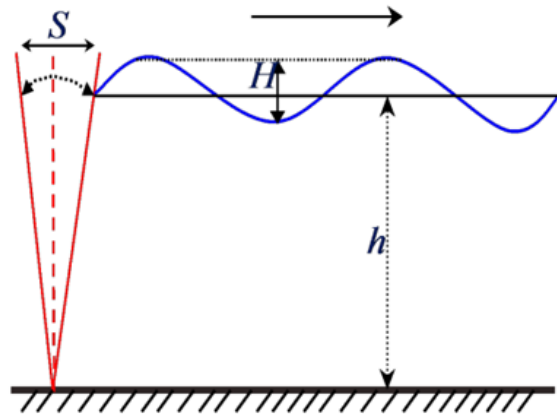
Figure 5.8. Mechanics of Flap wavemaker. (Galvin, 1963)

The relationship between H and S is given by Eq. (5.20).

$$\frac{1}{2}\,Sh = \frac{H}{k} = H\frac{L}{2\pi} = \frac{H}{2}\left(\frac{L}{2}\right)\frac{2}{\pi} \tag{5.19}$$

Where S- Piston stroke, H – Wave Height

The factor $2/\pi$ is the ratio between the area formed by the wave profile. From the relationship 1/2 S h = H /k, we can find out the ratio between the wave height H and the stroke S, namely

$$\frac{H}{S} = \frac{1}{2}\mathrm{kh} \tag{5.20}$$

The above relation is valid for shallow water conditions. In the present study, the Stokes theory equations specify the waves' velocity field and surface elevation. The inlet boundary is assigned with the displacement given by Eq. 5.19. A step function based on free-surface location or air domain at the top surface is used to generate the air volume fraction at the inlet.

5.5.5 Influence of beach slope

Various researchers have investigated several methods and techniques to dissipate the wave attenuation at the downstream end of the NWF. Maguire (2011), Fatemeh (2007) Neves (2021) and Wang et al. (2020) have investigated the comparison study of the three major types of phase-resolved wave models and the differences among those wave models.

In the present study, the numerical wave flume is tested in a water depth of 0.50 m with varying wave heights (0.12 m to 0.18 m) and wave periods (1.4 sec and 2.8 sec).

(a)
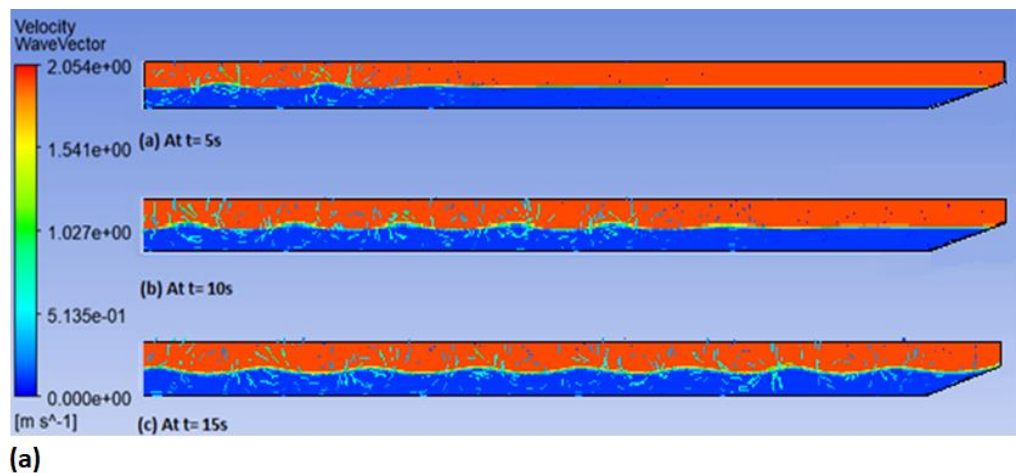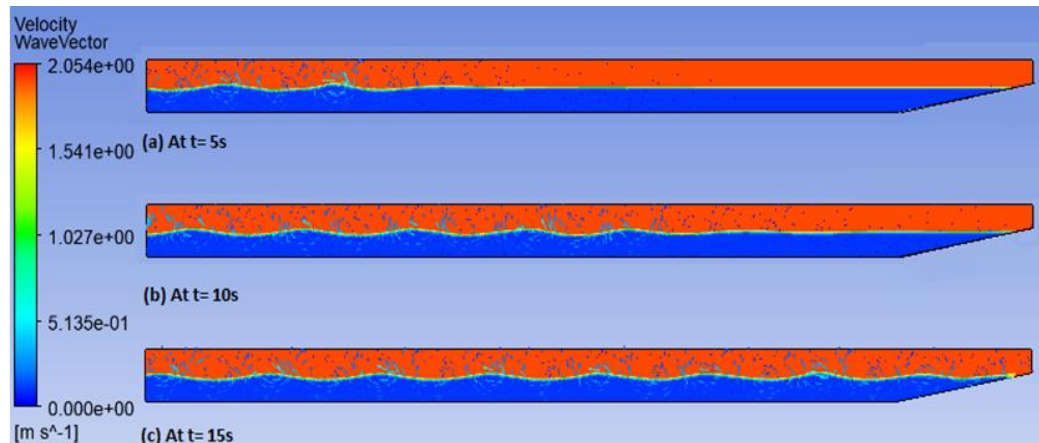
(b)
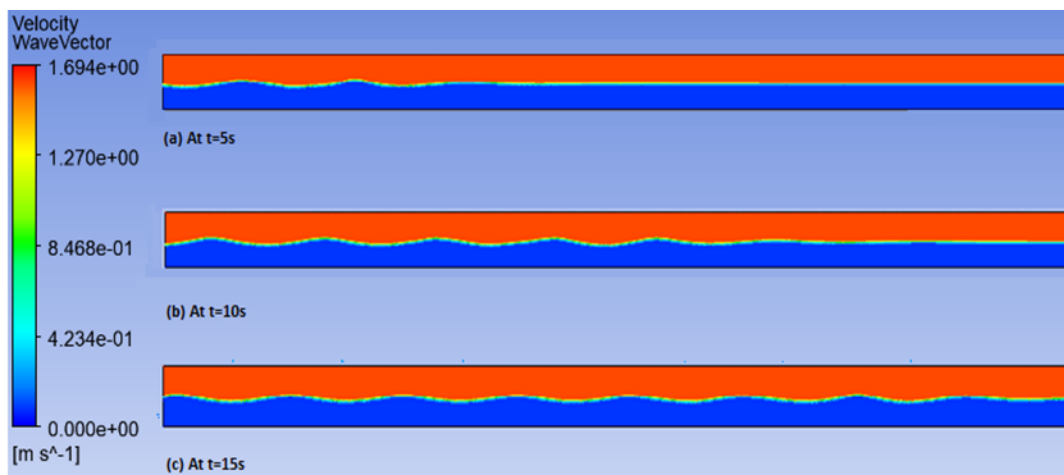
(c)

Figure 5.9 Propagation of waves in numerical wave flume for a) 1: 3 beach slope b) 1:5 beach slope c) numerical beach condition at the various instant of time (For H=0.12 m, T=1.4 sec)

The numerical waves generated for (H, T) = (0.12 m, 1.4 sec) for various beach slopes a) 1:3 b)1:5 & c) numerical beach conditions are illustrated in Figure 6.9. Two beach slopes (1:3 & 1:5) and numerical beach conditions are employed to dampen the wave energy and investigate optimum beach slopes for NWF. The measured wave elevations for different beach slopes at 3 m from the end of the beach are shown in Figure 5.9. A 3m is chosen from the downstream end of the beach to avoid the nonlinearities resulting from the wave breaking. The beach slope of 1:5 is optimum as the difference in the degree of wave damping, and the phase shift is insignificant compared to a slope of 1:3. Further, Figure. 5.10 shows the free surface elevations of the fully matured wave and

the dissipated wave near the downstream end of the numerical beach. It is observed that the sloping beach effectively dampens the wave compared to numerical beach conditions.
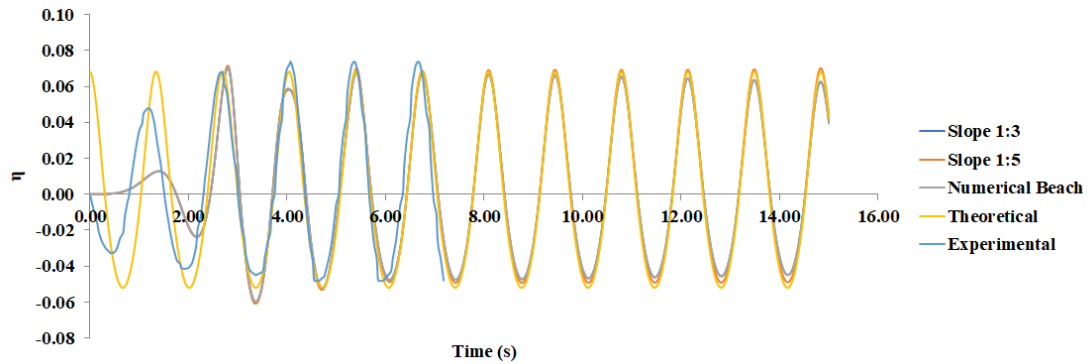
Figure 5.10: η v/s t graphs for comparison of numerical, theoretical & experimental results (For H=0.12 m, T=1.4 sec)

Furthermore, the horizontal and vertical components of wave-particle velocity of numerical study are shown in Figure 5.9 (a, b). The scalar wave particle velocity is obtained by combining these vector plots. The results obtained show excellent correlations with the analytical solutions. The waves are very close in phase, despite a slight difference in the surface elevation height. This occurs mainly due to a large time step interval, coarse mesh in the required domain, a small length of the NWF, or a steeper beach slope.

5.5.6 Analysis of errors

The error analysis is performed to check the significance of the developed numerical model. The key factors affecting the wave generation are analyzed, considering the cells and the number of points per wave height. The theoretical solutions are used as the reference solution. A regular wave with the wave period $T = 1.4$ sec and wave height $H = 0.12$ m at a water depth of $d = 0.5$ m is propagated in the numerical wave flume for 15 wave seconds. In each wave period, a uniform distribution of 10 points is used to calculate the diffusive error.

In each case, the diffusive error, ε, was calculated using:

119

$$\varepsilon = \frac{1}{H}(\eta - \eta') \qquad\qquad (5.21)$$

Where η and η` denote the numerically computed free-surface elevation and the reference point elevations (Zhang et al., 2019) the results obtained in the numerical wave flume after about the initial 4 seconds of simulation are used for the analysis to avoid any spurious results at the beginning of the test. The variations of diffusive error with time normalized by the wave period for (t/T) = (0.12 m, 1.4 sec) are plotted as follows in Figure 5.11
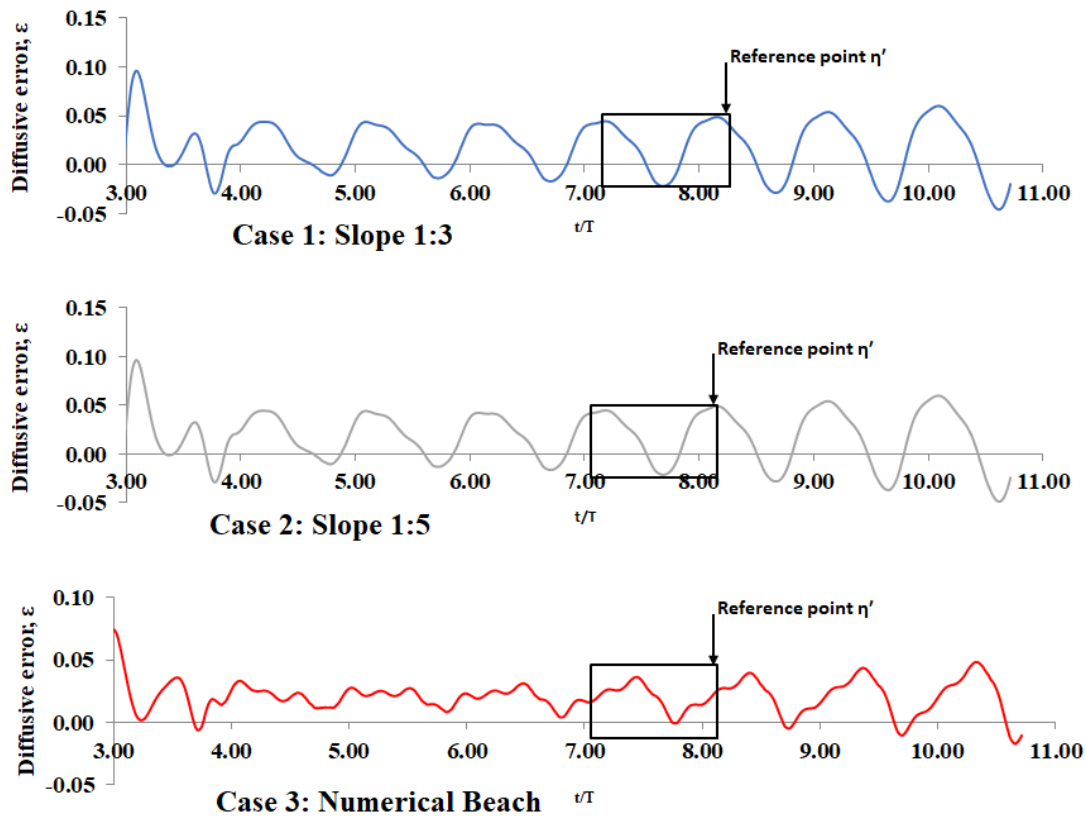
Figure 5.11: Diffusive Error v/s t/T (For H=0.12 m, T=1.4 sec)

The relative error is calculated by taking the analytical solution and reference point as reference. As evident from the graphs, in all three cases, it can observed that the error through all the domain lengths is minimal. The maximum diffusive error for the slope 1:3 (Case 1), 1:5 (Case 2), and numerical beach (Case 3) are 5.2 %, 4 %, and 4.5 %, respectively, all of which are within the acceptable limit. (Oberkampf and Blottner , 1997).

5.5.7 Influence of the numerical wave flume length

Numerical simulations are carried out for different wave tank lengths L (20 m, 30 m, 40 m). The comparison plots are illustrated in Figure 5.12. The water surface elevation at t=15 s for different tank lengths is noted that a reduction in the length of the NWF to 20m causes the reflection of the waves to affect the surface elevation at the downstream end and a shift in nature. At the same time, increasing the NWF length to 30 m and 40 m does not show any improvements, but it results in higher simulation time for conditions considered in the present study.
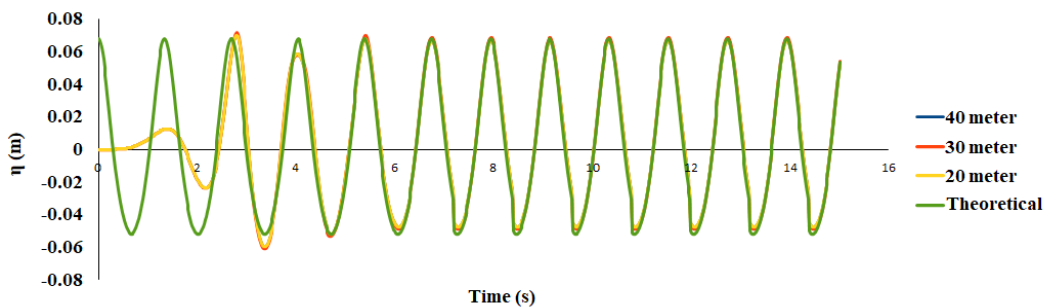
Figure 5.12: η v/s t graphs for comparison of various tank lengths & theoretical results
(For H=0.12 m, T=1.4 sec)

Increasing the tank length is an effective solution to prevent wave reflection; on the other hand, a 20 m wave tank (twice the maximum wavelength consider in the study) gives better results.

5.5.8 Validation of the NWF against experimental results

To validate the results from NWF against the experimental results, the time series of free surface elevations for all the cases from the numerical procedures are plotted. A comparison with experimental results is illustrated in Figure 5.13.
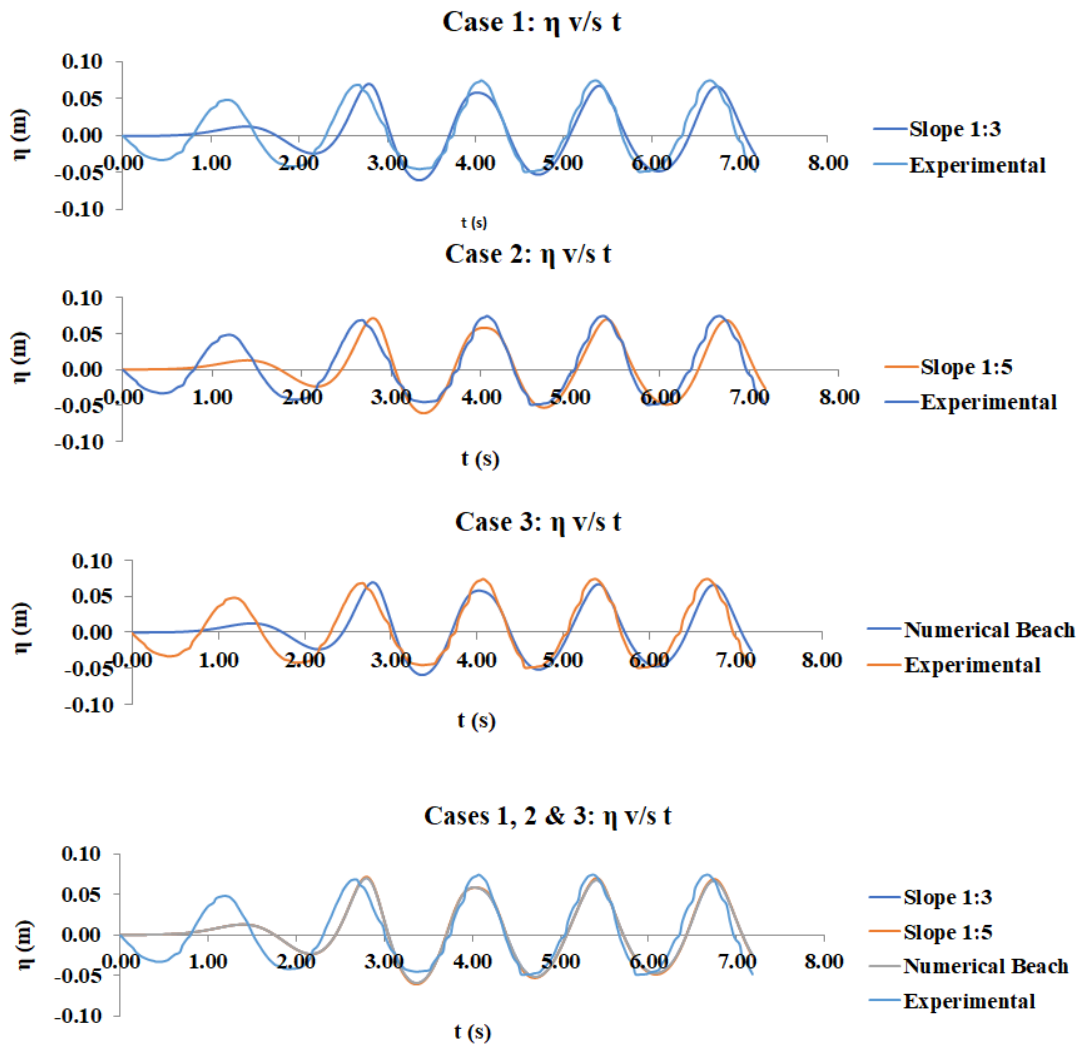
Figure 5.13: Comparison of η v/s t plots for different NWF with experimental results
(For H=0.12 m, T=1.4 sec)

A UDF is defined for the components of inlet velocity to generate ocean waves numerically to simulate the wave theory. This numerical wave flume gave considerably good results in-line with the experimental results. For the time step of 0.01 s (T/200), surface elevation in the wave crest and trough obtained from the numerical study closely correlates with the analytical study. Hence the time step of 0.01 sec is considered for all CFD simulations.
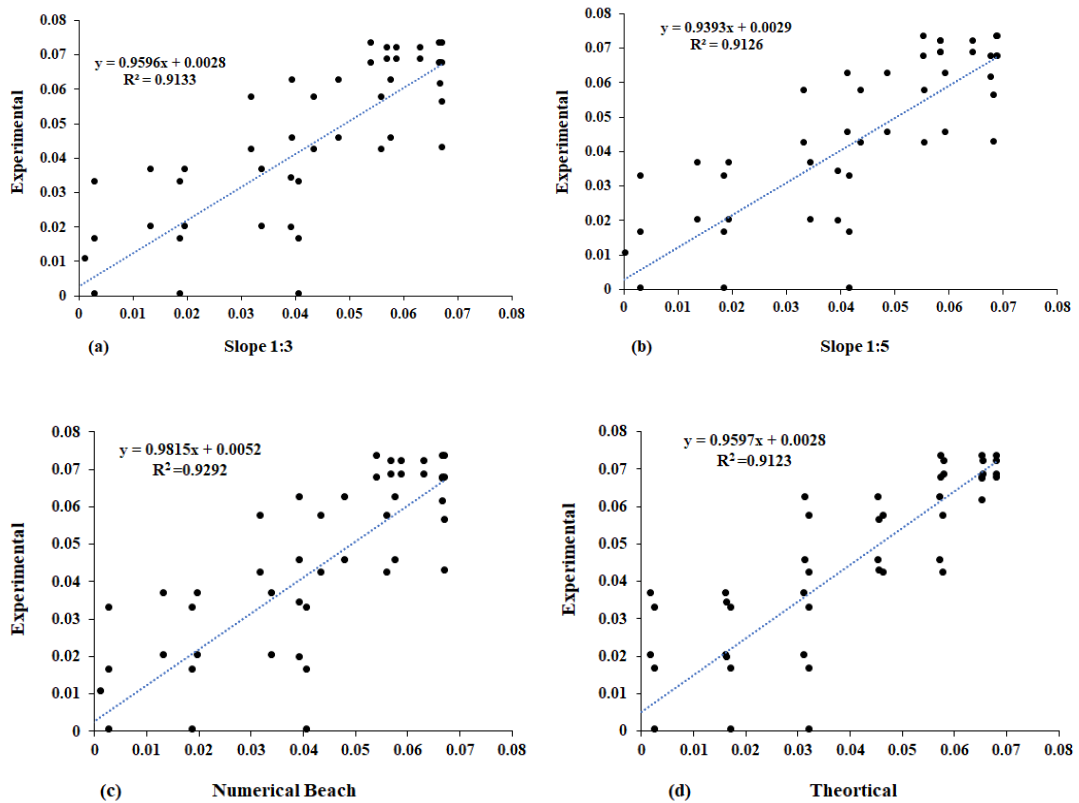
Figure 5.14: Comparison Scatter plot of different beach slopes & theoretical values v/s experimental data.

For better clarity, the scatter plots are plotted with the help of the statistical parameters illustrated in Figure 5.14. The coefficient for the determination (R^2) is more than 0.9 for all the cases considered in the study. However, for the numerical beach conditions, the obtained R^2 value is 0.9292.

Finally, it is concluded that the numerical simulations with a mesh size of 0.02 m x 0.02 m, with time, step 0.01 s, 20m NWF, and numerical beach condition, provide a good result, with an admissible correlation with experimental and theoretical approaches.

5.5.9 Comparison of wave profile obtained from the recommended NWF with experimental results

The comparisons of the wave surface elevations (η) between the simulated results and the experimental results for a case of H_i/d=0.24, T = 1.4 sec with the recommended mesh size of 0.02 m x 0.02 m, timestep 0.01 s, 20 m tank length and numerical beach condition are illustrated in Figure 5.15. The minor discrepancies in height and phase for a few waves are observed. But a general agreement between the numerical results and the experimental results is reasonable. The relative error is used to analyze the numerical and experimental results are quantitative.
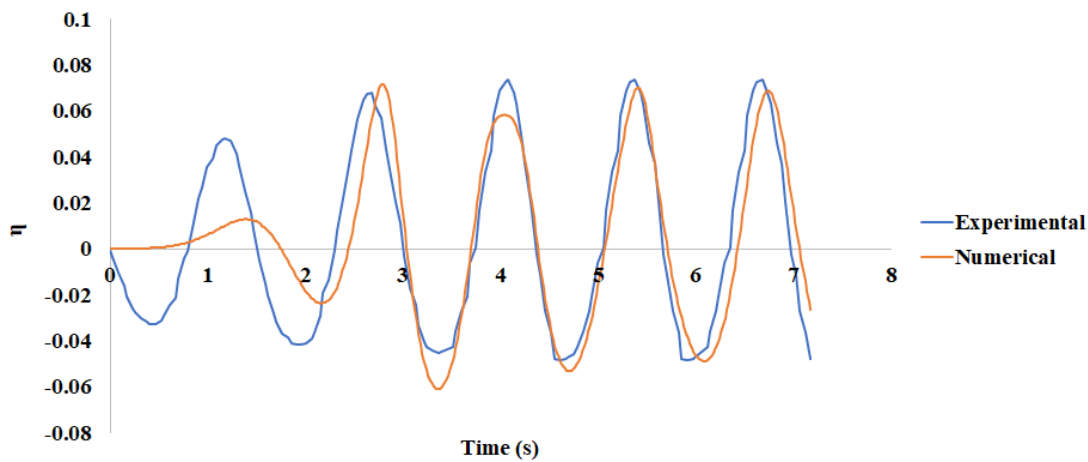
Figure 5.15 Variation of free surface elevation (η) between experimental and computational results; Relative Wave height (H_i/d) =0.24, Wave period (T)=1.4 sec

$$\text{Relative error} = \frac{Ep - Np}{Ep} \times 100$$

Where E_p - Experimental results

N_p - Numerical results

The mean relative error in wave height measured by the wave probe is 3.8 %, and the free surface elevation variation shows good correlations between experimental study and numerical solutions.

From the outcome of preliminary investigations. Here the various effects of beach slopes (1:3, 1:5, and a numerical beach state) in reducing the wave reflection characteristics, and the validation of the numerical model is done by comparing it with an experimental and theoretical approach with an acceptable error for better numerical solutions. The following input parameters remain fixed throughout the numerical study, such as the water depth (d = 0.5 m), mesh size (0.02 m), Numerical flume length (20 m) and NWF wave theory unless otherwise mentioned.

The conclusions arrived are:

1. Increasing the computational grid or mesh size results in wave damping and a small shift in the peak of results providing insignificant numerical solutions. To overcome these three mesh sizes (0.0 m x 0.01m, 0.02 m x 0.02 m and 0.03 m x 0.03 m) are considered. It is noted that (0.02 m x0.02 m) agrees with experimental and theoretical approaches and is effective in computational time compared to a lower mesh size (0.01m x 0.01m). NWF doesn't significantly affect varying beach slopes concerning the mesh size.

2. The beach slopes of (1:3, 1:5, and numerical beach conditions) are implemented in the downstream end of NWF to address the wave reflection and concluded that the beach slope of 1:5 and numerical beach conditions are similar in the performance wave absorbing nature. In addition, a 36 % reduction in the simulation time is observed in the case of numerical beach conditions.

3. To optimize the length of NWF, several factors are considered. Finally, the numerical simulations with a mesh size of 0.02 m x 0.02 m, with timestep 0.01 s, 20m NWF length, and numerical beach condition provide a good output with an excellent agreement with theoretical and experimental results.

With the knowledge of the preliminary investigations, further, the numerical simulations are carried out with test models such as vertical caisson breakwater with the protection of toe and slotted barriers in front of vertical caisson breakwater. In the subsections, the numerical performance characteristics of the wall-type breakwater are discussed in detail.

5.6 GEOMETRICAL AND MESHING DETAILS OF THE WALL-TYPE BREAKWATER

A two-dimensional numerical wave flume is modelled with dimensions of length 16 m, the height of 1.1 m. The water depth of 0.5 m and test model height of 0.9 m are considered for the present numerical investigation. The schematic of the numerical flume model and its dimensions are given in Figure 5.16. The test model is located at a distance of 14 m from the wave generation zone. To obtain the surface elevation at required positions (at a distance of L, L+(L/3), and L+(2L/3) from the test model) even at maximum wavelength conditions (6 m), 14 m distance is maintained between the test model and wave generation point. The obtained data are used to calculate the wave reflection coefficient (K_r).
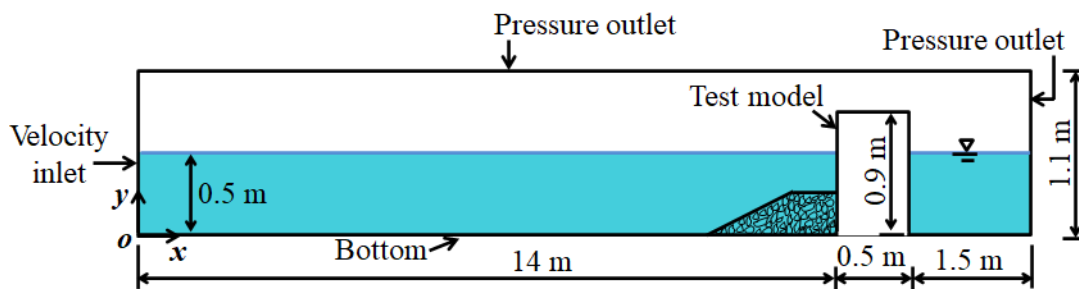
Figure. 5.16: Geometry of the flume model with boundary conditions.

Initially, under the hydrostatic condition (water at rest) of the flume, the generation of the wave process is initiated by assigning a regular wave motion in the wave flume using a user-defined function with the movement of the flap-type paddle. The governing equations (conservation of mass and moment) are solved by making the computational space into a finite number of a control volume. As an initial condition, static pressure is given for the liquid face, and the volume of the fluid model is used to generate the free surface between the air and water medium. The no-slip wall boundary condition was assigned for the test model and the flume walls. The upper domain boundary and the right-side wall of the flume model are defined as pressure outlets. Zero-gauge pressure is determined at the upper domain boundary by considering the atmospheric pressure as the reference pressure.

The inappropriate selection of mesh can affect the accuracy of simulation results, computational efficiency, and solution stability of the output. The proper wave

formation can be obtained when the model is developed with a minimum of 200 grids per wavelength (Kamath, 2012) and the aspect ratio (ratio of higher dimension to lower dimension of element) of an element should be less than 10 (Marques Machado et al., 2018). In the present study, to generate waves at a maximum wavelength of 6 m conditions maximum element length of 0.03 m is required. Hence, all the experiments are simulated with a mesh size of 0.02 m and at an element aspect ratio of 1.
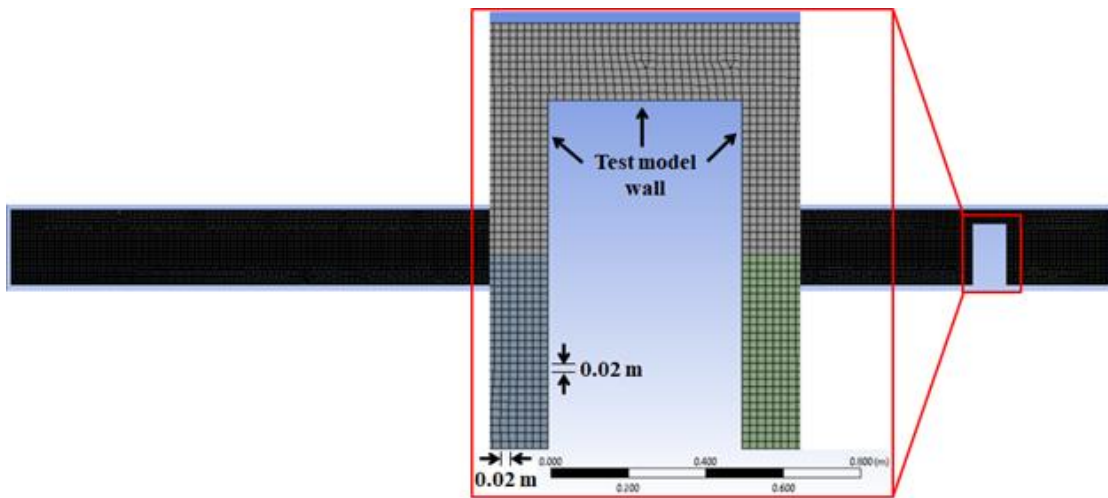
Figure. 5.17: Fluent mesh model closer to the test model.

Figure 5.17 illustrates the two-dimensional free mesh used nearer the test model. The total number of nodes and elements used are 40676 and 40002 respectively. The quality of results also depends on time discretization and the type of transient formulation used for the study. Implicit schemes are more stable than explicit schemes, even at lower time step sizes. Hence, the second-order implicit method with a time step of 0.01 seconds is used in this study. Marques Machado et al. (2018) concluded the time step of a maximum $(1/200)^{\text{th } 0.94}$ of the corresponding wave period was the optimum time step size for numerical modelling. All the experiments are simulated for up to 15 seconds to get the proper reflected wave data to calculate the reflection coefficient. The transient gravity-based model is chosen for the present study. VOF model with open channel wave boundary conditions is adopted, and the implicit formulation is used for the volume fraction parameter. The simulations are modelled with two-phase incompressible fluids (air and water) having a constant density of 998 kg/m^3 for water

and a constant density of 1.225 kg/m^3 for air. K-epsilon viscous models are more suitable for turbulent open-channel flows (Poguluri, 2020).

 In this study, the standard k-epsilon viscous model is used for wave generation. The selection of wave boundary conditions and wave theory depends on wave steepness and relative water depth. Recommended code practice DNV RP C 205 (2010) explained the suitable wave theories for various wave conditions (shallow to deep water). Shallow/intermediate wave boundary condition is applied at the velocity inlet, and Stokes's third-order wave theory is used for all the Numerical simulations.

5.7 MESH INDEPENDENCE STUDY

 Figure 5.18 shows the variation for different grid sizes with reflection coefficient (K_r) for the area of interest (test model). The quality of results also depends on time discretization and the type of transient formulation used in the study. The different grid sizes considered for the present study are 0.1 m, 0.01m, 0.02 m and 0.04 m.

$$\text{RMSE} = \sqrt{\frac{1}{N}\sum_{i=1}^{N}(y_{Numerical}-y_{Experimental})^2} \tag{5.22}$$

The convergence of the solution independent of mesh is obtained for 0.02 m and 0.01m grid sizes, and the corresponding solutions are compared with experimental values. The grid size of 0.02 m is considered for the present study owing to the fact that it takes less computational time on an account of a smaller number of elements.
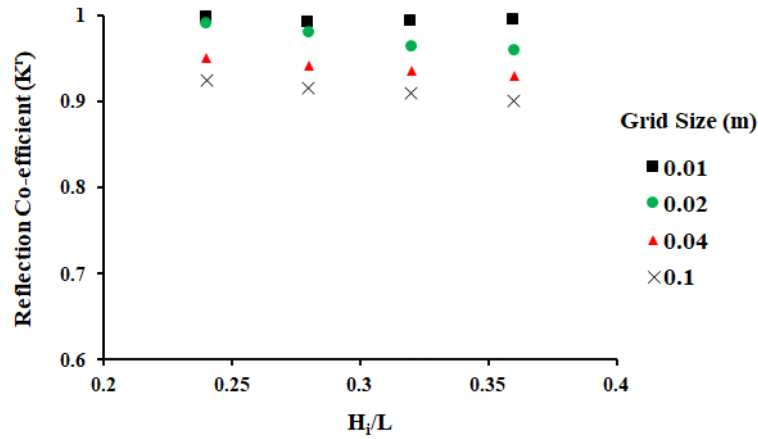
Figure 5.18: Mesh Independence

Table 5.4, Illustrates the statistical comparison of Fluent output with experimental results. Root Mean Square Error (RMSE) is used as an index of comparison. The RMSE formula is given in Eq. (6.18). The statistical results obtained at different wave heights (0.12 m and 0.18 m) and different wave periods (2.2 sec and 2.8 sec) are introduced in Table 6.1. The statistical results show that Fluent outputs have less deviated from experimental results.

Table 5.4 Statistical comparison of Fluent and Experiments

Experimental parameters	RMSE
$H_i = 0.12$ m, T = 2.2 sec	0.0210
$H_i = 0.12$ m, T = 2.8 sec	0.0341
$H_i = 0.18$ m, T = 2.2 sec	0.0258
$H_i = 0.18$ m, T = 2.8 sec	0.0198

5.8 DATA ANALYSIS FOR INCIDENT AND WAVE REFLECTION

The DHI wave synthesizer analysis software, MIKE ZERO is used for the analysis of incident and wave reflection. The method of analysis for regular waves and different parameters (wave transmission, reflection), are explained. The wave data from the wave Probe are measured in the absence of the test model in the flume, are used as incident wave input for the tests, and the incident wave height, H_i, is determined from these data. The wave up-crossing analysis is used for regular wave runs, and the average value of

all the wave heights within the 30 s span is used as the measured incident wave height. The data from wave probes are used to estimate the reflected wave height and coefficient of reflection, K_r, which is defined as $K_r = H_r/H_i$, where H_r is the reflected wave height. The reflection analysis software in MIKE ZERO is based on the method described by Mansard and Funke (1987) and extended by Zelt add Skjelbreia (1992). The distance between wave probes is used as inputs for the reflection analysis. Using three-wave probes is preferable to using two-wave probes in order to avoid singularity problems during reflection analysis. According to the law of the conservation of energy, the incident wave energy must be equal to the sum of transmitted wave energy, reflected wave energy, and wave energy loss. Hence, the equation, representing the law of conservation of energy can be used as follows:

$$E_i = E_t + E_r + E_l \qquad\qquad (5.23)$$

Where E_i represents the incident wave energy, E_t, E_r, and E_l denotes the energy transmitted, energy reflected, and energy loss respectively. The CFD results and the experimental results are compared for a wide range of input conditions and are discussed in the following sections.

5.9 COMPARISON BETWEEN NUMERICAL AND EXPERIMENTAL RESULTS

Numerical analysis is carried out to find the wave force, reflection coefficient, and run-up on a wall-type breakwater. The results obtained from numerical computations are validated using the experimental findings. The numerical simulations are performed at different wave periods (2.2 sec, 2.4 sec, 2.6 sec & 2.8 sec) and different wave heights (0.12 m, 0.14 m, 0.16 m & 0.18 m) at a water depth of 0.5 m.
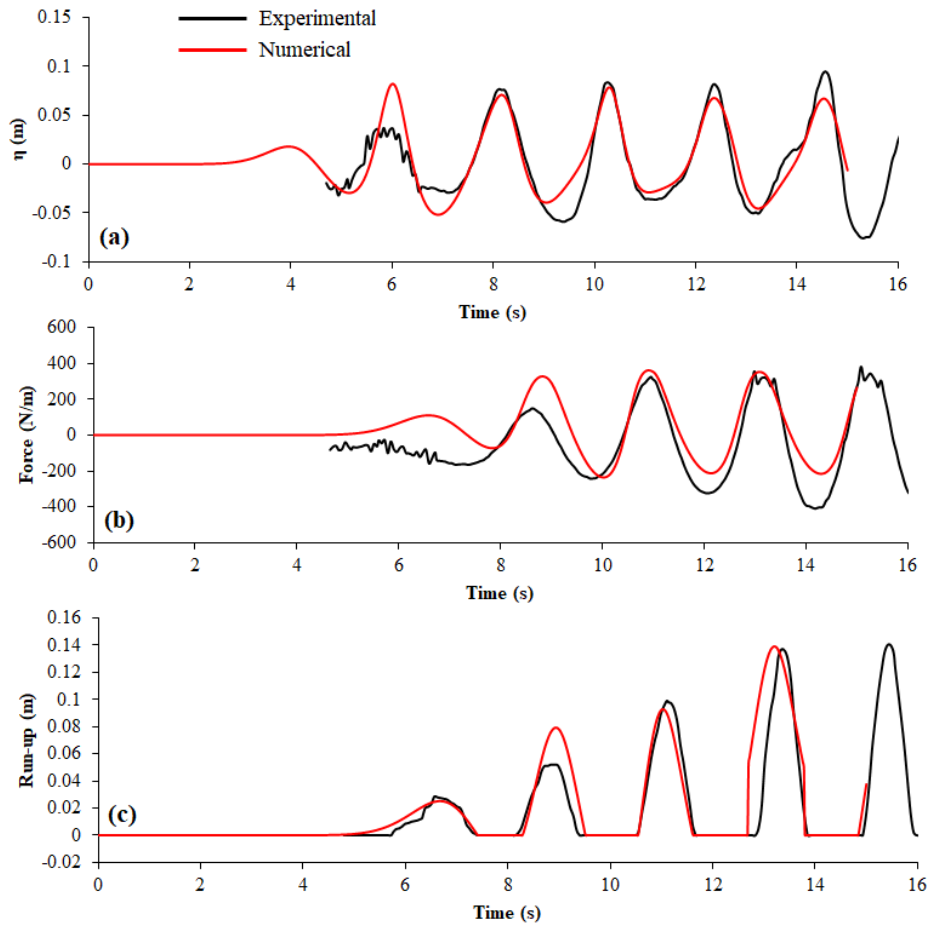
Figure 5.19: Comparison of experimental and numerical (a) surface elevation, (b) force on a vertical caisson, and (c) run-up for wave height 0.12 m and wave period 2.2 s condition.

The surface elevations at a distance of L, L+(L/3) & L+(2L/3) from the vertical caisson are measured during each set of experiments. The same data is used to validate the surface elevation data at respective positions computed from the numerical analysis. Figure 5.19 (a) and Figure 4.20 (a) shows a comparison of both numerical and experimental surface elevation data at L+(L/3) distance from the test model. Experimentally, the wave force on the test model at each instant of time is calculated from the measured wave pressure data at each moment at selected locations on the test model. During experimentation, the wave forces on the test model are measured in the x-direction.

Hence in the numerical analysis, the sum of forces in x-direction on test model walls at an instant of time is considered as a force on the test model at that particular instant of time. Figure 5.19 (b) and Figure 5.20 (b) show the comparison of force on wall breakwater over time obtained from experimental and numerical results.
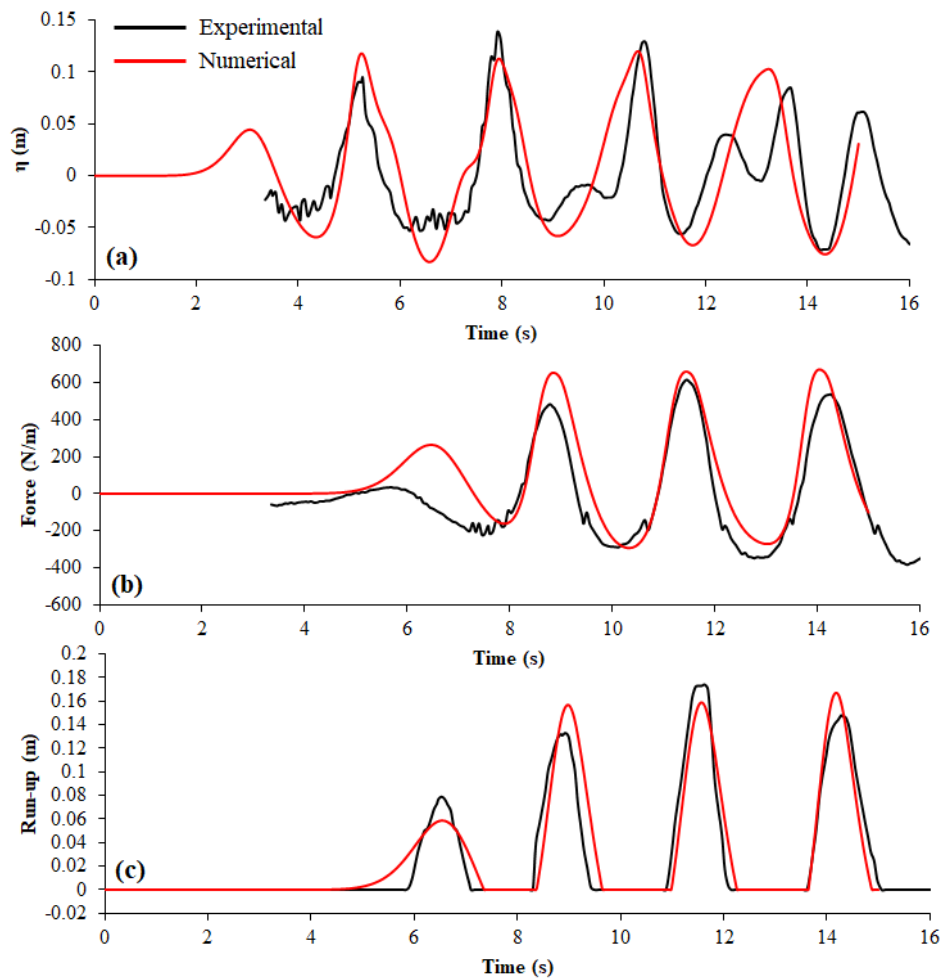
Figure 5.20: Comparison of experimental and numerical (a) surface elevation, (b) force on a vertical caisson, and (c) run-up for wave height 0.18 m and wave period 2.8 s condition.

The run-up is measured using a capacitance-based run-up meter placed on the front face of the test model. In the numerical analysis, the length of water volume fraction on the sea sidewall (front face) of the test model is considered for the run-up analysis Figure 5.19 (c) and Figure 5.20 (c) shows the temporal variations of run-up obtained from experiments and numerical analysis. Figure 5.19 and Figure 5.20 show that the computed numerical surface elevations, wave force, and run-up results showed good

agreement with experimental findings. Unstable wave formation is observed from both experimental and numerical results at 0.18 m wave height and 2.8 sec wave period test condition due to a higher Ursell number.
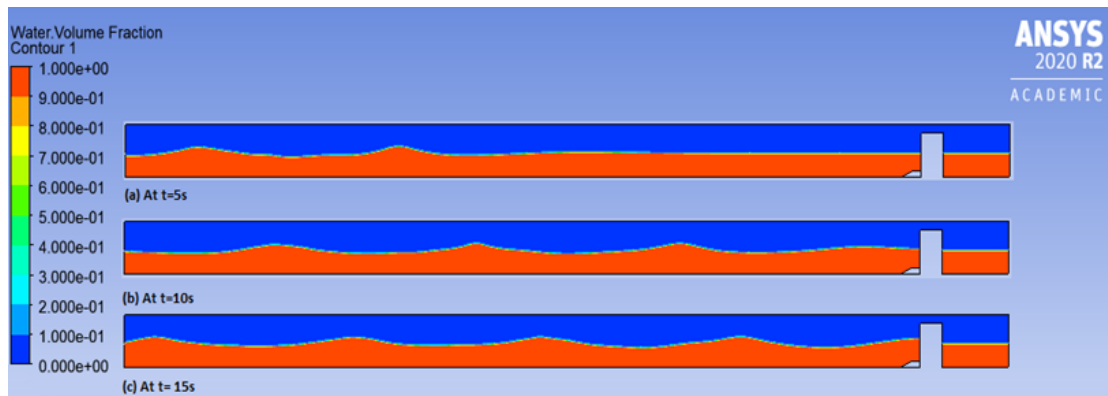
Figure 5.21: Propagation of waves in the numerical wave tank at an instant of time (a) 5 sec, (b) 10 sec, and (c) 15 sec (at a wave height of 0.12 m and a wave period of 2.2 sec condition).

In the VOF model, two phases (air & water) are not interpenetrating, and the fraction of the volume of a phase in a particular cell is calculated as a fraction of volume. The two phases (air and water) flow fields are assumed to be unsteady and solved by the Navier-Stokes and the (RANS) equations. The wave propagation and interaction of the wave with the test model shown in Figure 5.21 represent the water volume fraction in a numerical wave tank during waves' progress.

Figure 5.21 shows that the wall breakwater experienced the initial wave force at 6 sec, maximum force at 11.1 s, and minimum force at 12.2 sec. The water volume fraction graph (Figure 5.21) is the numerical evidence for forces acting on wall breakwater at different instants of time and also evidence for run-up at the different instants of time.

The pressure distribution in the numerical wave flume is shown in Figure 5.22 at 6 sec, 11.1 sec & 12.2sec. It is also observed the pressure on the lee side of the test model is not varied with time, indicating no transmission of energy from the lee side of the test model to the right side of the test model.
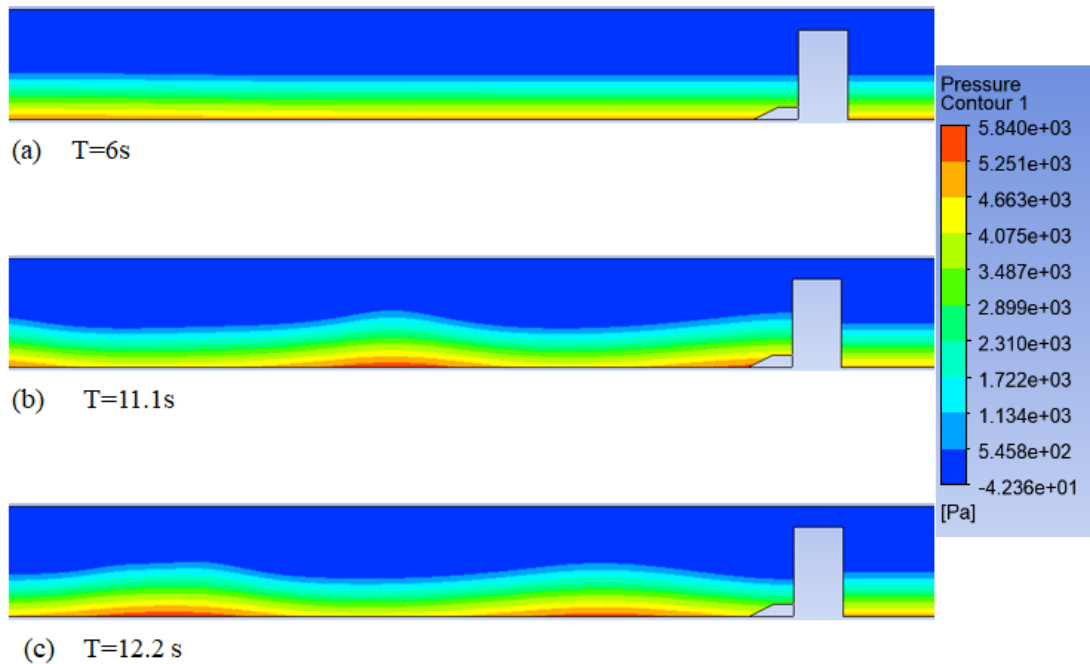
Figure 5.22: Pressure distribution in the numerical wave tank at (a) 6 s, (b) 11.1 sec, and (c) 12.2 sec (at a wave height of 0.12 m and a wave period of 2.2 sec condition).

The velocity of water and air particles during wave structure interaction at a wave height of 0.12 m and a wave period of 2.2 sec condition are illustrated in Figure 5.23. The velocity profiles are depicted along with the air volume fraction. The colour intensity of the arrows indicates the magnitude of the velocity, and the direction of the arrows shows the path of particle velocity. The motion of water particles is towards the test model before the wave starts interaction with the test model (Figure 5.23 (a)). The backflow of water particles from the test model is observed when the structure attained maximum run-up (Figure 5.23 (b)). The velocity of water particles is more at 11.1 s when compared to the velocity of water particles at 6 sec, which increases the run-up on the test model and subsequently wave forces. Figure 5.23 (c) shows the fully developed wave interacting with the test model. The water particle velocities are maximum at a fully developed wave crest location.
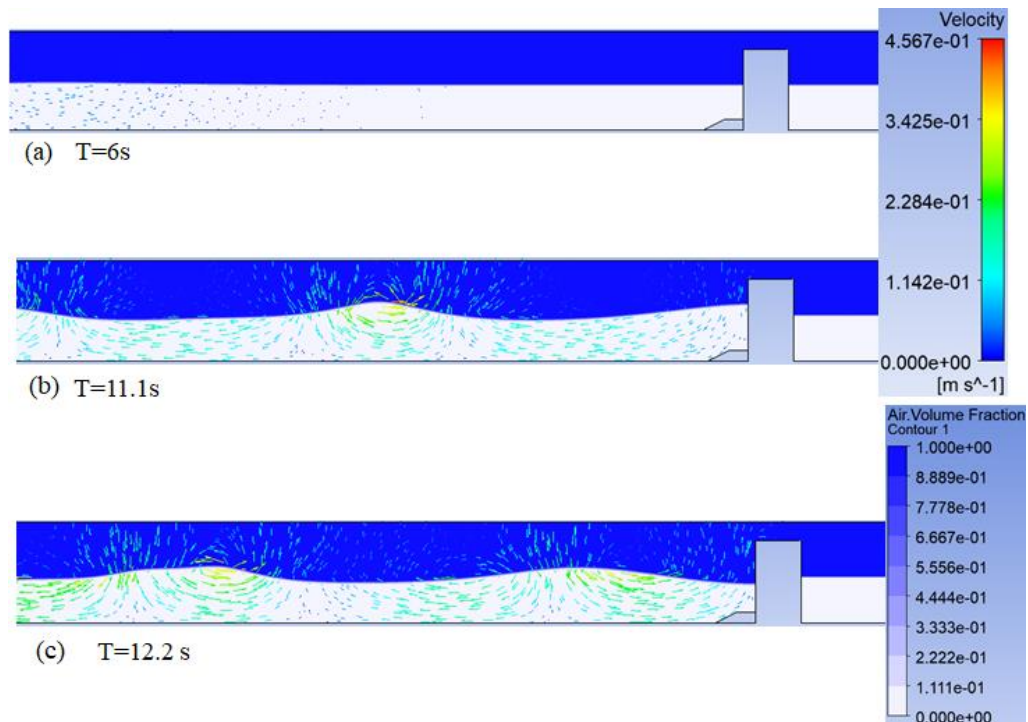
Figure 5.23: Magnitude and direction of fluid-particle (water and air) velocity in a numerical flume during propagation of wave under wave height of 0.12 m and a wave period of 2.2 sec condition.

In the present study, at all experimental conditions, water depth is less than half of the wavelength, which implies the water particles move in an elliptical shape. Figure 5.23 is evident of the elliptical motion of water particles due to the interaction of the wave with the sea bed.

5.10 VARIATION OF RELATIVE WAVE FORCE ($F/\rho g d^2$) WITH WAVE STEEPNESS (H_i/L) ON THE WALL FOR EXPERIMENTAL, NUMERICAL, AND THEORETICAL APPROACHES

Figure 5.24, illustrates the variation of relative wave force ($F/\rho g d^2$) with wave steepness (H_i/L) on the wall for the present experimental measured values. It is compared with the corresponding values calculated by theoretical formulae Goda and also by numerical approach. The wave force P is made non-dimensional by dividing over the term ($\rho g d^2$) and plotted on the y-axis. The x-axis indicates the wave steepness (H_i/L). The dashed line, solid line, and dotted circle represent the theoretical, experimental, and

135

numerical results, as shown in Figure 6.9. It is observed that the relative wave force is increasing with the increase in the wave periods and wave heights.
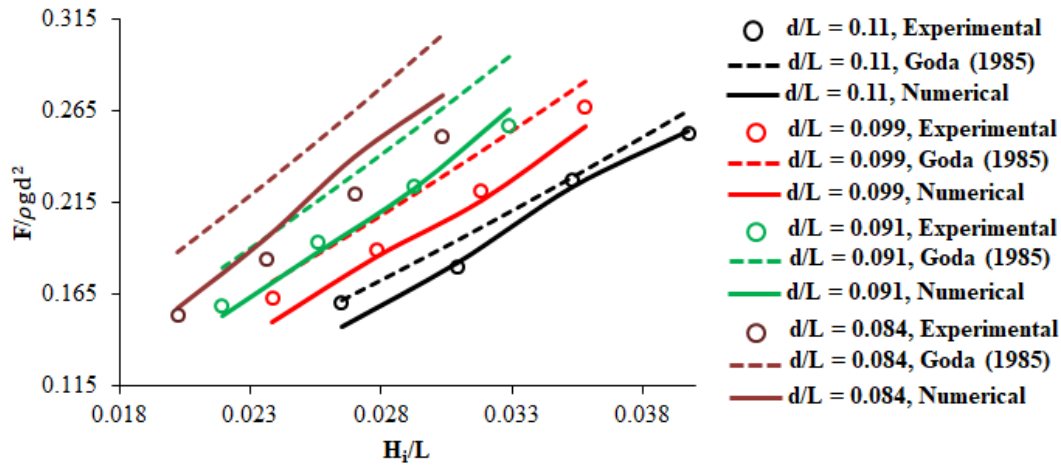
Figure 5.24: Variation of Wave force Parameter ($F/\rho gd^2$) with the incident wave Steepness (H_i/L)

5.11 VARIATION OF WAVE FORCE PARAMETER ($F/\rho gd^2$) WITH INCIDENT WAVE STEEPNESS (H_i/L)

The wave force is calculated using Goda's theoretical approach, and it is observed that the relative wave force increases with the increase in wave steepness. This may be due to the long-period waves exert more pressure than short-period waves. Goda's method provides a reasonable estimation of wave force distribution which is comparable with the experimental results. This is due to that long-period waves exert more force than short-period waves (Yung-Fang Chiu, 2007). The numerical results provide a reasonable estimation of wave force comparable with the experimental results for waves of small Ursell numbers. It is noticed that the theoretical approach overestimates 11 % of wave force for longer period waves.

5.12 VARIATION OF RELATIVE WAVE RUN-UP (R_u/H_i) WITH RELATIVE WATER DEPTH (d/L) ON THE WALL FOR EXPERIMENTAL AND NUMERICAL APPROACHES

The variation of relative wave run-up (R_u/H_i) and relative water depth (d/L) is illustrated in Figure 5.25 for various relative wave heights (H_i/d). In general, the wave run-up is defined as the vertical rise of water above the still-water level to which the water rushes up on the front face of the test model. This helps in determining the design wave crest level of the structure depending on the allowable overtopping level.
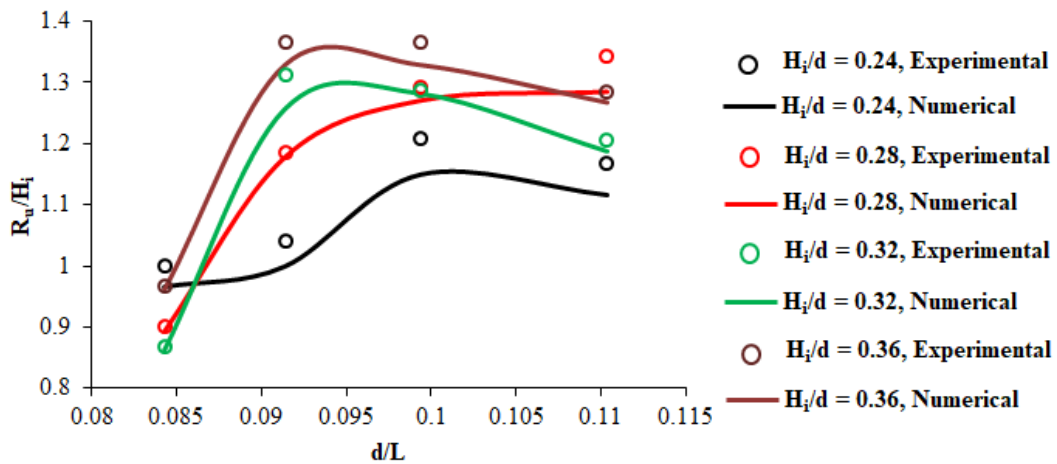
Figure 5.25: Variation of relative wave run-up (R_u/H_i) with relative depth parameter (d/L)

The relative run-up (R_u/H_i) decreases for an increase in the relative depth (d/L). The (R_u/H_i) increases with an increase in H_i/d because the higher waves of heights rush above the still water level. From the experimental results, the relative run-up (R_u/H_i) ranges between 0.85 to 1.4.

5.13 INFLUENCE OF WAVE STEEPNESS PARAMETER (H_i/L) ON WAVE REFLECTION COEFFICIENT (K_r)

Figure 5.26 shows the effect of wave height on the coefficient of reflection K_r, in terms of wave steepness, H_i/L for different wave periods (d/L = 0.084, 0.091, 0.099, and 0.11) on caisson breakwater. The wave surface elevation time histories from the wave probes are used to estimate the reflected wave heights (H_r). Three-wave probes are positioned

at L (wavelength), L/3, and 2L/3 distance from the test model used to measure incident and reflected wave heights. (Issacons, 1991)
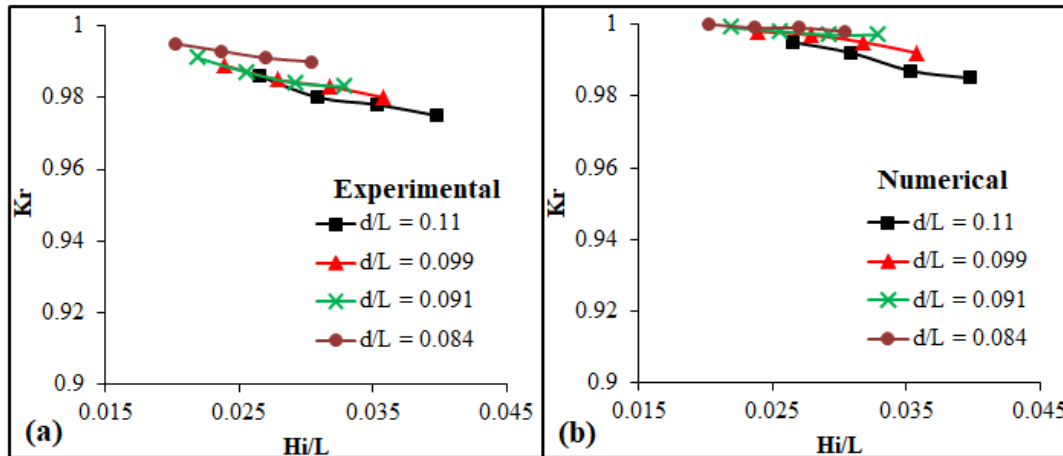
Figure 5.26: Variation of wave reflection coefficient (K_r) with wave steepness parameter (H_i/L)

The reflection coefficient (K_r) is obtained from the analysis of composite wave elevation using the transfer function method discussed by Shutang Zhu (1999). The reflection coefficient (K_r) is obtained from the study of composite wave elevation using the transfer function method discussed by Shutang Zhu (1999) and also calculated using MIKE Zero WS reflection analysis module, which is used for wave reflection analysis. The governing equations using the least-squares fit approach are based on the method proposed by Mansard and Funke (1987) and extended by Zelt and Skjelbreia (1992). And also, the analysis requires measurements of waves at a minimum of two different locations are more to solve.

The wave reflection coefficient (K_r) is defined as the square root of the ratio of the area between the reflected wave energy spectrums to the incident wave energy spectrum. From the observation, the reflection coefficient (K_r)is more than 0.97 for all the approaches.

5.14 ERROR ANALYSIS

The results of the developed numerical wave flume and taking into consideration all parameters. It is concluded that simulations using mesh size 0.02, with a time step 0.01 s, 16 m flume length, provide the best solution, with good agreement with experimental results. Figure 5.27 represents the percentage of relative force error with wave heights. It can be seen that the error through all the domain lengths is minimal. For a particular wave period, the percentage of error increased with an increase in wave height.
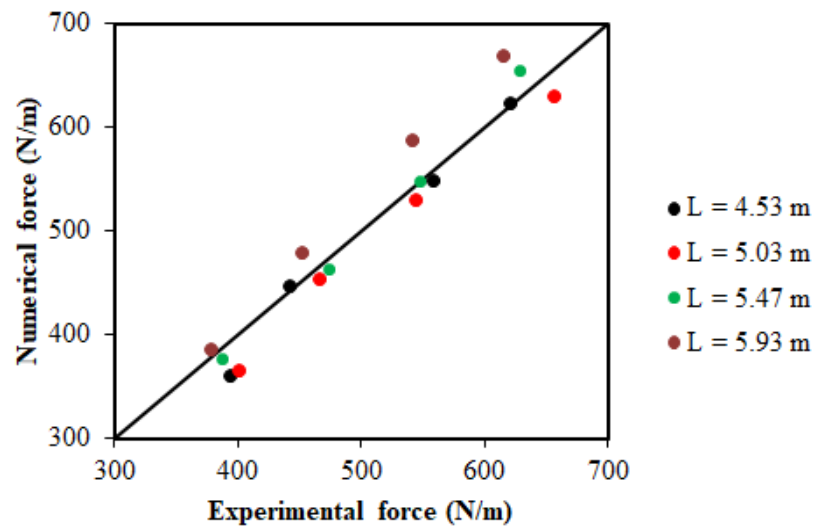
Figure 5.27 Error Analysis

The maximum percentage of error (i.e 9.3 %) is observed at a wavelength of 5.93 m. The increase in the percentage of error with increase in wave height and wavelength are due to higher Ursell numbers, which influence the nonlinearity in the wave nature.

5.15 CLOSURE

In the present chapter, an attempt is made to select the proper numerical model to study the hydrodynamic characteristics of the wall-type breakwater. The Hydraulic performances of the wall-type breakwater are estimated using numerical modelling under different wave characteristics.

The numerical results are validated using experimental findings, and the following conclusions are drawn.

- VOF model with a standard k-epsilon viscous model with Stokes third-order wave theory is appropriate to simulate the experimental conditions considered in this study, with a permissible error.
- The numerical model used in this study can estimate hydrodynamic characteristics of wall-type- breakwater with less error at smaller wave heights and wave periods. The error in estimated force on caisson breakwater is increased up to 6.8 % for wave height of 0.18 m conditions.
- The wave forces on vertical caisson type breakwater obtained from the numerical analysis showed a good correlation with experimental and theoretical (Goda, 1985) approaches.
- In numerical analysis, for shallow/intermediate wave conditions, the increase in wave height and wave period form unstable waves due to a rise in Ursell number, leading to increasing error in the estimated numerical results. At the same time, the grid resolution at specific regions of interest, and different mesh sizes can be used in a computation simulation. This will result in more accurate and efficient computation.

WAVE STRUCTURE INTERACTION ON VERTICAL CAISSON BREAKWATER WITH SLOTTED BARRIERS; PHYSICAL APPROACH

6.1 GENERAL

In recent years the new modern construction techniques are developed and implemented more economically. The demand and supply of big stones are one of the major drawbacks of the construction of the traditional breakwater. The wall-type breakwaters are designed generally built-in larger water depths for jetties for oil refineries, tsunami protection structures, etc. It requires less space, fewer quantity materials, and is more easily constructed than rubble mound breakwaters. The main disadvantages of the caisson type breakwater are strong reflections occur at the front wall, and it causes damages variety of problems such as ship navigations, waves overtopping, scour at the foundation, etc. To reduce such problems, Jarlan (1961) introduced a new method to dissipate the energy by providing perforated walls and a chamber inside. The incident wave energy is partially reflected at the permeable seaward wall and is partially transmitted through the opening of the perforated wall, and energy will dissipate due to vortices in between the perforated front wall and impermeable back wall. The main factors that select the type of breakwaters for attenuating the waves inside the harbours or ports are the easy availability of raw materials, project costs, and maintenance costs. The most commonly adopted breakwaters are rubble mound and caisson-type breakwaters. To reduce the costs and easy construction of breakwaters, slotted vertical barrier type breakwaters are constructed for this type of breakwater the water circulations maintained inside the ports and save the life of fish. Historically, perforated wall-type caisson breakwater was first introduced by Jarlan (1961), who proposed a single perforated wall on the front side and the impermeable wall on the backside. And a chamber between the impermeable and permeable wall reduces the wave forces and runup of the structure, and it is named Jarlan type breakwater Kondo (1979) and Chwang (1983) focused on the porosity effects. Fugazza and Natale (1992) observed

that when the reflection coefficient is minimum, the incident wave passes through the perforated front wall without changing the wave phase, while the non-perforated back wall reflects the waves the incident wave at the front wall has opposite phases. Many researchers have studied the benefits of multiple perforated front walls. A caisson-type breakwater with five slotted barriers was constructed for the Dalian chemical production terminal in China Huang et al. (2011) & Koraim et al. (2011) conducted an experimental investigation on a double vertical wall's hydrodynamic characteristics with an impermeable upper part and permeable lower part.

In this chapter, detailed physical investigations are highlighted to assess the wave-induced dynamic pressure, wave forces, wave runup and wave reflection on the vertical caisson breakwater with the presence of vertical and horizontal slotted barriers. At the same time, the porosity and the seaward location of the slotted barrier are varied from 10 % to 50 %, 1 m and 3 m respectively.

6.2 TEST MODELS

The test model is constructed using concrete and the dimensions of the model are 0.70 m in length, 0.5 m in breadth, and 0.90 m in height for the present study. The dimensions are selected based on the prototype of two caisson breakwaters integrated with OWC plants one in Vizhinjam port, Kerala and another from Sakata harbour, Japan. (Antonio F.O Falcao 2016).
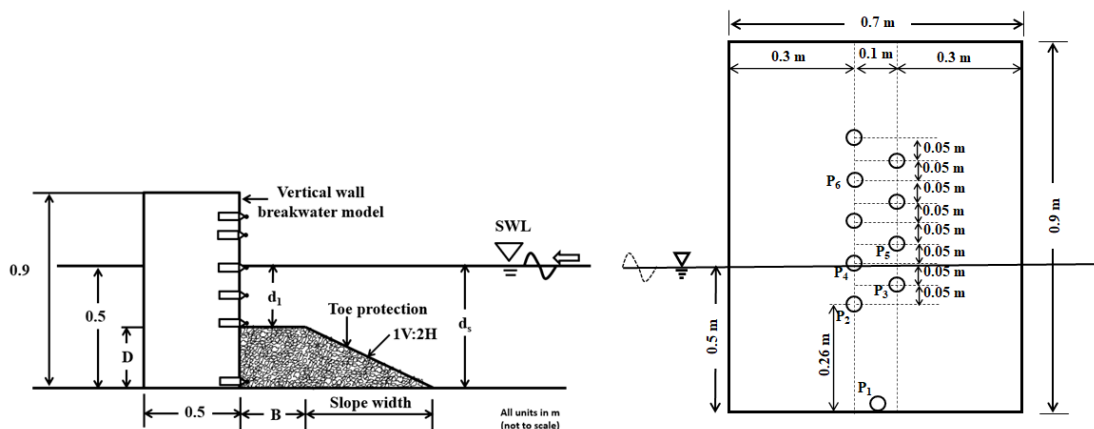
Figure 6.1: Positions of Pressure Transducer

Also, the height of the Vertical caisson breakwater is selected in such a way that there is no wave overtopping occurs. On the seaside of the model, rubble mound toe protection is constructed. The toe protection is designed as SPM (1984) Vol-II. The seaside slope of the toe is 1V:2H and the value of the d_1/d_S ratio used in the present study is 0.25d. SPM design procedure is based on the experimental work conducted by Brebner and Donnelly (1962). The cross-section of the test model with toe protection is shown in Figure 6.1.

Table 6.1 Dimensions of the toe cross-section for vertical/ caisson breakwater as per Brebner and Donnelly (1962) / SPM (1984)

Water Depth (d) (m)	Depth of Toe D=0.25d (m)	Width of Toe B=0.4 d (m)	Depth from MSL to top of Toe d_1=0.75d (m)
0.50	12.5	20	37.50

The toe is constructed and the relative depth ratio is maintained constant for all four varying water depths, the dimensions of the cross-section are depicted in Table 6.1. The trapezoidal cross-section of the toe consists of a homogenous pile of stones of 20g weight (i.e., nominal diameter, d_{n50} of 0.019 m) on the seaward side of the vertical caisson breakwater.

6.2.1 Slotted barriers

Slotted vertical and horizontal barriers are placed in front of the vertical caisson by varying the seaward spacing from 1 m to 3.0 m from the main structure and the porosity of 10, 20, 30, 40 and 50 % are used for each wave characteristic. The slotted barrier model is fabricated using a GI sheet of a thickness of 10 mm and the complete experiments are carried out at the depth of water 0.50 m. The artist and experimental view of the typical horizontal and vertical slotted barrier setup are shown in Figure 6.2. The range of experimental variables used in the present study is illustrated in table 6.2.
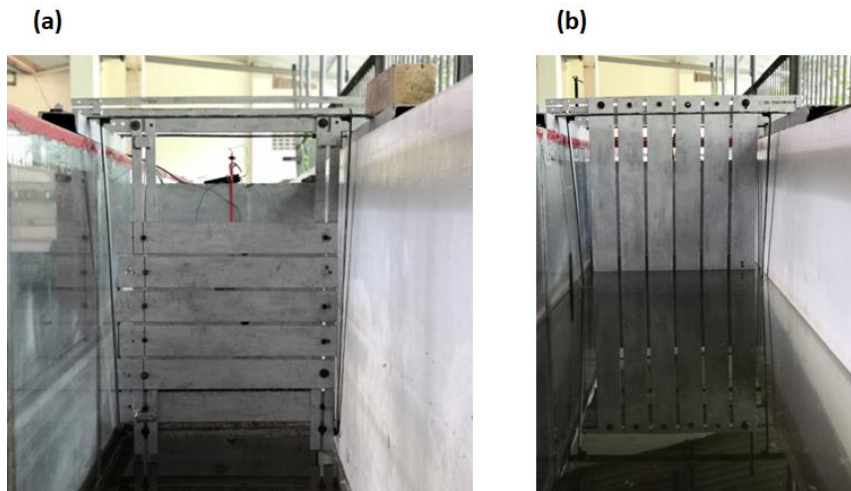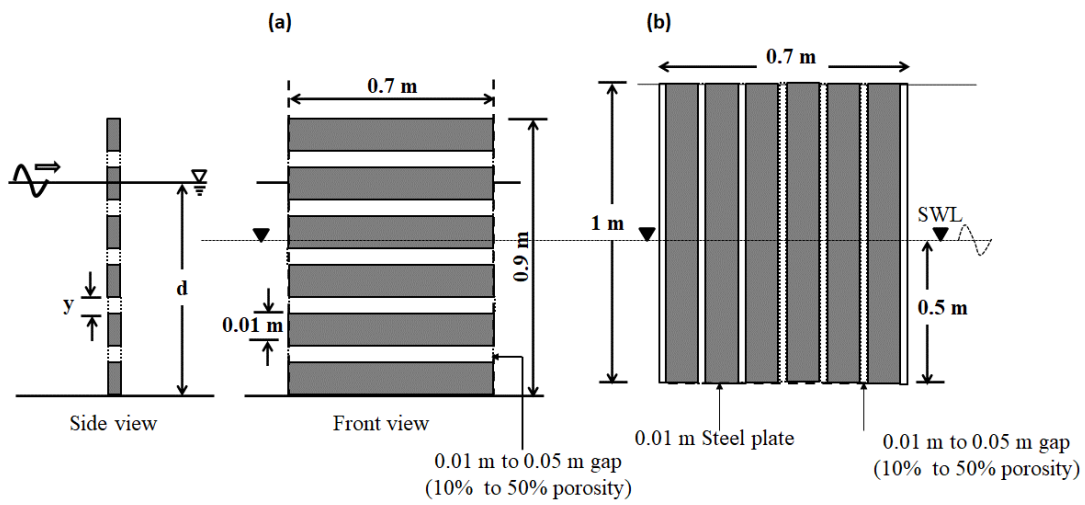
Figure 6.2. Typical slotted Barrier a) Horizontal Barrier b) Vertical Barrier

6.3 RANGE OF EXPERIMENTAL VARIABLES

Table 6.2. Wave and structural specific parameter

Parameters	Experimental range of values
Wave specific parameters	
Incident wave height, H_i (m)	0.12, 0.14, 0.16, 0.18
Wave period, T (sec)	2.2, 2.4, 2.6, 2.8
Depth of water, d (m)	0.50
Wave Length, L (m)	4.05 - 6.10
Porosity, μ (%)	10, 20, 30, 40 & 50

Spacing, S (m)	1-3
Structure specific parameters	
Vertical caisson breakwater	
Height of structure (m)	0.90
Width of structure (m)	0.70
Breadth of structure (m)	0.50
Vertical slotted barrier	
Height of structure (m)	1
Width of structure (m)	0.70
Thickness (m)	0.01
Horizontal slotted barrier	
Height of structure (m)	0.90
Width of structure (m)	0.70
Thickness (m)	0.01

6.4 VARIATION OF RELATIVE WAVE PRESSURE (P/ρgd) WITH RELATIVE DEPTH PARAMETER (z/d) ON THE VCB WITH THE PRESENCE OF A HORIZONTAL SLOTTED BARRIER (HSB)

During the experiments, wave pressures are noted and recorded for different wave heights and wave periods and depth of water 0.5 m. The wave pressures acting on the model are obtained using pressure transducers for different wave heights and wave periods. Wave pressures on the front face of the caisson are measured at six positions by using six pressure transducers installed on the front face of the caisson, which is converted by the program from millivolts to head of water. The artist's view of the test model with toe protection and the location of pressure transducers is presented in Figure 6.1. These values are then converted to pressures in kN/m^2 by multiplying the pressure head value with (ρg). From the unsteady Bernoulli equation, the pressure response factor kp becomes 1, at z = 0 (at SWL). At any water depth (–z) under a wave crest, the wave pressure is at its peak and consists of the static pressure and dynamic pressure is given by:

P = -ρgz (static Pressure) + ρgHKp(z) / 2 (dynamic pressure)   (6.1)

Where the first term is static pressure and the second one is dynamic pressure.

At still water level (z = 0), the vertical particle accelerations are maximum and are negative. The wave pressure has a trapezoidal distribution both above and below the still water level, while the uplift pressure acting on the bottom of the upright section is assumed to have a triangular distribution which is similar to Goda's approach. The pressure transducers are placed along with the depth of the caisson, at dimensionless depth z/d, where z is the distance from the still water level (measured positive above SWL and negative below SWL) to the pressure transducers and d is the depth of water at the structure.
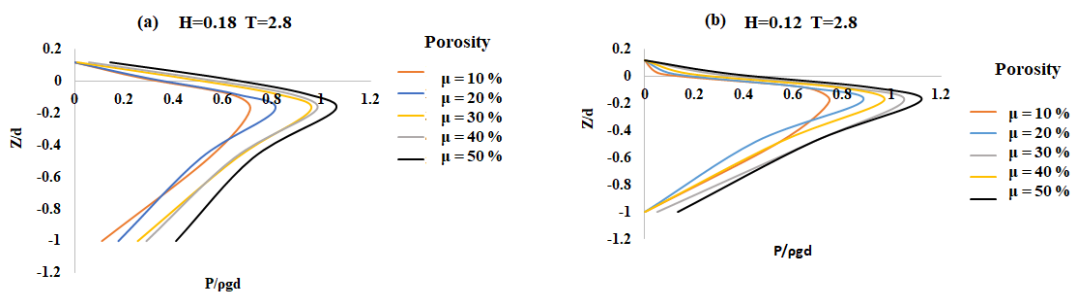
Figure 6.3 a) Variation of relative wave pressure (P/ρgd) with relative depth parameter on the wall (z/d), a) For d=0.5 m, S=1 m, H=0.18 m T=2.8 sec

b) For d=0.5 m, S=1 m, H=0.12 m T=2.8 sec
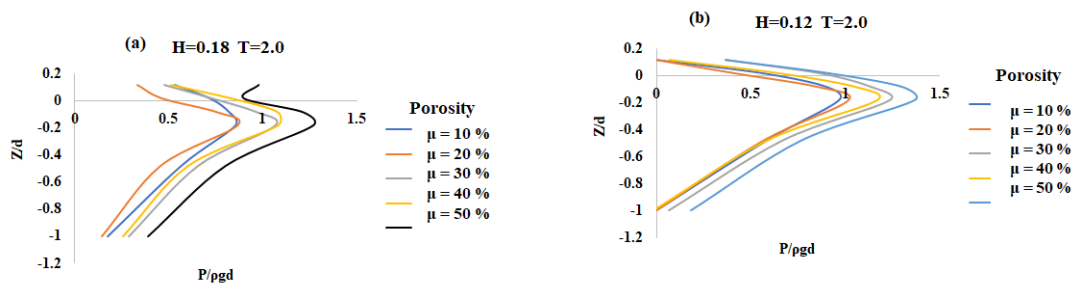
Figure 6.4 a) Variation of relative wave pressure (P/ρgd) with relative depth parameter on the wall (z/d), a) For d=0.5 m, S=1 m, H=0.18 m T=2.0 sec

b) For d=0.5 m, S=1 m, H=0.12 m T=2.0 sec

146
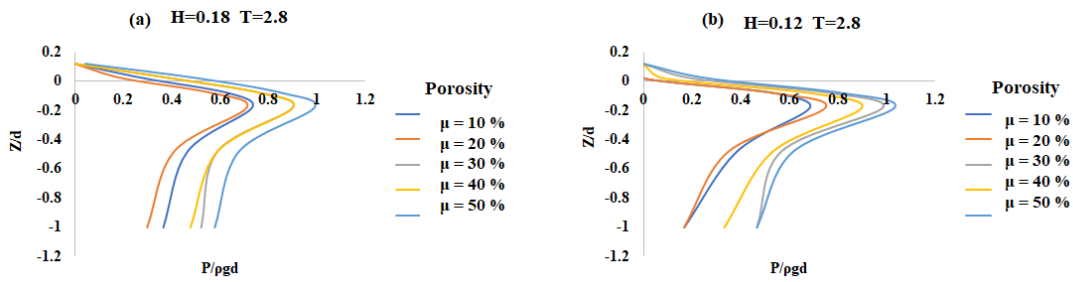
Figure 6.5 a) Variation of relative wave pressure (P/ρgd) with relative depth parameter on the wall (z/d), a) For d=0.5 m, S=3 m, H=0.18 m T=2.8 sec

b) For d=0.5 m, S=3 m, H=0.12 m T=2.8 sec
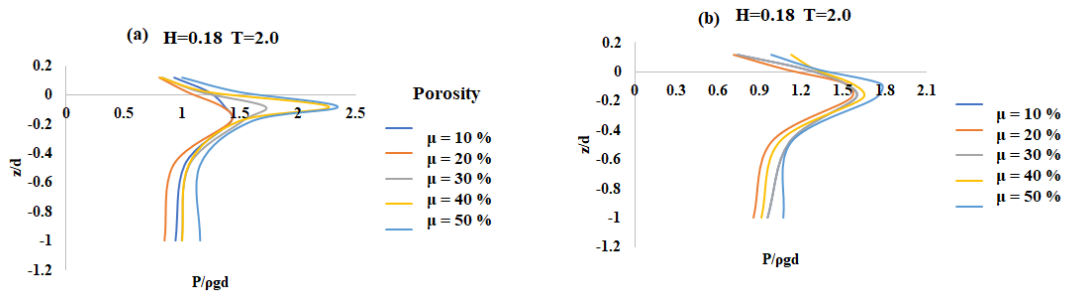
Figure 6.6 a) Variation of relative wave pressure (P/ρgd) with relative depth parameter on the wall (z/d), a) For d=0.5 m, S=3 m, H=0.18 m T=2.0 sec

b) For d=0.5 m, S=3 m, H=0.12 m T=2.0 sec

The wave pressures exerted on the VCB structure along the depth of the wall (z/d) for different wave periods and spacing are illustrated in Figures 6.3 - 6.6. The results are plotted with the non-dimensional pressure parameter (P/ρgd) on the X-axis with the non-dimensional depth parameter (z/d) on the Y-axis for varying porosities and spacing of the slotted barrier. Pressure transducers, P1 immersed at bottom of the test model, P2 sensor placed at a distance of 0.26 m from the position of P1 and P3, P4, P5, and P6 are positioned in a zigzag manner at an equal height of 0.05 m. It is observed that the relative pressure increases with relative water depth till the still water level, where it reaches the maximum value and then decreases with z/d having a minimum value at the bottom of the wall. Further, the relative pressure increases with an increase in wave period and wave height as long-period waves exert more pressure than the short period waves. In this study, pressure transducer number four placed near SWL with z/d= 0.08 experienced the maximum dynamic pressure and the porosity of the slotted barrier

increased from 10% to 50%, dynamic pressure acting on the caisson also increases since 50% porosity barriers allow passage of more amount of water than 10%. As the slotted barrier is moved from 1m to 3 m, there is a reduction of 25 % in dynamic pressure is observed in comparison with the 1m position.

In the case of a vertical slotted barrier, similar observations are observed and in the performance of pressure reduction 11% differences are observed.

6.5 VARIATION OF RELATIVE FORCE PARAMETER (F/ρgd^2) WITH RELATIVE WATER DEPTH (d/L)

To have a clear understanding of the effect of the porosity in front of the VCB and varying the position of the slotted barrier is needed for its cost-effective design. Figs. 6.7 to 6.10 illustrates the effect of porosity and position of slotted barrier in front of VCB for WFV for varying relative wave height H_i/d. The wave force F is made non-dimensional by dividing over the term (ρgd^2) and plotted on the y-axis. The x-axis indicates the relative depth of water (d/L). It is found from these figures that increasing the porosity from 10% to 50% consistently reduces the value of WFV. For the HSB (Horizontal Slotted Barrier) with H_i/d = 0.24, µ=10 % and position = 3m, it is noted that the WFV values varies from 0.31 to 0.135 for relative depth of 0.09 to 0.13.

Similarly, the HSB with H_i/d = 0.28, µ=50 % and position = 3m, it is noted that the WFV values varies from 0.485 to 0.306. The HSB placed at 1m distance, the relative force value varies in the range of 0.45 to 0.70 for (d/L) varying between 0.085 to 0.125. The reduction in the value of WFV is significant when the porosity of the slotted barrier is changed from 0% to 30% and the position from 1m to 3m. It is observed 19 % of reduction in total wave force when the HSB is at 3m When the porosity is more than 30%, the wave force reduction is marginal. Hence, varying the porosity from 15% to 25% is very sensitive in reducing the WFV. Like the spacing of the barrier increase from 1m to 3m, the wave force acting on the caisson decreases. When the barrier is away from the caisson, wave energy dissipation occurs, reducing the force acting on the caisson. It can also be inferred from the graph that relative wave force (F/ρgd^2)

increases with decreasing relative water depth (d/L) for a given wave steepness (H_i /L), since wave force F is directly proportional to wave period T.
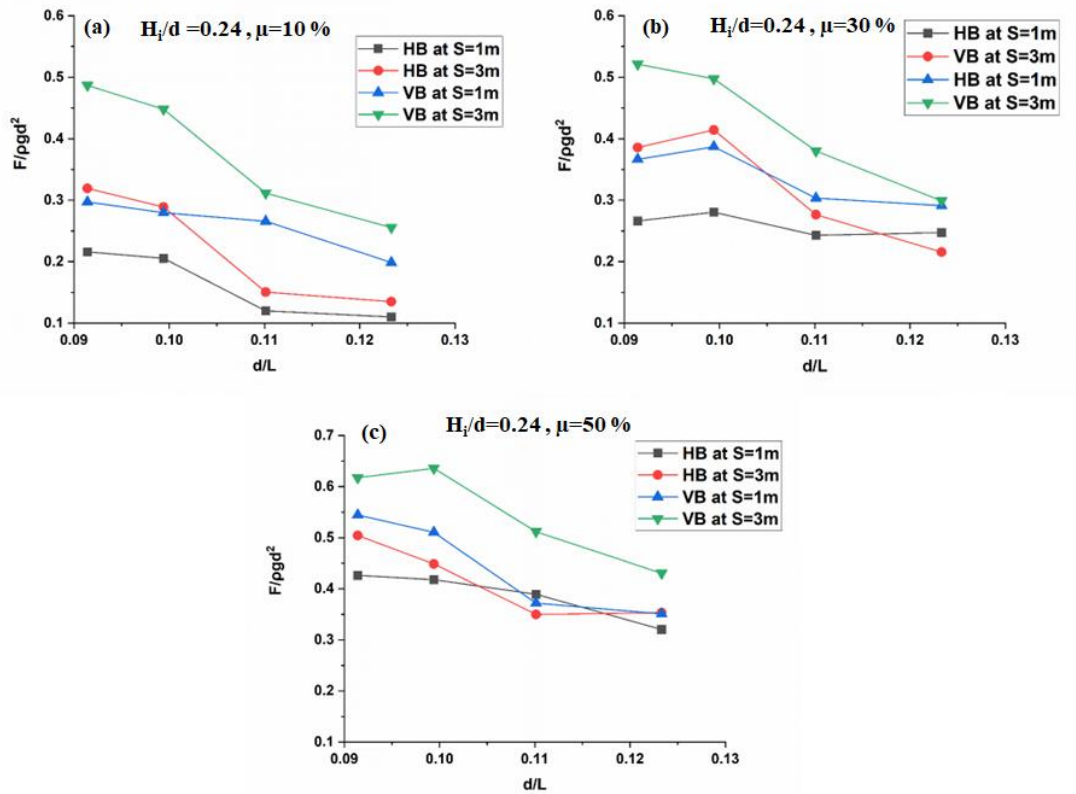
Figure 6.7 Variation of relative wave force parameter (F/ρgd^2) for VCB with relative water depth (d/L), For d= 0.50 m, H_i/d=0.24

Figure 6.8 Variation of relative wave force parameter (F/ρgd²) for VCB with relative water depth (d/L), For d= 0.50 m, Hᵢ/d=0.28
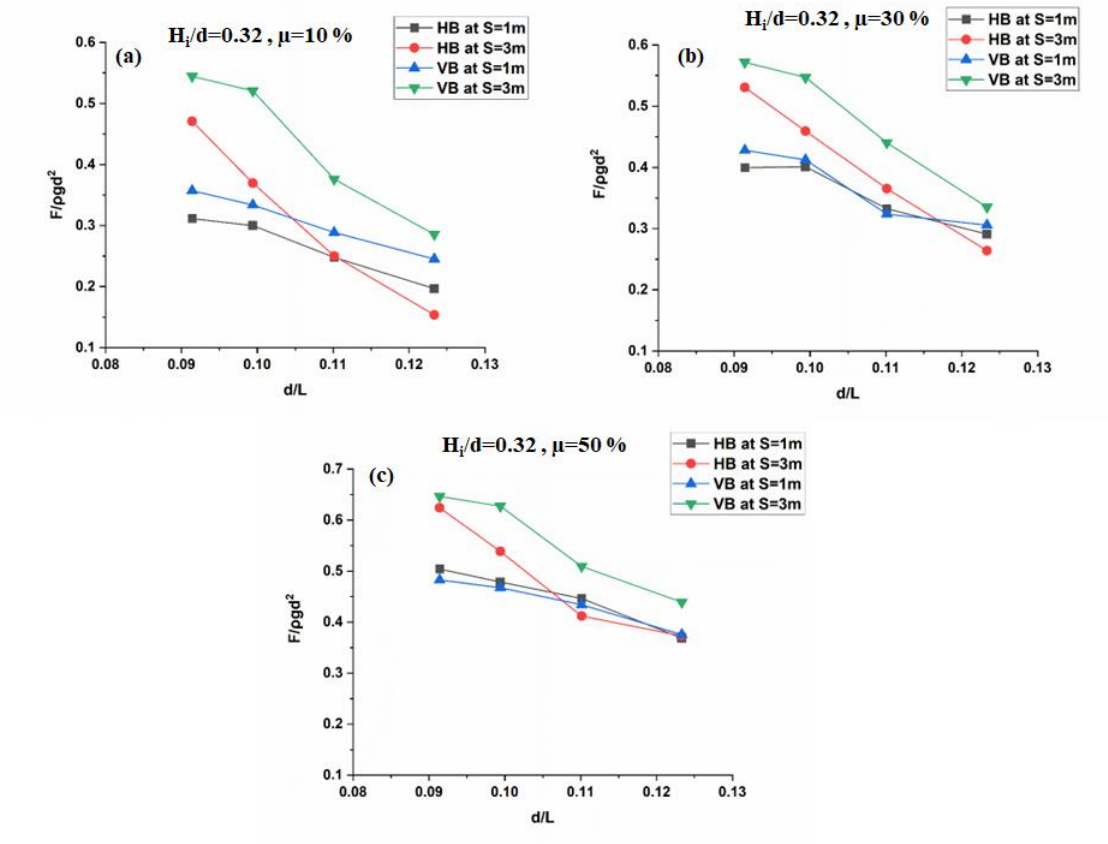
Figure 6.9 Variation of relative wave force parameter (F/ρgd^2) for VCB with relative water depth (d/L), For d= 0.50 m, H$_i$/d=0.32

Figure 6.10 Variation of relative wave force parameter ($F/\rho gd^2$) for VCB with relative water depth (d/L), For d= 0.50 m, H_i/d=0.26

In the case of vertical slotted barrier (VSB), similar trends are observed but in the total wave forces in comparison with HSB 17 % of differences are observed at the 3m position, in the case of 1m position, 12 % of differences are observed. Overall, it is found that increasing the porosity of the barrier from 10% to 50% helps to reduce the WFC progressively. Long waves and low porosity results in the highest value of WFC (more than 0.7). Short waves and high porosity help to reduce the value of WFC significantly (less than 0.3). Meanwhile, increasing the porosity of the barrier results in a minimum projected area for wave action on the barrier and more penetration of wave energy through the slots, resulting in less wave force transfer on the VCB. Hence, to reduce the wave force, it is essential to increase the porosity of the barrier.

6.6 VARIATION OF WAVE REFLECTION COEFFICIENT (K_r) WITH RELATIVE WATER DEPTH (d/L)

Figures 6.11 to 6.14 illustrates the trends in the variation of reflection coefficient (K_r) with different wave parameters. The reflection coefficient (K_r) is plotted with the relative depth parameter (d/L) for different porosity and relative wave height (H_i/d). The DHI wave synthesizer analysis software, MIKE ZERO was used for the wave reflection analysis. The wave up-crossing analysis is used for regular wave runs, and the average value of all the wave heights within the 30 sec span is used as the measured incident wave height. Data from three wave probes are used to estimate the reflected wave height and coefficient of reflection, (K_r) which is defined as $K_r = H_r/H_i$, where H_r is the reflected wave height.
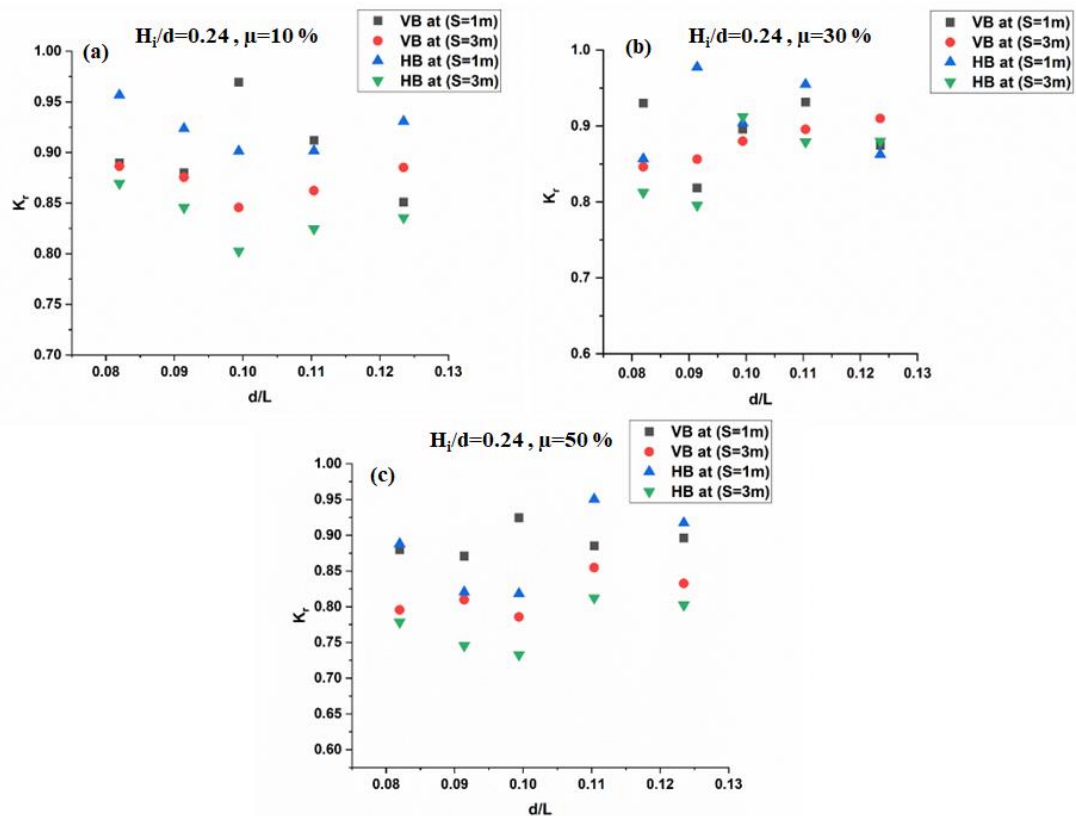
Figure 6.11 Variation of wave reflection coefficient (K_r) with relative water depth (d/L), For d= 0.50 m, H_i/d=0.24
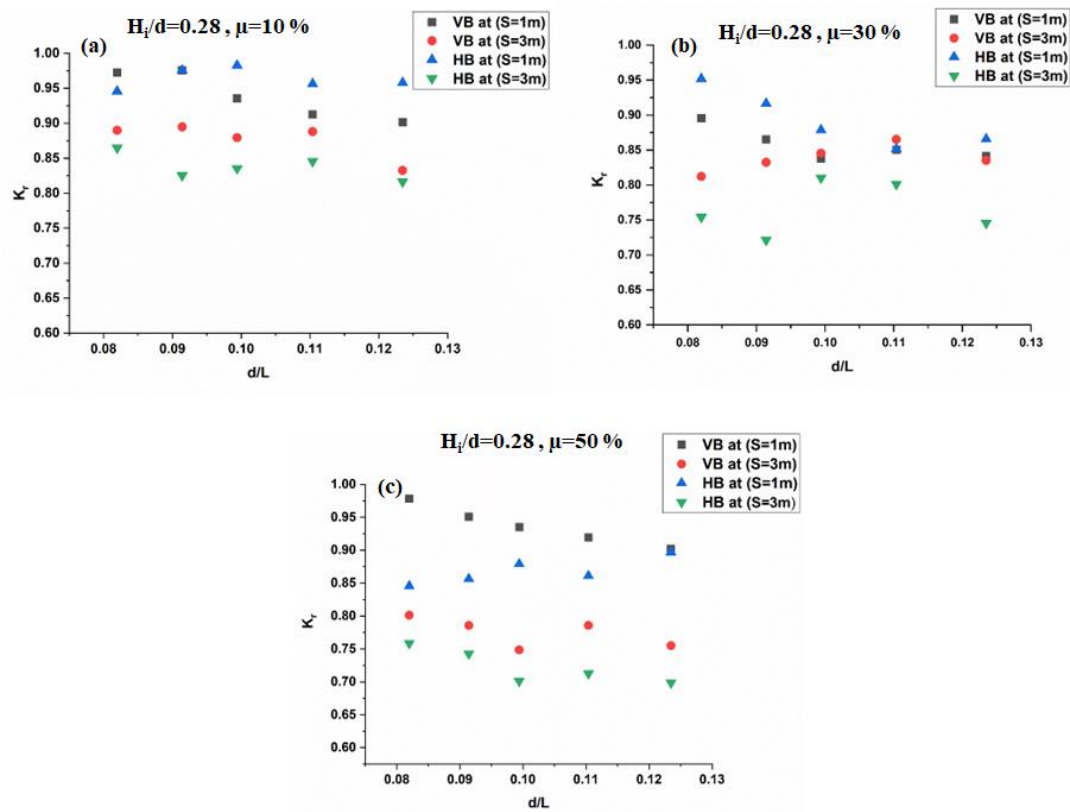
Figure 6.12 Variation of wave reflection coefficient (K_r) with relative water depth (d/L), For d= 0.50 m, H_i/d=0.28
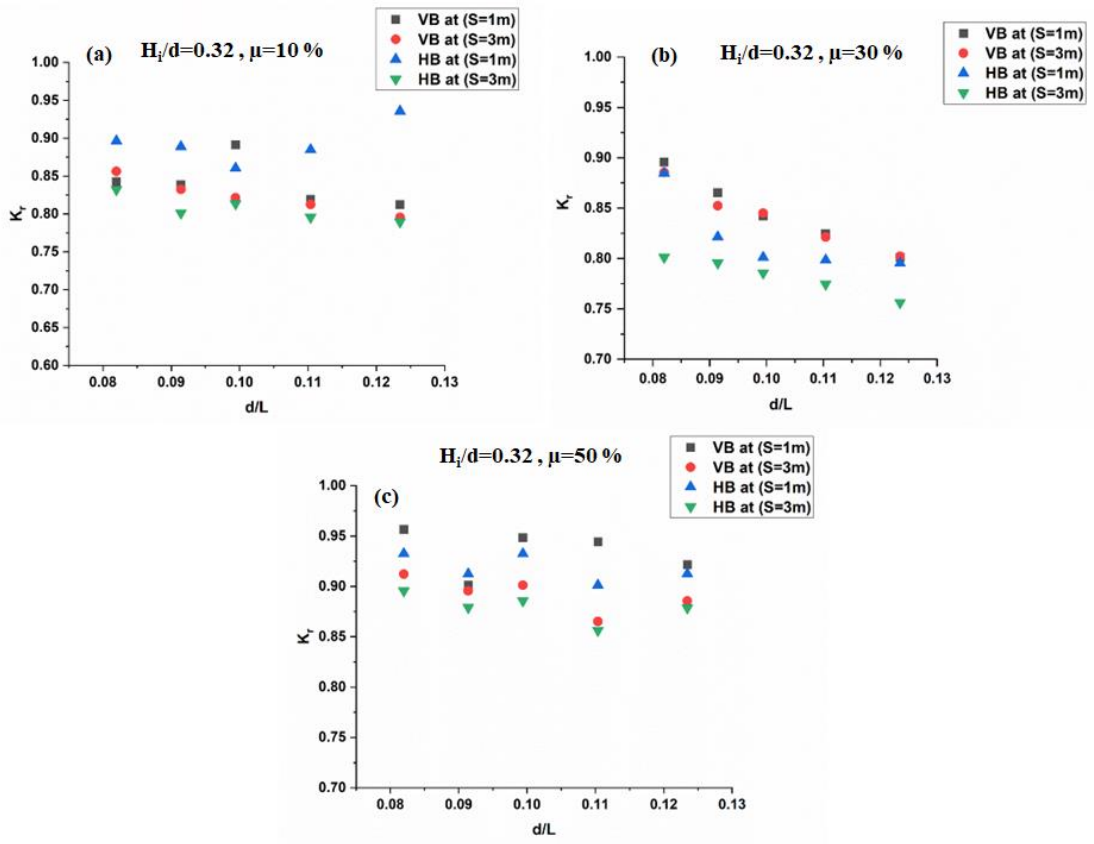
Figure 6.13 Variation of wave reflection coefficient (K_r) with relative water depth (d/L), For d= 0.50 m, H_i/d=0.32
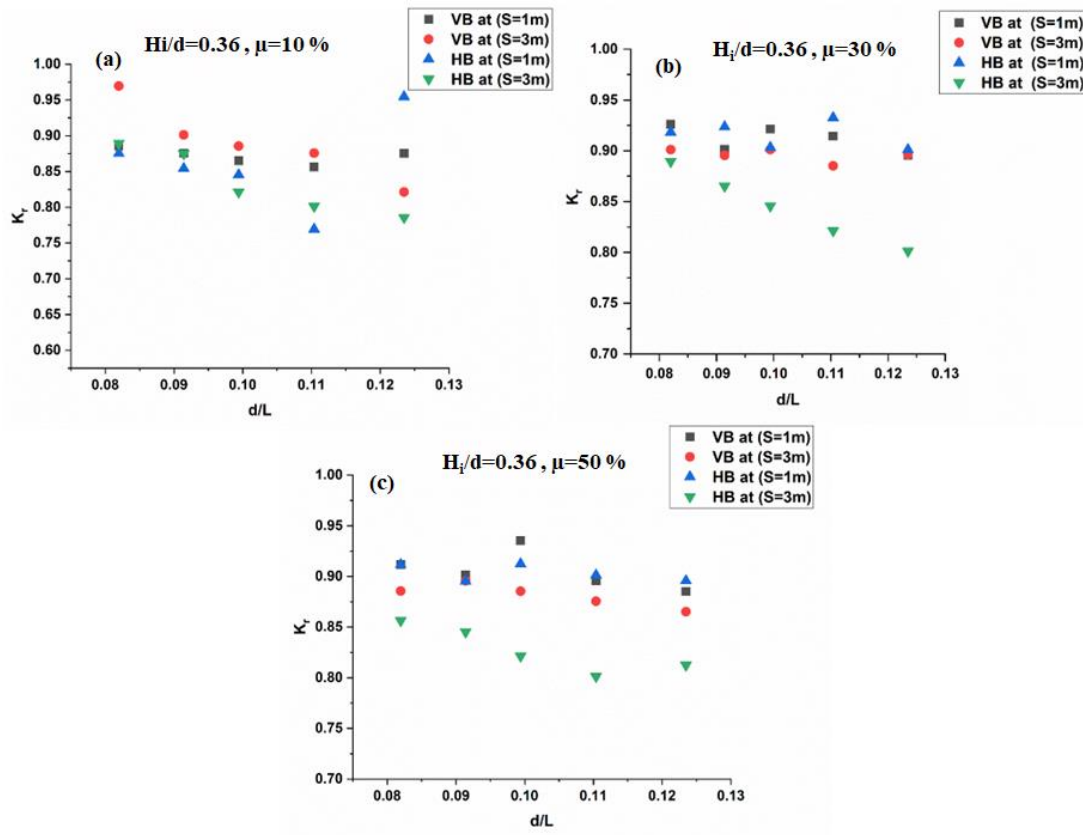
Figure 6.14 Variation of wave reflection coefficient (K_r) with relative water depth (d/L), For d= 0.50 m, H_i/d=0.36

The reflection analysis software in MIKE ZERO is based on the method described by Mansard and Funke (1987) and extended by Zelt add Skjelbreia (1992). The distance between Wave Probes is kept L, L+(L/3) & L+(2L/3) from the test model these distances are used as inputs for the reflection analysis. Using three-wave probes is preferable to using two-wave probes in order to avoid singularity problems during reflection analysis.

From the analysis of results, the HSB are found to be efficient in enhancing the reduction of wave reflection as it increases the energy loss through the slots in comparison with VSB. As the incident relative wave height increases reflection coefficient K_r also increases. The value ranges from 0.65 to 0.94 as relative incident wave height increases from 0.24 to 0.36.

For a given relative depth, the K_r value is found to be highest for 50% porosity for both H_i/d = 0.24 and H_i/d =0.36 because most of the wave energy is penetrated the slots and

156

is reflected by the VCB. By placing HSB in front of the caisson, the reflection coefficient can be brought down to values of 0.69 for a porosity of 30% at a barrier position of 3m. At the same time, a 32 % reduction in the values of K_r is observed in comparison with the position of 1m. In the case of VSB, it gives higher K_r values for all cases in comparison with HSB, when the flow of wave passes through the HSB, the wave is easily accommodated in the HSB as it has more penetration spacing and results in reducing the wave reflection. Whereas in the case of VSB, barrier arrangements obstruct the wave flow more which results in less penetration and result in more wave reflection.

Overall, the HSB, with 30 % porosity at a position of 3 m is observed more significant in the performance compared with VSB.

6.7 VARIATION OF RELATIVE RUN-UP (R_u/H_i) WITH DEPTH PARAMETER (d/L)

The variation of relative wave run-up (R_u/H_i) as a function of relative water depth (d/L) is illustrated in Figures 6.15 -6.18, for various relative wave heights (H_i/d). In general, the wave runup is defined as the vertical rise of water above the still-water level to which the water rushes up on the front face of the test model. This helps in determining the design wave crest level of the structure depending on the allowable overtopping level. From the graph, it is observed that the relative run-up (R_u/H_i) is increasing with an increase in the relative depth (d/L) for the depths of water.

The value of R_u/H_i varies between 0.25 and 1.4, as the relative depth varies from 0.084 to 0.13. The (R_u/H_i), increases with an increase in H_i/d because the higher wave heights rush up the waves above still water level and the short period waves have more runup on both HSB and VSB.
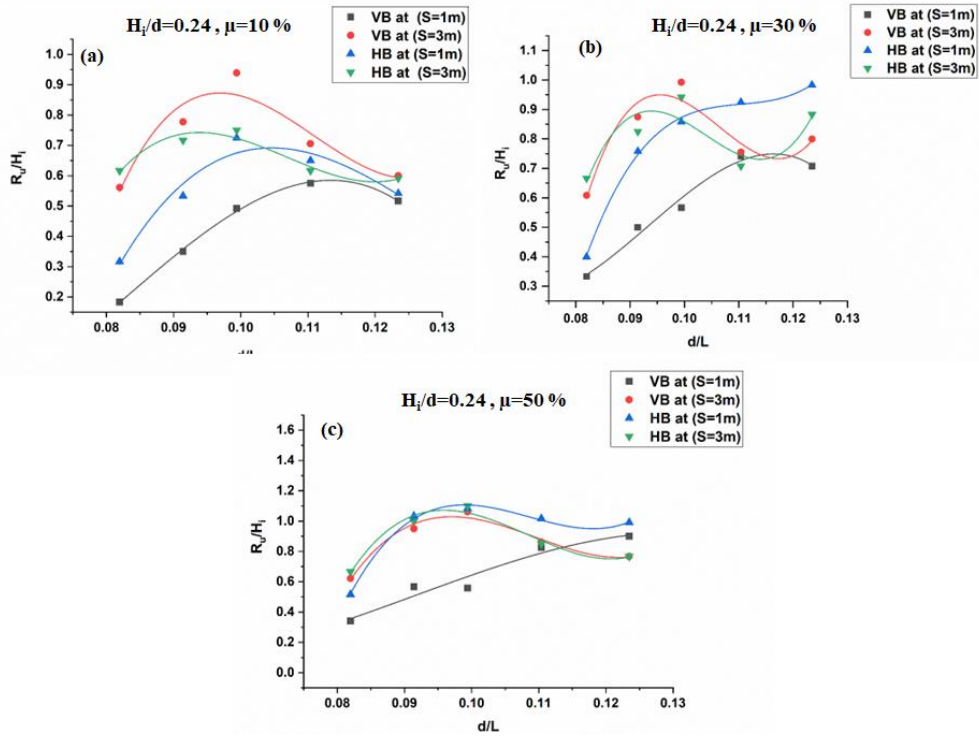
Figure 6.15 Variation of wave runup (R_u/H_i) with relative water depth (d/L)
(For d= 0.50 m, H_i/d=0.24)
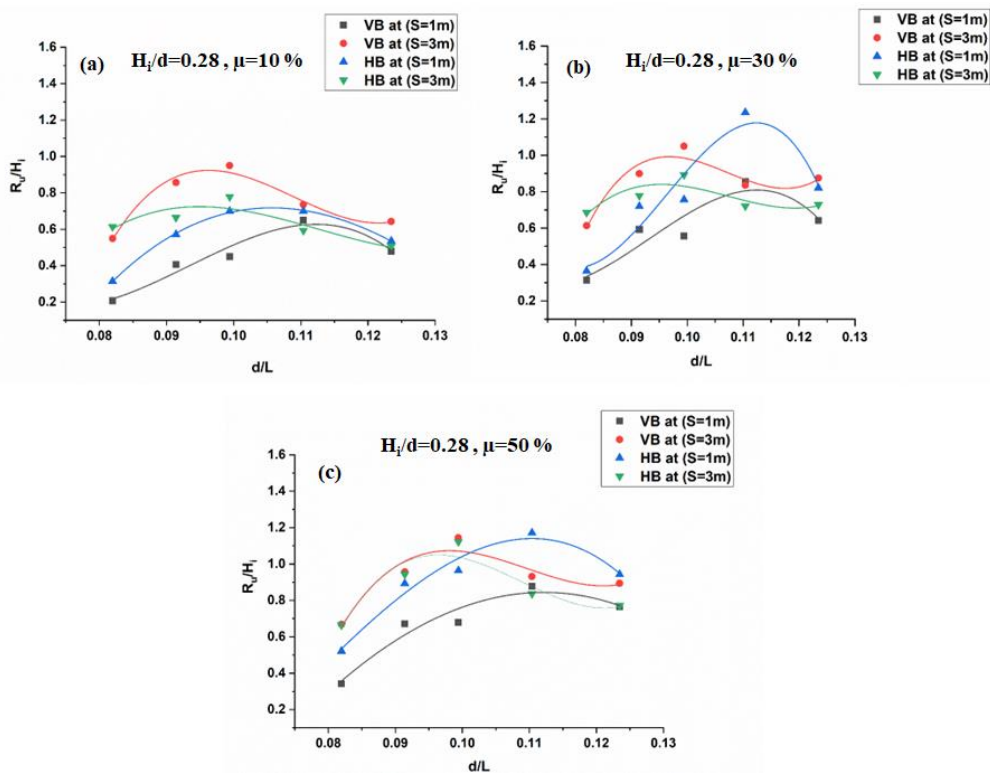
Figure 6.16 Variation of wave runup (R_u/H_i) with relative water depth (d/L)
(For d= 0.50 m, H_i/d=0.28)

158
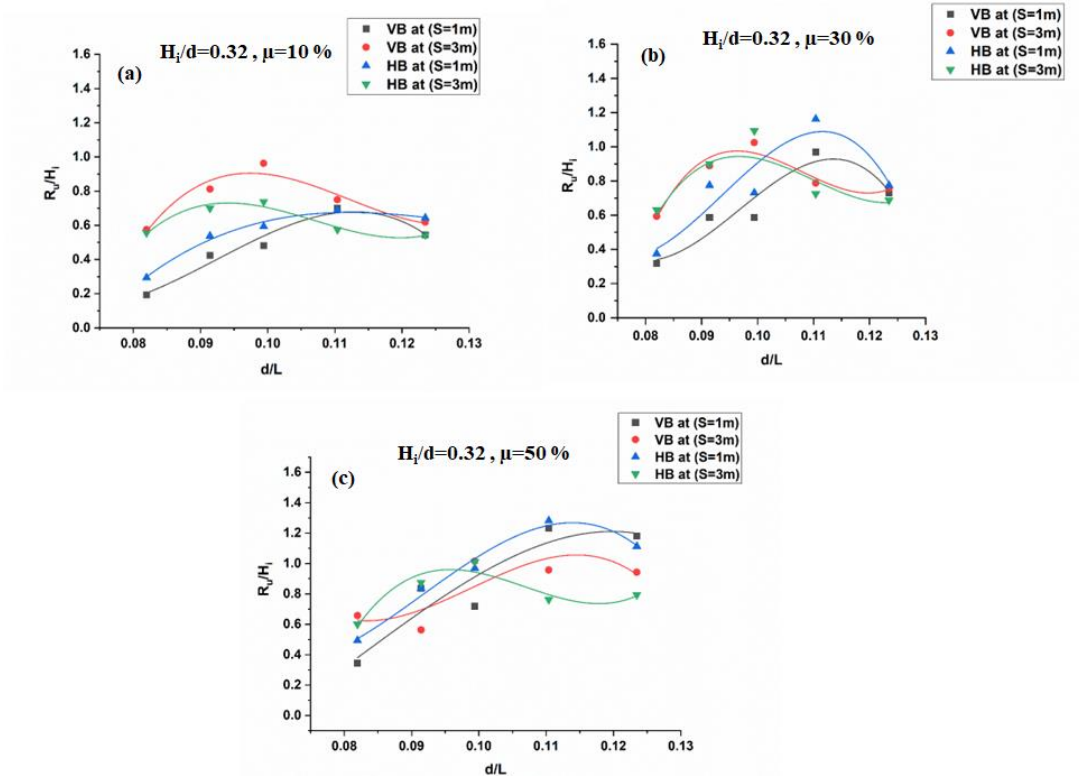
Figure 6.17 Variation of wave runup (R_u/H_i) with relative water depth (d/L)
(For d= 0.50 m, H_i/d=0.32)
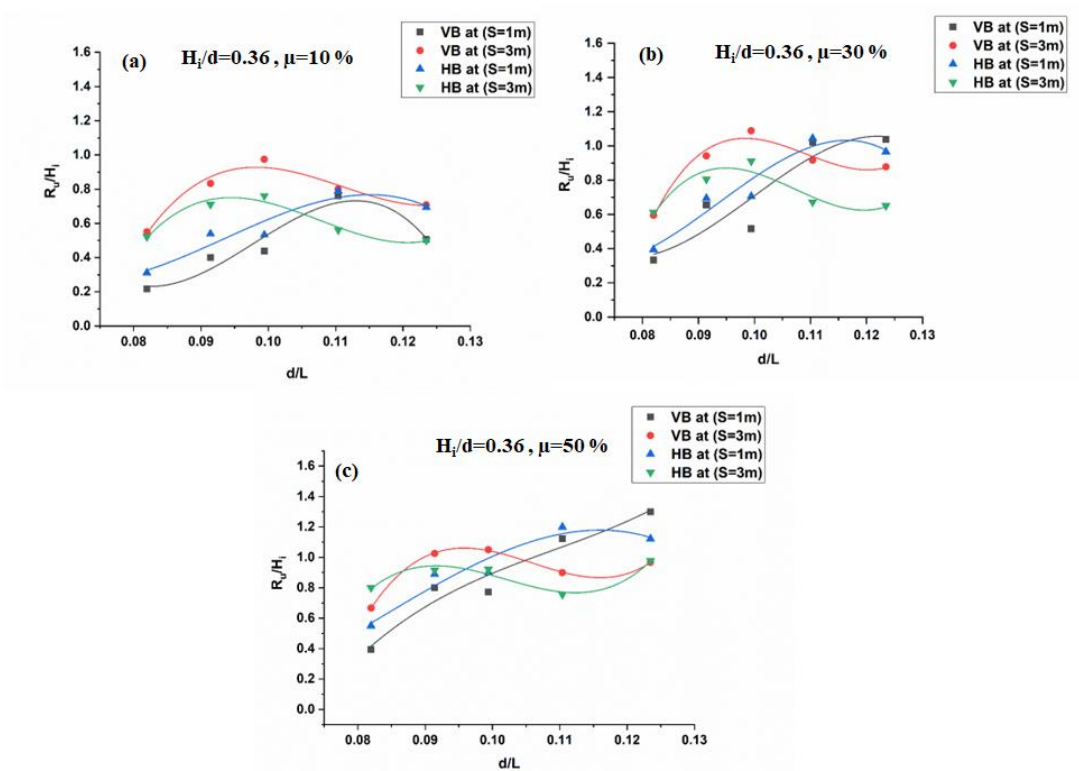
Figure 6.18 Variation of wave runup (R_u/H_i) with relative water depth (d/L)
(For d= 0.50 m, H_i/d=0.36)

As the porosity of the barrier increases from 10% to 50%, the run-up increases on the caisson, as higher porosity barriers interrupt less on wave passage through them, more water is hitting on the caisson and thus more run up on the surface. For 10% porosity, the relative run-up varies from 0.25 to 0.7 similarly, for 30% porosity relative run-up is varying from 0.45 to 1.2 and for 50% porosity from 0.5 to 1.3. Increasing the porosity after 30 % the reductions are marginal in both HSB and VSB.

In the case of wave runup, VSB gives better performance than SHB because the flow of wave passes through the HSB, is easily accommodated and has more penetration spacing and resulting in increasing the wave runup on VCB. Whereas in the case of VSB, barrier arrangements obstruct the wave flow more which results in less penetration and result in lower wave runup.

6.8 NUMERICAL APPROACH

From the outcome of the experimental investigations, the HSB gives better performance than VSB. So, it is decided that the numerical simulations are carried out with horizontal slotted barriers (HSB) in front of a Vertical caisson breakwater with the protection of the toe using a commercial CFD code, ANSYS Fluent.

In the subsections, the numerical performance and the results obtained using the numerical method are evaluated with experimental results to quantify errors within the model and to check whether the errors are within acceptable levels. Simulations are carried out for conditions varying the porosities of the slotted barrier from 10% to 50% and spacing from 1 meter to 3 meters with a VCB.

6.9 GEOMETRICAL AND MESHING DETAILS OF THE TEST MODEL

A two-dimensional numerical wave flume is modelled with dimensions of a length of 20 m, and a height of 1.1 m modelled using the Design Modeler in Fluent. The water depth of 0.5 m and test model height of 0.9 m are considered for the present numerical investigation. The schematic of the numerical flume model with VCB and its dimensions are given in Figure 6.19. The test model is located at a distance of 18 m from the wave generation zone. To obtain the surface elevation at required positions (at a distance of L, L+(L/3), and L+(2L/3) from the test model) even at maximum

wavelength conditions (6 m), 18 m distance is maintained between the test model and wave generation point.
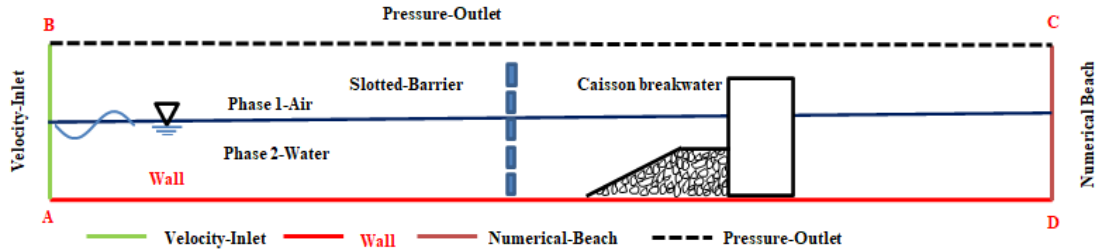
Figure 6.19: Geometry of the flume model with boundary conditions.

The meshing details are explained in the previous chapter 6, and the same is adopted in this chapter.

6.10 SOLVER SETUP

Figure 6.19 shows the boundary conditions with various coloured lines assigned to the Numerical Wave Tank. Boundary AD represents the inlet of the wave tank which describes the wave maker. An inlet velocity type wave generator is given, which generates regular waves. Boundary DC represents the wave flume bottom, which is assigned wall boundary condition so that no-slip wall condition is maintained. Boundary BC represents the end of the wave tank and boundary AB represents the free surface of the flume, both of which are assigned as pressure outlets. The gauge pressure is set at zero at the upper boundary, with atmospheric pressure as the reference pressure. The waves and currents are generated at the inlet of the tank while the reflected waves are absorbed at the outlet of the tank. Implementing a numerical beach at the end of the domain is a way of improving the absorption of incident waves and reducing their reflection. Hence, numerical beach condition is assigned at the end of the tank. The toe protection is defined as a porous layer to mimic granite stones from a regular heap of building materials as used in the experiment bounded by an interior boundary condition.

The interior of the domain is set to a fluid zone for which all active equations will be solved. The temporal discretization plays a quite important role in the quality of the solution. Large time step intervals cause wave damping. However, small-time step intervals significantly increase the computational time to reach the solution. Thus, the

161

choice of time step interval should be correctly evaluated. In this thesis, the time step chosen is 0.01 seconds, the total number of steps is 1500, k-ε turbulence model and the flume walls are assigned as No-slip wall conditions for all numerical solutions. The Volume of Fluid method is used because it is the most suitable method for tracking the free surface between air and water.

The VOF method can model two or more immiscible fluids by solving a single set of equations for the amount of movement and tracking the volume fraction of each fluid throughout the volume. The production and propagation of regular waves do not vary with the model of turbulence (Lal et.al (2008) and Finneganet. al (2012)). Hence in this study, the k-ε turbulence model is chosen. The flume walls are assigned as No-slip wall conditions.

6.11 FLOW FIELD ANALYSIS BASED ON CFD

The numerical wave tank with a caisson-type breakwater and horizontal slotted barrier are modelled in the designer modeller tool as explained in section 7.9. The input for numerical waves of wave parameters is taken from the experiment study as discussed in Table 6.2. Figures 6.21-6.24 illustrates the typical result of the numerical flow field near the slotted barrier for $H_i/d=0.36$, μ=30 %, T=2.2 s for 10 s, 50 s and 30 s. This helps for further understanding of the intensity and spatial variation of the kinematics of the water particle during its interaction with multiple slotted barriers.
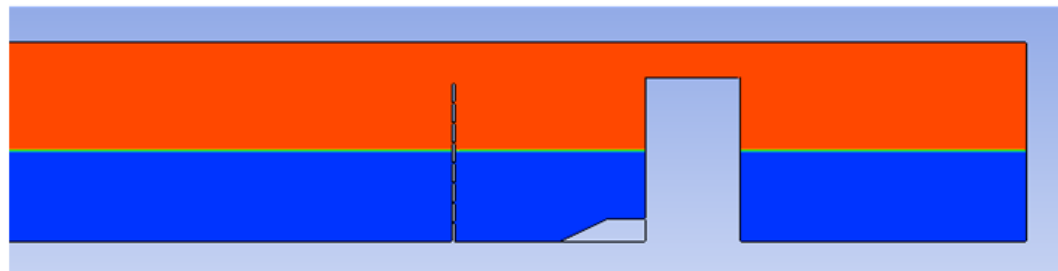
t= 5s
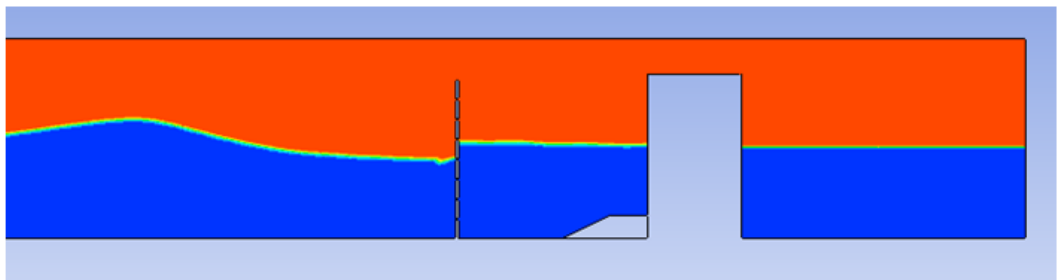
t= 5s
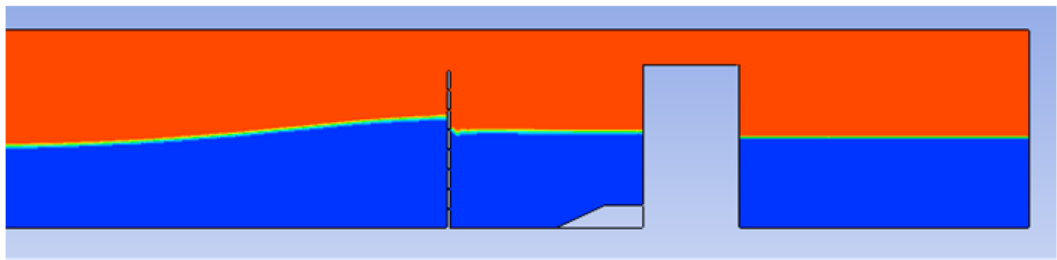
t= 10s

Figure 6.20: Numerical flow field near the HSB for 1 m position
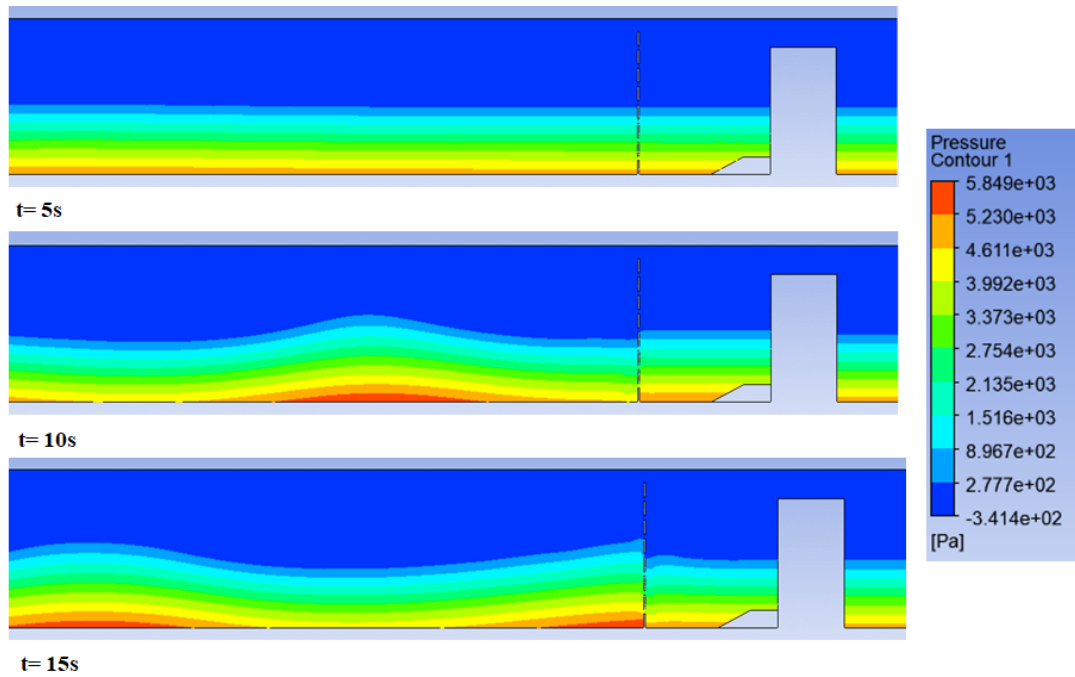
H_i/d=0.36, μ=30 % and T=2.2 s

Figure 6.21: Pressure contour field near the HSB for 1 m position
$H_i/d=0.36$, $\mu=30$ % and $T=2.2$ s
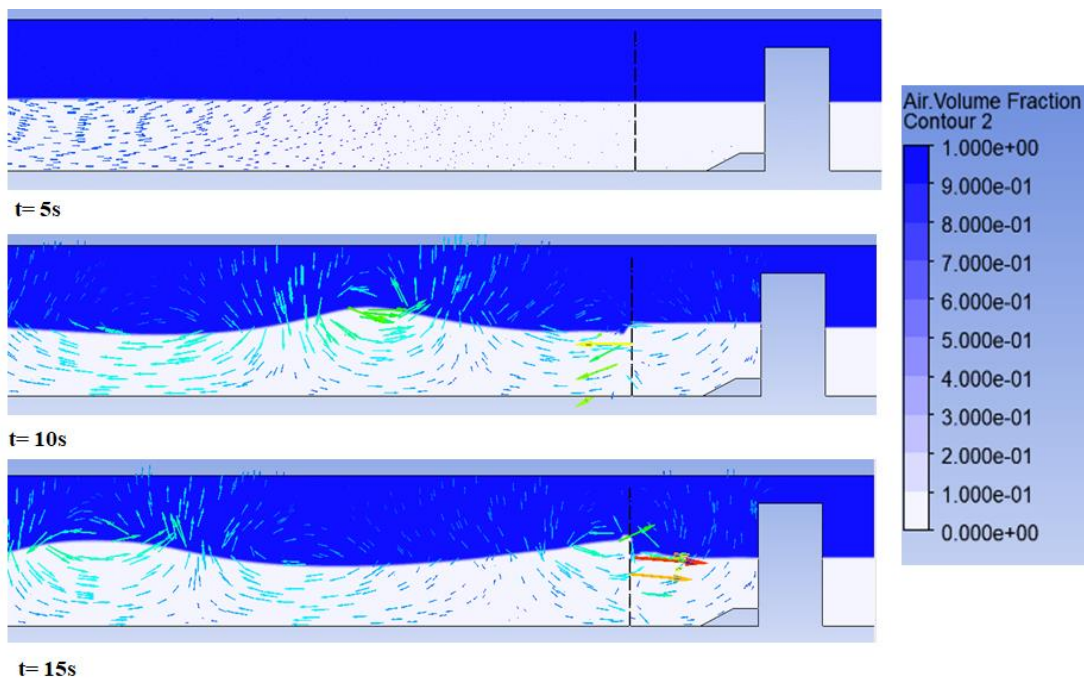
Figure 6.22: Velocity contour field near the HSB for 1 m position
$H_i/d=0.36$, $\mu=30$ % and $T=2.2$ s

164
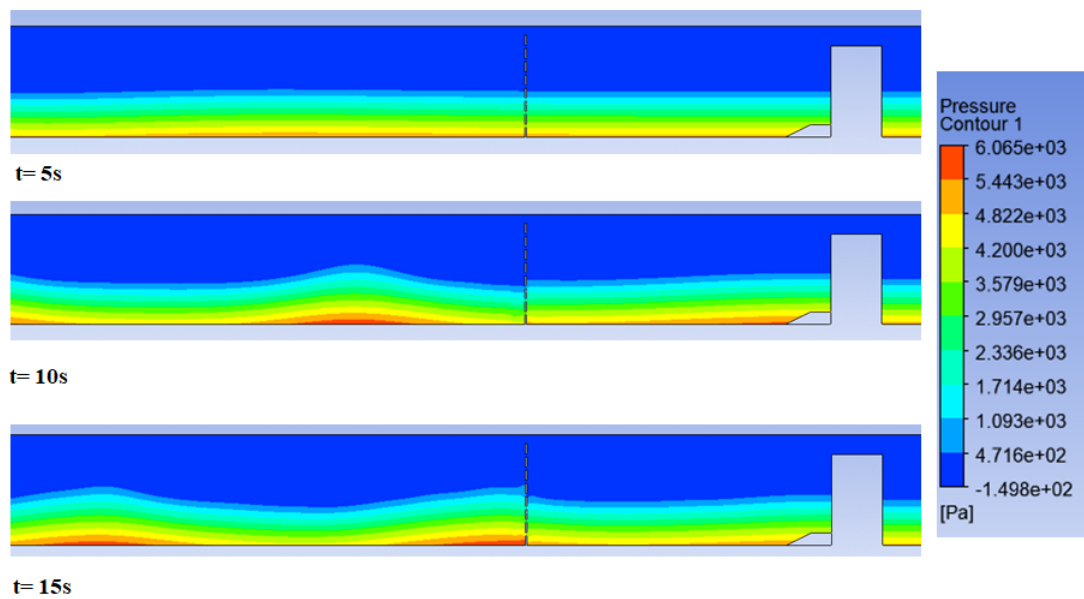
Figure 6.23: Pressure contour field near the HSB for 3 m position
H_i/d=0.36, μ=30 % and T=2.2 s
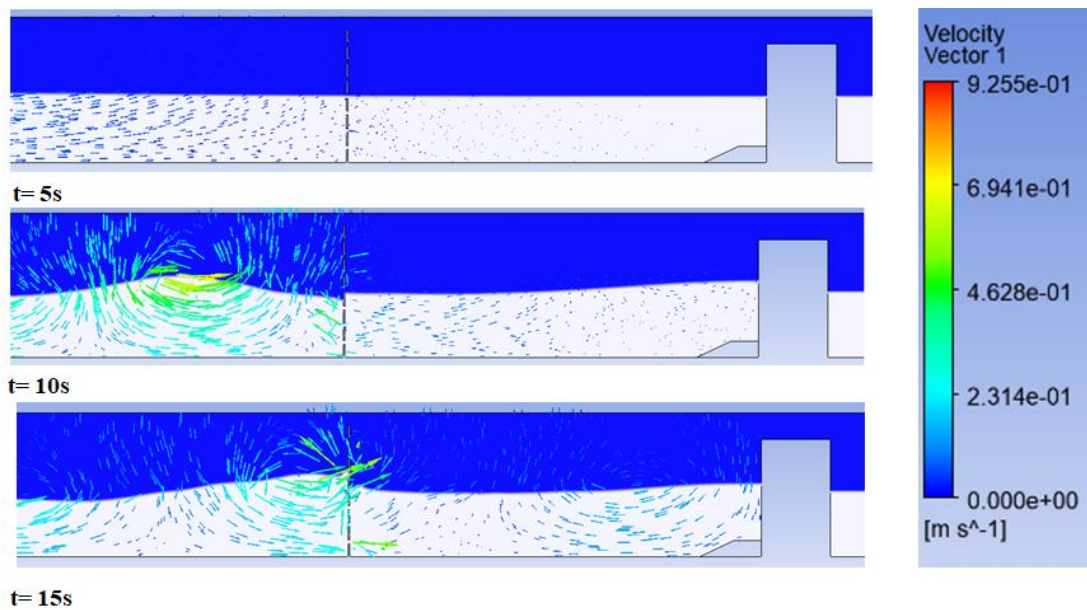
Figure 6.24: Pressure contour field near the HSB for 3 m position
H_i/d=0.36, μ=30 % and T=2.2 s

Figure 6.21 gives the velocity field during wave interaction with the slotted structure
and shows the generation of turbulence and jet-like flow in the vicinity of the slotted
barrier at 1m positioning from VCB, which is responsible for the wave energy losses
and at the same time the variation in pressure contours and velocity near the flow field

165

gives the better clarity at the vicinity of slots. Similarly, at 3m positioning of the slotted barrier from the VCB is illustrated in Figures 6.23 -6.24.

The snapshot clearly shows that the horizontal slotted barriers are very active in changing the water particle kinematics and the wave crest at 15s (Fig. 6.21), it is clear that the potential energy difference is a strong jet action and strong turbulence at the slotted. This is in line with the general understanding of the wave interaction with multiple slotted barriers during the physical model studies (Neelamani and Anjari, 2020). Further, the vector field around the barriers demonstrates the curl, flow separation, water jet, and free surface fragmentation, resulting in additional loss of energy. Because of the closely spaced multiple barriers, the water is set into piston mode for the initial duration and after which water recedes in the slots between the slats to the next partially confined chambers.

In this way, the flow reversal and the path to the next chamber are increased. It may also be noted that CFD-based results are having a good correlation with experimental results up to barrier porosities of 40% which is otherwise not viable with potential flow-based numerical models (Vijay et al., 2019).

6.12 VALIDATION OF DEVELOPED NUMERICAL MODEL WITH EXPERIMENTAL RESULTS

6.12.1 Effect of incident wave steepness (H_i/L) on horizontal wave force parameter ($F/\rho gd^2$)

From the experimental observation HSB with 30 % at 3m positioning gives better performance compared with all other cases and hence for validation, the same case has been used. Figure 6.25 illustrates the horizontal wave force F divided over the term (ρgd^2) and gives the non-dimensional parameter which is plotted on the Y-axis, against incident wave steepness (H_i/L) on X-axis.

166
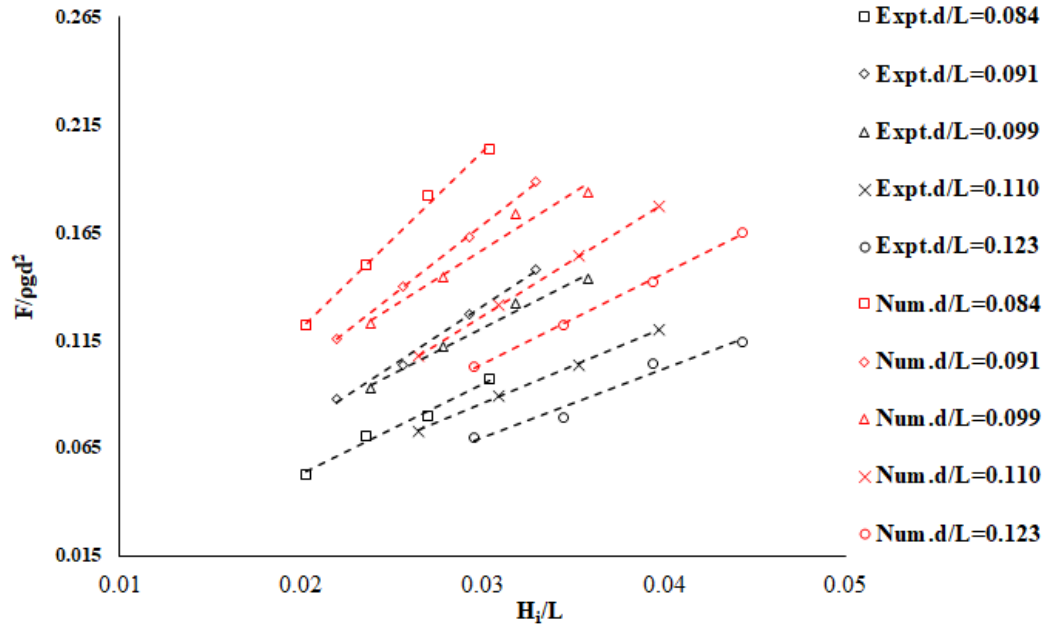
Figure. 6.25 Variation of relative wave force with incident wave steepness and relative wave depth for µ=30% and S=3 m

It is observed that the relative wave force parameter ($F/\rho gd^2$) increases with an increase in wave steepness (H_i/L) for a given relative water depth (d/L). As H_i/L increases from 0.020 to 0.044, $F/\rho gd^2$ increases by 22.5%, for d/L = 0.123. It can also be inferred from the graph that relative wave force ($F/\rho gd^2$) increases with decreasing relative water depth (d/L) for a given wave steepness (H_i/L). As d/L increases from 0.091 to 0.123, $F/\rho gd^2$ decreases by 18.2%. The deviation of the horizontal wave forces obtained using Experimental and the numerical wave force value is obtained as percentage error using the formula given:

$$\% \text{ Error} = \frac{1}{F_N}\left(F_{Exp} - F_N\right) * 100 \tag{6.1}$$

where F_N and F_{Exp} denote respectively the numerically computed force and the reference force value for various d/L values. And also, a slight deviation is observed for the range of (0.11-0.12) d/L and the mean relative error of 8.5 % with an acceptable range.

6.13 EFFECT OF INCIDENT WAVE HEIGHT (H$_i$/d) ON REFLECTION COEFFICIENT (K$_r$)

Figure 6.26 demonstrates the variation of K$_r$ as a function of relative water depth (d/L) for different values of relative wave height (H$_i$/d) in the case of a slotted barrier with 30% porosity placed and 3m spacing.
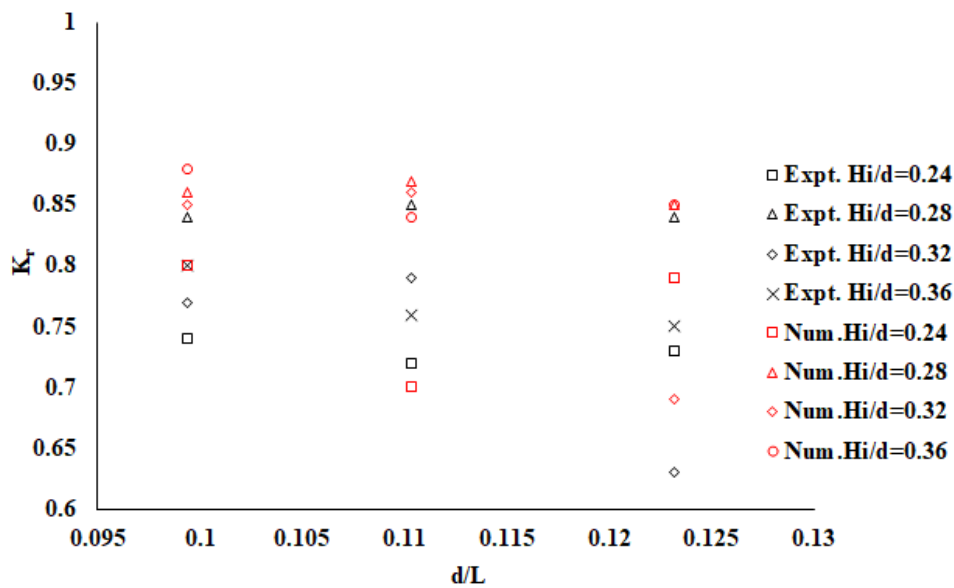
Figure 6.26 Comparison of numerical and experimental wave reflection coefficient (K$_r$), for μ=30% and s=3 m

From the figure, it is observed that the reflection coefficient (K$_r$) increases as incident wave height increases, for a given relative water depth (d/L) K$_r$ increases as H$_i$/d increases, for a given (d/L), because the energy under the wave with higher wave height will be more, and thus, more energy gets reflected the seaside. K$_r$ value increases by 10% as H$_i$/d 0.24 to 0.36 for d/L=0.099.

A similar trend is obtained by Vijay et.al (2019) which reveals that in the case of two slotted walls with 10% porosity, as wave height increases, the wave reflection increases in experimental and numerical methods. The deviation of the Reflection Coefficient K$_r$ obtained from the experimental method from the numerical wave force value is obtained as a percentage error using the formula given:

$$\% \text{ Error} = \frac{1}{Kr_{Exp}}\left(Kr_{Exp} - Kr_{Num}\right) * 100 \tag{7.2}$$

where Kr_N and Kr_{Exp} denote respectively the numerically computed reflection coefficient and the reference reflection coefficient value for various d/L values. On comparing, the experimental K_r values are found to be in good agreement with numerical K_r values with an error percentage lying between 3.33% and 9.98%, which is in the acceptable range. (Fabino et al. (2018)

6.14 EFFECT OF SPACING (S) ON REFLECTION COEFFICIENT (K_r)

To determine the effect of spacing on reflection coefficient K_r, a graph is plotted by varying the spacing of the slotted barrier (μ=30%) from 1m to 3m. On the Y axis, K_r is plotted against relative water depth d/L on X-axis as shown in Figure 6.27.
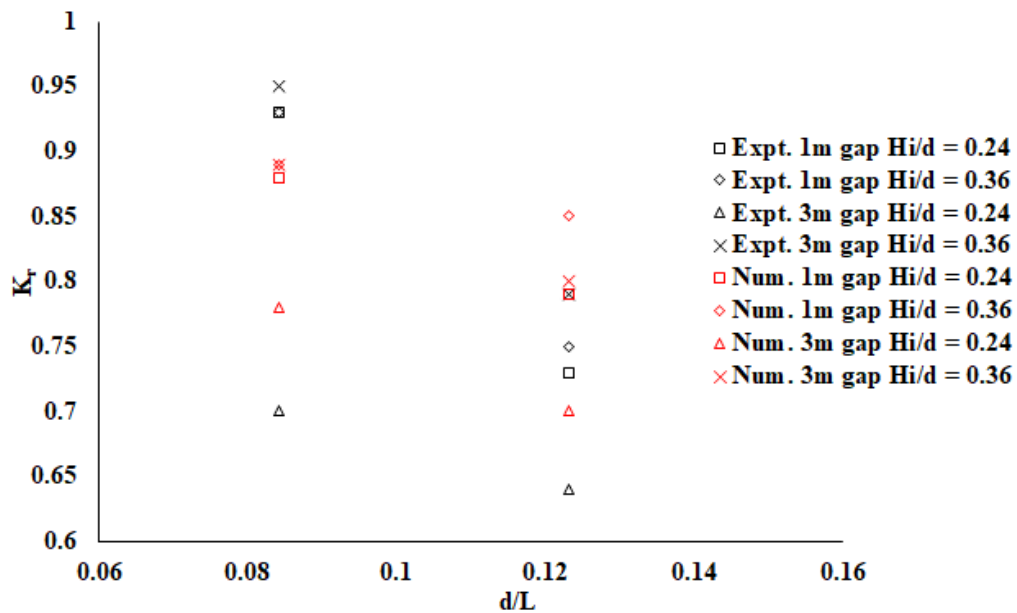
Figure 6.27 Comparison of numerical wave reflection coefficient (K_r) and

experimental wave reflection coefficient, for Hi/d=0.24,0.36 and μ=30%

From figure 6.27, it can be inferred that the reflection coefficient increases with decreasing in spacing, for a given relative water depth, i.e., higher K_r values are obtained for smaller spacing. As waves propagate through the wave chamber, energy dissipation of waves occurs which in turn results in lesser reflection. K_r value increased

by 12.82% when the spacing of the slotted barrier was decreased from 3m to 1m, for $d/L=0.084$ and $H_i/d=0.24$. It is also observed that the K_r value increases with H_i as waves of higher steepness, the energy under the wave will be more, and thus, more energy gets reflected on the seaside deviation of numerical K_r values from experimental values, expressed as in terms of % error is found to be within the range of 4.49% - 7.89%, which is acceptable.

6.15 CLOSURE

In this Chapter, the role of an HSB and VSB in front caisson breakwater on the mitigation of wave-induced response is analyzed using the experimental approach. The main findings are outlined below point-wise.

- For both HSB and VSB, the relative pressure increases ($P/\rho gd$) with relative water depth (d/L) till the still water level, where it reaches the maximum value and then decreases with (z/d) having a minimum wave pressure at the bottom of the wall. Similarly, when the spacing is increased from 1 m to 3 m, there is a reduction of 25 % in the dynamic pressure.
- The reduction in the value of wave force variation (WFV) is significant when the porosity of the slotted barrier is changed from 0% to 30% and the position from 1 m to 3 m. It is observed that 19 % of reduction in total wave force when the HSB is at 3m. At the same time, when the porosity is more than 30%, the wave force reduction is marginal. Hence, varying the porosity from 15% to 25% is insignificant in reducing the WFV.
- In the case of vertical slotted barrier (VSB), similar trends are observed. But the total wave force corresponding to S=3 m, is 17 % more than HSB, while for S=1 m it is 12 % higher.
- In the case of wave runup, VSB gives better performance than SHB because the flow of wave passes through the HSB, is easily accommodated, and has more penetration spacing and resulting in an increase in the wave runup for VCB. Whereas in the case of VSB, barrier arrangements obstruct the wave flow more which results in less penetration and lower wave runup.

170

- The observed value of wave reflection coefficient (K_r) is 0.69 for a porosity of 30% corresponding to spacing S =3 m. For a spacing of S=1 m, the (K_r) value is reduced up to 32 % in comparison with the spacing S=1 m.
- Finally, the developed numerical model shows an overall good agreement with the physical model study, with an error percentage of less than 10%. Hence, it can be used as a reliable method for determining hydrodynamic parameters.
- From the present study, it can be concluded that 30% porous HSB placed at 3 m from the caisson type breakwater is the most efficient in reducing the hydrodynamic parameter.

PERFORMANCE OF PERFORATED VERTICAL CAISSON TYPE BREAKWATER

7.1 GENERAL

The new modern construction techniques are developed and implemented more economically compared to plain caissons, perforated caissons are becoming more and more popular not only for anti-reflective quay walls inside sheltered harbours, but also for external caisson breakwaters, to partly overcome the typical drawbacks of vertical coastal structures: namely large reflections, forces, overtopping and toe scour. Perforated vertical breakwaters are intended to absorb part of the wave energy through various mechanisms, such as turbulence, viscous friction and resonance. The larger the water level difference at the two porous wall sides the larger the energy dissipation, which is strongly dependent on the wavelength L in the case of chamber systems. The wall porosity, defined as the ratio of the area of the front wall openings to the total wall area, is typically within the range of 15-40% and the chamber width.

Jarlan (1961) introduced a breakwater with a perforated front wall, a wave energy dissipating chamber, and a solid back wall. The generation of eddies and turbulence can achieve significant damping of incoming waves near the perforations in the front wall (Jarlan, 1961) and a substantial reduction of wave impact loads (Takahashi & Shimosako, 1994; Takahashi et al., 1994) and wave overtopping (Isaacson et al., 1998 a, b) can be achieved. It also allows water circulation and rubbish clearance creating a clean environment inside the harbour, and providing passage for fishes and microorganisms. It became very popular in engineering practice due to its high effectiveness in energy dissipation and has been investigated intensively and used increasingly worldwide. It improves hydraulic performance, total cost, quality control, environmental aspects, construction time, and maintenance. The first application of perforated caisson breakwater is at Comeau Bay (Canada) and various examples also exist in Italy (Franco, 1994), France and Japan (Takahashi, 1996).

In this chapter, an attempt is made to assess the dynamic pressure, wave forces, wave runup and wave reflection for the perforated caisson type breakwater. At the same time, the diameter of the perforations is maintained constant (0.04 m) and varying the percentage of perforation ((i.e, (a) 20 %, (b) 15 % , (c) 13 %, (d) 10 % & (e) 8%) on the seaside of the test model is investigated.

7.2 TEST MODELS

The test model is constructed using concrete and the dimensions of the model are 0.70 m in length, 0.5 m in breadth, and 0.90 m in height for the present study. The dimensions are selected based on the prototype of two caisson breakwaters integrated with OWC plants one in Vizhinjam port, Kerala and another from Sakata harbour, Japan. (Antonio F.O Falcao 2016).
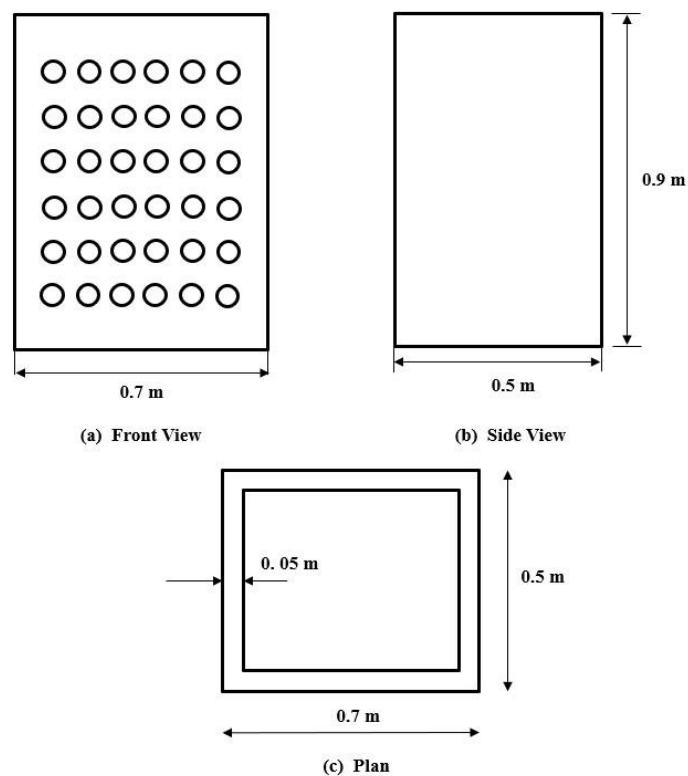
Figure 7.1: Cross-section of the perforated caisson breakwater

Also, the height of the vertical caisson breakwater is selected in such a way that there is no wave overtopping. On the seaside of the model, rubble mound toe protection is constructed as discussed in the earlier chapters.

The cross-section of the test model is illustrated in Figure 7.1. The front-facing of the test model perforations are introduced (i.e, (a) 20 %, (b) 15 % , (c) 13 %, (d) 10 % & (e) 8%) the spacings and diameter as shown in Figure 7.2. (MAST III-PROVERBS-CT95-0041 Grenoble, France).

The details of the experimental parameters used in the present chapter are illustrated in Table 7.1.
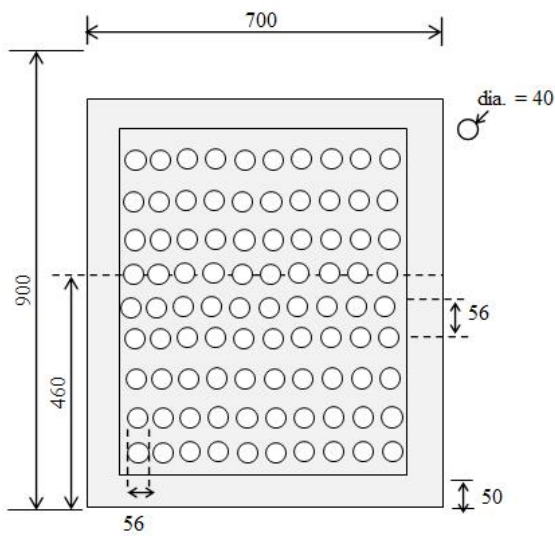
(All units in mm)

Figure (a). 20 % Perforation
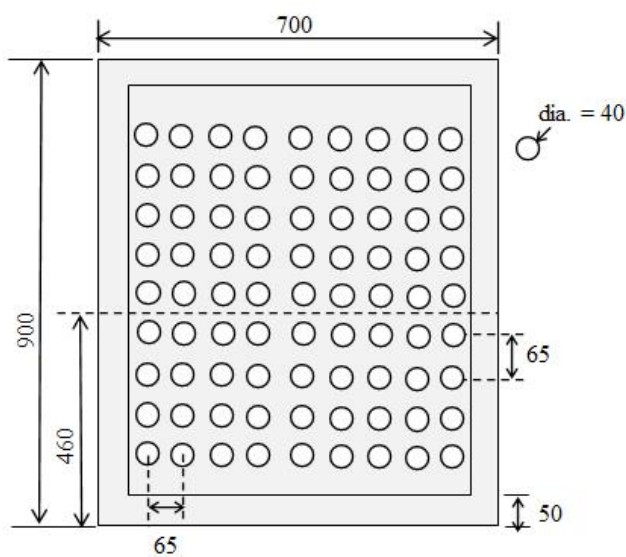
(All units in mm)

Figure (b). 15 % Perforation
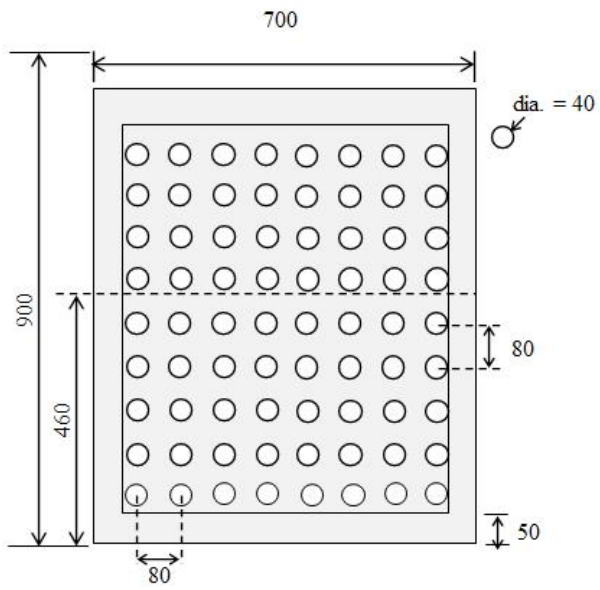
Figure (c). 13 % Perforation
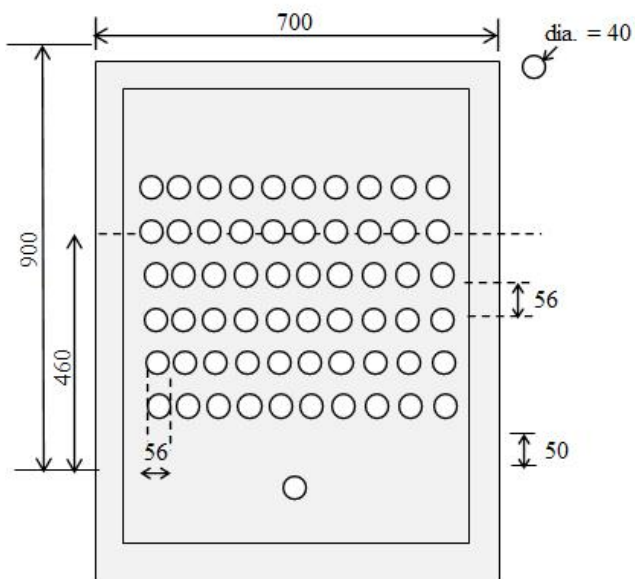
(All units in mm)

Figure (d). 10 % Perforation

(All units in mm)

176
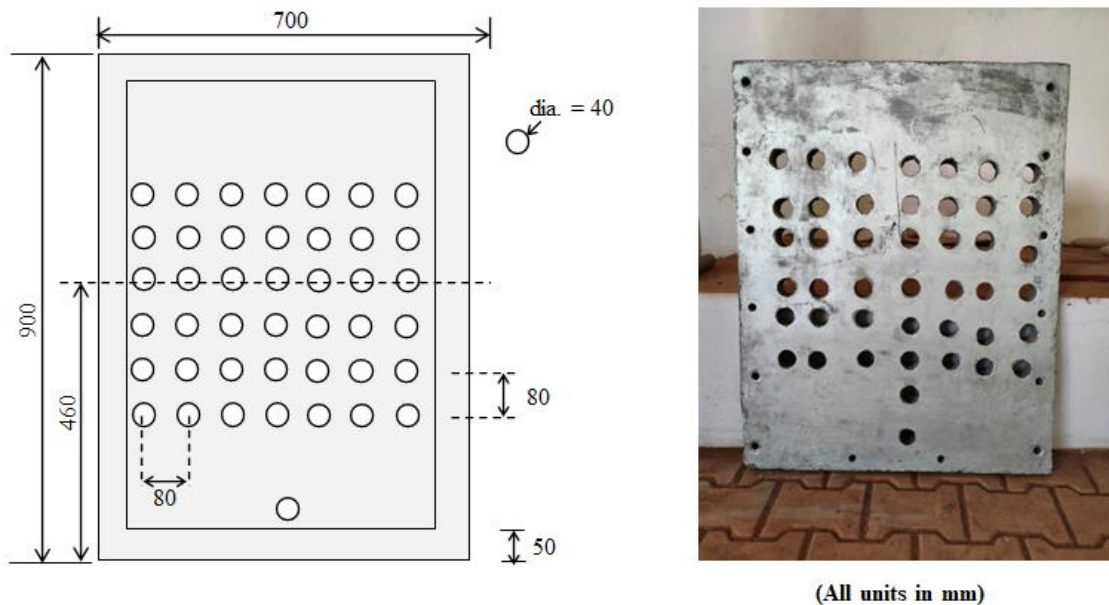
Figure (e). 8 % Perforation

(All units in mm)

Figure 7.2: (a-e) Perforated test model

Table 7.1. Wave specific parameter

Parameters	Experimental range of values
Wave specific parameters	
Incident wave height, H_i (m)	0.12, 0.14, 0.16, 0.18
Wave period, T (sec)	2.2, 2.4, 2.6, 2.8
Depth of water, d (m)	0.40 and 0.50
Wave Length, L (m)	4.05 - 6.10
Perorations, μ (%)	8, 10, 13, 15 & 20

7.3 VARIATION OF RELATIVE WAVE PRESSURE (P/ρgd) WITH RELATIVE DEPTH PARAMETER (z/d) ON FRONT WALL

The wave pressure acting on the perforated caisson breakwater is recorded using pressure transducers placed in the front and rear wall of the test model. The values of wave pressure are then converted into pressures in kN/m² by multiplying the pressure values (PSI) obtained through transducers with suitable conversion factors. From the unsteady Bernoulli equation, the pressure response factor kp becomes 1, at z= 0 (at SWL). At any water depth (–z) under a wave crest, the wave pressure is at its peak and consists of the static pressure and dynamic pressure is given by:

177

P = -ρgz (static Pressure) + ρgHKp / 2 (dynamic pressure)   (7.1)

Where the first term is static pressure and the second one is dynamic pressure. The pressure transducers are placed along with the depth of the caisson, at dimensionless depth z/d, where z is the distance from the still water level (measured positive above SWL and negative below SWL) to the pressure transducers and d is the depth of water at the structure.
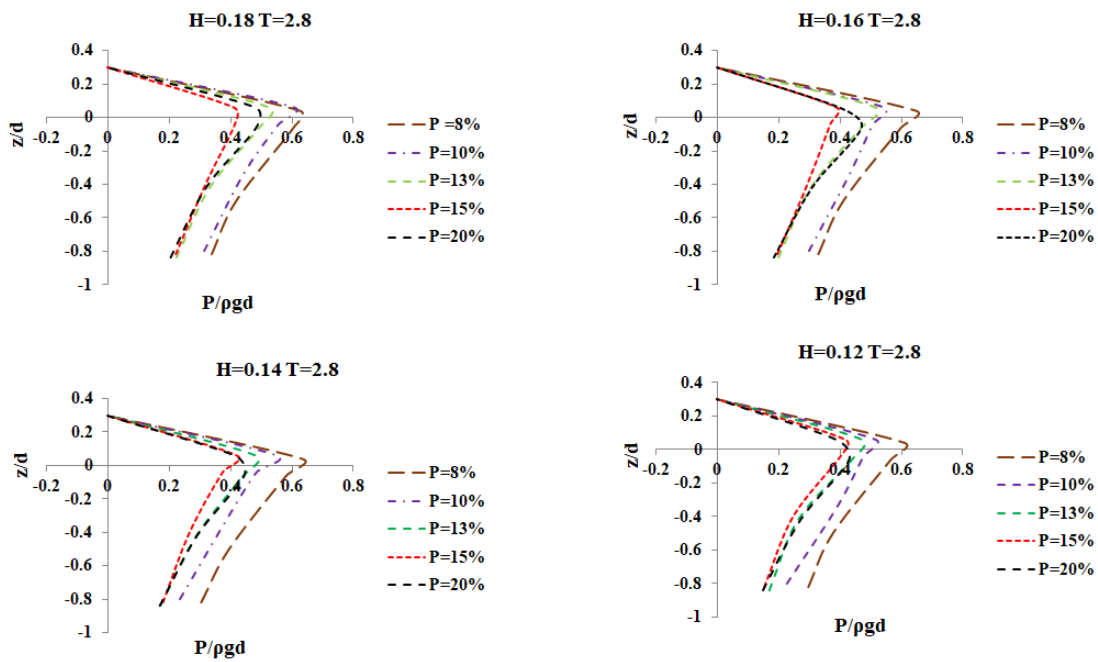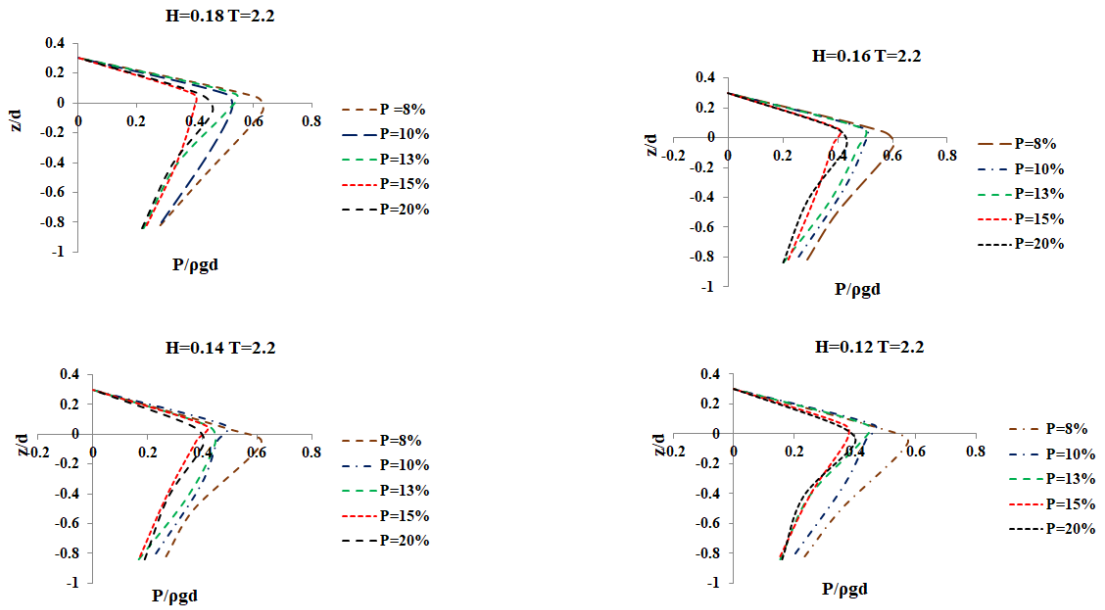
Figure 7.3: Variation of relative wave pressure (P/ρgd) with relative depth parameter
on the wall (z/d), d=0.50 m
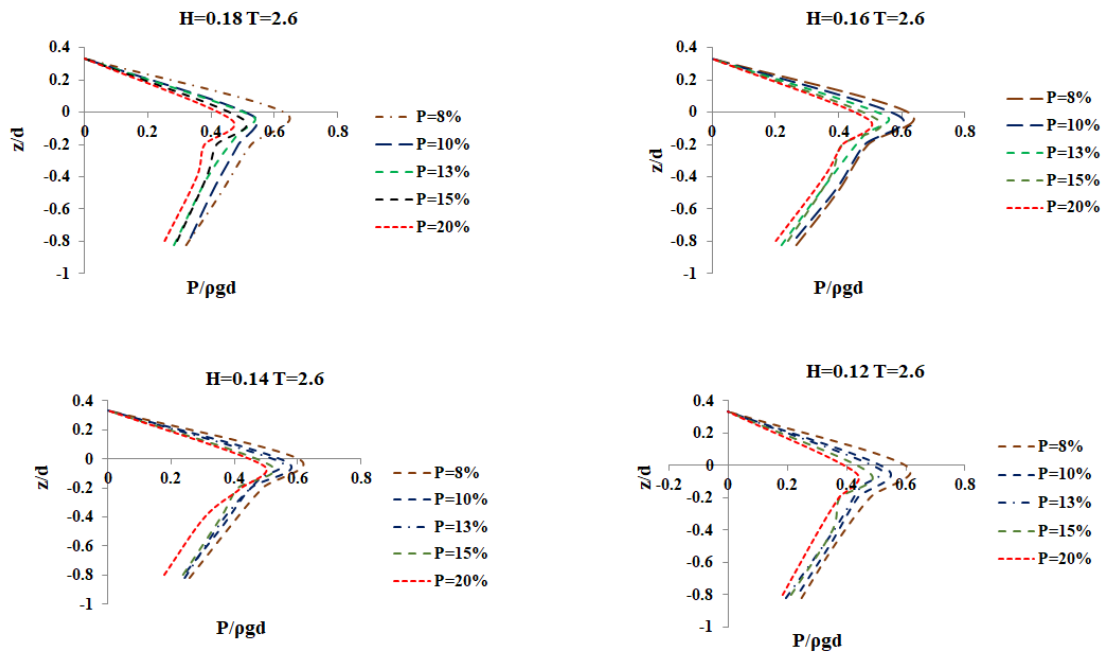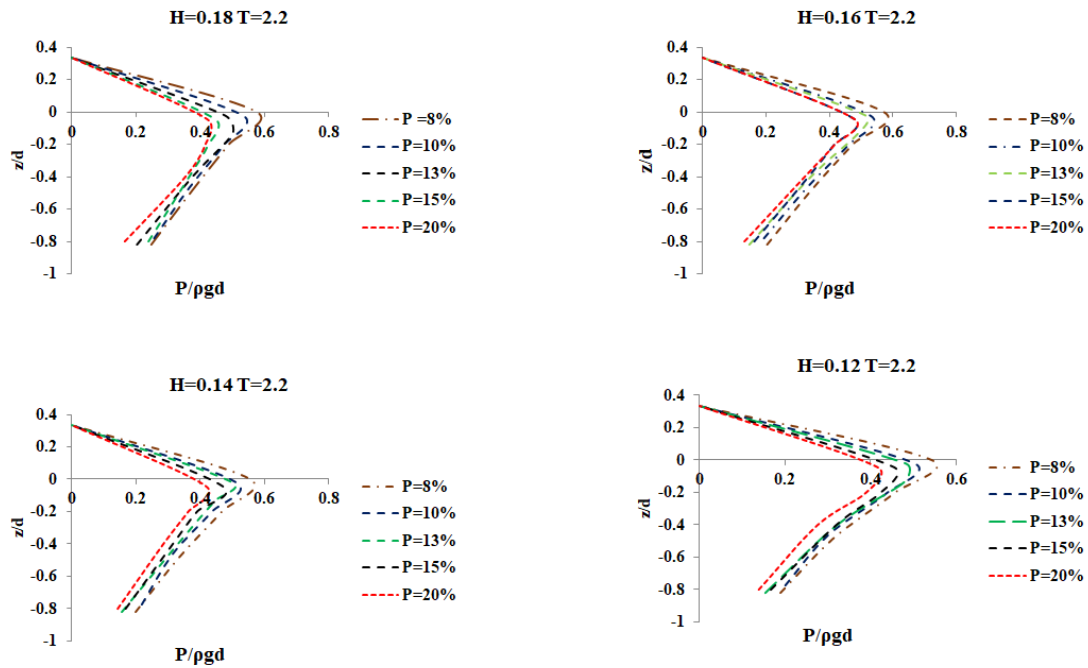
Figure 7.4: Variation of relative wave pressure (P/ρgd) with relative depth parameter
on the wall (z/d), d=0.40 m

Figures 7.3 and 7.4, illustrate the variation of relative wave pressure (P/ρgd) variation
with relative depth parameters on the perforated wall caisson (z/d). It has been observed
that relative pressure increases with relative water depth till the still water level (SWL),
where it reaches the maximum and then decreases with z/d having a minimum at bottom
of the wall. The dynamic pressure value reduces towards the bottom of the test model
according to the hyperbolic cosine function. From the unsteady Bernoulli equation, the
pressure response factor K_p becomes 1, at z=0 (at SWL). At still water level (z=0), the
vertical particle accelerations are maximum and are negative. Similar observations are
observed in the case of the non-perorated case also as discussed in chapter 4.

It is observed that when the porosity of the front wall is increased from 8% to 20%,
dynamic pressure values are found to be decreasing. Since higher porosity allow more
wave passage than the lower porous wall, i.e. 8%. Further, the relative pressure
increases with an increase in wave period and wave height as long-period waves exert
more pressure than short-period waves. A maximum reduction of 26 % in the dynamic

pressure is observed for the 20 % perforated model, in comparison with the 8 % perforated model.

7.4 VARIATION OF RELATIVE WAVE FORCE PARAMETER (F/ρgd²) ON PVCB WITH WAVE STEEPNESS (Hi/L)

The horizontal wave force generated by the regular wave field is illustrated in Figures 7.5-7.6. For the range of wave steepness (H_i/L), relative water depth parameter (d/L), and different perforations. The wave force F is made non-dimensional by dividing $\rho g d^2$ and plotted on the y-axis. The x-axis indicates the wave steepness (H_i/L). The perforated front face ((i.e, (a) 20 %, (b) 15 % , (c) 13 %, (d) 10 % & (e) 8%)) wave force parameter are compared with modified Goda's approach suggested by Tabet-Aoul et al. (2003) and also with non-perforated caisson breakwater.
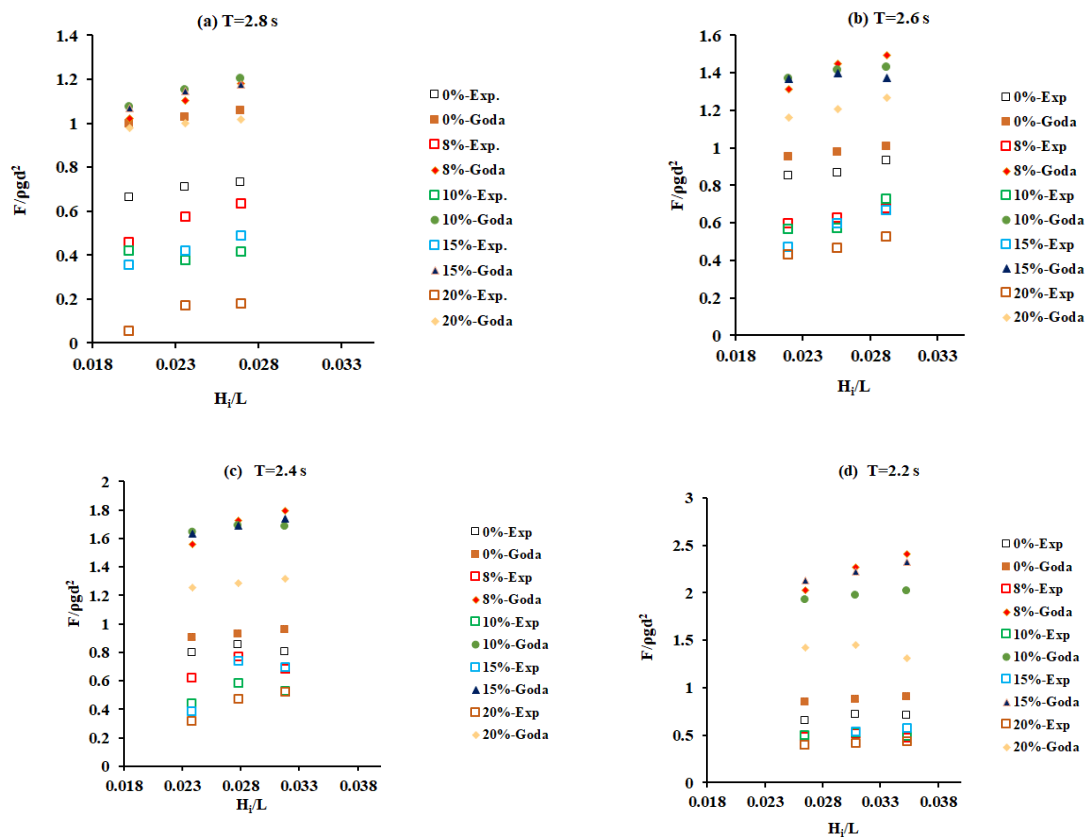
Figure 7.5: Variation of relative wave force parameter (F/ρgd²) on PCVB With Wave Steepness (Hi/L), d=0.50 m

181
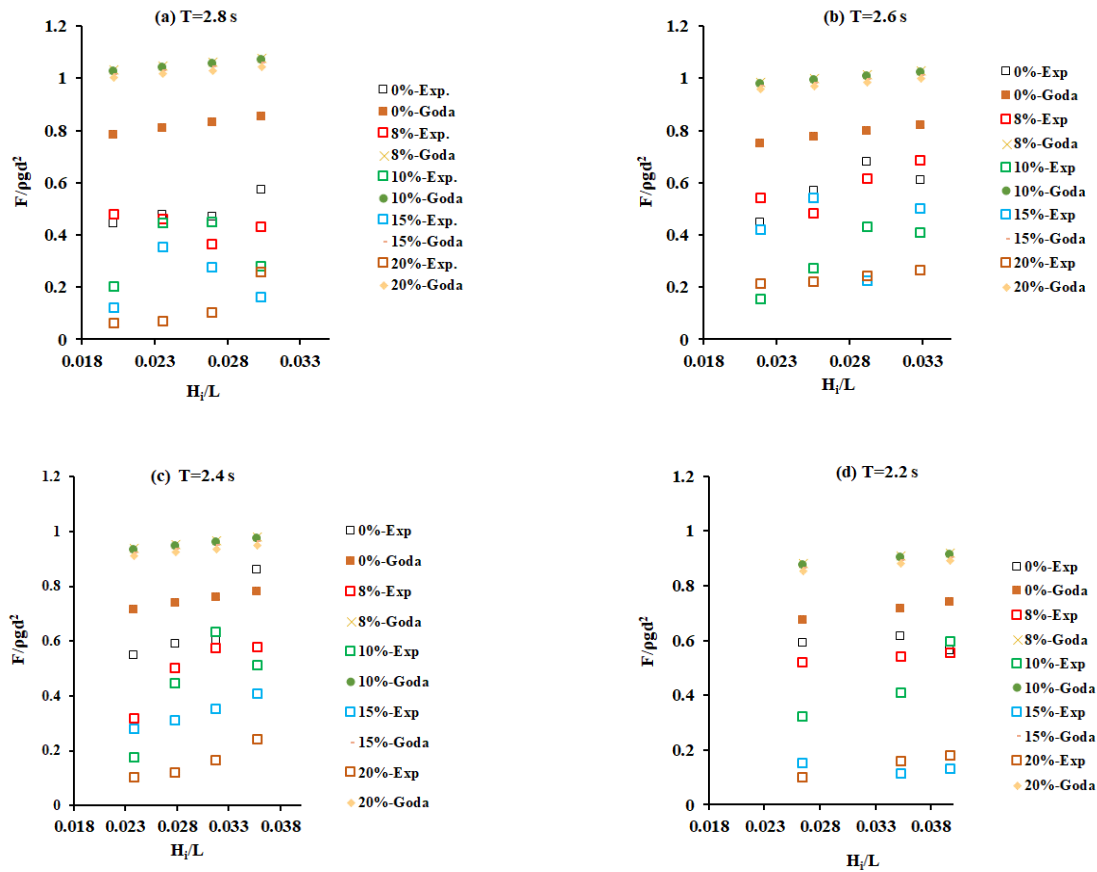
Figure 7.6: Variation of relative wave force parameter ($F/\rho gd^2$) on PCVB With Wave Steepness (H_i/L), d=0.40 m

It is observed that the relative wave forces are increasing with the increase in the wave periods, wave heights, and decreasing with μ. This is due to that long period waves exert more pressure than short-period waves. Similarly, model pressure data, recorded in the external and internal walls, have been integrated over the vertical face and compared with the modified Goda's formula suggested by Tabet-Aoul et al. (2003). The results reveal that the modified Goda's method overestimates the wave forces in all cases.

By increasing the perforations in the front face of VCB from 5% to 20% helps to reduce the horizontal wave force. Long waves and low porosity results in the maximum wave force parameter. Short waves and high porosity help to reduce the value of the wave force parameter significantly (less than 0.5). Finally, it is

observed that 15 % and 20 % perforated model gives a better reduction in wave force in comparison with all other perforations.

The total force is reduced by 40 % for 20 % perforated breakwater in comparison with non-perorated caisson for 0.50 m water depth. Similarly, for 0.40 m depth 28 % reduction is observed.

7.5 VARIATION OF WAVE REFLECTION COEFFICIENT (K_r) ON PVCB WITH WAVESTEEPNESS (H_i/L)

Figures 7.7 – 7.8 illustrates the trends in the variation of reflection coefficient (K_r) with different wave parameters. The reflection coefficient (K_r) variation is plotted with the wave steepness (H_i/L) for different porosity and wave period (T). The DHI wave synthesizer analysis software, MIKE ZERO IS used for the wave reflection analysis. Data from three wave probes are used to estimate the reflected wave height and coefficient of reflection, K_r, which is defined as $K_r = H_r/H_i$, where H_r is the reflected wave height.
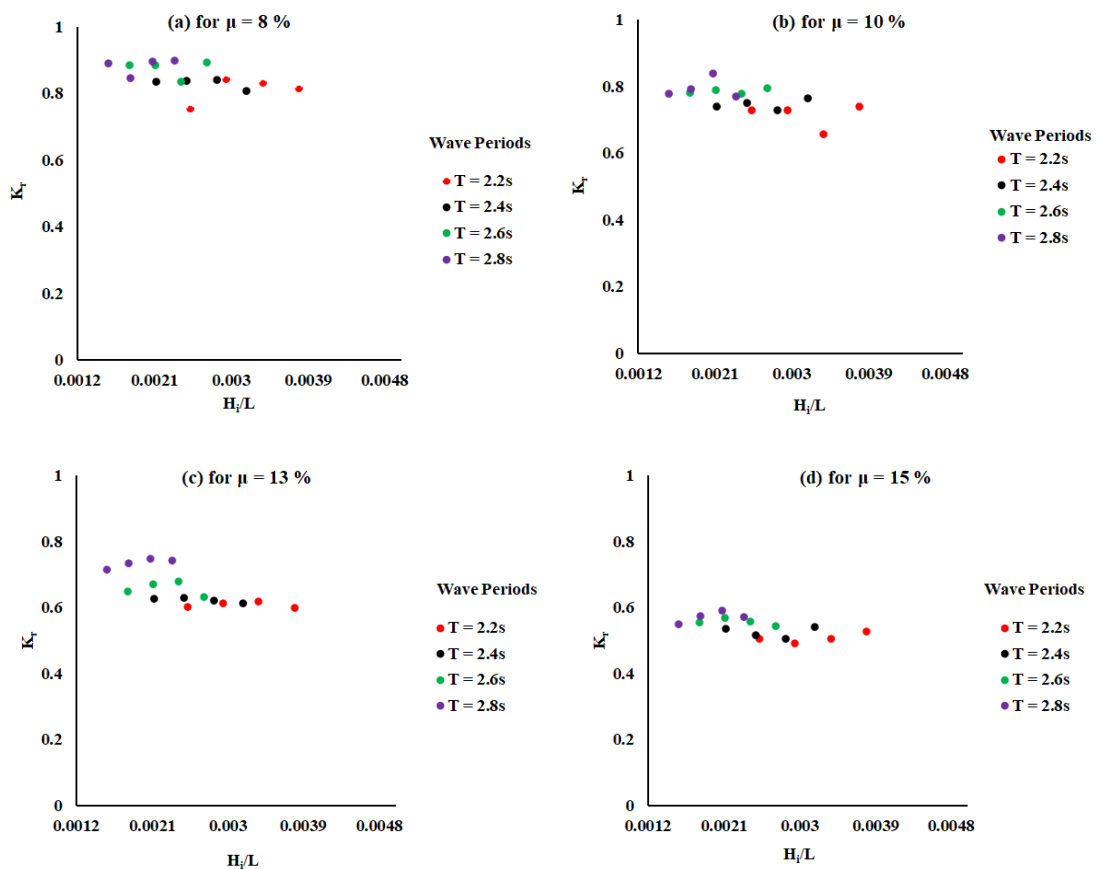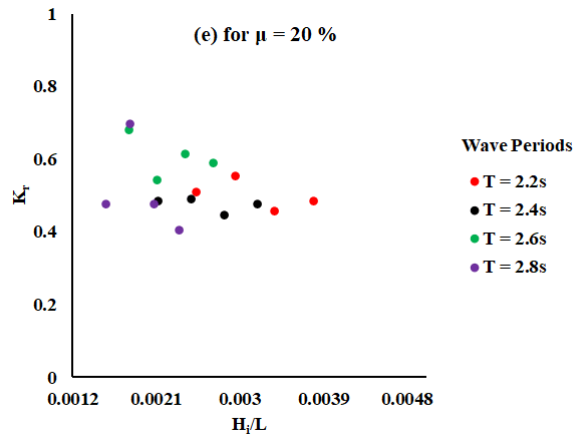
Figure 7.7: Variation of wave reflection coefficient (K_r) with wave steepness (H_i/L), for d = 0.50 m
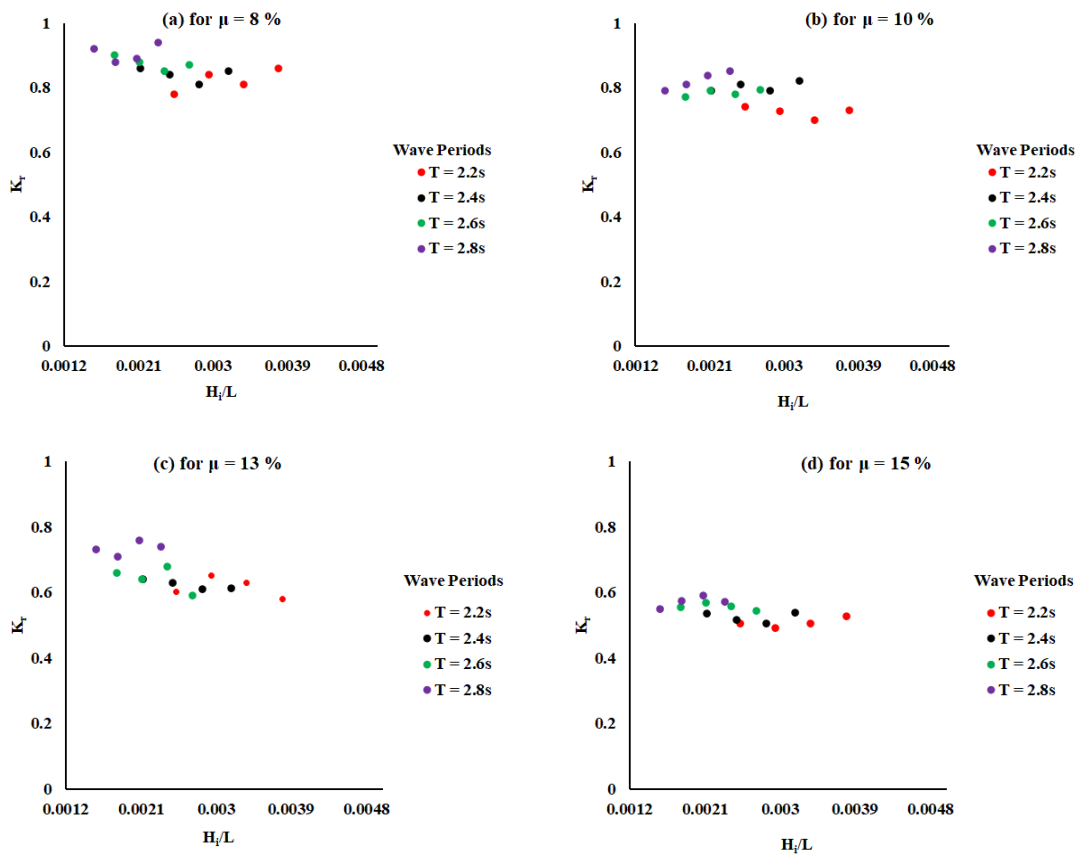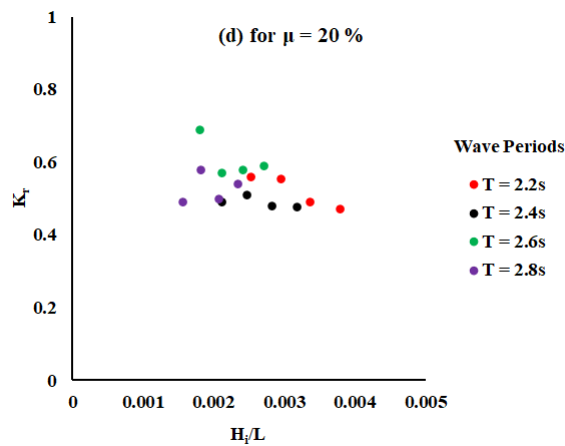
Figure 7.8: Variation of wave reflection coefficient (K_r) with wave steepness (H_i/L), for d = 0.40 m

The reflection analysis software in MIKE ZERO is based on the method described by Mansard and Funke (1987) and extended by Zelt add Skjelbreia (1992). The distance between wave probes is kept L, L+(L/3) & L+(2L/3) from the test model these distances are used as inputs for the reflection analysis (Issacon, 1991). Using three-wave probes is preferable instead of two-wave probes, (Munni Reddy et.al (2007)) in order to avoid singularity problems during reflection analysis as discussed in earlier chapters.

The perforations provided in the front wall are found to be efficient in enhancing the reduction of wave reflection as it allows energy passage through the structure. For a given H_i/L value, as incident wave height increases reflection coefficient generally showed an increasing trend. For a depth of 0.50 m, the value of K_r ranges from 0.42 to 0.89 as relative wave height increases from 0.24 to 0.36. K_r is highest for lower porous structure, i.e. 8% which reaches a maximum of about 0.89. The higher value is due to a lesser area for penetration of waves to resist and hence more reflection occurs at the caisson.

Lower K_r values are obtained for higher porous structures, (i.e for 20%) and the wave reflection co-efficient (K_r) drops to 0.45 which is due to more wave passage allowed through the structure. The value of the reflection coefficient increases with an increase in relative wave height. For waves of higher steepness, the energy under the wave will be more, and more energy gets reflected after hitting the structure.

Similar, results are observed for the case of 0.4 m depth of water with increase in porosity (8% to 20%) the reflection coefficient is reduced from 0.857 to 0.635. There is a reduction of 26% in reflection coefficient when porosity is increased from 8% to 20%. For an 8% perforated wall, the K_r value ranges from 0.84 to 0.86.

7.6 VARIATION OF RELATIVE RUN-UP (R_u/H_i) WITH DEPTH PARAMETER (d/L)

The variation of relative wave run-up (R_u/H_i) with relative water depth (d/L) is illustrated in Figures 7.9 -7.10, for various relative wave heights (H_i/d) and water depths. In general, the wave runup is defined as the vertical rise of water above the still-water level to which the water rushes up on the front face of the test model. This helps in determining the design crest level of the structure depending on the allowable overtopping level. From the graph, it is observed that the relative run-up (R_u/H_i) is increasing with an increase in the relative depth (d/L) for varying relative wave heights.

(e) for μ = 20 %
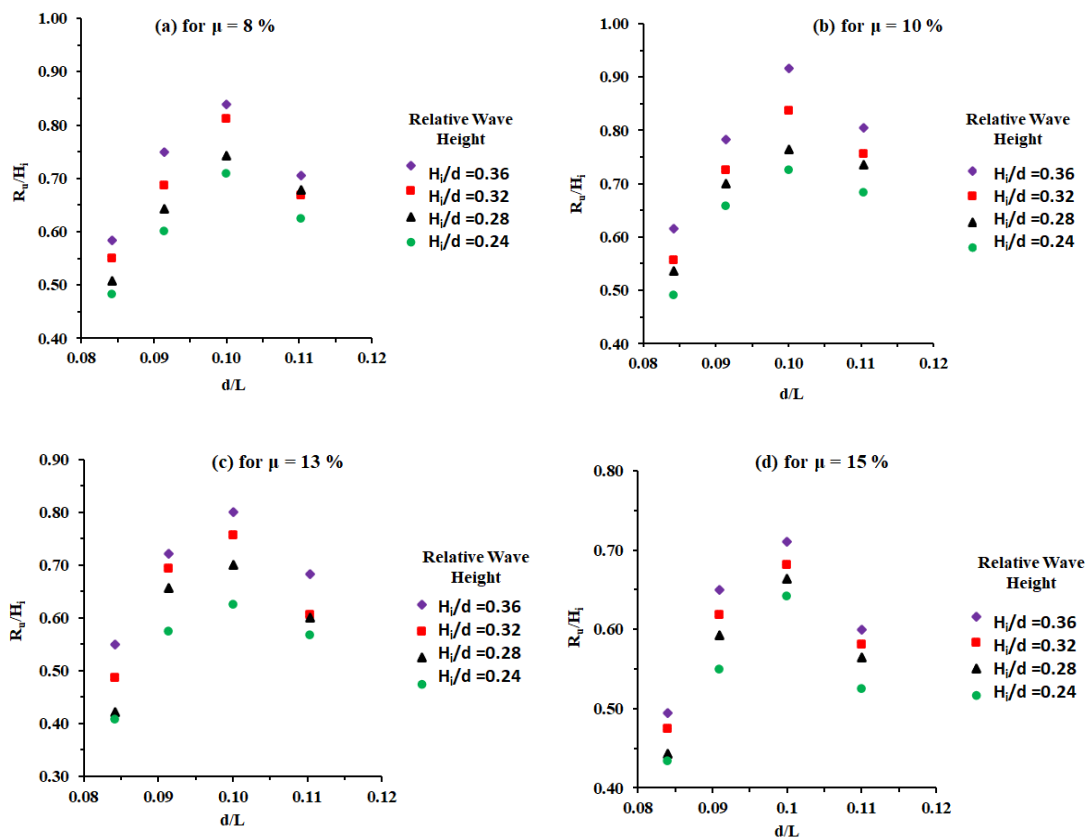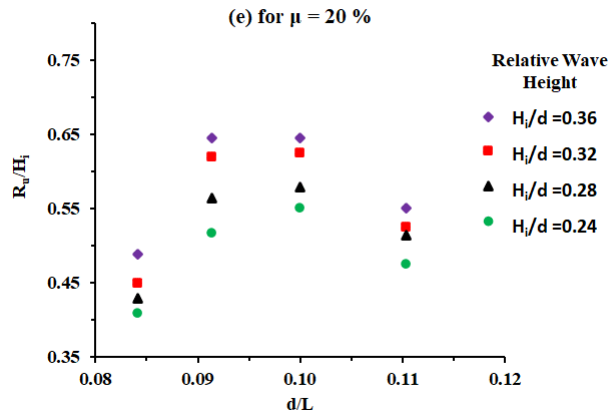
Figure 7.9: Variation of relative wave runup (R_u/H_i) with relative water depth (d/L) for d=0.50 m

187
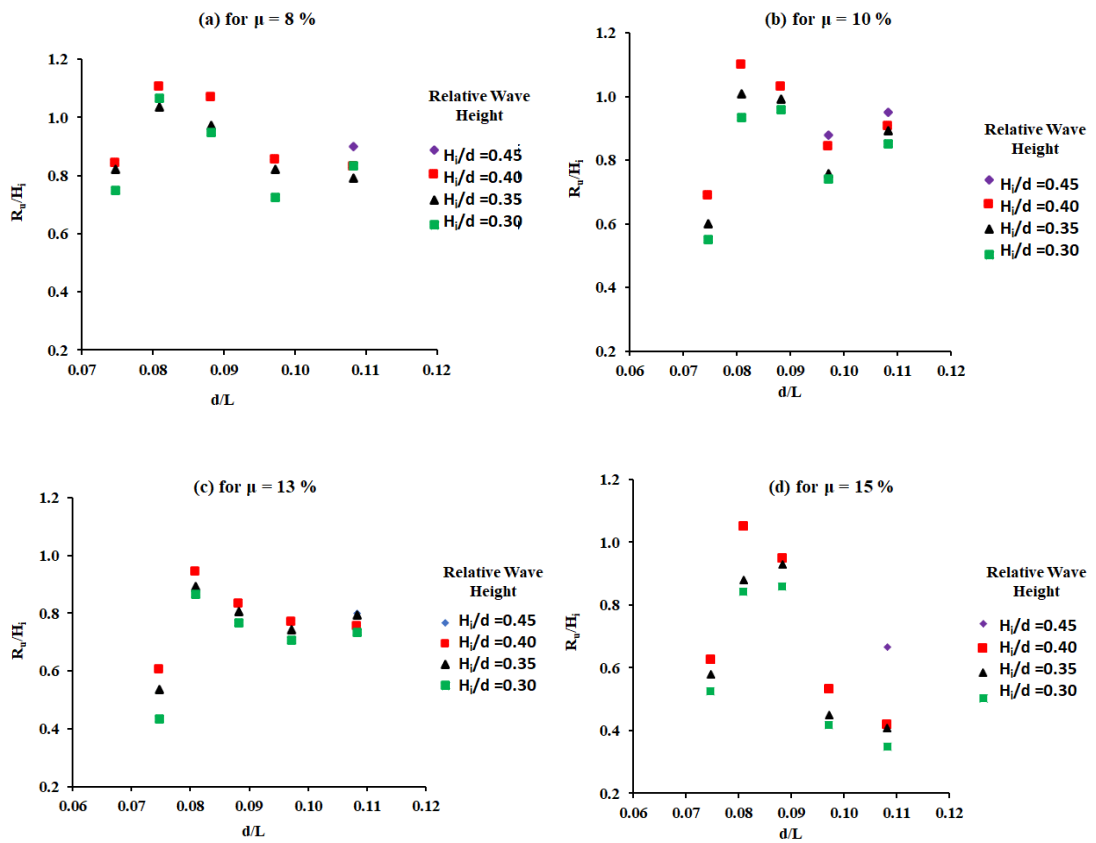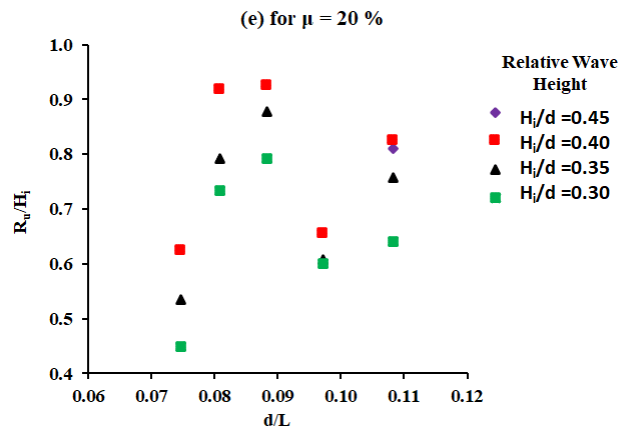
Figure 7.10: Variation of relative wave runup (R_u/H_i) with relative water depth (d/L) for d=0.40 m

For the depth of water of 0.50 m, it is found that R_u/H_i increases for an increase in d/L. the value of R_u/H_i varies between 0.35 and 0.9, as the relative depth varies from 0.084 to 0.11. As the porosity of the caisson increases from 8% to 20%, the run-up decreases. This may be due to the high percentage of porosity, and more wave passage through the pores. structure, causing a reduction in the rise of water level in front of the structure. For 8% porosity, the relative run-up varies from 0.45 to 0.85 and for 20 % porosity from 0.38 to 0.65.

For the case of 0.4 m water depth, the relative run-up varies from 0.575 to 0.994 for 8% porosity. Similarly, for 20% porosity relative run-up is varying from 0.475 to 0.828 Overall, making a sea-facing wall porous reduces the wave run-up considerably and hence the structure height can be reduced.

7.7 CLOSURE

In this chapter, an attempt has been made to investigate the hydrodynamic performance characteristics such as dynamic pressure acting on the front face, wave forces, wave run-up, and reflection coefficient on the perforated vertical caisson breakwater. The influence of porosity on the perforated caisson is studied with various perforated models ranging from 8 % to 20 % and their relationship is analysed through plotting graphs.

The main findings are outlined below.

- It is observed that when the porosity of the front wall is increased from 8% to 20%, dynamic pressure values are found to be decreasing. A maximum reduction of 26 % in the dynamic pressure is observed for the 20 % perforated model, in comparison with the 8 % perforated model.

- By increasing the perforations in the front face of VCB from 5% to 20% helps to reduce the horizontal wave force. Overall, In the total force, a 40 % of reduction is observed in comparison with non-perorated caisson for 0.50 m water depth. Similarly, for 0.40 depth 28 % reduction is observed.

- The perforations provided in the front wall are found to be efficient in enhancing the reduction of wave reflection coefficient (K_r) as it allows energy passage through the structure. For a depth of 0.50 m, the value of K_r ranges from 0.42 to 0.89 as relative wave height increases from 0.24 to 0.36. K_r is highest for lower porous structure, i.e. 8% which reaches a maximum of about 0.89. The higher value is due to a lesser area for penetration of waves to resist and hence more reflection occurs at the VCB.

- For the depth of water of 0.50 m, it is found that R_u/H_i increases for an increase in d/L. the value of R_u/H_i varies between 0.35 and 0.9, as the relative depth varies from 0.084 to 0.11. As the porosity of the caisson increases from 8% to 20%, the run-up decreases. This may be due to the high percentage of porosity, and more wave passage through the pores. structure, causing a reduction in the rise of water level in front of the structure. For 8% porosity, the relative run-up varies from 0.45 to 0.85 and for 20 % porosity from 0.38 to 0.65.

- For the case of 0.4 m water depth, the relative run-up varies from 0.575 to 0.994 for 8% porosity. Similarly, for 20% porosity relative run-up is varying from 0.475 to 0.828 Overall, making a sea-facing wall porous reduces the wave run-up considerably and hence the structure height can be reduced.

SUMMARY AND CONCLUSIONS

8.1 SUMMARY

In the present study, a detailed experimental and numerical investigation is conducted on a vertical caisson-type breakwater. In the first phase, the hydraulic stability of the toe is investigated in a 2D wave flume. In the second phase, an investigation of the non-perforated caisson type breakwater is performed considering different wave conditions. The variation of dynamic wave pressure, wave force, wave run-up, and wave reflection are determined for this structure. In the third phase, a numerical model of caisson breakwater is developed to study its performance using the computational fluid dynamics (CFD) approach using Ansys-Fluent and validated the same using experimental data. In the fourth phase, the experimental investigations are carried out on non-perforated vertical wall breakwater with the presence of a vertical and horizontal slotted barrier. In the fifth phase, the perforations (i.e 7 %, 10%, 13%, 15%, 20%) are introduced in the front face of the caisson breakwater to analyse the hydraulic performance to arrive at better perforations in reducing the wave forces, wave reflection and wave runup.

From the study, the following conclusions are drawn:

8.2 TOE STABILITY OF CAISSON-TYPE BREAKWATER

- Wave steepness is an influencing parameter for the damage development of the toe. Such behaviour is observed in very shallow water. As the incident wave steepness increases, the percentage damage increases for the range of variables considered in the present study. The maximum percentage damage observed for the depth of water of 0.35 m is 5.2 %. For other depths of water (i.e. 0.4 m and 0.50 m) it is in the acceptable range (< 5 %) (CEM, 2011).

- The damage to toe structure is more for lower water depth due to exposedness of toe and hence breaking of waves at toe level. This concludes the toe structures in shallow water condition is experiencing more damage.

- The stability number is significantly affected by the depth of toe below the still water level and by the relative depth of water (d/L) at the breakwater. Further increase in wave height causes steeper waves resulting in more damage. Similarly, it is observed that the surf similarity parameter decreases up to a maximum of 20 % for the relative depth (d/L) of 0.1233.

8.3 HYDRODYNAMIC PERFORMANCE OF CAISSON-TYPE BREAKWATER

- The dynamic pressure near the seabed is significantly less compared to the still water level because the vertical particle acceleration is maximum and it is negative. Goda's formula provides a good estimation of wave force distribution compared with the experimental results for certain d/L (0.8 – 0.11) ratios. Similarly, the Sainflou method is overestimating the wave forces by 15 % compared with the experimental results.

- The reflection co-efficient K_r values decrease with an increase of H_i/L, due to more excessive dissipation of wave energy for the steeper waves. The reflection coefficient K_r is more than 0.95 for both Zhu et al. (1999) and MIKE 21 (WS) reflection analysis.

- The factor of safety against sliding ranges from 5.9 to 2.1, and for overturning it ranges from 10.5 to 2.2 for the wave heights of 0.12 m to 0.18 m. The factor of safety against sliding should not be lesser than 1.2 in the case of Goda's (1985) approach, and should not be lesser than 1.5, as per IS 9527 (Part I)-1981. Hence the test model is safe against both sliding and overturning.

8.4 NUMERICAL MODELLING OF CAISSON-TYPE BREAKWATER

- In numerical modelling, the effect of beach slopes at the end of the numerical wave tank plays a significant role in the performance of wave reflection. In the present study, three cases of beach slopes namely 1:3, 1:5, and the default numerical beach condition are performed and the results reveal a beach slope of 1:5 and numerical beach conditions shows similar wave absorbing trend.

- The error in the wave force on caisson breakwater is increased up to 6.8 % for a wave height of 0.18 m. The increase in wave height and wave period form

unstable waves due to a rise in Ursell number, leading to increasing error in the estimated numerical results.

- The relative runup is observed to increase with an increase in relative water depth. For a water depth of 0.5 m, the value of relative runup varies from 1.05 to 1.7 for the relative water depth (d/L) of 0.084 to 0.110. The percentage deviation is in the range of 1.96% to 9.88% ($< 10\%$).

8.5 CAISSON-TYPE BREAKWATER WITH THE PRESENCE OF SLOTTED BARRIER

- For a given (d/L) the relative wave force parameter ($F/\rho gd^2$) increases proportionally with slotted barrier porosity. As the porosity of the slotted barrier increases from 10% to 50%, the relative wave force parameter ($F/\rho gd^2$) increases by 48 %, for a relative water depth (d/L) of 0.084. Similarly, as the spacing of the slotted barrier varies from 1 m to 3 m from the test model the relative wave force parameter ($F/\rho gd^2$) decreases up to 36 % for a d/L =0.084 and H_i/d =0.24.

- The reflection coefficient (K_r) increases with a decrease in the spacing of the slotted barrier. The (K_r) value increases by 12.82 %, when the spacing of the slotted barrier is decreased from 3 m to 1m, for d/L=0.084 and H_i/d=0.24.

- The study concludes that a 30% porous slotted barrier positioned at 3 m from the caisson-type breakwater is efficient in reducing the wave force and wave reflection.

8.6 PERFORATED CAISSON TYPE BREAKWATER

- The seaside perforated caisson breakwater has a decreasing trend in the oscillatory pattern of wave reflection with an increase in relative water depth (d/L). This demonstrates that for a higher porosity, wave reflection decreases in the case of short waves compared to long waves. This is due to the concentration of energy near the free surface in the case of short waves.

- The overall wave force acting on perforated caisson breakwater is reduced by about 40 %, when compared with non-perforated caisson breakwater.

193

- The reflection coefficient (K_r) values decrease with an increase of H_i/L. The reflection coefficient (K_r) is found to be decreased from 0.97 to 0.6 as the porosity increase from 7 % to 20 %.

8.7 SCOPE OF FUTURE STUDIES

- The physical model study on caisson-type breakwater may be carried out under irregular wave conditions.

- The numerical study on caisson-type breakwater may be carried out in 3D- simulations.

- The physical model study on multiple chambered perforated caisson type breakwater for different conditions may be carried out.

REFERENCES

Allsop W., and Muller G. (1995). "Comparative study on breaking wave forces on vertical walls", Journal of Waterway, Port, Coastal and Ocean Engineering ASCE, Vol 121, (pp 270-272).

Allsop, W., Alderson, J., & Chapman, A. (2009). Defending buildings and people against wave overtopping. In Coastal Structures 2007: (In 2 Volumes) (pp. 1253-1262).

Andrea Marzeddu, Tiago C. A. Oliveira, Francesc Xavier Gironella & Agustin Sánchez- Arcilla (2017) "Variability of wave impact measurements on vertical breakwaters", Journal of Hydraulic Research, 55:6, 772-786.

Arun Mulky Kamath (2012): Wave Forces on Structures Using Reef 3d., M.sc Thesis, NTNU.

Anand, K. V., and Sundar, V., F. ISH (2010). "Comparison of pressures due to random waves on Vertical and curved seawalls", ISH Journal of Hydraulic Engineering, 16:sup1, 26-34. doi: 10.1080/09715010.2010.10515013.

Brebner and Donnelly (1962). "Laboratory study of rubble foundations for vertical breakwaters", Coastal Engineering, Vol-1, Chapter 24, pp. 408-429.

Chakrabarti, S. K. (1996). Hydrodynamics of offshore structures. WIT press.

Chiu, Y., Lin, J., Chang, S., Lin, Y., & Chen, C. (2007). "An Experimental Study of Wave Forces on Vertical Breakwater". Journal of Marine Science and Application, 15(3), 158–170.

CIRIA/CUR (1991). "Manual on the Use of Rock in Coastal and Shoreline Engineering", CIRIA, Special Publication 83, CUR Report 154, A. A. Balkema, Rotterdam.

Dai, J., Wang, C. M., Utsunomiya, T., & Duan, W. (2018). Review of recent research and developments on floating breakwaters. Ocean Engineering, 158, 132-151.

Dattatri, J.; Raman, H., and Jothi Shankar, N., (1979). "Height and Period Distribution for Waves off Mangalore Harbour-West coast of India". Journal of Geophysical research 84, pp 3767-72.

Dattatri, J. (1994). "Waves off Mangalore harbour-west coast of India." Journal of Waterway, port, coastal, and Ocean Engineering, ASCE, 99(2), 39-57.

De Gerloni, M. (1998). Forces on perforated structures: Proposal for a Goda modified formula. MAST III-PROVERBS-CT95-0041 Overall Workshop, Grenoble, France (in French).i

Delft Hydraulic (1990). "Manual Breakwater - Design Tool for Rubble Mound Structures", Part B Technical Manual.

Dentale, F., Reale, F., Di Leo, A., and Carratelli, E. P. (2018). "A CFD approach to rubble mound breakwater design". Int. J. Nav. Archit. Ocean Eng., 10(5), 644–650.

d'Angremond, K. (2018). Breakwaters and closure dams. CRC Press.

Det Norske Veritas (2010): Environmental conditions and environmental loads, recommended practice. DNV-RP-C205, Oslo.

Du, Q., and Leung, D. Y. C. (2011): 2D Numerical Simulation of Ocean Waves, Proc. World Renew. Energy Congr., 57, 2183–2189.

Ergin A and Abdalla S. (1993). "Comparative study on breaking wave forces on vertical walls", Journal of Waterway, Port, Coastal and Ocean engineering ASCE, Vol 119, No. 5 (pp560-567).

Engineer Manual (1995). "Engineering and Design. Design of Coastal Revetments, Seawalls, and Bulkheads", Dept. of the Army, U. S. Army Corps of Engineers, Washington, DC.

Fabio, M., Marques Machado, António, M., Gameiro Lopes, Almerindo, D., and Ferreira (2018). "Numerical simulation of regular waves: Optimization of a numerical wave tank", Ocean Eng., 170, 89-99.

Franco, L. (1994). "Vertical breakwaters: the Italian experience." Coastal Engineering Journal, 22(1–2), 31–55.

Gao, X., and Inouchi, K. (1998). "The Characteristics of Scouring and Depositing in Front of Vertical Breakwaters by Broken Clapotis". J. Coastal Eng., 40(1), 99–113.

Gedda A.B., Manu, Rao S. (2019). "A Review on Stability of Caisson Breakwater". In: Rathinasamy M., Chandramouli S., Phanindra K., Mahesh U. (eds) Water Resources and Environmental Engineering I. Springer, Singapore.

Giovanni Cuomo, Rodolfo Piscopia, William Allsop (2011). "Evaluation of wave impact loads on caisson breakwaters based on joint probability of impact maxima and rise times", Coastal Engineering, Volume 58, Issue 1, Pages 9-27. doi.org/10.1016/j.coastaleng.2010.08.003.

Goda, Y., (1973b). "A new method of wave pressure calculation for the design of composite Breakwaters". Rept. Port and Harbour Res. Inst., Ministry of Transport, Vol. 12, No, 3, pp. 31-69.

Goda, Y., and Suzuki, Y. (1976). "Estimation of incident and reflected waves in random wave experiments". 15th International Conference on Coastal Engineering (ASCE), Honolulu, Hawaii.

Goda Y. (1985). "Random seas and maritime structures" University of Tokyo Press, Tokyo.

Goda, Y. (2000). "Random Seas and Design of Maritime Structures. World Scientific", Singapore. http://dx.doi.org/10.1142/3587.

Goda, Y. & Takagi, H. (2000). "A reliability design method of caisson breakwaters with optimal wave heights," Coast. Eng. J. 42(4), 357–387.

Hiroi, 1. (1919 J): "On a method of estimating the force of waves", KeJloirs of Engg. Faculty, Imperial University of Tokyo, Vol. X, No.l, p.19.

Hajivalie, F., and Yeganeh-Bakhtiary, A. (2009). "Numerical study of breakwater steepness effect on the hydrodynamics of standing waves and steady streaming". Journal of. Coastal Research.

Hajivalie, F., Yeganeh-Bakhtiary, A., and Hashemi-Javan, A. (2010). "Numerical simulation of wave breaking over a vertical breakwater". Int. J. Civ. Eng., IUST.

Hughes, S.A. (1993). "Physical Models and Laboratory Techniques in Coastal Engineering". World Scientific, Hong Kong.

I.S: 9527 (Part-I). "Code of practice for the design of Ports and Harbour Structures", Bureau of Indian Standards, New Delhi.

Isaacson, M. (1991). "Measurement of regular wave reflection. Journal of Waterway, Port, Coastal", and Ocean Engineering, 117(6), 553-569.

Kamphuis, J. W. (2010a). "Perspective on coastal engineering practice and education. In Handbook of coastal and ocean engineering", ed. Young C. Kim, 1135–1163. Singapore: World Scientific Publishing.

Kasem, T., and Sasaki, J. (2011). "Multiphase Modeling Of Wave Propagation Over Semicircular Obstacles Using Weno And Level Set Methods", Coastal Engineering Proceedings, 32, https://doi.org/10.9753/icce.v32.waves.57.

Kim, T. M. & Takayama, T. (2003). "Computational improvement for expected sliding distance of a caisson-type breakwater by introduction of a doubly-truncated normal distribution," Coast. Eng. J. 45(3), 387–419.

Le Mehaute, B., Divoky, D., & Lin, A. (1969). Shallow water waves a comparison of theories and experiments. In Coastal Engineering 1968 (pp. 86-107).

Mani, J. S. (2012). Coastal Hydrodynamics. PHI Learning Pvt. Ltd..

Mamak, M., Guzel, H. Theoretical and Experimental Analysis of Wave Impact Pressures on Curved Seawalls. Arab Journal of Science Engineering 38, 817–828 (2013). https://doi.org/10.1007/s13369-012-0521-x.

Mansard, E.P.D., and Funke, E.R. (1980). "The measurement of incident and reflected spectra using a least squares method." Proc. 17th Coast. Eng. Conf., ASCE, 154–172.

Mansard, E. P. D., and E. R. Funke. (1987). "On the reflection analysis of irregular waves". Tech. Rep. TR-HY-017, NRCC No. 27522, National Research Council of Canada.

Minikin R.R. (1963). "Winds, Waves and Maritime Structures'2nd ed., Griffin, London.

MIKE Zero [Computer software]. Danish Hydraulic Institute, Hørsholm, Denmark.

Muller G.U. & Whiftaker T.J.T. (1995). "On the vertical distribution of wave impact pressures" Proc Sth ISOPE conf., The Hague, The Netherland.

Munireddy, M. G., & Neelamani, S., (2004). "Wave pressure reduction on vertical seawalls/caissons due to an offshore breakwater". Indian Journal of Marine Sciences, 33(4), 329–337.

Muller, G.V. (2016). An appropriate size of toe rock for vertical seawalls.

Misra SC (2001) Uncertainty analysis in hydrodynamic tests. Proceedings, International Conference in Ocean Engineering, 200-207.

Minikin, R. R. [1950]: Winds, Waves and Maritime Structures, Griffin, London, pp.38-39. Muller, G. V. (2016). "An appropriate size of toe rock for vertical seawalls by", Stellebosch University, pp. 1-117.

Ning D. Z., Wang, R. Q., Zou, Q. P., and Teng, B. (2016). "An experimental investigation of hydrodynamics of a fixed OWC Wave Energy Converter"., Appl. Energy., 168, 636–648.

Oumeraci H. (1994c) "Review and analysis of vertical breakwater failures - lessons learnedo Coastal Engineering, Special issues on Vertical Breakwaters, Vol22, pp3-30, Elsevier Science BV, Amsterdam.

Owen, M. W., & Briggs, M. G. (1986). Limitations of modelling. In Developments in Breakwaters (pp. 91-101). Thomas Telford Publishing.

PIANC (1991). "Guidelines for the Design and Construction of Flexible Revetments Incorporating Geotextiles in Marine Environment", Report of the Working Group 21 of the Permanent Technical Committee II.

Pilarczyk, K. W. (1990. "Coastal Protection", A. A. Balkema, Rotterdam.

Rajendra K, Balaji R, Mukul P (2017) Review of Indian research on innovative breakwaters. India J Geo Mar Sci 46:431–453.

Rundgren, L. Water wave forces, Bulletin, Royal Institute of Technology, Division of Hydraulics, Stockholm, Sweden, No. 54.

Shutang Zhu, (1999). "Separation of regular waves by a transfer function method", Ocean Engineering, Volume 26, Issue 12, Pages 1435-1446.https://doi.org/10.1016/S0029-8018(98)00041-9.

Shore Protection Manual. (1984). 4th ed., 2 Vol U.S. Army Engineer Waterways Experiment Station, U.S. Government Printing Office, Washington, DC.

Sainflou, M. (1928). Essai sur les Digues Maritimes Vertical. (Test on vertical sea dikes) Annales des Ponts et Chaussees 98, 5-48. (in French).

Steven Hutchinson, Young M., and Macleod A., (2010), "Caisson Breakwater Design for Sliding", Coastal Engineering, V-27, pp. 1–14.

Sunny Kumar Poguluri and Cho, I. H. (2020). "Analytical and numerical study of wave interaction with a vertical slotted barrier, Ships and Offshore Structures", DOI: 10.1080/17445302.2020.1790299.

Takahashi, S., Shimosako, K. & Hanzawa, M. (2001). "Performance design for marine structures and its application to vertical breakwaters: Caisson sliding and deformation-based reliability design," Proc. Advanced Design of Maritime Structures in the 21st Century, Port and Harbour Research Institute, Yokosuka, Japan, pp. 63–73.

U.S. Army Corps of Engineers, 2011. "Coastal Engineering Manual. Washington, D.C., Engineer Manual" 1110-2-1100 (in 6 volumes).

Vijay, K. G., and Sahoo, T. (2019). "Scattering of Surface Gravity Waves by a Pair of Floating Porous Boxes." ASME. J. Offshore Mech. Arct. Eng. October 2019; 141(5): 051803. https://doi.org/10.1115/1.4043415.

Venkateswarlu, V., & Karmakar, D. (2019). "Numerical investigation on the wave dissipating performance due to multiple porous structures". ISH Journal of Hydraulic Engineering, pp 1–18. doi.org/10.1080/09715010.2019.1615393.

Williams, A. N., Lee, H. S., & Huang, Z. (2000). Floating pontoon breakwaters. Ocean Engineering, 27(3), 221-240.

Xuan Li, Wei Zhang (2019). "3D numerical simulation of wave transmission for low-crested and submerged breakwaters, Coastal Engineering, Volume 152, 103517. doi.org/10.1016/j.coastaleng.2019.103517.

Zelt, J. A., and J. E. Skjelbreia. (1992). "Estimating Incident and Reflected Wave Fields Using an Arbitrary Number of Wave Gauges". Coastal Engineering, ASCE, 777–789.

MEASUREMENT OF WAVE REFLECTION

AI-1 GENERAL

The present section describes the measurement of regular wave reflection carried by Michael Isaacson (1991). There are three methods for measuring wave reflection by using either two or three fixed probes which will give for the incident wave height, reflection coefficient, and the phase of the reflected wave train. The method involving three height measurements is the most common one. By the use of three probes, recommendations are made for the relative probe spacing to avoid conditions at which the methods fail or become inaccurate.

The three methods used are

Method I: two fixed probes—two heights and one phase angle measured.

Method II: three fixed probes—three heights and two-phase angles measured.

Method III: three fixed probes—three heights measured.

The calculation of the reflection coefficient is based on the three height measurements method proposed by Isaacson (1991).
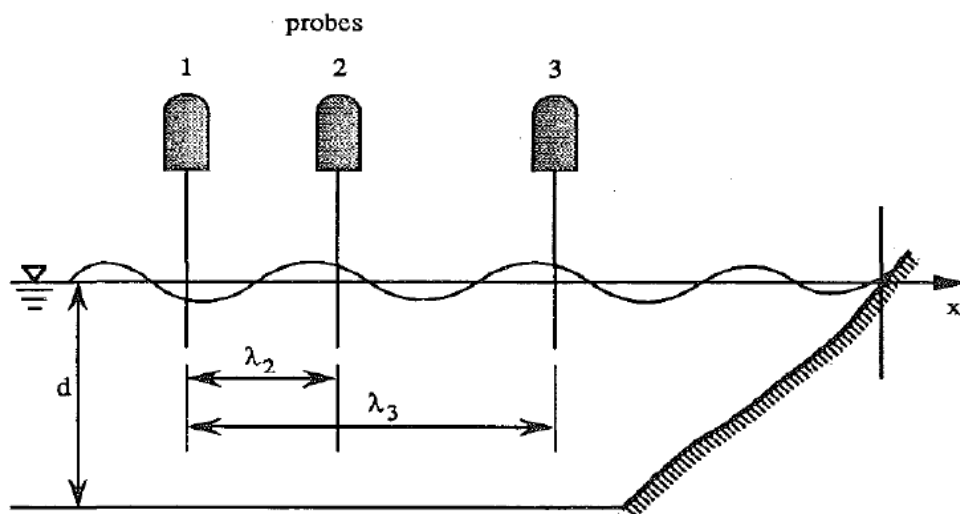
Figure AI-1 Typical sketch for wave reflection Isaacson (1991).

The flow of the calculation is given as,

$$\Delta n = k\lambda n$$

Where $k = 2\pi/L$ and λn is the distance between the nth probe and the first probe

$$\Lambda = \frac{A_1{}^2 sin[2(\Delta_3 - \Delta_2)] - A_2{}^2 \sin(2\Delta_3) + A_3{}^2 \sin(2\Delta_2)}{\sin[2(\Delta_3 - \Delta_2)] + \sin(2\Delta_2) - \sin(2\Delta_3)}$$

$$\Gamma = \frac{1}{2}\left\{\left[\frac{A_1{}^2 + A_3{}^2 - 2\Lambda}{\cos(\Delta_3)}\right]^2 + \left[\frac{A_1{}^2 - A_3{}^2}{\sin(\Delta_3)}\right]^2\right\}^{1/2}$$

$$H^2 = 2\left(\Lambda + \sqrt[1]{\Lambda^2 - \Gamma^2}\right)$$

$$K^2 = \frac{4\Lambda}{H^2} - 1$$

For slotted barrier kept at 1m, T = 2.6 sec, H = 0.16m and μ=10% , the probe readings are:

Wave 1 = 61.106 , Wave 2 = 23.871 , Wave 4 = -56.019

Where:

$$A_1 = \frac{Wave1}{2} , \qquad A_2 = \frac{Wave2}{2} , A_3 = \frac{Wave4}{2}$$

k=2π/L = $\frac{2\pi}{5.47}$ = 1.148

where Δn=kλn ,, is the dimensionless distance between the nth probe and the first probe

$\Delta_1 = 0.$

Δ_2=kλ2 = Δ_2=2π/3 = 2.09

Δ_3=kλ3 = Δ3=4π/3 = 4.19

For A1 = 30.55 , A2 =11.93 and A3 = -28.00

$$\Lambda = \frac{30.55^2 sin[2(4.19-2.09)] - 11.93^2 \sin(2*4.19) + -28^2 \sin(2*2.09)}{\sin[2(4.19-2.09)] + \sin(2*2.09) - \sin(2*4.19)}$$

$$\Lambda = 2686.11$$

$$\Gamma = \frac{1}{2}\left\{\left[\frac{30.55^2 + -28^2 - 22686.11}{\cos(4.19)}\right]^2 + \left[\frac{30.55^2 - -28^2}{\sin(4.19)}\right]^2\right\}^{1/2}$$

$$\Gamma = 2684.72$$

$$H^2 = 2\left(\Lambda + \sqrt[1]{\Lambda^2 - \Gamma^2}\right)$$

$$= 5545.64$$

$$K^2 = \frac{4*2686.11}{5545.64} - 1 = 0.93$$

K = 0.96

For some probe values, the value of $\Gamma > \Lambda$, and the value of H_2 is obtained as negative value. For such values, K2 is obtained as a negative value and is ignored.

WAVE FORCE

SPECIMEN CALCULATION OF WAVE FORCE ON SOLID WALL
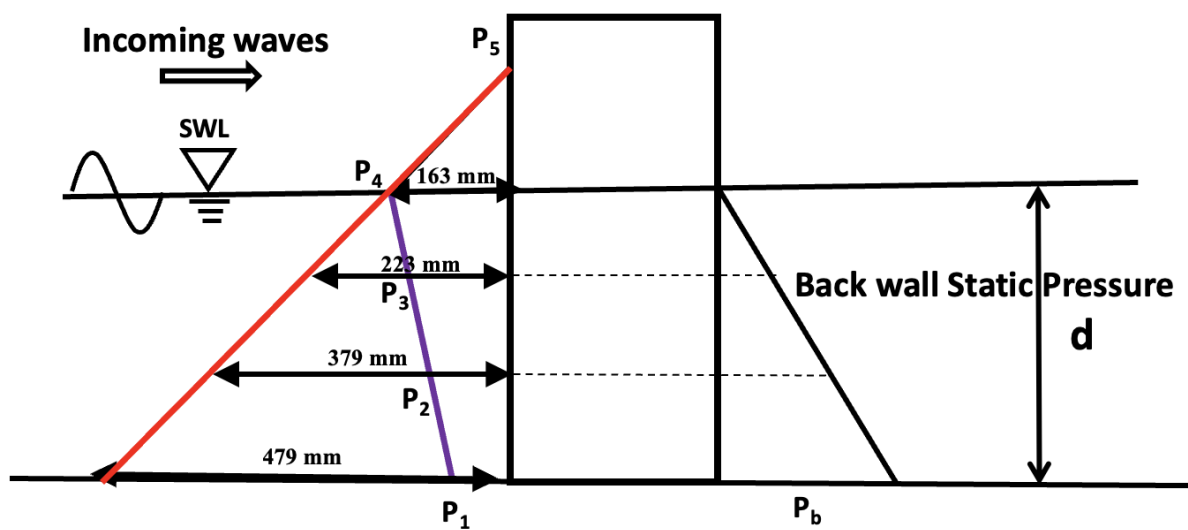
Static Pressure = ρgh

$$P_1 = 1000 \text{ x } 9.81 \text{ x } (0.479)\text{-}P_{b1}$$

$$P_2 = 1000 \text{ x } 9.81 \text{ x } (0.379)\text{-}P_{b2}$$

$$P_3 = 1000 \text{ x } 9.81 \text{ x } 0.223)\text{-}P_{b3}$$

$$P_4 = 1000 \text{ x } 9.81 \text{ x } 0.163)\text{-}P_{b4}$$

$$P_5 = 0$$

Force per meter length

$$F_1 = (\tfrac{1}{2})(P_1 + P_2) \text{ x } h_1$$

$$F_2 = (\tfrac{1}{2})(P_2 + P_3) \text{ x } h_2$$

$$F_3 = (\tfrac{1}{2})(P_3 + P_4) \text{ x } h_3$$

$F_4 = (\frac{1}{2})(P_4 + P_5) \times h_4$

Net Force (F) = $F_1 + F_2 + F_3 + F_4$ (per m length)

Total Force on Solid wall = F x 0.7 m N (length of wall or width of flume)

WAVE FORCE CALCULATION ON PERFORATED FRONT WALL

Total Force on Perforated front wall = Total Force on Solid wall x Area Factor

Area Factor = [Area of Solid wall – Area of Perforation] / Area of Solid wall

Similarly, the total force on Rear Wall is also calculated

Total Force on Perforated breakwater (F_{total}) = Front wall force + Rear wall force

UNCERTAINTY ANALYSIS

AII-1 GENERAL

The hydrodynamic test facilities differ from one another with regard to facilities, instrumentation, experimental procedures and scale. Hence, it becomes necessary for a test facility to provide possible lower and upper margins, which can be adopted with a fair confidence level. Such a study for an experimental test procedure in a particular facility is termed an uncertainty analysis. Uncertainty describes the degree of goodness of measurement or experimentally determined result. It is an estimate of experimental error. It is possible to conduct experiments scientifically and predict the accuracy of the result (Misra, 2001) with the help of uncertainty analysis. Experimental error sources should be identified and the error (δ) should be determined from manufacturers brochures, calibration and conducting simple experiments respectively (Kline, 1985).

The use of uncertainty analysis is indispensable in physical model studies. There is no single way to describe uncertainty in measurements and there are many different situations that demand somewhat differing descriptions. The distribution of uncertainty between precision and bias is arbitrary. Whatever may the method used for calculating uncertainty, the method used should be reported in some appropriate way and the report includes the method employed (Kline, 1985). It is also generally agreed that the inaccuracies can be appropriately expressed by an "uncertainty" and these values could be obtained by an "Uncertainty analysis". The confidence interval gives an estimated range of values, which is likely to include an unknown population parameter. From a given set of observations the estimated range is calculated. The 95% confidence interval limits must always be estimated and this concept of confidence level is fundamental to uncertainty analysis (Misra, 2001).

AII-2 PROCEDURE FOR UNCERTAINTY ANALYSIS

A best-fit curve can include both the 95% confidence band and the 95% prediction band. The confidence band tells about 95% sure that the true best fit curve (if an infinite number of data points are available) lies within the confidence band. The prediction band tells about the scatter of the data. If data points are considered, 95% of points are expected to fall within the prediction band. Since the prediction band has to account for uncertainty in the curve itself as well as scatters around the curve, it is much wider than the confidence band.

Fig. AII-1 shown below, confidence bands contain a minority of data points. The confidence bands shown have a 95% chance of containing the true best fit curve and the dashed prediction bands include 95% of the data points. Also, the 95% confidence and prediction bands have been accepted to be reliable enough for usage under the adoption of uncertainty analysis.
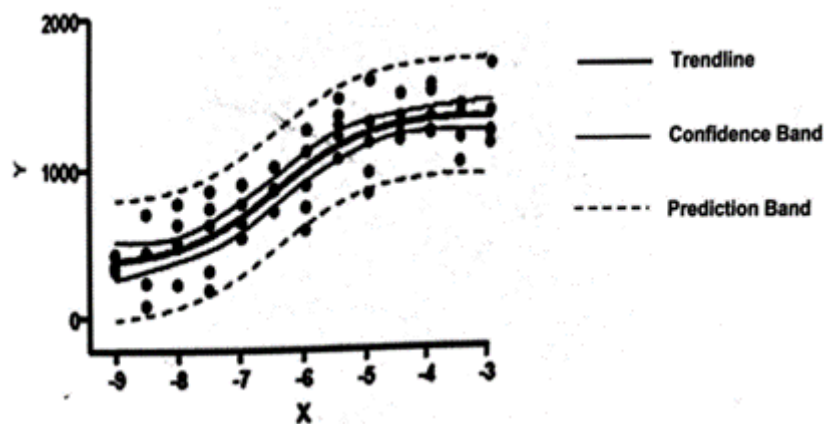
Figure AII-1 combined specimen graph for 95% confidence and prediction band

Figure AII-2 to AII-5 shows the plot of 95% confidence and prediction bands for the variation of K_r with H_i/L and R_u/H_i with H_i/L for 0.50m water depth for the typical cases in which the trend lines have a correlation coefficient of more than 0.90. From the figures, it is observed that the plot contains the best fit curve with 95% confidence that the trend line lies within these confidence bands and data points lie within the prediction

bands drawn. From the bands drawn, the results may be analyzed with 95% confidence i.e. the conclusions drawn from these graphs are 95% reliable. Also, from the figures, it is visualized that experimental data points are bounded within the 95% prediction bands and this particular observation strengthens the conclusions derived from these graphs.
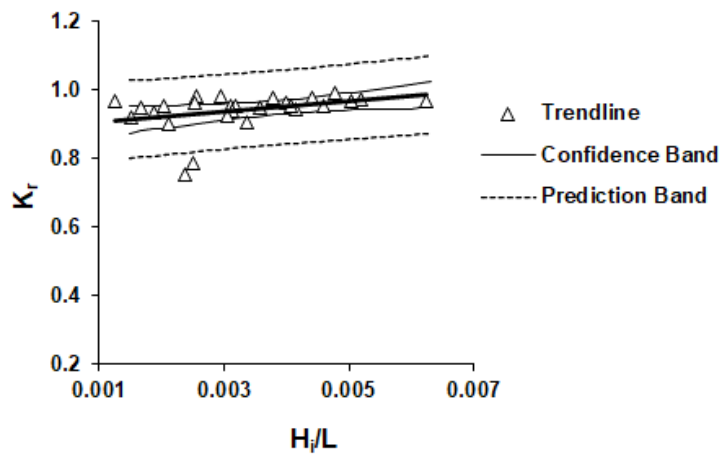
Figure AII-2   Plot of 95% confidence and prediction bands for variation of K_r with H_i/L (VCB)
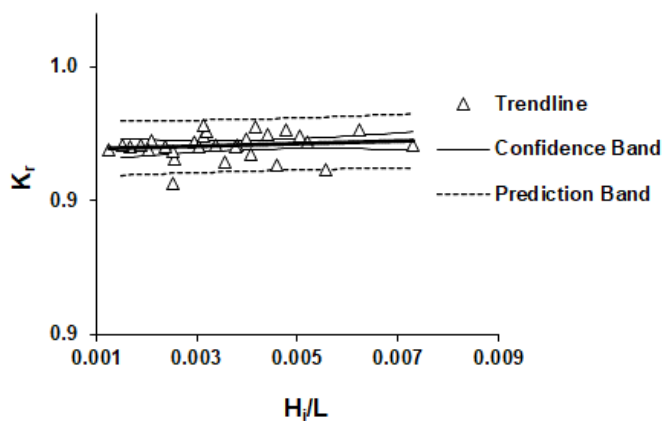
Figure AII-3   Plot of 95% confidence and prediction bands for variation of K_r with H_i/L (PVCB)
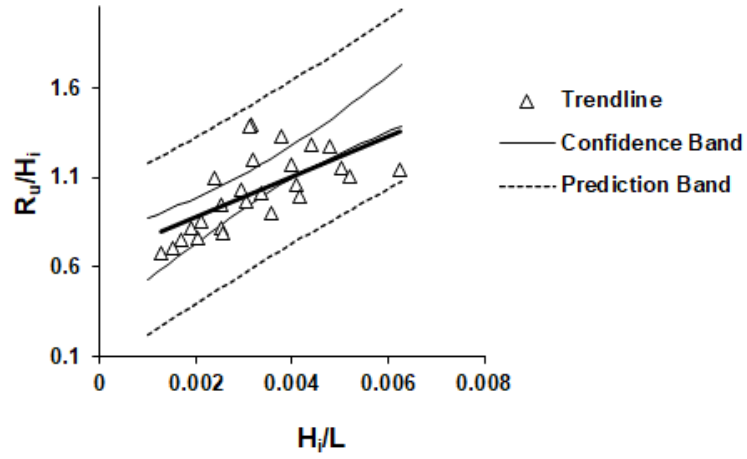
Figure AII-4 Plot of 95% confidence and prediction bands for variation of
R_u/H_i with H_i/L (VCB)
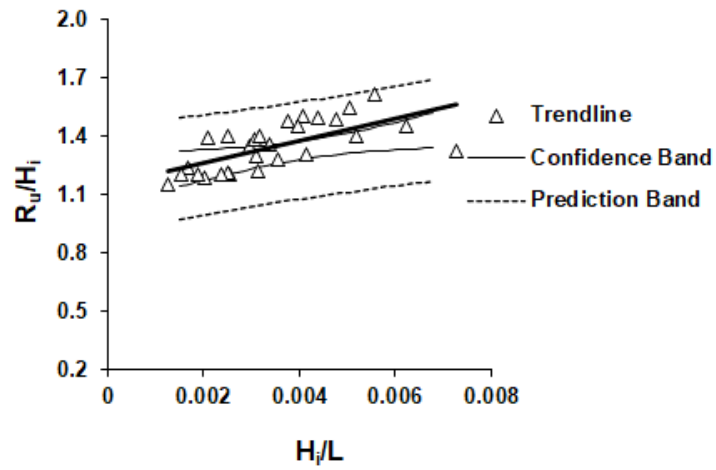
Figure AII-5 Plot of 95% confidence and prediction bands for variation of
R_u/H_i with H_i/L (PVCB)

EQUATIONS USED FOR THE ANALYSIS

95% confidence band

$$\mu_{y/x_o} \pm t_{\propto/2, n-2} \sqrt{\left[\sigma^2 \left\{\frac{\frac{1}{n} + (x_o - x)^2}{S_{xx}}\right\}\right]}$$

95% prediction band

$$\mu_{y/x_o} \pm t_{\propto/2, n-2} \sqrt{\left[\sigma^2 \left\{\frac{1 + \frac{1}{n} + (x_o - x)^2}{S_{xx}}\right\}\right]}$$

Where,

$\mu_{y/x_o} = \beta_o x + \beta_1$ computed from the fitted regression model

α   = Significance level used to compute the confidence level

σ^2 = Variance

x_o = Data sample

x   = Sample mean

t   = Value from 't' distribution table

n   = number of samples

$$S_{xx} = \sum_{i=1}^{n} x_o{}^2 - \frac{x_i{}^2}{n}$$

SAMPLE CALCULATION OF CONFIDENCE AND PREDICTION INTERVALS $(R_u/H_i$ vs $H_i/L)$

X_i (H_i/L)	Y_i (R_u/H_i)	$\hat{Y}_i$	SS_E	S_{xx}	K	K'	Upper limit	Lower limit	Prediction Band	
									Upper limit	Lower limit
0.0015	1.1502	1.234	0.00701297	7.03197E-06	0.0904	0.2617	1.324	1.144	1.496	0.972
0.001696	1.2375	1.241	1.411E-05	6.02878E-06	0.0855	0.2600	1.327	1.156	1.501	0.981
0.001893	1.3901	1.249	0.02003097	5.10276E-06	0.0807	0.2585	1.329	1.168	1.507	0.990
0.002089	1.3987	1.256	0.02039698	4.25391E-06	0.0761	0.2571	1.332	1.180	1.513	0.999
0.002286	1.3475	1.263	0.00710736	3.48222E-06	0.0716	0.2558	1.335	1.192	1.519	1.007
0.002482	1.3575	1.271	0.00756766	2.78771E-06	0.0674	0.2546	1.338	1.203	1.525	1.016
0.002679	1.2012	1.278	0.00587071	2.17036E-06	0.0633	0.2536	1.341	1.214	1.531	1.024
0.002875	1.1875	1.285	0.00953228	1.63018E-06	0.0596	0.2527	1.345	1.226	1.538	1.032
0.003268	1.3833	1.300	0.00698466	7.8133E-07	0.0531	0.2513	1.353	1.247	1.551	1.049
0.003464	1.2857	1.307	0.00045615	4.72656E-07	0.0506	0.2507	1.358	1.256	1.558	1.056
0.003661	1.5031	1.314	0.03561345	2.41151E-07	0.0486	0.2503	1.363	1.266	1.565	1.064
0.003857	1.2032	1.322	0.01404167	8.68144E-08	0.0472	0.2501	1.369	1.274	1.572	1.072
0.004054	1.2102	1.329	0.01411591	9.64605E-09	0.0465	0.2499	1.376	1.283	1.579	1.079
0.00425	1.2210	1.336	0.01329945	9.64605E-09	0.0465	0.2499	1.383	1.290	1.586	1.086
0.004446	1.4801	1.344	0.0186224	8.68144E-08	0.0472	0.2501	1.391	1.296	1.594	1.094
0.004643	1.4921	1.351	0.01992645	2.41151E-07	0.0486	0.2503	1.400	1.302	1.601	1.101
0.004839	1.5502	1.358	0.03684412	4.72656E-07	0.0506	0.2507	1.409	1.308	1.609	1.108
0.005036	1.2012	1.366	0.02700915	7.8133E-07	0.0531	0.2513	1.419	1.312	1.617	1.114
0.005232	1.4011	1.373	0.00079595	1.16717E-06	0.0561	0.2519	1.429	1.317	1.625	1.121
0.005429	1.4502	1.380	0.00490136	1.63018E-06	0.0596	0.2527	1.440	1.321	1.633	1.128
0.005625	1.4895	1.388	0.01040132	2.17036E-06	0.0633	0.2536	1.451	1.324	1.641	1.134
0.005821	1.6141	1.395	0.04803726	2.78771E-06	0.0674	0.2546	1.462	1.327	1.649	1.140
0.006018	1.3001	1.402	0.01041192	3.48222E-06	0.0716	0.2558	1.474	1.330	1.658	1.146
0.006214	1.3031	1.409	0.01130642	4.25391E-06	0.0761	0.2571	1.486	1.333	1.667	1.152
0.006411	1.4054	1.417	0.00012779	5.10276E-06	0.0807	0.2585	1.498	1.336	1.675	1.158
0.006607	1.4506	1.424	0.00070664	6.02878E-06	0.0855	0.2600	1.510	1.339	1.684	1.164
0.006804	1.3214	1.431	0.01209784	7.03197E-06	0.0904	0.2617	1.522	1.341	1.693	1.170

APPENDIX III: TOE DAMAGE PHOTOGRAPHS

INITIAL CONDITION   **FINAL CONDITION**

For T=1.6 sec, H= 0.12 m

(a) No. of displaced units: 1   Percentage Damage: 0.34

For T=1.8 sec, H= 0.12 m

(b) No. of displaced units: 6   Percentage Damage: 2.02

For T=2.0 sec, H= 0.12 m

(c) No. of displaced units: 1   Percentage Damage: 0.34

For T=2.2 sec, H= 0.12 m

(d) No. of displaced units: 8   Percentage Damage: 3.0

INITIAL CONDITION   FINAL CONDITION

For T=2.4 sec, H= 0.12 m

(e)   No. of displaced units: 09   Percentage damage: 4.0

For T=2.4 sec, H= 0.14 m

(d)   No. of displaced units: 13   Percentage damage: 4.6

PUBLICATIONS BASED ON PRESENT RESEARCH WORK

Publications in Journals (Indexed in SCI / Scopus /Web of Science)

1. Kumaran V., Manu, and Subba Rao, (2021), "Assessment of Dynamic Pressure/ Force on Vertical Caisson type Breakwater." *Marine Geo Resources and Geo Technology*. DOI: 10.1080/1064119X.2021.1873469.

2. Kumaran V., Manu and Subba Rao (2021), "Hydrodynamic Characteristics of Caisson Type Breakwater -A Physical and Numerical Approach." *International Journal of Naval Architecture and Marine Engineering*, DOI: 10.3329/jname.v18i2.52134.

3. Kumaran V., Manu and Subba Rao (2022), "Damage Analysis of Toe for Wall Type Breakwaters." *Journal of the Institution of Engineers (India): Series A*, DOI: 10.1007/s40030-021-00591-4.

Scopus Indexed Book Chapter

1. Kumaran V., Manu and Subba Rao (2020), "An Experimental Investigation on Toe Stability for Vertical- Caisson Breakwaters." In the book titled "Lecture Notes in Civil Engineering" Springer, Singapore/ *Lecture Notes in Civil Engineering*/ LNCE Vol 99/pp 593-602. DOI:/10.1007/978-981-15-6828-2_43.

Journal Articles (Submitted for Publication)

1. Kumaran V., Manu and Subba Rao (2022), "Reduction of wave force on wall type breakwater with slotted barriers: Physical and Numerical approach", **Ocean Engineering**.

International Conferences / Symposium

1. Kumaran V., Sajid K, Subba Rao and Manu (2021) "Experimental Investigation of Dynamic Pressure on Wall Type Breakwater with Slotted Barrier," First International Conference on Recent Advances in Civil Engineering (ICRACE - 2021), held at National Institute of Technology, Silchar 2021, has been honored with **BEST PAPER AWARD.**

2. Kumaran V., Manu and Subba Rao (2019), "Analyzing the Wave Forces on Vertical Caisson Breakwater- A Numerical Approach" in International Symposium on Advances in Coastal Research with special reference to Indo Pacific [AdCoRe IP-2019], National Centre for Coastal Research (NCCR), Chennai, India. Book of abstracts AdCoRe IP-2019, p. 161, 17-19th Dec 2019.

3. Kumaran V., Manu and Subba Rao (2019), "Experimental Investigation on the performance of vertical- caisson type breakwater with and without toe protection" in 24th HYDRO-2019-International conference on Hydraulics, water resources & coastal engineering, Dept. of Civil Engg., University College of Engg., Osmania University, Hyderabad, India. Proc. of HYDRO-2019, Vol I, pp. 526 – 534, 18-20th Dec 2019. (ISBN- 978-93-8935-484-3).

CURRICULUM VITAE

Name : KUMARAN V.

Permanent Address:

R. Viswanathan, Plot 23, Tami Residency, Saravana Bhavan, Padur Link Road, Padur, Chennai, Tamil Nadu. PIN: -603103.

Contact No.   : +91-9003665164.

Email ID   : vkumaranms@gmail.com. ; **Scopus ID:** 56829063400

Experience:

Senior Research Fellow (2016-2022)

College   : National Institute of Technology Karnataka, Surathkal.

Project Title   : Hydrodynamic performance characteristics of caisson type

                Breakwater (Funded by MoES, Government of India)

Education:

Master of Science (By Research) (Dec 2013- May 2016)

Discipline   : Civil Engineering

College   : College of Engineering, Guindy, Chennai.

Thesis Title   : Application of numerical model for analyzing the wave climate of

                Agatti Island, Lakshadweep, India

Bachelor of Engineering (2009-2013)

Discipline   : Harbour and Ocean Engineering

College   : AMET University, Chennai.

Project Title   : Estimation of settlement of soil group by action of piles using

                PLAXIS 3-D